Biophysical modeling of effects of ionizing radiation and associated uncertainties

Biophysikalische Modellierung der Effekte ionisierender Strahlung und damit verbundener Unsicherheiten

Zur Erlangung der Habilitation
genehmigte Habilitationsschrift von Thomas Friedrich aus Groß-Umstadt
Tag der Einreichung: 5. Februar 2016
Darmstadt — D 17

1. Gutachten: Prof. Dr. Barbara Drossel
2. Gutachten: Prof. David J. Brenner, Ph.D., D.Sc
3. Gutachten: Prof. Harald Paganetti, Ph.D.

TECHNISCHE
UNIVERSITÄT
DARMSTADT

GSI

Biophysical modeling of effects of ionizing radiation and associated uncertainties
Biophysikalische Modellierung der Effekte ionisierender Strahlung und damit verbundener Unsicherheiten

Genehmigte Habilitationsschrift von Thomas Friedrich aus Groß-Umstadt

1. Gutachten: Prof. Dr. Barbara Drossel
2. Gutachten: Prof. David J. Brenner, Ph.D., D.Sc
3. Gutachten: Prof. Harald Paganetti, Ph.D.

Tag der Einreichung: 5. Februar 2016

Darmstadt — D 17

Abstract

Ionizing radiation is a health hazard to humans, but is exploited at the same time in various applications, in particular in diagnostic and therapeutic medicine. A profound understanding of the underlying processes, starting from the physical energy deposit up to the biological radiation response, is the basis for a reliable prediction of radiation effects. The subject of this work is the formulation of predictive dose response models.

Special emphasis is set on two aspects, namely the prediction of radiation effects as well as their uncertainties: First, the dependence of radiation effects on physical properties like particle type and energy of the radiation used is discussed. The physical characterization of radiation to which cells or tissues are exposed to is one of the most important determining factors for the effect. Particularly the spatial and temporal pattern of radiation damage induction have to be considered: High ionization densities give rise to clustering of lesions to the DNA, and such complex DNA damage is most critical for the fate of individual cells. Based on experimental findings and theoretic considerations, strategies are developed on how to implement the complex involved physical and biological processes into mathematical models. Such models must be sufficiently simple, testable against experimental data, and practical for application purposes. A set of requirements for radiation effect models has been identified, which is proposed as a list of general criteria for successful models in radiobiology. Based on these requirements, a comprehensive radiobiological model framework for the prediction of radiation damage is introduced. The model applicability to many different aspects of radiobiology is demonstrated, based on one consistent set of concepts, strongly supporting the model assumptions. Second, in addition to effect predictions, strategies to assess the corresponding uncertainties are discussed theoretically and at hand of experimental data. The variability of biological targets as well as errors inferred by model applications are regarded side by side. This is of importance, e.g., for evaluating the accuracy of treatment planning in radiation therapy of cancer.

The developed model framework is put in perspective of current radiobiologic research. The core of the work are six research publications, focusing on various aspects in effect modeling for different radiation qualities. They cover strategies of model set-up and benchmarking using experimental data, as well as aspects of effect uncertainty estimates.

Zusammenfassung

Ionisierende Strahlung stellt ein Gesundheitsrisiko für den Menschen dar, wird aber gleichzeitig in verschiedenen Anwendungsbereichen wie zum Beispiel der diagnostischen und therapeutischen Medizin genutzt. Ein tiefgreifendes Verständnis der zugrunde liegenden Prozesse von der physikalischen Energiedeposition bis hin zur biologischen Strahlenantwort ist die Grundlage für eine verlässliche Vorhersage von Strahlenwirkungen. Das Thema dieser Arbeit ist die Formulierung von prädiktiven Dosis-Wirkungs-Modellen.

Einen Schwerpunkt bilden die beiden Aspekte der Vorhersage von Strahlenwirkungen sowie deren Unsicherheiten. Zunächst wird die Abhängigkeit der Strahlenwirkung von der Strahlenart und der Energie diskutiert. Die physikalische Charakterisierung der Strahlung, der Zellen oder Gewebe ausgesetzt sind, ist einer der wichtigsten bestimmenden Faktoren für die Wirkung. Besonders berücksichtigt werden die räumlichen und zeitlichen Muster der induzierten Schäden: Hohe Ionisationsdichten führen zur Clusterung von Schäden an der DNA. Sich so formierende komplexe DNA Schäden bestimmen maßgeblich das weitere Schicksal der bestrahlten Zellen. Basierend auf experimentellen Befunden und theoretischen Überlegungen werden Strategien entwickelt, wie die beteiligten physikalischen und biologischen Prozesse in mathematische Modelle implementiert werden können. Solche Modelle müssen hinreichend einfach, an experimentellen Daten verifizierbar und praktisch für Anwendungszwecke sein. Eine Reihe von Anforderungen für Strahleneffektmodelle wurde zusammengetragen, die als eine generelle Aufstellung von Kriterien für erfolgreiche Modelle in Radiobiologie vorgeschlagen wird. Auf der Grundlage dieser Anforderungen wird ein konsistentes radiobiologisches Modellgebäude zur Vorhersage der Strahlenwirkung vorgestellt. Die Anwendbarkeit des Modells auf viele verschiedene Aspekte der Radiobiologie wird auf der Basis eines einheitlichen Satzes von Konzepten und Parametern gezeigt, die nachdrücklich die Modellannahmen unterstützen. Den Zweiten Hauptaspekt der Arbeit bildet die Entwicklung von Methoden, um die entsprechenden Unsicherheiten zu beurteilen. Diese Unsicherheiten werden theoretisch sowie durch die Untersuchung experimenteller Daten quantifiziert. Die Variabilität biologischer Systeme in ihrer Reaktion auf Strahlung sowie die durch die Modellannahmen eingebrachten Fehler werden nebeneinander betrachtet. Dies ist beispielsweise für die Bewertung von Unsicherheiten bei der Bestrahlungsplanung in der Krebstherapie von Bedeutung.

Die entwickelten Modellkonzepte werden in den Rahmen aktueller strahlenbiologischer Forschung gestellt. Der Kern der Arbeit besteht aus sechs Publikationen, die sich auf eine Reihe von Aspekten der Effektmodellierung für verschiedene Strahlenqualitäten konzentrieren. Sie decken Strategien der Modellformulierung, deren Validierung durch experimentelle Daten sowie Abschätzung verbundener Unsicherheiten ab.

Contents

1 Introduction **1**
- 1.1 Motivation . . . 1
- 1.2 Objective . . . 3
- 1.3 Outline . . . 3

2 Physical and biological basics **5**
- 2.1 The standard paradigm of radiation damage . . . 5
- 2.2 Endpoints and dose response . . . 7
- 2.3 Impact of cell or tissue type on the effect . . . 10
- 2.4 Impact of radiation quality on the effect . . . 11
  - 2.4.1 Sparsely and densely ionizing radiation . . . 12
  - 2.4.2 Ion radiation . . . 13
  - 2.4.3 Ultrasoft X-rays . . . 16
- 2.5 Relative biological effectiveness . . . 18
- 2.6 Particle therapy . . . 20

3 Modeling concepts and application **23**
- 3.1 Requirements for radiation effect models . . . 23
- 3.2 Historical perspective and classification . . . 25
- 3.3 Interpretation of the linear-quadratic model . . . 28
- 3.4 Levels of clustering and complexity . . . 30
  - 3.4.1 Biological target size . . . 30
  - 3.4.2 SSB clustering on the nanometer scale . . . 31
  - 3.4.3 DSB clustering on the micrometer scale . . . 32
- 3.5 The Local effect model . . . 33
  - 3.5.1 Principles . . . 33
  - 3.5.2 Applications . . . 36
- 3.6 The Giant Loop Binary Lesion model . . . 38
  - 3.6.1 Principles . . . 38
  - 3.6.2 Applications . . . 40

4 Accuracy and uncertainty considerations **42**
- 4.1 Types of uncertainties in RBE . . . 43
- 4.2 Parameter sensitivity analysis . . . 43
- 4.3 Uncertainties induced by data processing . . . 44
- 4.4 Uncertainty and variability in observed experimental radioresponse . . . 45

5 Discussion of the articles A1-A6 **48**
- 5.1 Effect modeling: Articles A1-A3 . . . 48

5.2 Uncertainty considerations: Articles A4-A6 49

6 Perspectives **52**

7 Reprints of selected publications **56**
7.1 Article 1: The mathematical framework of the Local Effect Model 56
7.2 Article 2: The Giant Loop Binary Lesion Model 62
7.3 Article 3: Modeling the radiation action of ultrasoft X-rays 74
7.4 Article 4: Sensitivity analysis of high LET modelling 86
7.5 Article 5: Mathematical aspects of RBE uncertainties 110
7.6 Article 6: A data base of cell survival experiments 116

Bibliography **138**

1 Introduction

1.1 Motivation

Ionizing radiation is a part of nature. It occurs in space as cosmic radiation and on earth as terrestrial radiation. Ionizing radiation is exploited in various ways by mankind in scientific, industrial and medical applications. Examples are accelerator-driven research, material testing and diagnostic and therapeutic methods of radiology, respectively.

Energetic photons like X-rays or γ-rays and massive charged particles like electrons or ions deliver energy to a target, giving rise to energy deposition by excitations and ionizations in the target material. When interacting with biologic target material ionizing radiation is therefore able to inflict damage to the cells and tissue on the molecular level [1,2]. This might be harmful, but also beneficial in some situations. Knowledge about the consequences of ionizing radiation and underpinning mechanisms facilitates to prevent from unwanted radiation exposures or to mitigate the associated effects. Likewise, radiation can be delivered on purpose and its biologic effects may be exploited. For all that, a proper quantification of radiation effects is needed.

In particular mathematical modeling of radiation is a fruitful approach to a predictive quantification of radiation action and the associated damage. The underlying model assumptions may be verified or falsified by testing such models against measured data of radiation damage. Predictive modeling of radiation effects has large impact and relevance for different fields of application and research:

- **Radiation cancer therapy:** Cancer is one of the leading mortality reasons ranks as the second most mortal disease worldwide after heart diseases [3]. For solid tumors, radiation therapy is besides surgery and chemotherapy the most important therapeutic strategy. The aim is to inactivate tumor cells by irradiation of the tumor tissue, while sparing the surrounding healthy tissue as good as possible [4]. Conventionally this is done by irradiation with photon radiation. Typically ^{60}Co was used as radiation source in earlier times, while nowadays high energetic (MV) synchrotron radiation is delivered from small electron linear accelerators. Convenient beam delivery techniques like irradiation from various angles to the tumor and a shaping of the beam contours optimize this method. Clearly, an understanding of how tumor conformity, the dose coverage of healthy tissue and various other factors affect the control of the tumor (i.e. the growth prevention) and the side effects in the normal tissue is mandatory. In particular novel promising forms of treatments with protons and heavier ions (typically carbon) emerged, primarily driven by their favorable physical properties for therapy [5–7]. Carbon ion therapy was promoted at GSI during a pilot project in 1997 - 2008 [8–10]. Currently, dedicated clinics for particle therapy are raised all over the world [11]. As charged particles carry an enhanced effect as compared to comparable doses of conventional photon radiation, again the question for the dose-effect relation arises. In turn, to plan a patient specific irradiation treatment, the prediction of the radiation effects are needed. Mathematical effect modeling facili-

tates a safe treatment planning considering the physical and biological aspects of radiation effectiveness.

- **Radiation protection on earth and in space:** Exposure of the human body to ionizing radiation bears a potential to induce cancer as a late effect, e.g. typically occurring years after exposure [12]. This is important to be considered in e.g. in medical diagnostics with X-ray computer tomography (CT) scans [13, 14], for occupational exposures [15, 16], but also in radiation therapy [17] to minimize side effects. For space travelers, e.g. on a planned Mars mission, radiation exposure by the cosmic galactic radiation and the radiation delivered by the sun is a hazard with a mortality risk to the astronauts [18, 19]. The carcinogenic potential is particularly relevant for lower doses where the received dose is not large enough to cause cell death, which is regarded as a self-protecting mechanism of organisms against the development of cancer. The relation between dose (and possibly dose rate) and the enhanced risk to develop cancer is derived from epidemiological studies and interpreted in terms of appropriate models [20]. Again, the dose-effect relation, accounting for the radiation and biologic factors for radio response, is a key aspect to be considered.

- **Other therapy modalities using radiation:** In medicine also different forms of radiation-involved therapies for non-tumor diseases have been established [21]. For instance, high doses of very small radiation beams are given to treat arteriovascular malformations. Moreover the treatment of artrial fibrillation with radiation beams is possible [22]. In these cases tissue degradation by high doses of ionizing radiation is exploited. On the other hand, low doses of α radiation are known to show anti-inflammatory effects, which is why patients with rheumatic diseases benefit from radon inhalation [23]. Suspiciously a close interference of the radiation action with the immune system plays a role. To understand and predict these effects and related side effects, modeling will be needed.

- **Radiation as research tool in cell biology:** The induction of damage to cells on the molecular level and the observation of subsequent processes can be used in radiobiology to learn about these processes. It is clear by now that after the initial damage induction to the DNA, which is considered to be the most radio-sensitive site of the cell contained in the cell nucleus, cells attempt to repair the damage, which exploits complicated pathways involving cascades of proteins. Finally, harmed cells either have their damage repaired successfully, have persistent but viable damage, or enter a form of cell death [1, 2]. To explore the mechanism of DNA repair, radiation is frequently used as a damaging agent [24]. Mathematical models of radiation effects have to explicitly or implicitly reflect these processes, and a joint consideration of experimental studies and model assumptions helps to confirm or reject hypotheses about how cells react to radiation.

Summarizing, quantitative modeling of radiation damage is an inherent part of research in radiation biophysics with a strong impact to radiation protection and medical applications. Many models aiming at different aspects of radiation damage and / or processing have been developed throughout the last decades and find applications in the related disciplines. However, as the physical processes, namely the interaction of radiation with matter, as well as the biological processes, namely damage induction and processing, are very complex, up to now still many basic questions remain unsolved and an comprehensive understanding of all processes is lacking.

Consequently models have to restrict to essential parts, allowing for reasonable predictions. The exploitation of model limits and associated uncertainties is therefore of great importance.

1.2 Objective

The basic problem in modeling radiation effects is that both the interaction processes of radiation with biologic matter and the subsequent damage processing are highly complex. Thus the observed dose response is a product of this complexity, which has to be reflected in proper modeling. Different approaches to tackle this problem have been developed, but most of them are limited either in predictive power or applicability to different endpoints, i.e. biological observable such as cell kill or skin reddening. A sound modeling, however, should provide reliable predictions for a wide span of situations varying in the radiation quality used or the cells or tissue under investigation. Moreover, if it reflects reality a transition between different endpoints should be possible within the same model framework.

The objective of this work is to argue on a very general level which modeling strategies are promising or even mandatory for successful predictive modeling of radiation effects. In particular the decision between explicit (mechanistic) or implicit (empiric) simulation of complex processes but also the choice of relevant scales of radiation damage and damage repair play a role in this context. A balance of detail level included and the overall model simplicity is a further aspect to be considered.

Besides point predictions, also associated uncertainties of such modeling have to be quantified. The presented work thus also emphasizes on possible approaches to assess uncertainties. This covers not only the uncertainties of model input data and model results but also the propagation into quantities relevant in applications. As an example, in particle therapy of cancer not only thorough predictions of the enhanced effectiveness of ion radiation is needed, but also the related uncertainties in patient treatment plans must be considered.

These two main focus points will be illustrated in this work at hand of the model framework of the Local Effect Model (LEM) and the complementary Giant Loop Binary Lesion (GLOBLE) model. While the former one was invented to predict the enhanced effectiveness of ion radiation, the latter one is a general dose effect model originally designed for photon radiation. Both models are based on the same assumptions, in particular regarding the spatial scales relevant for lesion formation and processing. A thorough model benchmarking and the successful widespread applicability of the models can be regarded as a strong support for the underlying assumptions. Consequently the correct predictions made by LEM and GLOBLE shed light on the nature of the relevant biological targets.

1.3 Outline

Integral part of this Habilitation thesis are six embedded publications which have been peer reviewed and published in scientific journals. They are labeled and referenced as [A1-A6] throughout the work and compiled in the last chapter of the thesis. Three of the publications aim at model formation and applications, while the other three are concerned with uncertainty considerations. Table 1.1 contains an overview of the publications.

The main text in chapters 2-6 of the present work includes a comprehensive framework and puts the publications into relation and perspective of current research. The thesis is organized

Table 1.1: Publications regarded as part of the present Habilitation thesis.

Label	Title	Journal & Year	Ref.
A1	Calculation of the biological effects of ion beams based on the microscopic spatial damage distribution pattern	Int. J. Radiat. Biol. 2012	[25]
A2	Modeling cell survival after photon irradiation based on double-strand break clustering in megabase pair chromatin loops	Radiat. Res. 2012	[26]
A3	Modeling cell survival after irradiation with ultrasoft X Rays using the Giant Loop Binary Lesion Model	Radiat. Res. 2014	[27]
A4	Sensitivity analysis of the relative biological effectiveness predicted by the local effect model	Phys. Med. Biol. 2013	[28]
A5	Accuracy of RBE: experimental and theoretical considerations	Radiat. Environ. Biophys. 2010	[29]
A6	Systematic analysis of RBE and related quantities using a database of cell survival experiments with ion beam irradiation	J. Radiat. Res. 2013	[30]

as follows: In the second chapter physical and biological basics for the context of the presented research are recalled. General concepts of radiation effect modeling are introduced and discussed in chapter 3. Also the concept of the LEM/GLOBLE formalism and the spectrum of its applications are presented. In chapter 4 uncertainty considerations are introduced. The interrelation of the articles [A1-A6] and their general impact in current research are briefly discussed in chapter 5. Finally, in chapter 6 the perspectives of the presented research and possible future developments are highlighted, in particular in the scope of current radiobiologic research and developments in particle therapy of cancer.

2 Physical and biological basics

In this chapter physical and biological aspects relevant for effect modeling will be recalled. Within the standard model of radiation damage different stages are classified from damage induction up to late consequences on the organism level. As model approaches typically are designed for specific observables, these biologic endpoints emerging in this general picture are discussed subsequently along with their radiation response.

Radiation action can only be understood by considering both biological and physical factors. Hence the impact of the inherent radiosensitivity of cells and tissues as well as the radiation quality are regarded. Finally this facilitates the definition of the relative biological effectiveness, i.e. the effect of any radiation quality expressed relative to the response after photon irradiation, and its application in the clinical context of cancer radiation therapy.

2.1 The standard paradigm of radiation damage

The course of radiation damage is commonly summarized within a standard model or standard paradigm [1, 2, 31, 32]. This is presented in Fig. 2.1 in a graphical representation. Interestingly, this course extends over several orders of magnitudes in time from femtoseconds to years and in space from atomic scales to meters. The associated processes cover physical interactions over radiochemical and biological processes up to medical implications. This clearly shows why the investigation or simulation of radiation induced biologic effects must always be research conducted in an interdisciplinary context.

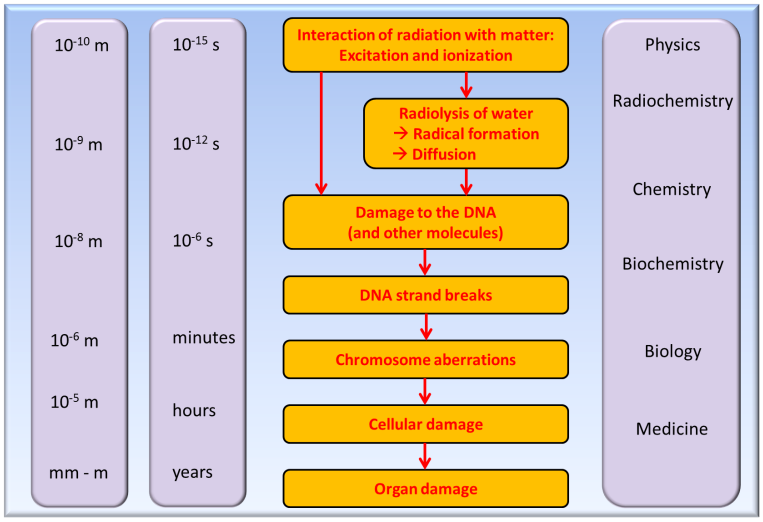

Figure 2.1: Standard paradigm of radiation damage.

The first step in the process of radiation damage is the point-like energy transfer of the radiation or secondary electrons via excitation and ionization to the surrounding medium [33]. Damage to biologically relevant targets by means of physical energy deposition occurs either

directly by these processes or indirectly by formation of reactive radicals which diffuse to these targets. The most sensitive target for sustainable damage of tissues turned out to be the DNA within the cell nuclei [34]. This is because it contains all genomic information, it is the basis of protein expression and therefore responsible for cell functionality, and it is also transmitted in each cell division from mother to daughter cells. Within the DNA, different types of damage like single strand breaks (SSB), double strand breaks (DSB), base damages or sugar damages of the backbone can be inflicted. Then cascades of proteins of the cell are engaged to repair damage [35, 36]. Within so-called *repair pathways* different proteins have different tasks like damage recognition, preparation for repair or actually inducing a proper DNA restoration. From all elementary damages, DSB are hardest to repair, but it is known that even these can be repaired efficiently with a high fidelity, where the exact repair capability depends on cell type and cell cycle phase [37]. Hence it is believed that lesion sites which contribute efficiently to cellular damage show composite lesions, like two DSB close to each other or DSB and other damage types in close proximity [36]. Whether or not this complex damage can be viably taken by the cell depends again on the repair capacity and on the particular characteristics of the damage. In the next step of the standard paradigm unrestored neighboring breaks eventually may lead to erroneous connections of open DNA ends [38, 39]. In the phase of mitosis of the cell cycle, where the cell attempts to divide itself, the DNA chromatin is condensed and these lesions become visible as chromosome aberrations. Most likely cell division will fail or the damage will be transmitted to progeny of the cells. So with a radiation dose as stimulus the cells loose gradually their functionality or proliferative capacity, i.e. their potential to divide into daughter cells. In this perspective, DNA repair mechanisms presumably exist to prevent cell death: This becomes clear by considering that each individual human life started from a single fertilized egg cell and results in 10^{14} cells in adults by successive cell division [40], and moreover many cells in our body are renewed from time to time. Hence retaining high fidelity cell reproduction is important, and failure of DNA repair finally might lead to failure in functionality of entire organs or even tissue degradation, which is the next level in the standard paradigm. In particular, the consequences on organ or organism level are usually separated in early and late effects. The former occur quite early after irradiation and, if not mortal, vanish after some time (such as skin reddening or radiation disease). Late effects occur after long latency times and include second (radiation induced) cancers and chronic irreversible normal tissue complications (such as radiation pneumonitis or radiation effects in the central nervous system). In therapy these side effects are limiting the dose that can be given to the tumor, as parts of the radiation field unavoidably extents into normal tissue.

For a proper radiobiological effect modeling the key features of each step in this picture have to be figured out and implemented in modeling assumptions. Again it becomes clear, that both physical and biological factors have to be considered for determining a prediction of radiation damage side by side.

A most critical issue for radiation effect modeling in this perspective is how physical alterations of the biologic matter are translated into functional damage of cells or tissues. Most important but still barely understood is the question what type of complex damage is most relevant. This question is strongly connected to the relevance of different spatial scales of radiation damage and the associated biological target, i.e. conformation unit of the DNA [41]. Moreover, repair of lesions of different complexity implies different time scales of damage processing, bringing in also the question for temporal aspects of damage processing. Hence the standard paradigm comprises spatiotemporal aspects which need to be addressed for a proper understanding of

radiation effects. This is a long standing problem in radiobiology which experiences a renaissance debt to both new experimental techniques and modeling approaches. The present work makes assumptions on that within the presented modeling framework, and agreement with experimental results support these assumptions.

From the standard paradigm a number of lessons can be learned for radiation therapy as one of the most important applications of radiobiological research. These are summarized as the famous 4 R's of radiotherapy [1, 42]. They comprise repair of damage, tumor repopulation during and after treatment, reassortment of the cell cycle after irradiation and reoxygenation of cancerous cells. Cancer cells are often hypoxic due to lack of tumor vascularization, and thus the indirect radiation action via radical formation is less efficient compared to normal cells, making them more radioresistant. Again, for dedicated modeling the relevance of these processes has to be considered and eventually to be covered by the model.

However, besides the standard picture there is some current debate about the impact of so-called *non-targeted effects* like the influence of signaling from irradiated to non-irradiated cells [43]. Likewise, the damage capacity of radiation is known to depend on the immune status of the organism, and also alternative targets within the cell like mitochondria are discussed. These considerations might give rise to modifications of the standard paradigm in future. At the moment the relative importance of non-targeted effects is not clear. Concerning radiobiologic modeling, a change of the current paradigm might require to embed these new ideas in established modeling concepts in cases where non-targeted effects are of relevance.

2.2 Endpoints and dose response

The standard paradigm allows to distinguish between different stages of radiation damage, starting from the initial damage right after exposure of the DNA up to late radiation effects to the organism. Techniques have been developed to quantify radiation effects at these different stages by looking at corresponding endpoints. Quantification of the radiation damage for different endpoints helps to set them into relation and to understand in detail the course of radiation damage from one stage to the next. Here only the endpoints of relevance for the presented work are briefly discussed, namely DNA lesion induction, cell survival as well as tumor control and normal tissue complications. Besides these, further endpoints like formation of chromosome aberrations, protein expression, pathway investigation of repair and of cell death, cell transformation as a first step of cancer development and many more are of interest in the field [1]. In Fig. 2.2 the dose response curves of endpoints considered in the present work are illustrated schematically. Temporal aspects, either implied by DNA repair mechanisms leading to tissue regeneration or by alteration of the time course of dose delivery are represented in Fig. 2.3.

DNA damage induction and repair

In the early stages of radiation damage lesions are inflicted to the DNA. As these lesions can not be directly observed by conventional methods - the DNA in the cell nucleus can not be resolved even with electron microscopy - indirect experimental approaches have been developed. Two main techniques were established: The method of gel electrophoresis discriminates between intact, long DNA segments and smaller DNA fragments, which have been produced by DSB, by measuring size dependent molecule migration in an electric field [44]. The DSB yield can be derived from migration velocities. Regarding DNA at various times after irradiation, repair kinetics can be obtained depending on the time allowed for repair prior to damage fixation.

The second method exploits antibody staining to proteins involved in repair of DNA lesions, letting them appear as fluorescent foci. A prominent example is the investigation of γH2AX foci marking DSB of the DNA [45]. Again, kinetics of repair can be investigated by fixation of the damage at different times after the irradiation.

Both methods allow to quantify different DNA lesions and among them in particular the DSB yield, i.e. the number of initially induced DSB per Gy and cell. Depending on the cells under investigation the determined values have been observed between 10 an 50 DSB per Gy and mammalian cell for high energetic photon radiation [46, 47]. It has been also demonstrated that the DSB yield is constant over several magnitudes of dose [48], as indicated in Fig. 2.2a. It is instructive to consider some physical properties of radiation exposure: The energy deposition associated with a dose of one Gy results with the average ionization energy of water (W-value, [49]) of about 34 eV in about 1000 ionizations at the DNA molecule, considering that the DNA only covers about 1 % volume of the nucleus. This means that most lesions are not DSB but presumably less severe forms of damage like SSB or base damages with higher yields. In contrast, more severe complex lesions, which only a fraction of all DSB is involved in, are extremely rare but turned out to be the more effective.

Beyond the initial damage induction the temporal aspects of repair processes is also of interest. Here, after an initial phase of damage recognition and protein recruitment [50] typically a biphasic repair kinetics is observed [48, 51, 52], exhibiting a fast decrease of lesions at early times followed by slower repair rates at larger times, see Fig. 2.3a. This phenomenon has different interpretations which might go side by side as correlations: The proportion of fast and slow repair might depend (i) on the choice of the repair pathways, (ii) on the complexity of the damage to be removed, (iii) on the density of chromatin where the damage is induced or (iv) on whether the two open DNA ends after a DSB are rejoined directly or connected to other neighboring open ends [53]. Misrepaired or unrepaired lesions (persistent damage) might give rise for either viable mutations or further consequences on the cell level.

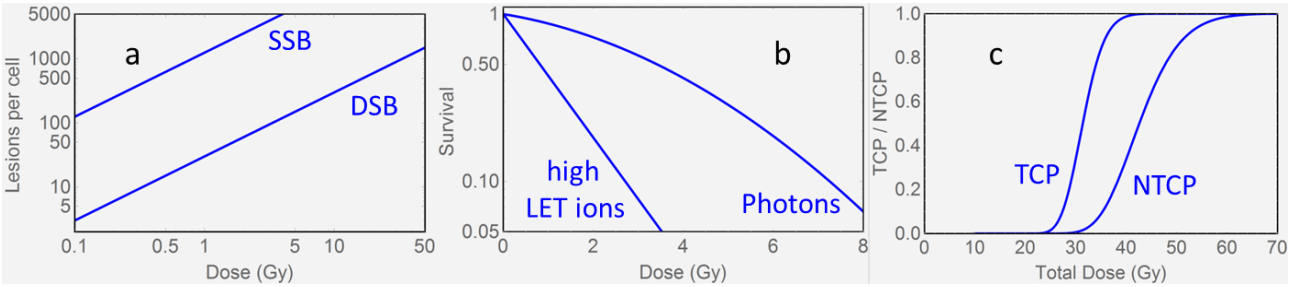

Figure 2.2: Schematic dose response curves for (a) DSB and SSB induction, (b) cell survival and (c) tumor control and normal tissue complication probability, reflecting radiation effects on the DNA, cell and tissue level, respectively.

Cell survival

Considering radiation damage on the cell level suggests no unique definition of what is meant by the death of a cell. Indeed many forms of a cell's fate after severe damage like apoptosis, necrosis or senescence are known, and complicated pathways lead to these forms of cell death [54]. Clonogenic cell survival is defined as the probability of cells to keep up their proliferative capacity. Since the seminal work of Puck and Marcus [55] the clonogenic cell survival assay

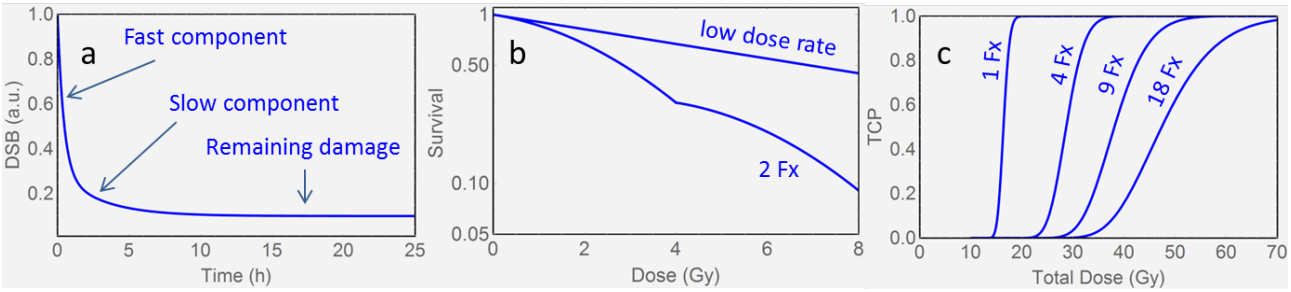

Figure 2.3: Temporal aspects associated with repair mechanisms: (a) Repair kinetics of DNA DSB repair, (b) elevation of cell survival by means of low dose rates or fractionated dose delivery and (c) dependence of TCP curves on fraction number.

measures the fraction cells from in-vitro cultured cell lines to further proliferate after irradiation. Typically, the dose response curves, also termed *cell survival curves*, show a shoulder in a semilog plot for photon radiation and are described empirically by a second order curve,

$$S = e^{-(\alpha D + \beta D^2)} \quad , \tag{2.1}$$

where S is the cell survival probability, D the dose and α and β coefficients reflecting initial slope and curvature of the survival curve, respectively. Equation 2.1 became famous as linear-quadratic (LQ) model. Considering the complex underlying processes leading to damage induction and processing, cell survival curves appear to be surprisingly simple in shape, c.f. Fig. 2.2b. The interpretation of the shoulder shape is that at higher doses more severe damage might be induced, which might be harder to repair for the cell, resulting in higher effectiveness per dose increment (for details see section 3.3). Although the radiosensitivity of in-vitro cell lines as measured in survival experiments might not be directly transferable to an in-vivo situation the general characteristics of cell inactivation persists. As connected tissue might change its properties if many of the cells are damaged, cell inactivation is a strongly impacting factor on endpoints of connected tissues, organs or the entire organism.

The temporal aspects of DNA lesion repair have direct consequences also for the shape of cell survival curves [56–58]: When radiation is delivered in fractions (i.e. in multiple portions with time gaps in the order of the cell cycle duration in between), the pause allows for repair of lesions between the fractions. In the subsequent fraction the LQ shape of dose response is repeated, indicating that repair processes have finished in meantime. Thus fractionation results in an overall lower effect as for a single exposure with the full dose. Likewise, if radiation is delivered protracted (i.e. with low dose rates), repair of lesions can take place already during radiation delivery. This mitigates the formation of more complex damage compound of more elementary lesions, and the survival curve appears straightened. Again, repair leads to a lower overall effect. Survival curves accounting for repair are presented schematically in Fig. 2.3b. These observations suggest the existence of sublethal damage [59, 60] which might become lethal for the cell by means of additionally accumulated lesions, or repaired otherwise before such additional lesions are created.

Endpoints on the tissue level

The investigation of endpoints of radiation damage on the organ or tissue level was highly promoted by clinical investigations in the framework of cancer radiation therapy. In clinical

endpoints generally one has to distinguish between two regions of radiation exposure, the target region where radiation is desired to inactivate cells and the healthy surrounding tissue which should be spared out as good as possible. Corresponding, different clinical endpoints play a role to quantify tumor control and side reactions.

One of the hallmarks of cancer is uncontrolled proliferation [61] which needs to be stopped for a successful cancer therapy. The inactivation of tumor cells is thus the ultimate goal of radiotherapy of cancer. Since a tumor may grow as long as reminiscent tumor cells are not inactivated, the probability to control a tumor is given by the probability of jointly inactivating all tumor cells [62, 63]. This leads to a sigmoid like dose response curves of tumor control probability (TCP) as shown schematically in Fig. 2.2c. As indicated above, individual radiosensitivity of patients as well as cell repopulation are factors also to be considered for a full understanding of the tumor control probability. The TCP curves usually refer to local control, i.e. considering only the primary tumor and not metastases which might have developed.

For the normal tissue the specification of the endpoint is very case specific. Generally one can consider early or late radiation side effects, but there is no clear scale that measures damage to entire organs. Hence scoring systems for various side effects have been developed. Then the normal tissue complication probability (NTCP) measures the probability for exceeding a predefined score. Again the dose response curves appear as sigmoid curves, c.f. Fig. 2.2c. Different modeling approaches exist which take into account the dose distribution across the considered organ and functional aspects of the organ exposed [64–67]. The dose range between the TCP and NTCP curves is termed *therapeutic window*, and strategies in treatment planning aim to maximize the width of this range, in order to carry out successful treatment with least amount of side effects.

If tissue is exposed not instantaneously to dose, tissue regeneration has to be considered for the overall effect. Hence again temporal aspects become important. In radiation therapy of cancer, e.g., normal tissue can regenerate between the fractions, while tumor tissue has less capability to do so as it was exposed to higher dose. As presented in Fig. 2.3c the overall dose to be given for a required TCP depends on the fractionation schedule. A large number of fractions requires a higher total dose, as the amount of initial damage per fraction is smaller and a larger overall time is given for tissue regeneration.

2.3 Impact of cell or tissue type on the effect

The consequences of radiation do not only depend on properties of the agent (radiation type, c.f. 2.4) but also on the biological target. Different cell or tissue types react differently to radiation. This becomes most evident when considering targets of different sizes: Mammalian cells are typically inactivated within a few Gy of photon radiation, while for yeast cells which have a much smaller DNA much higher doses of hundreds of Gy are needed. This is intuitively plausible as the probability to damage a piece of DNA goes down with its size, so the dose has to cope up for this decrease.

But also within mammalian cells, which approximately have the same DNA content, differences between different cell types are evident. Most normal cells with an intact repair system are quite resistive to radiation, while other cell lines appear to be rather sensitive, i.e. they show a higher effect at a given dose. There are numerous biological reasons for this variation, ranging from different distributions in the cell cycle to different pools of available repair proteins [68–71]

Besides the sensitivity of cells at a given dose the entire shape of the cell survival curves is another important parameter characterizing the reaction to radiation. Above it was argued that the shoulder shaped dose response curves as typically seen for photon irradiation are due to the increasing influence of more complex lesions induced at higher doses which are harder to repair. A prominent shoulder shape therefore is an indication, that the less severe lesions at lower doses can be effectively repaired. More straight survival curves are usually steeper even at low doses, hence indicating a less efficient repair system. The expression of a shoulder thus bears important information about the repair capability of the cells. This property is commonly parameterized by the α/β-ratio, which is the dose above which the quadratic component has more influence than the linear component [1].

This concept is also used in clinical context or for in-vivo experiments for the parameterization of tissue reaction to radiation. Here, the repair capability becomes visible as regeneration between fractions in fractionated radiation therapy. The α/β-ratio is then derived from the sensitivity to fractionation [72].

Hence the α/β-ratio is a basic quantity generally used for both in-vitro cultured cells and tissues to characterize the biological response to radiation. The following systematics becomes evident:

- Low α/β-ratio (about 1-4 Gy): These cells are likely to have an intact repair system. Often their α-component is low which means they are rather radioresistant to photon radiation. In organs the cells are rather slowly proliferating and mostly differentiated. Examples are organs of the central nervous system and slowly proliferating tumors like prostate or tumors of the skull base. In therapy tissues of that kind are sensitive to changes in the fractionation scheme.
- High α/β-ratio (about 4-10 Gy): These cells are rather sensitive even to photon radiation. In organs the cells are quickly proliferating. Examples are skin and all fast proliferating tumors.

However, one should keep in mind that the radioresponse observed in in-vitro assays is not necessarily correlated to that of corresponding in-vivo tissues [73]. The dose response of cells within tissues might be influenced by cell to cell communications, by their microenvironment and metabolic factors. Likewise, the sensitivity of in-vitro cell lines is subject to change due to culture conditions and the history of a cell line, which is why cells of equal type in different labs are hardly comparable in their characteristic response to radiation.

2.4 Impact of radiation quality on the effect

Different radiation qualities, i.e. radiation type and energy, vary in their energy deposition patterns in a target. Thus the local energy (or ionization density) distribution caused by the radiation is a relevant factor for the radiation effects which are established in biological targets. An inhomogeneous energy deposition gives rise to an enhanced formation of complex damage as compared to a homogeneous distribution of dose. This is reasoned in enhanced local ionization densities, leading to more complex damage, and explains why radiation qualities differ in their biological effectiveness. Consequently it makes sense to characterize radiation qualities according to their dose deposition patterns and investigate the effect with respect to this property. This is one of the basic ideas adopted by almost all modeling concepts predicting the effect of radiation.

It is worth to note that all radiation qualities have one feature of energy delivery in common: While the primary particles undergo interaction processes in the target material, as a result of their ionization processes mostly secondary electrons are produced which deliver the main part of the energy [74]. Hence most radiation damage locally induced is mediated by secondary electrons, no matter what the primary particle is. However, the ionization density of the secondary electrons varies considerably between radiation qualities.

2.4.1 Sparsely and densely ionizing radiation

As argued above mainly the spatial arrangement of energy transfer sites is of interest to understand the influence of the radiation quality on the observed effects. As the concept of dose expresses by definition the deposited energy relative to the considered mass, always an averaging over a volume containing that mass is involved. Hence dose is a macroscopic quantity, neglecting the microscopic arrangement of the energy deposition sites. In the field of microdosimetry researchers went one step further and investigated the spatial distribution of dose depositions [75, 76]. The insights gained suggested to differ between sparsely ionizing radiation qualities where the energy is rather distributed homogeneously across the irradiated volume and densely ionizing radiation qualities where energy is delivered inhomogeneously to the target and only small fractions of the volume are subject to high energy depositions while others are spared. Commonly the expression *local dose* refers to a rather microscopic concept of dose where such inhomogeneities are resolved.

The most prominent example for sparsely ionizing radiation is energetic photon radiation. This includes X-rays produced in X-ray tubes of typically more than 100 kV acceleration voltage, bremsstrahlung in the MeV region produced by small electron linear accelerators as often used in clinics for radiotherapy, as well as hard γ radiation from radioactive decays. The high energetic photons typically undergo inelastic Compton scattering and are finally absorbed by a photoionization process at lower energies. Due to their large initial energies the interaction lengths of the photons are quite large (ranging from centimeters to meters), which is why X-rays can be used for medical imaging. The secondary electrons produced by the X-ray photons or in cascades by other electrons typically have large energies. Hence their tracks will overlap, and an overall homogeneous pattern of energy transfer points across the target with low an approximately uniformly distributed ionization density is established. Combined with the notion that a condensation of energy transfer points would result in a more localized and thus more effective damage distribution, sparsely ionizing irradiation gives a lower bound for the biologic effect of a given dose, and any induced inhomogeneity will result in effect enhancement.

Beams of accelerated ions or α-particles in contrast are typical examples for densely ionizing radiation. Along the path of the primary particles lateral scattering plays only a marginal role and secondary electrons are produced originating from the straight trajectory of the primary particle. The secondary electrons cause further ionizations. If they have a strong radial momentum component they are called δ*-electrons* and carry out energy with radially decreasing density with respect to the primary particle's trajectory. This gives rise to the formation of a track structure of ionization events around the primary particle path [74, 77–79]. Local doses attributed to regions in the track structure can be very high, causing severe damage in the target. Hence, as the overall energy deposition after charged particle radiation is much more inhomogeneous as compared to a photon radiation field, it results in a higher effectiveness.

2.4.2 Ion radiation

Energy loss
Ions loose energy when penetrating a target primarily by Coulomb interaction. This gives rise to a gradual deceleration of the ion. For a particle of energy E the stopping power, i.e. the energy loss along the penetration path of length x through matter is described by Bethe's formula [80, 81], which in a very schematic, non-relativistic form can be written as

$$-\frac{dE}{dx} = k(E)\frac{Z_t Z_p^2}{E} \quad , \tag{2.2}$$

where Z_t and Z_p are the charge numbers of the target material and the particle, respectively, and $k(E)$ is a function absorbing all constants and varying slowly (logarithmically) with energy. It becomes evident that Eq. (2.2) is a differential equation, and when neglecting the slow energy dependence in $k(E)$, integration and solving for dE/dx results in an energy loss increasing with penetration depth, culminating at a singularity where the particle stops at a finite range [82,83]. An intuitive interpretation for the anti-correlation of stopping power and energy is that at lower energies the interaction times with electron shells of target atoms and thus interaction cross sections are larger. This again implies that energy loss is most efficient for stopping particles.

From a radiobiology point of view the absorbed energy by the target per path length is of interest and *termed linear energy transfer* (LET). By its value it equals - up to negligible radiation losses by bremsstrahlung - the stopping power. The energy released by particles slowing down has been measured and compared to theory which has been enriched over the last century with numerous relativistic and quantum mechanical corrections [74, 84–88]. Practically, stopping power is available resulting from both measurements and predictions or interpolations in cases where no measurements are available.

The connection between energy, LET and depth in water for protons is illustrated exemplarily in Fig. 2.4. As demonstrated in panel a, the LET decreases with particle energy approximately as $LET \propto E^{-0.8}$ over a large energy range, closely to the expected behavior $LET \propto 1/E$ as derived from Eq. (2.2) when discarding the slow energy dependence of $k(E)$. When penetrating through matter the particle energy decreases continuously (c.f. Fig. 2.4b) with increasing energy loss at larger depths. For an ion beam of defined initial energy the LET decreases with depth as demonstrated in Fig. 2.4c, and the particles stop approximately at the same depth, i.e. they have the same range. The range depends on the initial energy of the particles: The higher the initial particle energy is, the deeper they penetrate into matter. When particles are just about to stop, LET is high, implying a peak of energy loss right at the end of their range. As, however, the particle deceleration is a stochastic process, the range is not exactly the same but subject to a small distribution, giving rise to a so-called *range straggling*. Hence a depth dose distribution pattern is established with a strong peak where particles are stopping, which is termed *Bragg peak*.

Macroscopic dose
Considering a particle beam, all particles crossing a volume will accumulate dose to that volume. Hence the macroscopic dose D, defined as energy deposited per mass, is connected to LET and the particle fluence F of the beam as

$$D = \frac{F \times LET}{\rho} \tag{2.3}$$

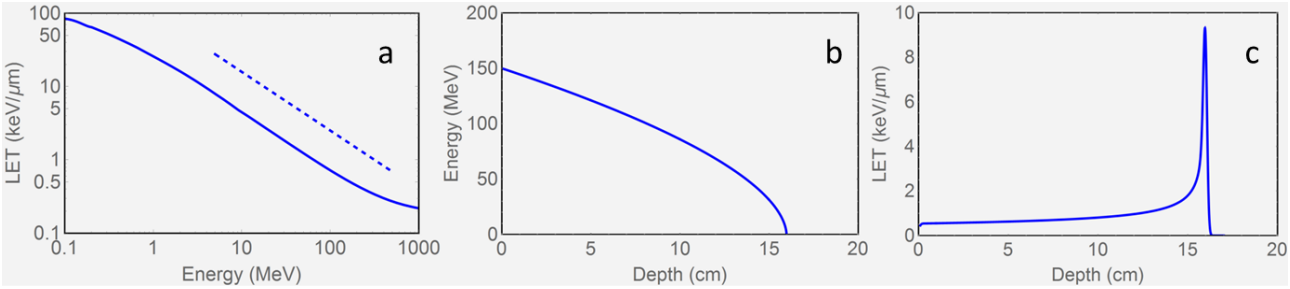

Figure 2.4: Connection between particle energy, stopping power (LET) and depth in water: (a) Anti-correlation between LET and energy for protons. The dashed line indicates a power law $LET \propto E^{-0.8}$. (b) Energy profile in water for a 160 MeV proton beam, demonstrating the deceleration with increasing depth. (c) Variation of LET with penetration depth, where the profile has been convoluted with a Gaussian function of small width to simulate range straggling in the Bragg peak. Thus the convoluted curve represents the depth dose profile.

in SI units, where the LET is given for the target material of density ρ [1]. This shows that for a requested dose with high LET particles a rather low fluence is needed, while higher particle fluxes of low LET ions are needed for the same dose.

Track structure

The LET as considered above parameterizes the entire energy loss per path length of the primary particle trajectory. The energy transferred to the target medium is carried outwards by δ-electrons, and a dose deposition pattern forms around the primary particle track, usually termed *track* structure. Figure 2.5 displays a typical example of a track structure of carbon ions. Obviously the ion causes a large ionization density along its path, which decreases rapidly with distance to the primary particle trajectory.

Using gas filled detectors, microdosimetric measurements of dose depositions in some distance to the ion track revealed that the radial ionization density decays as approximately r^{-2} with increasing radial distance r to the particle trajectory [77]. This was understood by a theoretic consideration of inelastic electron scattering cross sections along with relativistic electron ballistics. Essentially, the production rate of high energetic δ-electrons is much smaller as compared to lower energetic δ-electrons, so that energy deposits far from the track center occurs less often than close to the track. Generally, the energy of the primary particle determines largely the energy distribution of the caused secondary electrons. High energetic particles have therefore a wide track structure where δ-electrons can migrate up to 1 cm or even more. In the inner part of the track structure, the local doses can get very high. Due to conservation of energy, the integration over track structure must reveal the entire energy loss, i.e. the LET [77].

These considerations imply that particles of a given species with low energy have a high LET and moreover a narrow track structure, giving rise to very high local doses, and are thus densely ionizing. In contrast, high energetic particles have rather low LET and a wider track structure. However, in comparison to orthovoltage X-rays there is still enhanced inhomogeneity in dose deposition, and the term *low LET radiation* is usually used in perspective of the individual problem. Typical properties of carbon ions of low and high energy, as corresponding to a therapeutic

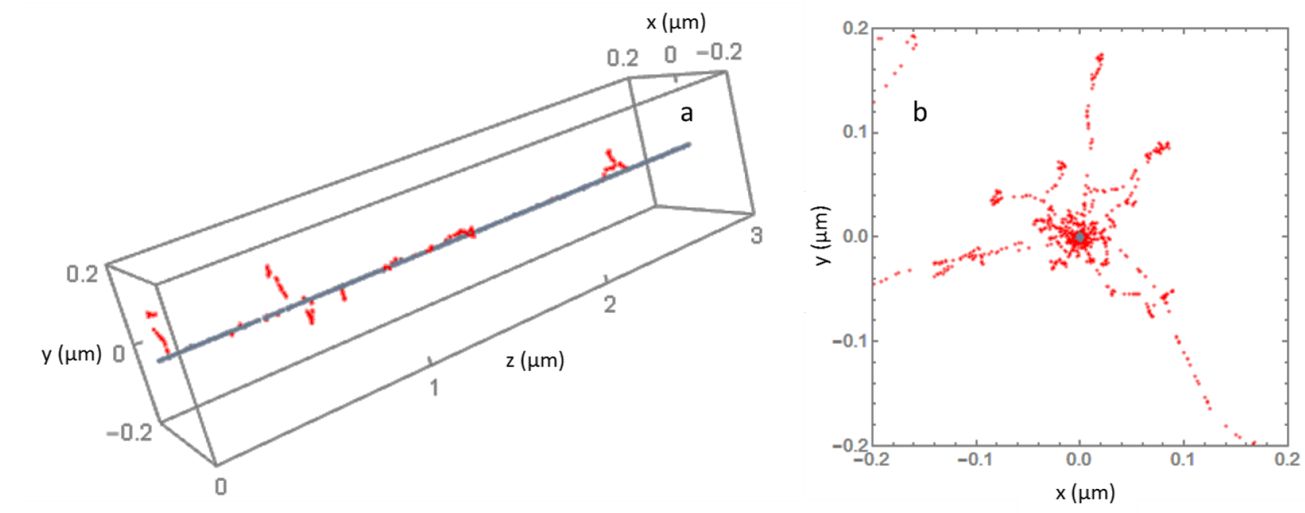

Figure 2.5: Track structure of a 100 MeV/u carbon ion: (a) View on a 3 μm segment of track structure in side perspective (drawn to scale). Ionization events in distance up to 5 nm to the ion trajectory are colored in blue, ionizations caused by δ-electrons carrying energy outwards in red. (b) Projection in ion propagation direction of 10 μm ion track length. Simulations have been performed with the track structure Monte Carlo code TRAX [89–92].

target and the surrounding areas within the radiation field (the so-called *entrance channel*), respectively, are summarized in Tab. 2.1.

Amorphous track structure parameterizations

While a full description of track structure as described above involves the accurate position and ionization or excitation energy portions of all point-like energy transfers, a more practical approach consists in an average description of these energy deposition patterns around ion trajectories. Then the ion track can be described by an *amorphous track structure* [93], which is a smooth function in space reflecting the probability for ionization events, or, in other words, ionization density. This effective description neglects correlations of neighboring energy depositions along individual secondary electron tracks, but is not limited in spatial resolution.

Table 2.1: Properties of therapeutic carbon beams.

	Entrance channel	Bragg peak
Energy (MeV/u)	290	25
LET (keV/μm)	13	77
Core dose (Gy)	1465	93000
Track radius (μm)	951	14.8
Radius at 1 Gy (μm)	0.16	0.45

The amorphous track structure is typically visualized by the radial dose profile, where the term *dose* has to be regarded as a local, microscopic dose. A simple amorphous track structure formulation is given by

$$D(r) = \lambda \,\mathrm{LET} \begin{cases} {r_{min}}^{-2} & \text{for } r \leq r_{min} \\ r^{-2} & \text{for } r_{min} \leq r \leq r_{max} \end{cases} \tag{2.4}$$

where the normalization factor λ is

$$\lambda = \frac{1}{\pi\rho\left[1 + 2\ln\left(\frac{r_{max}}{r_{min}}\right)\right]} \tag{2.5}$$

and determined such that the integral $\int_0^{r_{max}} 2\pi r \mathrm{d}r$, i.e. the amount of energy stored in the track structure, reflects the particle LET [94]. In Eq. (2.4), $D(r)$ is the local dose at distance r to the track center in the target material with density ρ. The track radius is given by $r_{max}[\mu\mathrm{m}] = 0.062\, E[\frac{\mathrm{MeV}}{\mathrm{u}}]^{1.7}$, which was revealed empirically by considering measurements in gaseous media as discussed above and reflects that δ-electrons have a maximum possible energy. The radius r_{min} labels the core radius of the track above which the $1/r^2$ decrease of the dose starts. The core region is not accessible by measurements, but quantum mechanical considerations suggest a velocity dependent extension of that region as $r_{min} = \beta r_c$ where β is the relativistic velocity parameter, and r_c is the core radius for highly relativistic ions and is of the order of some nanometers [94]. Figure 2.6 shows the radial track structure according to Eq. (2.4) for various combination of ion type end energy. Notably, the local dose profile varies over several orders of magnitude across the track. It should recognized at this point that due to some reminiscent ambiguity in the parameterization of the track core, the presented equations set up a model, inspired by experimental results and theoretic considerations. An overview of various suggested amorphous track structure models is given in [95].

2.4.3 Ultrasoft X-rays

Ultrasoft X-rays are photons typically emerging from the characteristic X-ray spectrum emitted from atomic transitions from outer to inner shells and typically cover the energy range from about 100 eV to a few keV. Although still energetic enough to cause ionizations they differ significantly in their properties from high energetic photon radiation in various aspects. First, due to their low energy they interact solely via photoionization processes, while Compton scattering plays practically no role. Hence they will be absorbed exponentially with penetration depth, where the absorption length is in the order of a few to a few hundred micrometers in the range of about 280 eV (carbon K shell X-rays) to about 4.55 keV (titanium K shell X-rays), respectively [96]. Second, for heavier elements with occupied atomic L shells, the photoionization will be followed by an Auger emission. This has a typical energy of 500 eV for water as considered target [97, 98] and thus has similar properties as the photoelectron. Third, the energy is transferred to the photoelectron (except its binding energy), but as this energy is low a cascade of only a few further ionizations might follow, and the remaining range of these electrons is low. The ranges of the photoelectrons are about 7 nm for C_K X-rays and 550 nm for Ti_K X-rays [96]. Consequently, essentially a few ionizations will occur restricted to a small volume of the order of some nm to some hundred nm around the location of the photoioniztation. In this region a high

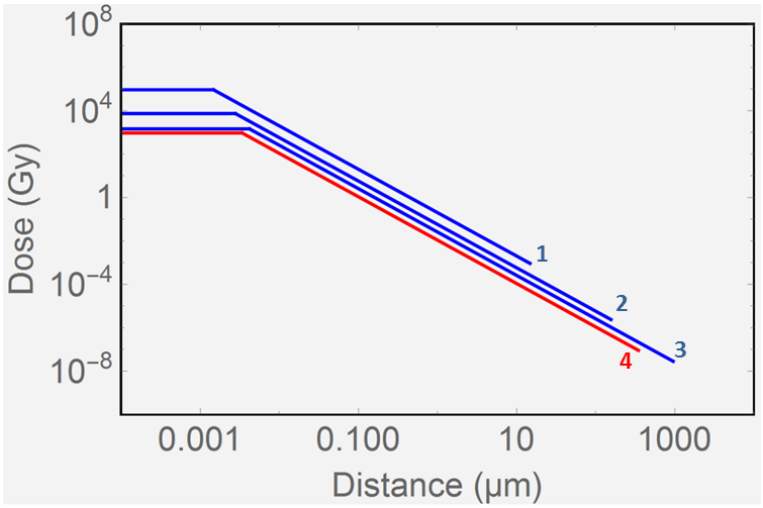

Figure 2.6: Radial dose for various combinations of ion species and energy according to the amorphous track structure model Eq. (2.4). Dose profiles are shown for carbon ions (blue) with energies of 25 MeV/u (1), 100 MeV/u (2) and 290 MeV/u (3) and protons (red) for an energy of 160 MeV (4) up to the maximum track radius. The different tracks are similar in shape, although highly differing in absolute doses and track extensions as evident in the double logarithmic plot.

ionization density occurs, while the gross part of the irradiated volume remains uncovered by ionizations. To investigate the ionization patterns caused by ultrasoft X-rays it is thus sufficient to consider the track structure of the photo- and Auger electrons. Typical ionization patterns for 1 keV electrons are visualized in Fig. 2.7. A clear correlation of ionization events along curved electron trajectories is visible, and eventually track bifurcation occur due to the generation of electrons by means of further ionization processes. Recently it was shown that the concept of amorphous track structure around photo- and Auger electron tracks can be applied in analogy to ion track structure to understand the effectiveness of ultrasoft X-rays [99].

The study of ultrasoft X-rays in radiobiology is of interest for the following reasons:

- Although photon radiation in general is regarded as low LET radiation because each particle infers just a small amount of energy, ultrasoft X-rays are densely ionizing as the energy is distributed inhomogeneously, giving rise to high local doses in small regions. This situation is in a way comparable with the track structure of high LET particle radiation [100].

- As has been discussed before, most radiation action is mediated by secondary electrons, no matter what the primary radiation type is. When slowing down, eventually at the end of any individual electron track, the electrons have a small portion of kinetic energy only, and a cluster of ionizations is expected as for photoelectrons produced by ultrasoft X-rays. Hence considering ultrasoft X-rays allows to study the properties of effective secondary electron track ends, which are found in any radiation quality where higher energetic secondary electrons are involved [101].

- While ion tracks occur in a cylindrical symmetry and dose is always deposited along the straight ion trajectory, the ionization clusters caused from ultrasoft X-rays are locally restricted in all dimensions, i.e. they form bubble like regions with high ionization density.

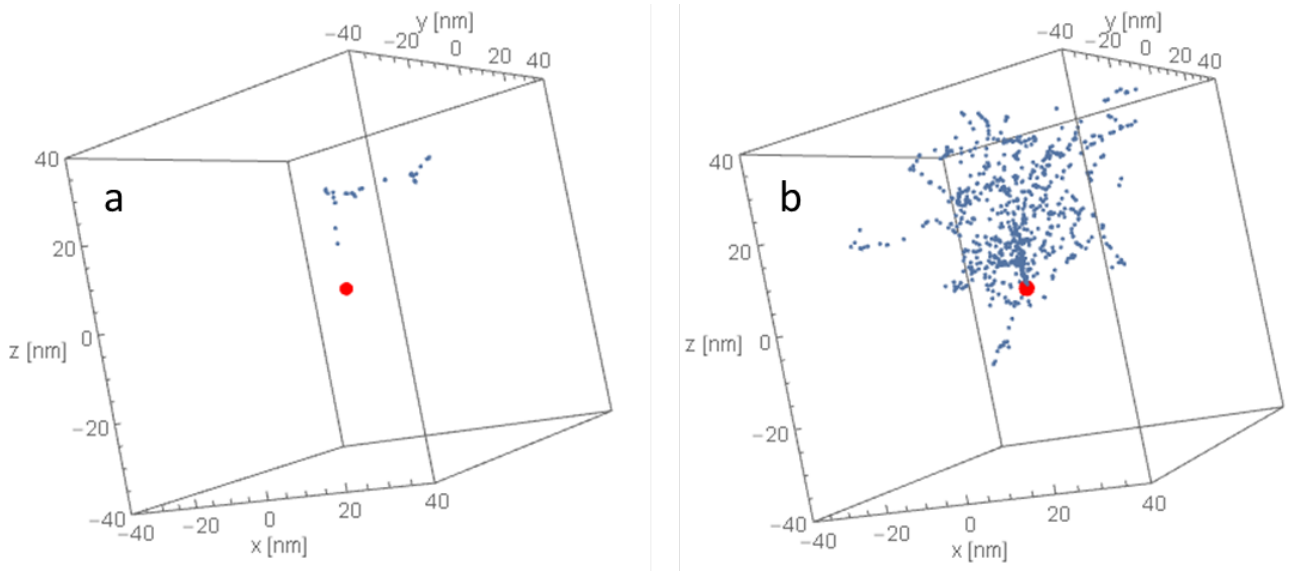

Figure 2.7: Track structure of 1 keV electrons emitted at the origin (red dot) in z direction: (a) Single electron and (b) overlay plot of 30 electrons. The blue dots show individual ionization events. Simulations have been performed with the track structure Monte Carlo code TRAX [89–92].

Hence ultrasoft X-rays can be exploited to study the formation of complex damage depending on the size of the ionization and lesion clusters.

Indeed it has been demonstrated that the effectiveness of photon radiation depends on energy [102–104], and that ultrasoft X-rays have a higher effectiveness than high energetic photons [96, 105, 106]. Historically, stimulated by the work of Goodhead and coworkers [107–109] these experiments lead to the enhancement of the field of microdosimetry, because it became evident that the increased effect of ultrasoft X-rays can be only understood by looking at a nanoscopic level rather than on the μm scale only. The interpretation of these findings is, that the spatially correlated ionizations arising from one photoionization process match the order of the width of the DNA which is about 3 nm or first higher order DNA conformation like the 30 nm fiber [36, 110, 111], giving rise to more complex damage on these structures. This is an example how the understanding of biologic effect is directly connected with the meaningful biological targets in radiobiology.

2.5 Relative biological effectiveness

As has been demonstrated above, different radiation qualities differ in their dose deposition pattern. Consequently, the spectrum of damage types induced and with that the repair capability of the cell to that damage depends largely on radiation quality, but also on biological factors such as the functionality of repair mechanism. To quantify the efficacy of different radiation types, the concept of relative biological effectiveness (RBE) is introduced as the dose needed to induce

a requested effect of some radiation quality Q relative to the dose needed for the same effect with high energetic photon radiation:

$$RBE = \frac{D_{\mathrm{Q}}}{D_{\mathrm{photon}}}|_{\mathrm{isoeffect}} \tag{2.6}$$

For the case of ion radiation the definition of RBE is schematically visualized in Fig. 2.8.

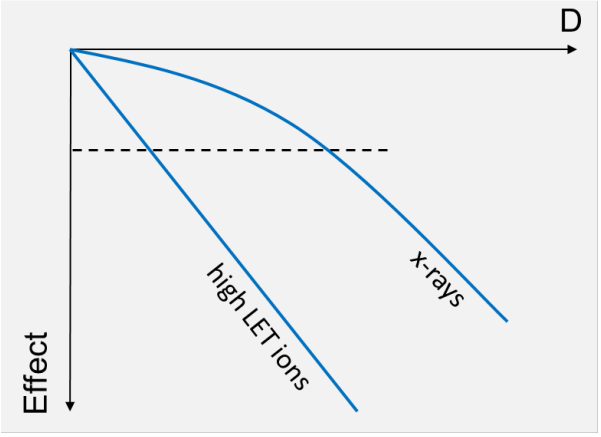

Figure 2.8: Definition of the RBE to parameterize the enhanced effect of high LET radiation. The dashed line marks an isoeffect level at which the RBE is evaluated as ratio of doses needed to reach this effect.

This definition is simple, very general and applicable to practically all end points. Referring to energetic photons as reference radiation is most practical because orthovoltage X-ray tubes are accessible in many labs all over the world and in radiotherapy vast experience has been made with ^{60}Co irradiators and clinic accelerators over decades. Furthermore as mentioned earlier photon radiation is regarded as more homogeneously and sparsely ionizing and thus constitutes a lower bound in effectiveness. Hence the RBE is expected to be larger than one in all other cases.

Despite its simple definition RBE turns out to be a complicated quantity. In particular, RBE depends on the following physical and biological factors:

- Dose and fluence: At higher doses RBE will decrease, as for the photon reference the incremental action per Gray typically increases with dose, while this is less the case for more inhomogeneous dose deposition. In this regard also geometric properties of the cell nucleus play a role, as it determines the number of photons or massive particles passing through the target cross section for a given dose. Hence the statistical properties of dose deposition in individual cells may vary, influencing RBE.
- Particle Species and energies: For charged particles like accelerated ions the energy transferred to the medium strongly depends on the charge number and the energy of the ion (c.f. 2.4). Typically for a given ion type RBE increases with LET and hence decreases with energy. At very high LET only hit statistics matters, and RBE decreases again. For photons of lower energy the limited range of photons and photoelectrons lead to inhomogeneous dose deposition patterns. Again, RBE increases with the degree of inhomogeneity of the ionization density.

- Endpoint: Dose response curves of different endpoints vary in their properties (c.f. 2.2). Hence RBE may vary between different endpoints.

- Radiosensitivity: Cells and tissues react differently to different types of damage (c.f. 2.3). Because the types of damage induced depend on the radiation quality, this has impact on RBE. Generally, cells or tissue types with a high α/β-ratio result in a low RBE and vice versa.

The characteristics of RBE with respect to these factors has been matter of investigation for several decades both for ions [112–115], and soft X-rays [96]. The entire RBE systematics is reflected best by considering dose response curves for the radiation quality of interest and the dose response of the reference radiation simultaneously. For high LET ion radiation and the endpoint of cell survival, e.g., the dose response is typically steeper right from the beginning and shows, if any, a less pronounced shoulder (see Fig. 2.2) than the dose response curve of the reference radiation. This is plausible as the high LET facilitates the induction of more severe lesions which are harder to repair even for lower doses - these lesions overcome the repair ability of the cell. The efficiency of lesion repair is moreover mostly reflected by the shape of the photon dose response curve, as discussed in section 2.2. The RBE can be evaluated from the relative difference of both dose response curves. Thus, in regard of these complex relations, mathematical RBE modeling must consider both the physical and biological aspects of radiation damage and processing.

2.6 Particle therapy

The goal of any cancer radiation therapy modality is to widen the therapeutic window, i.e. to maximize the distance of TCP and NTCP curves in dose. This allows at the end to reach a maximum in tumor control with tolerable side effects. Finally, endpoints like the probability of no recurrences in five years of follow up time after therapy or patient survival corrected for other mortality reasons are investigated in clinical studies.

Typically, external radiation therapy of cancer is performed using ^{60}Co γ-rays or X-rays produced by small clinic accelerators, typically electron linacs whose bremsstrahlung is used as therapeutic beam. Modern techniques like intensity modulated radiation therapy or volumetric arc therapy [116–118] combine beams irradiated from different directions to the target volume, i.e. the tumor, to achieve a maximum possible tumor conformity and low normal tissue exposure.

The use of protons instead was proposed in 1946 [119] and exploited for therapy since the mid fifties [120]. Also other hadrons like neutrons or pions were used or considered as particles for therapy [5]. While therapy with neutron irradiation was (and is in few facilities) in clinical practice for some decades but revealed comparably minor benefit, and other particle therapy modalities such as pions did not establish for various reasons, only proton and carbon ion therapy are nowadays broadly considered and implemented in dedicated treatment facilities, while the use of helium and oxygen is under discussion for special purposes [121–124].

Ion beam therapy bears a number of advantages, but also higher effort is needed for such therapy modalities. The beneficial properties of charged particles for therapy are more and more acknowledged, and the current rate of new facilities founded is still growing. When this thesis was completed more than 100.000 cancer patients have been treated with proton

beams and more than 15.000 with carbon ions world wide. Carbon ion facilities are currently available in Japan, Germany, Italy, and China, under construction in Austria and South Korea, and first planning is in progress in the United States [11]. Clinical outcome clearly shows the benefit carbon ion therapy for several tumor types [125–128], although randomized clinical trial studies are still in progress.

The discussed properties of charged particle radiation lead directly to the advantages of particle therapy [129–131]:

- In comparison to energy deposition caused by photons, the dose profile is inverted (c.f. Fig. 2.9(a)), which is the main rationale for hadron therapy, as it facilitates to bring in energy deposition where it is needed: in the target region. The inverted dose profile thus saves normal healthy tissue, while exposing the target region to high doses.

- The sharp Bragg peak allows for a good tumor conformity with relatively few channels, i.e. beam directions relative to the patient. In treatment plans various Bragg peaks are delivered to different depths in tissue in order to reach a homogeneous dose distribution across the tumor, see Fig. 2.9(b). The flat dose profile is extended Bragg peak or spread-out Bragg peak (SOBP).

- In particular for ions heavier than protons the small lateral scattering allows to design laterally strongly confined irradiation fields.

- The high LET leads to a high RBE in the target, even increasing the ratio of dose in the target to the entrance dose (peak-to-plateau-ratio), as can be seen in Fig. 2.9(b).

- Due to the damage complexity in the target, cell inactivation is less affected by the oxygenation status of the cells or different repair capabilities across the cell cycle as observed for low LET radiation.

- As radiation damage of high LET particles is less sensitive on biological factors of the target, inter-individual differences in radiosensitivity, i.e. the heterogeneity within patients, has less impact on tumor control curves derived from patient cohorts. Thus the uncertainty in doses needed to control the tumor is reduced.

- For high LET radiation, dose rate effects and sensitivity to fractionation, i.e. to the photon α/β-ratio of the tumor tissue, is less pronounced, higher fraction doses (hypofractionation) becomes possible (c.f. Fig. 2.2). As the target is covered by a higher dose, repair of tumor tissue is less effective, while due to the good tumor conformity the normal tissue is still exposed to tolerable dose levels.

On the other hand there are also a couple of disadvantages or issues to be discussed. Most of them are matter of current research:

- Hadron therapy facilities, in particular for heavy ions, are very expensive in construction and performance. Hence an appropriate selection of patients is needed, where these enhanced techniques are beneficial in terms of treatment results [129].

- To exploit the RBE of charged particles, it must be properly quantified prospectively. This is nontrivial due to its rich dependencies on biological and physical aspects. Radiation effect modeling is an essential tool for this purpose. The issue is not only the availability and

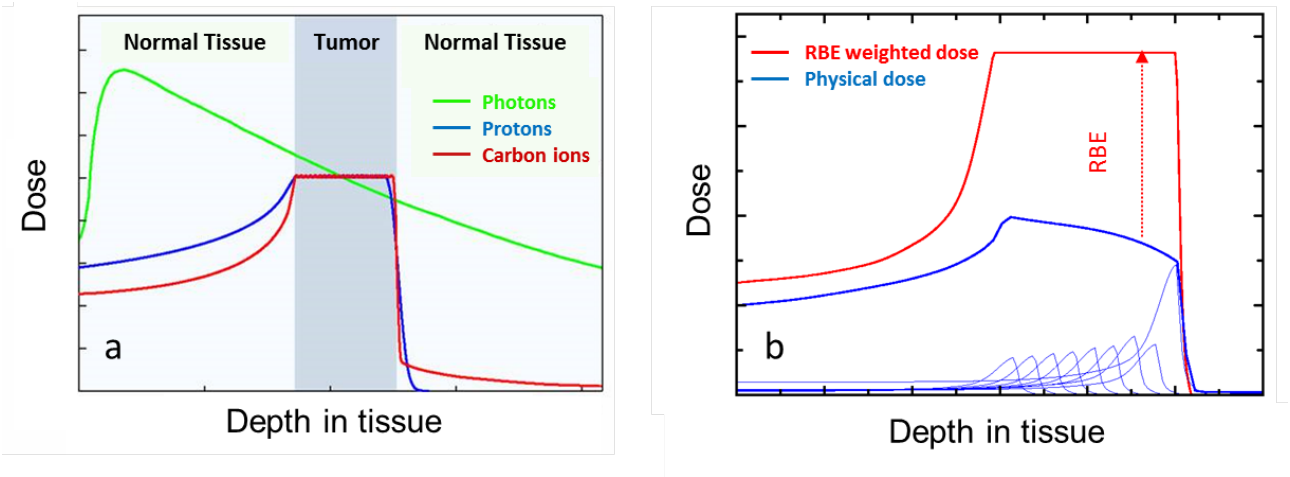

Figure 2.9: Depth dose profiles. (a) Depth dose profiles of photons, protons and carbon ions in comparison. The hadrons show an inverted dose profile. (b) Typical irradiation field for carbon ions, composed of several Bragg peaks forming a spread out Bragg peak, and resulting in a homogeneous RBE weighted dose distribution across the target region.

performance of such models, but also of requested model input data. The quantification of RBE and related uncertainties are a main focus of the present thesis.

- A proper patient positioning is a very delicate task. Due to the high tumor conformity and sharp fall-off of the dose beyond the margins of the target field, mispositioning immediately results in a high dose exposure of healthy tissue. This issue is even getting more complicated for moving targets, e.g. driven by breathing or heart beat motion [132].

- Nuclear processes like target fragmentation and for heavier ions also projectile fragmentation give rise to a multiple particle type mixture of radiation qualities, which has to be accounted for in treatment planning [133, 134]

- Out-of-field leakage doses are expected from the fragments and give rise to an additional low dose exposure of healthy tissue. An accurate dose quantification is, however, a demanding task. Exemplarily, much research has been performed on the exposure level of healthy tissue in the neutron stray field [135–138]. The development of secondary malignancies is of particular importance for the treatment of pediatric patients, whose expected lifetime exceeds typical latency times for second cancer expression.

In clinical practice the doses that are given in therapy are constrained predominantly by tolerance doses of exposed healthy tissue. The translation of these doses between different treatment modalities or different fractionation schedules requires an understanding of the dose response mechanisms. For carbon ion therapy the implementation of RBE in treatment planning is performed by exploiting radiobiologic models. In European facilities the LEM is used [139–141], which is largely discussed in this work, and in Japanese facilities the Microdosimetric Kinetic Model (MKM) is applied combined with an empiric scaling of the dose profile [142–146]. Again it is evident that the inherent entanglement of physical and biological properties and the spatiotemporal aspects of dose delivery have to be considered for determining the radiation effect.

3 Modeling concepts and application

Everywhere in science measurements and tests are performed to finally develop an idea or a picture how aspects of nature work. Strictly, all derived hypotheses are models, which can be supported or refuted by experimental data. However, as complexity increases models have to get more complex or to consider functional dependencies of the involved quantities. Here mathematical modeling becomes relevant. Throughout this work, by the term *modeling* in fact mathematical modeling is meant.

Modeling radiation effects is a matter of selecting the key features from the course of radiation damage and the appropriate mathematical tools. A proper development of model approaches depends on the creativity of the researcher. Model tests and benchmarking can then help to determine the limits of a model set-up.

The goal of this chapter is to introduce different aspects and ideas followed by radiation effect models. At first, some general considerations about requirements and constraints of mathematical effect modeling will be given. This contains also a general proposal of a set of necessary conditions such models have to fulfill in order to be useful and practical in radiobiology. Next, a historical view and a brief discussion of the basic strategies followed in various model demonstrates the broad variety of developments in the field. The LQ model is the most prominent model, although it is rather descriptive than predictive. As it is related to or even used as part of more sophisticated models like LEM and GLOBLE, the interpretations underlying the model will be discussed. The notion of lesion clustering on different scales is a key feature exploited in the LEM and GLOBLE and will be motivated, before the main ideas of LEM and GLOBLE will be considered. In this work the discussion will restrict mostly to the endpoint of survival, while in general the presented modeling work is applicable for other endpoints and phenomena as well, as demonstrated at the end of the chapter.

3.1 Requirements for radiation effect models

The great theories in physics like Newtonian mechanics, theory of relativity or quantum mechanics are all simple in the sense that they are formulated by a tiny set of basic rules or axioms, based on which many processes in nature can be explained provided the conditions and restrictions under which these observations have been made are known. These theories are thus fundamental. Complex systems obey these laws, too, but are much harder to describe. The reason for this is that they contain a high number of processes which run simultaneously and may interact, or a large number of variables and quantities to be considered for a full description.

Needless to say, cells are complex systems and their response to radiation exposure is a complex situation. Trying to construct models reflecting reality by taking into account as many aspects as possible, for instance by ab initio models describing all interactions, will be tedious and is not feasible at the moment for practical reasons (e.g. computer power) and because not all processes are investigated and known. On the other hand, a model which is oversimplified may fail to reflect relevant processes. Hence a compromise of the level of detail described in modeling has to be found.

On a more abstract level, a mathematical model describes an observable based on input parameters and internal model parameters which implement the situation to be modeled. A higher level of detail would thus mean to increase the number of degrees of freedom of the model and to introduce additional parameters. If the number of degrees of freedom is too high, when fitting the model to experimental data no significant parameter values can be expected any more. In contrast, if a model has too few degrees of freedom, the model is too incomplete and the predictive power is low [147]. The situation is visualized in Fig. 3.1. A compromising number of free parameters has to be determined, which should reflect the information contained in the curves to be described. For the description of shouldered dose curves for instance, two free parameters should be sufficient, as in the simple LQ approach. This reflects the small level of information contained in an individual set of experimental cell survival data, which adequately can be described by a second order polynomial.

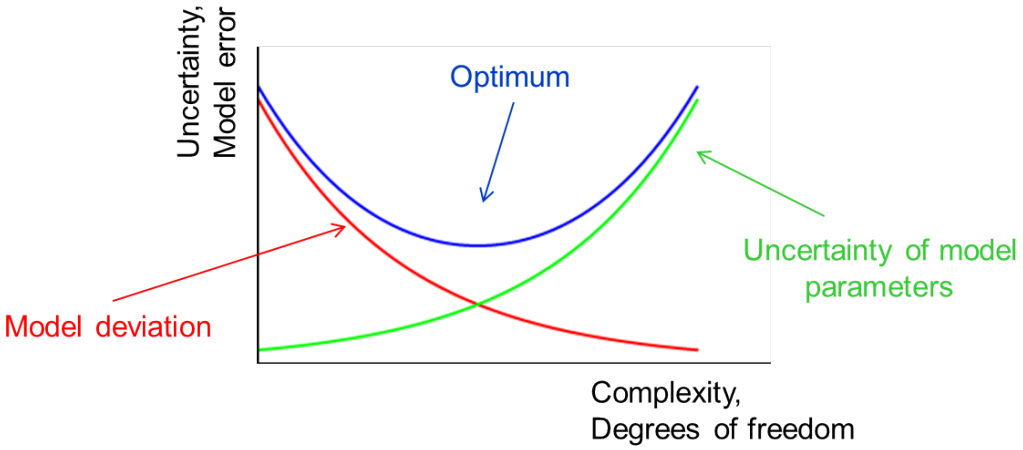

Figure 3.1: Uncertainty minimization in mathematical modeling.

Again it should be stressed that a complete picture can not be revealed by models, as underlying processes are only known to some extent. In this perspective current radiobiologic modeling is more than just an implementation of a set of rules, it is rather a prediction for the implication of assumptions, which in turn can be tested by comparison with experimental results.

Based on the state of research a minimum set of 'must have ingredients' and model abilities can be proposed which is essential for predictive effect modeling. This proposed list is a very general conjecture of the present thesis and finds support in the discussed research work of the publications [A1-A6]:

- Characterization of the spatial distribution of ionizations: The physical properties of the radiation as the agent triggering radiation damage must be considered.
- Target geometry: The sensitive sites have to be specified to define where ionizations can cause further radiation damage.
- Lesion induction: From the dose distribution the induced damage has to be quantified.
- Conversion to an observable endpoint: Hypotheses or techniques have to enter into modeling how, depending on radiosensitivity, initial lesions are processed and how un- or misre-

paired lesions will be converted to an observable endpoint such as chromosome aberrations or cell survival.

- Mechanistic interpretation: The model should allow for an interpretation of its model parameters in terms of a physical or biological meaning.
- Benchmarking: A model must be testable. Otherwise there is no way to support the model assumptions by comparison with experimental data. Only if such benchmarks succeed, the model can be regarded as predictive.
- Transitivity: A model which bases on justified assumptions should be able to describe several aspects of radiation damage within the same model framework.

In particular the last point of this list is where most models which have been published in the literature have drawbacks, or simply a spread out of application was not followed. The LEM and GLOBLE model framework presented in this work was applied to numerous endpoints and different observable aspects within the same framework and without changing the parameters used for description. This is one of the most convincing arguments for the applicability of these concepts.

3.2 Historical perspective and classification

Modeling cell survival has a vivid history, starting right from the early days of radiobiology. Figure 3.2 gives a chronological overview of the developments. Apparently many attempts have been made to understand the radiation response, exploiting different views on cellular mechanisms of radiation damage processing and considering specific aspects of interest, such as response to radiation at low or high doses, or temporal aspects of radiation delivery. The models labeled in red allow predictions also for high LET radiation. The set-up of the GLOBLE model goes back to article [A2], and all other models included in the figure were originally presented in [32, 142, 148–172]

Successful modeling points towards a confirmation of the underlying assumptions and thus promises a deeper understanding of radiation damage. All models listed in Fig. 3.2 are to some extent mechanistic and to some extent empiric, which will determine the information one can get from the models. In turn, models can only be used for predictions or interpretation of experimental results if meaningful model parameters are available. The point of view from which the various models have been derived from and with that the meaning of the applied parameters is different for each model. Nevertheless, some main concepts of radiation effect models can be distinguished. A list of concepts along with accomplishments and showstoppers is given below, though this list may not necessarily be complete and is not meant to reflect a classification scheme for different models:

- Target theory: A very physical view on inactivation of cells was suggested by considering a sensitive target, which has to be hit once or a certain number of times to induce cell inactivation. Likewise the joint hit probability for a number of subtargets has been considered. The target theory was developed by Lea [148] and has widespread applications especially for yeast cells and bacteria. However, a shortcoming was that the models predicts a vanishing slope at low doses, in contrast to experimental results. Phenomenological approaches to overcome this [149] bear of a clear justification.

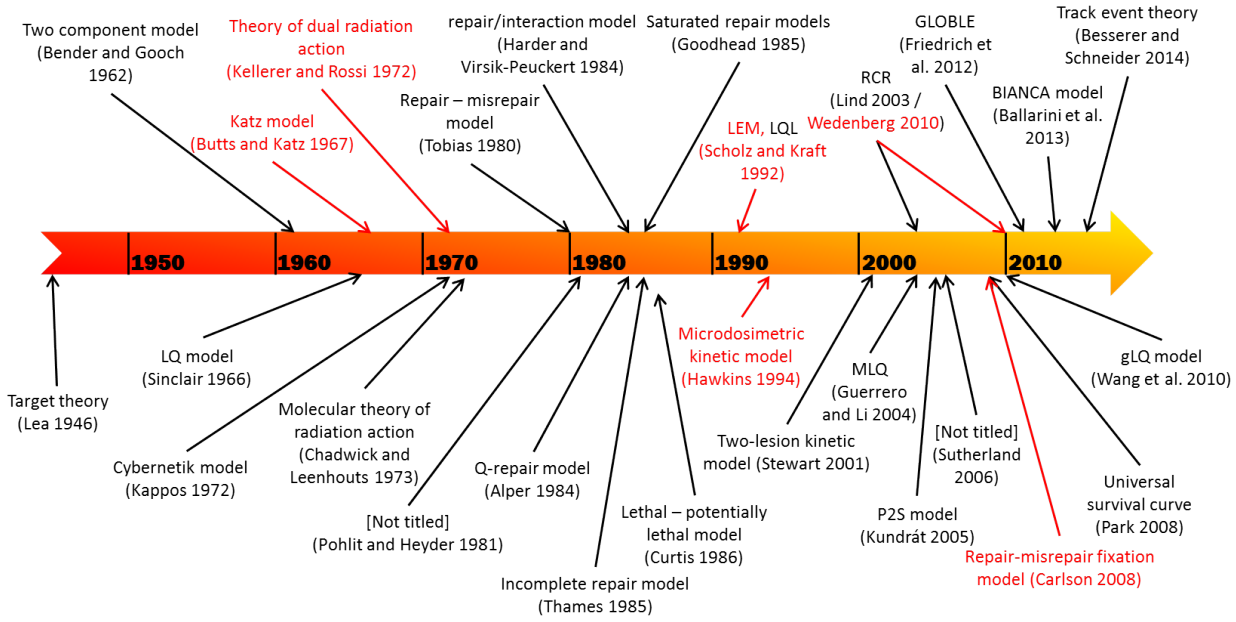

Figure 3.2: Timeline of most important descriptive or predictive cell survival model developments. Entries in red refer to models which explicitly have implemented mechanisms to predict high LET dose response. Monte Carlo models without analytical effect calculation have not been adopted into the figure. Also the list may not reflect all model developments that have been presented so far. See main text for references of the models.

- Microdosimetric model concepts: In microdosimetry the energy distribution in micrometer sized subvolumes was experimentally investigated with dedicated proportional counters in gaseous media [173]. Inspired by that, Kellerer et al. derived the theory of dual radiation action [153], a modeling approach considering the distribution width of energy within so-called *microdosimetric domains* whose size is one of the model parameters. The model started from the idea of a quadratic dose response within individual domains, resulted in a mechanistic interpretation of the LQ model and succeeded in explaining basic features of high LET radiation effects. Later on the concept was enhanced by the Microdosimetric Kinetic Model [142, 174] which also managed to explain time effects of repair, e.g. when radiation is given protracted instead of instantaneously. Drawbacks of such modeling are that averages over the microdosimetric domains are carried out, prohibiting the application to situations where a finer resolution would be required, as for example for the radiation action of ultrasoft X-rays [109]. These considerations triggered the development nanodosimetry, along with corresponding model work [175, 176], which could overcome this shortcoming. A further issue, however, is the lack of a clear biologic interpretation of the meaning of the microdosimetric domains: It was known that chromosome aberrations are formed by lesions within μm proximity [39], but there was no interpretation about why these lesions were not subject to repair processes within these sites. The concept of relevant sites is also adopted in the LEM, where such interpretation was added.

- Dynamic repair modeling: This type of models considers the induction and the successive removal of damage by means of differential equations. The development of the underlying

concepts goes back to [32, 160] in the formulation of the Repair-Misrepair model (RMR) and the Lethal-Potentially Lethal model (LPL), respectively. These approaches allowed in particular to explain temporal aspects of repair. The model setup is completely general while the assumption of different repair modes is somewhat specific. Furthermore, parameter determination by fitting the model to experimental data is a demanding task due to the mathematical structure of these models.

- Transport codes in combination with a DNA damage model: A number of models, in particular for the simulation of the radiation damage of charged particles, starts to describe the physical interaction processes by means of transport codes [177]. At the end, ionizations on the DNA are converted into DNA lesions, from which the fate of single cells will be derived. Examples are KURBUC [178], PARTRAC [179], RITRACKS [180] or Geant-DNA [181]. These approaches allow a detailed insight in the composition of the physical radiation field. However, when converting ionizations into biological lesions and simulating their processing, just as in all other model concepts a number of assumptions is needed, relativizing the level of detail exploited in the physical part of the simulation. A practical drawback is that transport codes and track by track biological interaction models often need extremely large computation power, thus usually generating model results of limited statistical power.

- Amorphous track structure models: Instead of considering all physical interactions of high LET radiation in detail, the concept of amorphous track structure considers continuous functions of local dose as spatial probability distributions for energy transfer, c.f. section 2.4.2. Amorphous track structure thus is regarded as the ensemble average of individual track structures. Such averaging over individual tracks of point-like energy transfer points allows a simple analytic description of track structure. An overview of applied models describing track structure is given in [95], and prominent examples of associated RBE models are the Katz model [151, 182, 183] and the LEM [139, 161, 184, 185]. From a theoretical point of view the justification of amorphous track structure is not trivial and debated. The transition from a distribution of point-like energy transfer events to a local dose distribution is comparable to the introduction of thermodynamic variables such as temperature in statistical mechanics. This requires an 'equilibrium state' of all energy transfer events described by local dose or of all particles in motion in a thermodynamic system, respectively. Hence the information loss by taking the average for local dose evaluation, where the exact positions of energy transfer points is neglected, is an important issue to consider. Nevertheless, in contrast to microdosimetric models, in the concept of amorphous track structure the deposited energy is not spatially averaged over μm sized domains, but rather reflected by a probability distribution which is unlimited in its spatial resolution.

A number of models also combine several of the concepts discussed above. For instance, the time course of repair modeled within the MKM follows ideas closely related to the LPL and RMR models, whereas the microdosimetric input data for the MKM are often obtained by Monte Carlo transport codes or amorphous track structure formulations. The Katz model applies elements of the early target theory for the effect calculation, while LEM applies the conventional LQ model. The Repair-Misrepair Fixation model [168] exploits detailed Monte Carlo simulations of the radiation field and a deterministic simulation of repair following the concept of the RMR and

LPL. Consequently the question for the most successful strategies to model particular aspects of radiation damage arises.

3.3 Interpretation of the linear-quadratic model

The most prominent model in radiobiology, probably due to its simplicity, is the LQ model. It was introduced in the framework of chromosome aberrations by Lea [38], in the clinical context by Fowler and Stern [186] and was later also applied to describe cell survival curves [150]. The model is purely empiric and from a mathematical point of view just a second order fit function to experimental data. Hence it could be used to describe experimental data, but not to predict them.

A general interpretation derives, however, from statistical considerations: Defining lesions which will lead to cell death as lethal lesions, only those cells will survive which do not receive any lethal lesions by definition. If one assumes a Poissonian distribution of lethal lesions, the probability for no lethal lesion is $\exp(-<L>)$, where $<L>=\alpha D+\beta D^2$ is the average number of lethal lesions. Hence a basic interpretation for the exponent is found.

Several more mechanistic interpretations have been developed, and also gave rise to further model developments. These approaches are listed below. Notably, again the importance of spatial and / or temporal aspects of radiation damage induction and processing becomes evident:

- In the early days of a mechanistic interpretation of the LQ model, DSB were thought to be the most lethal lesions. In their molecular theory Chadwick and Leenhouts [154] proposed that the linear component is due to DSB induced by one particle track and the quadratic component due to the accidental induction of two SSB on opposing strands of the DNA in sufficient proximity. Clearly, linear and quadratic dependence in dose would be expected for single and two particle processes, respectively. However, considering the number of SSB observed after irradiation (about 1000 per track and Gy) in perspective with the DNA content of mammalian cells (about 6×10^9 bp) it became clear later on that an effective formation of additional DSB by two-track processes is unlikely. Nevertheless this approach is of value as it tried for the first time to associate lesions directly with observed effects in cell survival.

- Later on, experiments with delayed plating of cells after irradiation and fractionated irradiation led to the concepts of potentially lethal damage, i.e. lesions which become lethal when the next critical step in cell cycle is reached, and sublethal damage, i.e. damage which gets lethal if additional sublethal lesions occur. The interpretation is that all lesions (α and β type) are subject to repair, but the binary accumulation of sublethal lesions only alters the β-component [187].

- Strongly related, also effects of protracted irradiation have been considered: The stronger β-component for acute as compared to protracted exposure (c.f. Fig. 2.2b) suggested that pairs of (sublethal) lesions might suffer from binary misrepair which makes them lethal. The lethal lesions should become visible as chromosome exchange type aberrations, i.e. two chromosomes have a break each and recombine in a cross-wise manner. Indeed a strong correlation between observed aberration frequencies and cell inactivation has been found [188]. For protracted irradiation such accumulation of sublethal lesions is

impaired as it occurs less likely due to repair taking place already during exposure. Hence the β-component is interpreted as an misrepair interaction of independently induced lesions [189]. Remarkably, although damage induction and repair are processes on different time scales, the interpretation of a shoulder reasoned by a less successful repair fidelity at high doses and interaction of lesions are indistinguishable and identical, as higher lesion densities imply higher misrepair rates. However, it should be noted that despite of a correlation between aberration frequencies and cell inactivation, so far there is no relation available that would allow a reconstruction of a full survival curve from observed chromosome aberrations or vice versa.

- For charged particle radiation the β-component is usually considered as a combined effect of two adjacent particle tracks (hence quadratic in dose), termed *inter-track effect*, while the α-component characterizes the damage each particle infers alone (hence linear in dose) and is termed *intra-track effect*. Hence, for high LET particles a shoulder is typically less visible because even within single tracks the lesion density is large, facilitating the interaction of lesions or hampering their repair. Therefore, α-components typically increase with LET of ion radiation. If a clear shoulder is visible in a dose response curve to ion radiation it is attributed to the overlap of their tracks.

- Most models explain the quadratic component by some interaction process or lack in repair. This means that the general notions are comparable, and indeed the LQ model follows approximately or even exactly (as in the MKM, e.g.) from the model hypotheses. This analogy even holds if the kinetics of lesion induction and repair is considered [58].

From a physical point of view an interaction of two lesions is associated with an interaction range, which suggests that a coincidence of damages within the interaction range can be regarded as some level of complexity. This idea is also exploited in the GLOBLE model, which has thus a strong connection to the LQ model (see article [A2]) by this link. Also the LEM makes for low doses use of the LQ model as a parameterization of dose response curves for photons (as model input) and ions (as model output).

While reliably representing dose response curves at low doses up to some Gy, the course of survival curves of the LQ model at high doses is a long standing debate. Whereas target theory as well as the dynamic repair models predict a constant final slope, the LQ model would predict an continuously increasing bending of the dose response curve with dose. This seems to be in contrast to some experimental and clinical findings [190–195] and attempts have been made for according modifications of the LQ model by simulating saturation effects at high doses [139, 165,169,170,196]. However, there are also arguments why the pure LQ model in its simplicity is sufficient to describe the data, although this would not exclude a different systematics at higher doses not observed in the experiments and clinical studies. There is a current renaissance of the debate about the validity of the LQ model [189, 197, 198] and the biologic mechanisms of radiation damage [199–201] at high doses, driven by the accelerated developments of treatment modalities like stereotactic body radiation therapy [202, 203] involving very high doses. The modeling work associated with the LEM uses a linear extension of the survival curves at high doses [139], which is nowadays known as the linear-quadratic-linear (LQ-L) approach.

3.4 Levels of clustering and complexity

As early as in the formulation of the Theory of Dual Radiation Action [153] Kellerer proposed, inspired by the observation of an approximate $D^{-1/2}$ dose dependence of RBE, that "the elementary lesions are of dual nature, i.e. that they are the result of two sublesions whose production is independent of energy concentration". In these days the duality of lesion formation was interpreted as the formation of exchange type chromosome aberration, and an interaction radius for such processes in the order of a micrometer had been revealed by Lea and Neary [38, 39]. Later on the concept of clustered or complex damage was generalized in the sense that the proximity of two lesions can be regarded as one more complex lesion.

3.4.1 Biological target size

As mentioned before, interaction of lesions requires always an interaction range and with that a corresponding target size which allows the interaction. Hence clustering and complexity is intimately related with the question for the biological target. Goodhead opened up this question and demonstrated that there might be a coincidence of scales which are relevant for radiation damage, each of which is associated to a conformation unit of DNA in the cell nuclei [41, 100].

The investigation of ultrasoft X-rays clarified that solely a consideration of micrometer sized targets as in microdosimetric concepts was insufficient and also targets on the nanometer scale, i.e. the level of several base pairs on the DNA, have to be considered. These findings led to the notion of complex damage, where the term *complex* refers to nm complexity. Such lesions could for instance be a DSB with another DNA lesion in closed proximity. The work of Nikjoo and coworkers [33, 204] followed this track and investigated their abundance and importance. Strongly related, also work going back to Ward [205, 206] suggested the existence of 'locally or regionally multiply damaged sites'. Later on other levels of complexity were suggested [171, 207, 208], corresponding to larger conformation units of the DNA in the sub kbp, kbp and Mbp range [110]. Experimental techniques have been developed relating gene loci with spatial distance in the chromatin. Different techniques provide support for the importance of different scales, and indeed up to now concepts like the existence of the 30 nm fiber of chromatin are questioned by some studies [209, 210].

However, as from the field of microdosimetry and investigations on chromosome aberration the relevance of the μm scale is evident, it was proposed that aberrations can form based on two DSB within about a micrometer distance. But again, general quantitative relationships between DSB induction and aberration yields were not established, leaving room for further mechanistic interpretation of lesion interactions on the micrometer scale. Here the LEM and GLOBLE models propose explanations, why spatial proximity of DSB facilitates enhanced formation of aberrations.

In a more general sense, complex or clustered damage can be defined as any proximity of lesion within a given volume. Thus a DSB can be regarded from the viewpoint of radiochemistry as a higher order damage as it results from ionization clusters [78], implying a composition of two SSB. Likewise, two DSB in micrometer proximity also constitute a higher complexity than single DSB, and might thus facilitate the formation of lethal chromosome aberrations. Recalling that single DSB can be usually repaired with quite good fidelity these considerations are of particular interest to reveal both the lesions and associated biological targets responsible for

radiation damage on the cell and organ level. However, up to now the discussion of complexity and its implications is by far not at the end and thus there is also some ambiguity in existing definitions and conventions - it is not clear what complex damage is or what types of complex damage are relevant.

3.4.2 SSB clustering on the nanometer scale

Paradigms for damage cluster on the nm scale were introduced by Ward as *locally multiply damaged sites* who pointed out the distinct role of OH radicals for the induction of these lesions [205, 206]. Nikjoo followed by a classification of nanoscopic damage, consisting of SSB and DSB and these lesions by accompanying themselves, like 2 DSB, 2 SSB or an SSB and a DSB in close proximity [33, 204]. The enhanced DSB yield of high LET radiation and of ultrasoft X-rays could be explained by this approach. Quantitative investigations were carried out based on Monte Carlo transport codes of secondary electrons.

In the framework of LEM a more simplistic picture was established for the calculation of DSB yields. Its simplicity consists of only considering DSB and SSB without discriminating between different levels of complexity of these lesions. In general, two SSB on opposite strands may form a DSB, if they are induced sufficiently close to each other. The formation of additional DSB is visualized in Fig. 3.3a. The model calculation starts by the yields of high energetic photons for SSB and DSB, where the values resemble average values found in the literature for mammalian cells. The yields are linear in dose up to at least 100 Gy [48], which means that the lesions are typically formed by single track processes. Hence for high energetic photons, DSB are usually induced by one electron or one ionization cluster, causing two SSB on opposite strands of the DNA in a small volume in a correlated way. This insight was inspiration for modeling additional DSB at very high photon doses due to the random coincidence of SSB. They are interpreted to be formed by different tracks at high photon doses, thus resulting in a quadratic component of the DSB yield. In [211] the model procedure is explained in detail, and a yield ratio of the linear and quadratic component in dose of $\alpha_{DSB}/\beta_{DSB} = 8300$ Gy was found, meaning that at this value as many inter- as intratrack DSB are produced and the yield will be doubled. To summarize the model in brief, for a given dose a random positioning of SSB on both DNA strands was simulated and opposite breaks within intervals of 25 bp counted as additional DSB. In the case of high ionization densities of ion tracks or at electron track ends, e.g. after ultrasoft X-ray photoionization, the local doses are comparably high. Therefore the concept of DSB enhancement can be applied in a straightforward manner to these situations. In LEM, the DSB enhancement makes up one part of the higher effectiveness of ion tracks. For ultrasoft X-rays as well as for ions, experimental values for DSB induction and cell survival could be explained with this approach.

In comparison to other model approaches based on the Nikjoo classification like PARTRAC or RITRACKS [179, 180] the main differences of LEM are the restriction to DSB and SSB only and the admittance of the interaction of 25 bp instead of 10 bp. The numbers are somewhat ambiguous as experimental indications derived from plasmid experiments only give an order of magnitude. Hence some more research is needed, and at the moment a validation of the modeling assumptions can only be gained indirectly by comparison of calculated vs experimental yields or effects, where all model approaches are comparably successful. It should be stressed again that the LEM approach is designed most simplistic, does not claim therefore to reflect the real diversity of complex lesion formation on the nm scale. However, it does claim to reveal

the right proportion of enhancement of such lesion formation for high ionization densities by probabilistic arguments.

3.4.3 DSB clustering on the micrometer scale

Within a classical view going back to Lea and Neary [38, 39] the micrometer scale is important for the formation of chromosome aberrations, where two lesions in different chromosomes but in close proximity of about a micrometer can result in exchange type aberrations. Evidence is also seen in cell survival curves, interpreting the quadratic component of the LQ model to result from these lesions by binary misrepair. This interpretation, however, is not in agreement with a large induction rate of simple chromosome aberration composed from two breaks which appears to be linear in dose [212], but would be expected to follow a quadratic dependence. One can ask at this point if the theoretic considerations are incomplete or the experimental dependencies are not revealed correctly, as aberrations are hard to quantify due to subtle time effects and detection uncertainties.

The approach of LEM and GLOBLE here does not consider the micrometer scale as interaction between lesions in different chromosomes, but rather clustering of DSB within subcompartments of DNA. A rationale for this is given by the concept of chromatin loops as subcompartments of the DNA. Chromatin loops are thought to be intervals of the 30 nm fiber of the DNA between attachment sites to the nuclear matrix at distinct gene locations. Such loops have been proposed by several studies [213, 214] relating genomic to spatial distances and estimated to be of about 2 Mbp in length. Also other techniques point towards a relevance of DNA conformation units of on average about 2 Mbp size, including DNA fragment size measurements [208, 215–217], Hi-C techniques [218, 219] or the phosphorylation length of γH2AX foci around damaged sites of the DNA [220]. This is supported by theoretic arguments [221–224].

The general idea is that *isolated DSB* within a loop can be repaired quite effectively, while the abundance of multiple DSB within one loop, termed as *clustered DSB* is more severe and repaired with less fidelity. Such lesions would disrupt the integrity of the DNA fiber and facilitate a formation of chromosome aberrations which might commit lethality when the cell enters into next mitosis. The typical size of chromatin loops would correspond to about half a micrometer, in line with the prior microdosimetric findings. Clustering of DSB in chromatin loops is visualized in Fig. 3.3b.

A recent different modeling concept also foots on the idea of in-site multiple lesions as a form of complex damage which facilitates chromosome aberration formation [171], but in this study the kbp, corresponding to rather than the Mbp scale was exploited. In this model the yield of clustered lesions is a fit parameter rather than a model result and thus there is limited predictive power of such modeling. Nevertheless this approach shows that there is discussion about the relevance of higher order clustering and about the relevant size and the corresponding target. There is also some experimental and theoretic evidence for the existence of smaller loop scales of about 100 kbp [225–227]. More experimental investigation could help to clarify the situation, and in the virtue of novel techniques [218] promising results can be expected within the next years.

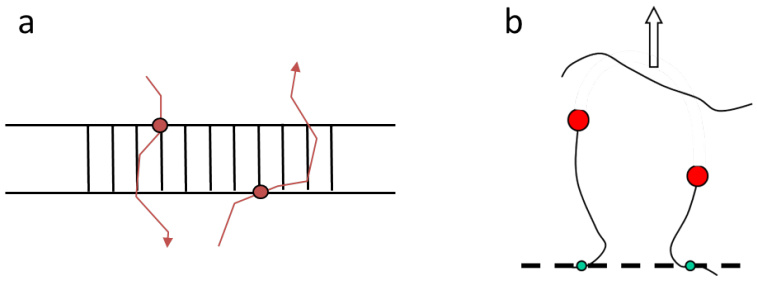

Figure 3.3: Levels of clustering in LEM and GLOBLE: (a) nanometer scale and (b) micrometer scale.

3.5 The Local effect model

The local effect model is a model approach combining several ideas to predict the radiation damage after high LET charged particle radiation. Its original version, LEM I, is used up to now in carbon ion therapy facilities in Europe as RBE predicting model in treatment planning. Over the years the model was refined and comprises in its current development stage, LEM IV, not only the consideration of local dose distributions but also of corresponding lesion distributions. It allows the reliable prediction of RBE for all therapy relevant particles and energies. All further discussion will relate to LEM IV. Table 3.1 gives an overview of the model versions.

Table 3.1: Model versions of the Local Effect Model.

Model version	Included feature	Reference
LEM I	Local effect calculation based on local dose	[139, 161]
LEM II	Radical diffusion and nm interaction of SSB resulting in DSB yield enhancement	[94]
LEM III	Energy dependence of the core radius in amorphous track structure	[228]
LEM IV	Conversion of dose to DSB distributions to determine local lesion complexity	[185] and [A1]

3.5.1 Principles

The LEM follows a number of basic strategies to estimate the high LET effectiveness. As a proof of principle, first results of LEM IV were published in [185]. The model set-up, a detailed mathematical implementation and further model tests are outlined in article [A1]. The main strategies followed in LEM are:

- The simple amorphous track structure model introduced in 2.4 is used to determine the local dose at any distance r to the primary ion's trajectory. The model reveals a $1/r^2$

dependence of local dose up to a finite range given by the maximum energy of δ-electrons. In the core, a maximum dose is proposed to assure a proper normalization of the radial local dose profile according to the LET.

- The yield of DSB based on LET is derived using the concept of nm clustering of SSB as outlined in [211, 229].
- A spatial distribution of DSB in cells is derived by a stochastic Monte Carlo sampling from the local dose distribution. The nuclei are considered as cylindrical objects with homogeneous DNA distribution. The arrangement of DSB after an ion passing a nucleus is sketched in Fig. 3.4.
- Proximity of DSB is evaluated to determine clustered DSB, defined as more than one DSB within chromatin loops, which are modeled as cubic subcompartments of the nucleus. From this the proportion of clustered to isolated DSB is evaluated and taken as a parameter quantifying the complexity of the damage milieu within the nucleus.
- A photon equivalent dose providing the same degree of complexity is determined and the associated photon effect calculated from the photon dose response parameters. The ion effect is determined as a fraction of this effect scaled by the total DSB number, as for ions not the entire cell is exposed with the same lesion complexity. Notably, thus the ion effect is determined as an extrapolation form the photon dose response curve.

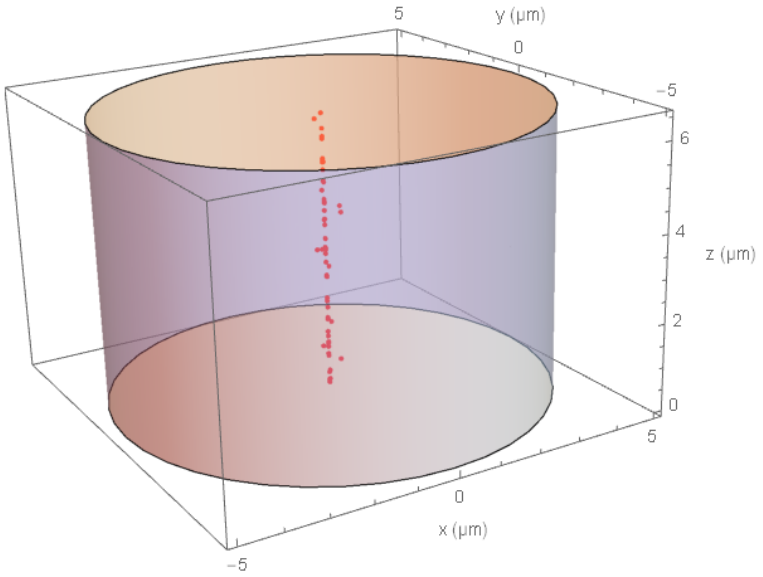

Figure 3.4: Set of DSB induced by a high LET carbon ion passing through a cylindrical model cell nucleus of 5 μm radius and 500 μm^3 volume. Along the particle track a high density of lesions becomes visible, while far off the center only eventually a DSB produced by a high energetic δ-electron occurs.

Summarizing, the main concepts of LEM are the exploitation amorphous track structure, of the coexistence of both nm and μm scales for lesion induction, and the extrapolation of the photon dose response to the high LET response scaled by the complexity of the lesion distribution. A basic insight justifying this step is, as described in [185], that the local radiation action is usually

mediated by means of secondary electrons and therefore the local response does solely depend on the local ionization density, regardless of the radiation quality causing these ionizations. The course of different steps in LEM is visualized in Fig. 3.5. Although the general concept is kept most simplistic as it works usually with average quantities and essentially only uses the photon dose response parameters as variable input parameters, the practical implementation in a computer code is somewhat tedious, because for instance the proper compartmentization of the nuclei in chromatin loops has to be arranged. The full mathematical framework and steps towards such an implementation are presented and discussed in article [A1].

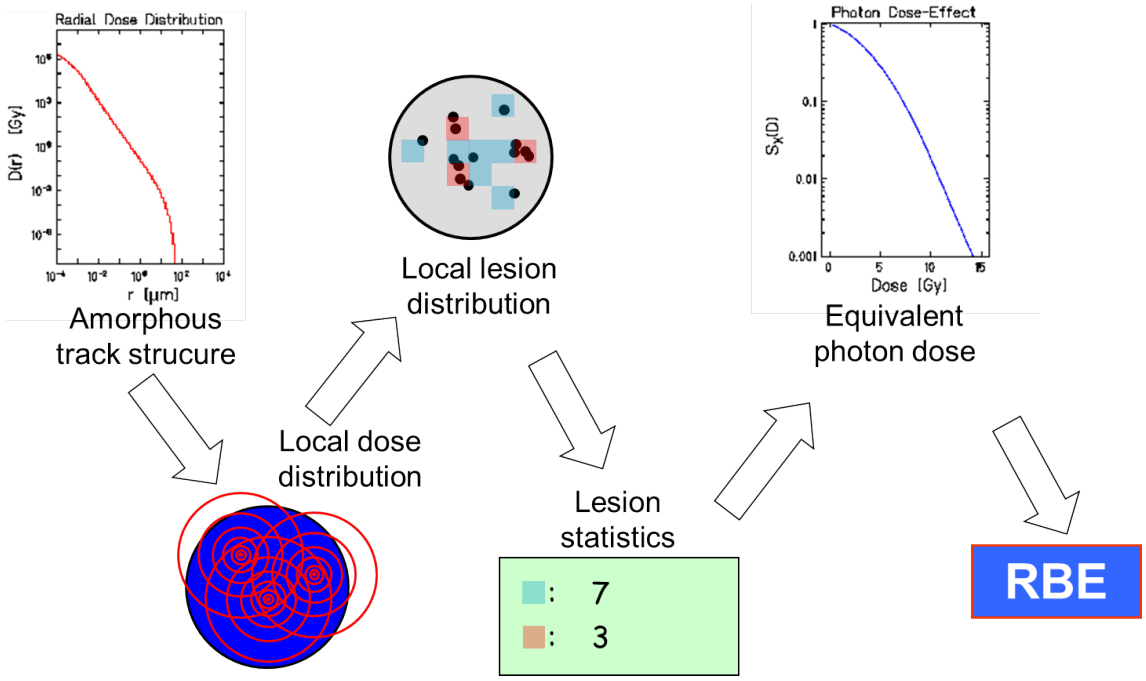

Figure 3.5: General set-up of LEM: Starting from an amorphous track structure parameterization of the local radial dose profile of individual particles passing through the cell, an overall dose distribution across the entire nucleus and from that a lesion distribution is derived by means of a Monte Carlo calculations. Next, lesions within box shaped chromatin domains are scored, and isolated (blueish boxes) and clustered (reddish boxes) DSB are counted. Their proportion is calculated as a representative quantity characterizing the average degree of complexity of lesions. Then a photon dose is determined where a lesion pattern after photon irradiation would produce the same average degree of complexity. Finally, the associated effect after photon irradiation of that dose is determined and reflects, weighted with the volume fraction covered by ion induced lesions, the effect of the ion. From this the RBE can be immediately calculated.

It should be stressed that the LEM has both mechanistic and empiric properties. It is mechanistic, as the distribution of lesions gives a clear interpretation of the complexity of initial lesion distributions. It is empiric as the complicated biologic processes involved in damage processing and repair is only implicitly considered in the photon dose response, parameterized by the LQ parameters. This allows taking into account repair without explicit modeling, using the reaction to photon radiation as template. Another remarkable property of the LEM approach is that the

assumption of the coexistence of two spatial scales directly enter in two separate contribution to RBE, one originating by the pure number of DSB and the other by the interaction of DSB.

In comparison to most other high LET dose response models the biggest advantages of LEM are a true consideration of nm resolution within the amorphous track approach, a clear paradigm of relevant targets and target sizes and effect computations based on a few assumptions and using a minimum sized set of parameters only. It has been thoroughly benchmarked against in-vitro and in-vivo data. It is used successfully in its original version for treatment planning in carbon ion therapy in the treatment facilities in Heidelberg, Marburg, Pavia, and Shanghai, and will also be used in the facility in Wiener Neustadt in future. As proposed before, a successful application to a broad range of different situations, as outlined in the next section, is one of the most intriguing arguments for the model approach.

3.5.2 Applications

Since the model set-up was completed the LEM IV was applied for different purposes. Here, published and ongoing work is listed in order to demonstrate the widespread applicability of the model, both in radiobiology research and the clinical context.

Applications in radiobiology

- Spatial measurement of dose distribution in tissues have been performed by means of biodosimetric methods. LEM predictions based on the amorphous track structure approach are in good agreement with radial distribution of DNA damage in tissue along individual ion tracks [230]. Before only physical measurements of track structure carried out in gaseous media were available. These studies thus confirm the validity of the radial track structure approach for biological applications.

- Due to gradual repair of induced damage protracted dose delivery will result in a smaller effectiveness than instantaneous dose exposure for photon irradiations, while this effect is less obvious for high LET radiation. The impact of temporal aspects of dose delivery for high LET radiation was investigated with LEM and is in agreement with experimental data [231].

- The distinction of damage classes of isolated and clustered DSB along with the track structure model in LEM allows a description of damage induction and repair kinetics after high LET irradiation. A further assumption in this context was, that clustered damage is likely to be subject for a slower repair than isolated DSB. A mechanistic description and prediction of kinetics of DNA damage after high LET irradiation was developed. The repair of isolated and clustered DSB were identified with the slow and fast component of damage repair (c.f. Fig. 2.3a) and compared to experimental data, where agreement was found [232, 233].

- An enhanced effect of high LET ion radiation is due merely to the inhomogeneous ionization pattern. This was shown by dedicated microbeam experiments where low LET protons showed en effect enhancement solely by focusing the beam to sub micrometer dimensions [234]. Experimental results for cell survival can be precisely described by the LEM. The experiments serve as a direct evidence for the relevance of micrometer lesion interaction. In comparison to the effect of carbon ions of comparable LET but higher ionization density also the effect of interactions on the nanometer scale is demonstrated. The

experimental results are revealed by LEM with good accuracy. This research is conducted within the BMBF founded project 'LET Verbund', and a corresponding publication is in preparation.

- To understand normal tissue radiation injury, the LEM has successfully predicted the RBE for side effects after spinal cord irradiation in in-vivo systems [235]. This proves that also endpoints on the organ level can be described by LEM and is a proof of principle on the way to clinical application.

Clinical applications

- As LEM I is the model version still used for clinical applications, a comparison of clinical results and treatment planning based on LEM I with the improved model version LEM IV was needed. For TCP of chordoma as well as for NTCP of temporal lobes after irradiation of craniosacral tumors it was found, that both model versions describe the clinical results adequately [236, 237].

- The determination of RBE for clinical purposes is important for a proper treatment planning, but the RBE depends on the model used. Hence comparing treatment plans where the RBE was derived with different models needs a mapping of the different RBE concepts. To understand clinical studies from Japanese ion beam treatments a translation of their clinical doses into European RBE weighted doses was necessary. The LEM helped to derive such translation recipes [238, 239].

- LEM was used to predict the dose dependence of RBE and to demonstrate the tissue type dependence of RBE at high doses. These findings are of relevance in therapy planning of modern regimens using high doses in few fractions (hypofractionation) such as in stereotactic body radiation therapy [240].

- In proton therapy conventionally an RBE of 1.1 in the entrance channel and the target is used by recommendations of the ICRU [241]. This is standard in proton facilities all over the world, while radiobiological studies clearly demonstrate higher RBE values at the distal part of extended Bragg peaks. Hence the question arises what impact a more explicit consideration of RBE in treatment planning would change and if possibly side effects of the therapy could be reduced. One aspect of the higher RBE is a shift of the biologically relevant range of the proton beams into the normal tissue. A quantification of the range dependence on tissue type and dose was possible with LEM [242]. This topic is of large current interest in medical physics, and clinical results are expected in the near future which will allow further comparison of the predictions with clinical data.

- LEM simulations are usually carried out with some approximations, shortening the Monte Carlo runs needed for convergent RBE results. However, for larger doses as of interest in hypofractionated regimens, systematic model errors increase. There a more time consuming full simulation was performed [A1], considering the exact stochastic nature of hit statistics of ions on cell nuclei. By modifications of the treatment planning system TRiP [140, 243] a usage of thereby calculated RBE information was enabled [244].

- Second cancer risk after particle therapy is an important topic of current research. A comparative study of carcinogenic risk after proton and carbon therapy was performed

by applying the LEM for the calculation of cell inactivation and adopting some ideas of LEM also for the simulation of carcinogenic trigger mechanisms. The cancer risks were exemplarily evaluated at hand of Hodgkin's Lymphoma patient plans [245]. These model approaches may become helpful for understanding and predict late side effects of radiotherapy and build a bridge between radiobiologic considerations and radiation protection.

- LEM was applied to assess benefits in ion therapy comparing protons, helium and carbon ions as different therapy relevant ion species [121]. As particle therapy is still to be considered as an emerging form of therapy, optimization with respect to benefit is a vivid field of research.

- One problem in hadron therapy treatment planning is intrafractional organ motion. For a quantification of the consequences of motion, the biological radiation action has to be considered in the target and normal volumes. Again, LEM can be applied for a proper analysis [246].

The list demonstrates that the relevance of biophysical modeling covers aspects of clinical applications, radiation protection as well as basic cell biology research. The methods used for these investigations all use LEM as introduced in [185] and article [A1].

3.6 The Giant Loop Binary Lesion model

Based on experiences made with LEM the idea arose to go one step further in the interpretation of the concept of distinguishing between two lesion types only for the effect prediction, namely of isolated and clustered DSB, and to associate these with individual lethalities. A straightforward application to photon irradiation led to the development of the GLOBLE model. Like LEM, GLOBLE is a very simple model approach based on a minimum of assumptions and parameters.

3.6.1 Principles

The GLOBLE model exploits a small number of assumptions, which makes it to a very simple photon model, based on a mechanistic interpretation. The details of the model development and first applications as a proof of principle are outlined in article [A2]. The underlying concepts are listed below:

- As for LEM, chromatin loops of 2 Mbp DNA are regarded as interaction regions of DSB. Again the distinction between isolated and clustered DSB is made.

- For high energy photon radiation dose is deposited quite homogeneously across cell nuclei. Henceforth to good approximation the number of isolated and clustered DSB can be calculated simply by Poissonian statistics.

- To convert the abundance of lesions with an effect, each isolated and each clustered DSB is associated with a inactivation probability of the entire cell. These two probabilities are fit parameters of the model and are considered as parameters of the individual radiosensitivity of the cells under investigation.

With this conceptual basis the cell survival probability S can be expressed as

$$S = e^{-(n_i \epsilon_i + n_c \epsilon_c)}, \tag{3.1}$$

where n_i and n_c are the dose dependent number of initial isolated and clustered DSB, respectively, and ϵ_i and ϵ_c are the corresponding cell inactivation probabilities of those lesions. For photon radiation at high energies the number of unaffected chromatin loop domains, n_i and n_c can be determined from Poissonian statistics for the DSB distribution. As demonstrated in Fig. 3.6 this results for low doses in a linear increase of n_i and a quadratic increase of n_c with dose. At very high doses, which are not accessible experimentally, essentially all domains are expected to have more than one DSB. Consequently, in terms of cell survival a transition from an iDSB- to a cDSB-dominated damage regime is expected.

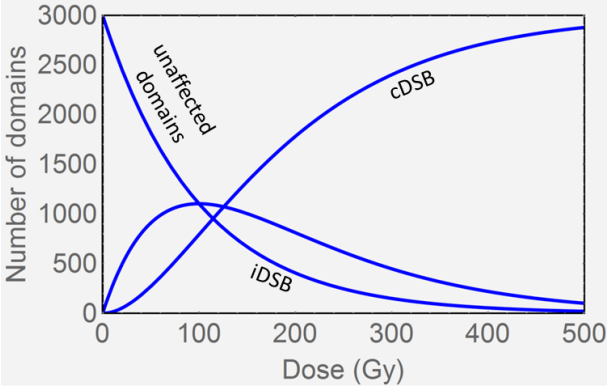

Figure 3.6: Number of unaffected chromatin loop domains, domains with exactly one DSB (iDSB) and with more than one DSB (cDSB) vs dose, assuming Poissonian statistics for the DSB distribution.

The model derivation and mathematical details are presented in article [A2]. There it also has been demonstrated that the simple approach along with the mechanistic interpretation allows to understand the dose response curves of repair deficient cell lines as well as an observed anti-correlation of α- and β values of the linear-quadratic model for various cell lines. Most inspiring, however, are the numerical values of the model parameters which revealed that isolated DSB are lethal to about 1 %, while clustered DSB typically are lethal in 20 % of all cases for cell lines with an intact repair system. These numbers are only indications as their exact values depend on the particular cell line under investigation, but reflect the general idea of different lethalities of different levels of lesion complexities. Although only considering lesion interaction in chromatin loops as closed compartments this approach does not forbid an impact of eventual formation of chromosome aberrations: Unrepaired clustered DSB facilitate the formation of aberrations which then determine cell death. The associated probabilities are implicitly contained in the lethality coefficients of the GLOBLE model.

It should be mentioned that the mathematical structure of the GLOBLE model as proposed in Eq. 3.1 - even without the mechanistic interpretation of chromatin loops and lesion clustering - is the most simple model distinguishing between less and more harmful lesions. Hence one can be faithful that the GLOBLE is a quite basic concept with a justification simply based on mathematical arguments. On the other hand one has to recall that the model parameters are average quantity over a cell population, which includes for instance different cell cycle stages of changing radiosensitivity in the case of asynchronous cells.

3.6.2 Applications

In the following published and ongoing work related to GLOBLE is listed:

- As outlined in article [A2], GLOBLE allows to understand the relation of wild type cells and derived cell lines of these with defects in the repair system, impairing DSB repair. The latter usually show a steep dose response curve [247], which suggests that even isolated DSB can not be repaired properly, and thus are comparable in effect to clustered DSB. Assuming that the lethality ϵ_i of iDSB is equal to the lethality ϵ_c of cDSB allows to understand the radiosensitive behavior of repair deficient cell lines.

- The GLOBLE was applied to explain the enhanced radiation action of ultrasoft X-rays. Based on the enhanced DSB yields and the dose response properties after high energetic photon radiation an accurate prediction of survival curve after irradiation with ultrasoft X-rays was found. Remarkably, also an mechanistic explanation could be given why in this case the RBE is not dependent on dose. Hence with GLOBLE also the entire shape of survival curves can be predicted, both for high energetic photons and ultrasoft X-rays. In article [A3] the whole model framework and the results are described and discussed. It became evident that both levels of inhomogeneity have to be taken into account, namely the localized ionization clusters due to the small range of secondary electron tracks as well as the decreasing dose profile across cell nuclei due to photoabsorption. In a following work the calculation of the yield based on the nanometer interaction of SSB is modeled, completing the full understanding of the radiation damage of ultrasoft X-rays. A publication is in preparation [99].

- As for high LET radiation qualities, the time course of repair was investigated at hand of γH2AX kinetics after photon irradiation. Experiment data could be adequately described by the kinetics predicted with GLOBLE [248]. The model procedure involved a proposed correlation of iDSB and cDSB with slow and fast repair components of biphasic repair kinetics. The applicability of biphasic repair as proposed within the GLOBLE model was shown to be justified at hand of a data collection [53].

- The GLOBLE model was successfully enhanced by a kinetic simulation of lesion induction and repair for protracted irradiation [249, 250], thereby simulating dose rate effects of photon radiation. Here the idea was that after induction of an isolated DSB a lesion can either be repaired or accompanied by induction of a further DSB, converting it into a clustered DSB. The kinetics could be described by formation and decay rate equations, strongly inspired by simulation of occupation states of laser media. This approach was later on also applied within LEM to high LET radiation qualities [231], demonstrating the strong link between these two model approaches. This work also demonstrates how mathematical modeling techniques of a field of pure physics can be transferred to the different context of radiobiological problems.

- An enhancement of GLOBLE led to the discrimination between the inactivation probabilities associated with different pathways of DNA repair after irradiation [251]. This allowed a cell cycle dependent description of cell survival curves.

All these applications are based on the model introduced in article [A2]. Despite of the simplicity of the GLOBLE approach the most obvious characteristics of photon irradiation experiments can be explained and the full dose response curve appropriately be calculated.

4 Accuracy and uncertainty considerations

Every measured quantity is subject to uncertainty. Moreover, variability is an ubiquitous phenomenon in biology. For most observables large uncertainties are rather the rule than the exception. For the application of radiation effect models a number of questions arise in this context:

- Experimental and clinical outcome is only reproducible in the sense of average values of the observable. This is due to inherent uncertainties related to damage processing and induction, but also to the variation in the inter-individual radiosensitivity cells and patient populations. What is the impact on biophysical modeling, if model parameters are subject to errors?
- What is the desired accuracy of such modeling, if the quantities to be described are anyway subject to large uncertainties?
- How can one separate the limits of a model, inducing systematic errors of the model results, from the potentially also systematic uncertainty of experimental data used to benchmark models?

Research on such questions in radiobiology is still a byproduct rather than a focus. Although some methodological problems of e.g. retrieving parameters of the LQ model from in-vitro or in-vivo data or the propagation to the RBE have been pointed out [252–255], usually few effort is made to account for such problems. However, interest has increased by the growing importance of modern radiation therapy modalities, where precise therapy planning is required.

From a clinician's perspective the relevance of uncertainty associated with effect modeling is embedded in a whole list of other uncertainties faced in practical treatment. These include: uncertainties of the CT image evaluation, uncertainties in the target delineation, positioning uncertainties, uncertainties in stopping power and beam properties, limited accuracy of dosimetry, uncertainties due to target motion and changing target volumes during the treatment due to tumor growth or regression [256]. Nevertheless in particular for carbon ion therapy where the RBE is large, uncertainties in the biological planning are significant and translate into uncertainties of doses to be delivered. Hence they need to be addressed properly. But also in proton therapy, where so far biological treatment planning is only applied within a fixed RBE of 1.1 [241], there is evidence in particular from in-vitro experiments for higher RBE values in the Bragg peak area [257], and the uncertainty due to the RBE at distal ends of applied fields is known and discussed [242, 256, 258, 259].

Although far from having a complete picture, the present chapter summarizes results that have been gathered on uncertainties of parameters and quantities of relevance for LEM. First, different types of uncertainty occurring in RBE modeling are discussed. Next, to understand the influence of parameter uncertainties in LEM a sensitivity analysis has been performed and will be presented in the next section. Then the possible induction of artificial systematic uncertainties by means of preparation of raw data is demonstrated. Having the need for caution in the interpretation of experimental data in mind, finally the investigation of uncertainty in cell survival data is covered in detail.

4.1 Types of uncertainties in RBE

Different types of uncertainty related to RBE modeling with LEM exist. A rough classification with reference to subsequent sections is given below:

- Experimental quantities used for input parameters of the model are subject to uncertainties. This comprises inter-individual variabilities between cells or patient populations under investigation. The uncertainties will propagate to uncertainties in the modeling results. They are considered in section 4.2.

- Starting from raw data, derived quantities like the α/β-ratio are often considered. By calculating these quantities bias errors can be induced by nonlinearities in the uncertainty propagation. This issue will be discussed in section 4.3. In modeling, the α/β-ratio is often used as input parameter. The impact of such bias errors has consequently to be accounted for.

- Experimental quantities used for model benchmarking are subject to uncertainties, which will be elucidated in section 4.4. These will determine how decisive model tests can be.

- The model will have, in particular due to its simplicity, limits. These can be apparent as systematic model errors like over- or underestimation of effects in some situations. Limits of LEM are briefly discussed in section 5.2.

Moreover, the LEM applies a Monte Carlo code to derive DSB distributions in nuclei. However, as Monte Carlo routines converge as $1/\sqrt{N}$ with the number of runs N to the asymptotic value, this error can be made arbitrary small by sufficient runtime. For published results usually a Monte Carlo error of lower than 1 % is assured. Hence this origin of uncertainty can be discarded for further discussion.

It is worthwhile to note at this point that the different origins of uncertainties consist a general difficulty when the predictive power of different models should be compared: As models typically refer to different sets of input parameters, different levels of uncertainties are involved and would have to be separated from the model inherent uncertainties. This is in general not feasible, and there is no clear recipe how to compare models under non-comparable boundary conditions. Hence most model comparisons actually suffer from some non-comparability, meaning that a fair and equal treatment of the models to be compared cannot be guaranteed. A comparison of LEM to other models has therefore been followed only qualitatively by comparing the model ingredients and underlying concepts. Solely on the level of clinical applications model comparisons have been performed based on established procedures for patient treatments with carbon ions, where the goal was to set predicted RBE values in relation rather than assessing the performance and accuracy of the underlying models [236, 238, 244]

4.2 Parameter sensitivity analysis

In conventional photon therapy a dose accuracy of 5 % in the target region is recommended and should be guaranteed by a proper quality assurance [260]. Due to the various sources of uncertainty, in carbon ion therapy this level of accuracy is not feasible. Although there are no official recommendations an uncertainty of the RBE weighted dose of about 10 % is regarded

as tolerable. Hence one of the important tasks is to quantify the RBE uncertainty and to make sure that RBE predictions are sufficiently accurate.

A first step to quantify uncertainties of predicted RBE is to investigate how the LEM propagates uncertainties of its input parameters. In practical applications, the input parameters may vary due to inter-individual differences between cells under investigation or different patients to be treated [261–263]. As LEM maps the effect after photon irradiation onto that after ion irradiation in a non-trivial way there is no analytic way of performing such an analysis. Hence a sensitivity analysis was performed starting from typical input values for both monoenergetic irradiation and for irradiation of a spread out Bragg peak as for clinical purposes. The sensitivity analysis demonstrates here the change of the RBE as model output stimulated by a change in one of the input parameters. The sensitivity analysis of LEM IV is presented in article [A4] along with an exemplary demonstration of how sensitivities can be converted into an RBE uncertainty estimate for clinical purposes based on plausible input parameter variabilities. Related work has been published focusing at particular input parameters of LEM IV [264] and impact on tumor control probability using LEM I [265].

The study of article [A4] showed within a systematical sensitivity analysis that the calculated RBE is most sensitive on the photon dose response parameters which are used as input for the RBE calculations. Therefore the associated uncertainties of the RBE are present already in the response to photon radiation. Moreover, the uncertainty in extended Bragg peaks decreases in comparison to monoenergetic radiation of comparable dose averaged LET. The reason is that across a SOBP a mixture of radiation qualities exist, leading to a damping of the uncertainties, but also a reduction of RBE. For proton therapy, where the RBE at distal ends of fields might be harmful as it is not taken into account in treatment planning, such a reduction is desired and could be realized by techniques like LET painting [266–268]. However, for carbon ion radiation a high RBE is beneficial as it provides a higher ratio of RBE weighted dose in the peak compared to the entrance channel. Hence a compromise between that high RBE and associated tolerable uncertainties has to be found. For this more radiobiological and clinical studies will be needed, and the provided methods in article [A4] will be helpful for a quantitative assessment of uncertainties. In the context of the current discussion of personalized medicine [269] such studies appear very promising and could facilitate a full exploitation of RBE for clinical treatments in future.

4.3 Uncertainties induced by data processing

In radiobiology the application of Gaussian error propagation is often inappropriate for two reasons. First, the distribution of the data is often not Gaussian, and second, the uncertainties of data are often of the same order as their mean, prohibiting a series expansion of the influence of deviations up to first order only. Consequently, more advanced techniques like simulated error propagation by Monte Carlo methods have to be applied for such quantities [270].

This becomes of particular importance, when based on measured data composite quantities are derived, like the α/β-ratio or RBE values as a ratio of two doses. As concluded in article [A5], caution is needed in the interpretation of RBE values reported in the literature, as these values might be systematically too large. The same argument applies again to α/β-ratios if they are directly derived from dose response curves. The reason for such a bias error is due to the properties of ratio distributions, as shall be outlined briefly in the following:

The distribution of ratios of random variables is an interesting statistical problem. For two Gaussian random variables X_1 and X_2 with realizations x_1 and x_2, respectively, the ratio X_1/X_2 is a new random variable which follows a long tailed distribution. In particular this implies $\overline{(x_1/x_2)} > \overline{x_1}/\overline{x_2}$. So the ratio x_1/x_2 of individual realizations is likely to be too large as compared to $(\overline{x_1}/\overline{x_2})$.

Article [A5] focuses on this issue and revealed that under the assumption of Gaussian distribution of numerator and denominator of the ratios the result will be distributed with a long tail, making large values more likely. This is demonstrated at hand of RBE values calculated from dose response curves, but the same argument also applies to α/β values, c.f. 4.4. A further complication is that the assumption of Gaussian distribution is not necessarily true and that in addition correlation between both quantities of the ratio might play a role.

Suggestions to overcome these difficulties are to consider, if possible, as many data as possible to obtain an impression of independent experimental results. Furthermore, if the uncertainties of the numerator and denominator quantities can be estimated, Monte Carlo error propagation allows to construct the theoretic ratio distribution and to assess the bias error induced. Generally, as outlined in article [A5] it is suggestive to use median values instead of average quantities because the median is less sensitive on the shape of the distributions. With these techniques bias errors can be quantified and taken into account. The work nicely shows that not only experimental results in terms of mean values, but also the underlying distribution have to be considered in order to fully understand characteristics of derived quantities. In article [A5] the necessary mathematical framework is provided for a profound error propagation.

4.4 Uncertainty and variability in observed experimental radioresponse

For tests of RBE models experimental data of ions over a wide LET range are needed. In addition, for LEM photon dose response data are needed as input parameters, where again a quantification of uncertainties is of interest. To follow the goal of obtaining a global view on available data and to quantify their uncertainty, for the endpoint of cell survival a data base has been established, containing over 800 combinations of survival curves for both low and high LET irradiation taken from the literature. It was termed *Particle Irradiation Data Ensemble (PIDE)* inspired by a data collection of energy levels in nuclear physics [271]. The PIDE contains besides the cell survival data, parameterized within the parameters of the LQ model, also relevant physical and biological information such as the cell types, particle species, energies and LET values and several more. It was introduced in article [A6], where also first evaluations were presented. The PIDE is the largest data base, while other data collections exist, focusing on certain aspects of dose response curves [257, 272, 273]

The data base was made available for the research community and can be retrieved over the GSI website [274]. Currently the data base has about 100 subscribers who use it for their own research. Ther are already some publications showing results derived from PIDE [6, 124, 275–281]. The most important features of PIDE are compiled in the following list:

- PIDE contains 845 pairs of cell survival curves (for photons and ions). These were taken from 74 publications.
- The cell lines used comprise sensitive and resistant cells, normal and tumor cells, cells in asynchronous populations and synchronized in particular cell cycle phases, and human and rodent cells. All properties are tabled in the data base.

- Irradiation conditions comprise monoenergetic beams as well as irradiation within spread out Bragg peaks. Various ions at different energies have been used, resulting in different LET values. Again, all properties are tabled in PIDE.

- Only experiments have been adopted into the data base which fulfill certain quality criteria, like irradiation under track segment condition where the LET does not vary considerably along the track segment through the cell nucleus.

Currently PIDE is being updated by including also raw data, i.e. the measured cell survival probabilities for each dose point, instead of only providing the LQ parameters. The benefit will be a more justified comparison between data sets of different labs or different researchers. A generic problem is that at different institutions various ways of e.g. normalizing survival data to the number of cells irradiated are applied. Likewise, error bars given for the raw data are determined by various strategies. Moreover, the number of data points underlying each survival curve differs, but has a strong impact on the precision of the derived parameters. Hence accessibility of the full sets of raw data will facilitate a reanalysis of all data with the same techniques.

One first insight confirmed by PIDE is that dose response after ion irradiation is rather robust against changes in the cell's radiosensitivity, while the photon dose response underlies a much larger variability. Hence uncertainties in RBE go back to uncertainties in the photon dose response curves to a large extent, in line with results from the sensitivity analysis, c.f. section 4.2. To demonstrate the large variability of photon parameters, Fig. 4.1 shows the distribution of α/β-ratios of photon dose response curves listed in PIDE for V79 hamster cells. The large spread of the values goes back to intra-individual and inter-individual uncertainties: Any cell damage and subsequent damage processing is a probabilistic process and is consequently associated with an inherent, also termed *intra-individual* uncertainty. Moreover, when comparing independent experiments, 'copies' of the cell lines in various labs differ in their history, which might give rise to changes in their radiosensitivity. Also, different ways of analyzing raw data and obtaining LQ parameters for the same cell line contribute to *inter-individual* differences. As discussed in the previous section, a systematic distortion by means of calculating ratio quantities (c.f. article [A5]) plays a role on top. Evidently, simply taking the calculated α/β values from one experiment is insufficient for a characterization of a cell line. Rather a set of experiments along with the distribution of the dose response parameters should be considered. The solid line in Fig. 4.1 indicates a calculation of the ratio distribution of α and β, taking the uncertainty of these parameters in the underlying experiments into account.

A number of further investigations have been carried out at hand of the PIDE and were presented in article [A6]:

- A precision analysis of the characteristics of RBE on its determining factors was provided. This confirms long-standing findings in radiobiology with a high statistical performance: RBE decreases with dose and decreases with the photon α/β-ratio. It increases with LET up to a maximum RBE, where the overkill effect causes RBE to drop for higher LET values. A profound particle specificity was determined in the increase of RBE vs LET and the position of the RBE maximum. The scatter of data allows to refine and better quantify these statements by appropriate statistical methods such as moving averages.

- An uncertainty and correlation analysis of the LQ photon parameters was provided. It turned out, that for independent experiments the photon α and β parameters are anti-

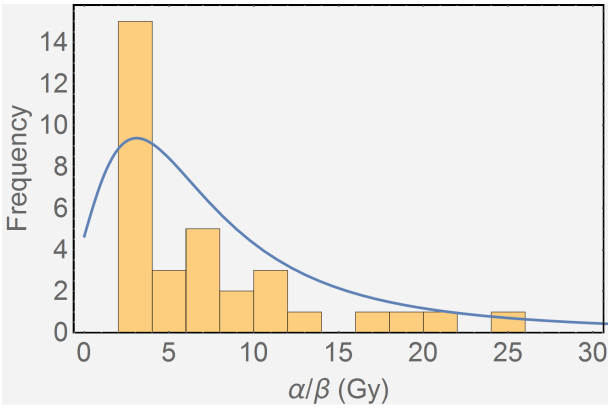

Figure 4.1: Distribution of the α/β-ratios derived from V79 cell survival experiments tabled in the PIDE. The solid line is a theoretic distribution function computed by methods discussed in articles [A5] and [A6]. A strong curtosis and thus a long tail of the distribution becomes evident. Hence simply considering individual α/β values or calculating means might induce bias artifacts.

correlated. While within individual experiments such anti-correlation is expected by means of the χ^2 minimization fit procedure, for independent experiments the reason is not obvious. An explanation is found within the GLOBLE model and outlined in article [A2]. The key idea is that the effect due to iDSB depends on α while the effect of cDSB depends on a linear combination of α and β. If the GLOBLE model is the correct photon dose response model this predicts the observed anti-correlation.

- The course the β-parameter of ion radiation in dependence on LET is largely debated (see [282] and references therein). While no statistical significant conclusion has been found so far, the results of the PIDE strongly indicate that RBE decreases for high LET values. Presumably the reason is that particle energies and hence track structure widths go down with increasing LET, impairing overlap of different tracks. A smaller inter-track effect implies a smaller β value of ion radiation dose response.

Generally, characteristics of RBE and related quantities can be experimentally explored with a high statistical power using the PIDE. A comprehensive view on the available data allows moreover to develop measures for the spread of existing data as well as to identify ranges of missing or scarce data, encouraging future experiments.

While of high interest for model benchmarking, such a data base is of limited benefit for clinical purposes. There, α/β-ratios have to be derived from fractionation studies for the clinical endpoint of interest. Usually the available data is scarce which is why for the development of RBE information for therapy purposes all available information has to be regarded and interpreted in the more complex clinical context. However, characteristic properties of uncertainty propagation in LEM as an RBE predicting model can also be investigated by means of in-vitro data only, and results can then be transferred to the clinical situation as indicated in article [A6].

5 Discussion of the articles A1-A6

Aim of this chapter is to put the articles [A1-A6] into relation to each other and to briefly discuss the main accomplishments. While each article contains an individual discussion part the focus is here the common view on the effect model concepts and the uncertainty considerations.

5.1 Effect modeling: Articles A1-A3

At the moment, the LEM is used for description of charged particle radiation damage while the GLOBLE model is applicable for photon radiation qualities. However, both models share most of their underlying assumptions and concepts as evident in articles [A1] and [A2]:

- Both models carry out effect simulations in two stages: At first the distribution of radiation induced DSB is simulated and interpreted in terms of isolated and clustered DSB, and then from the lesion pattern the effect is derived. While the first step follows mechanistic concepts, the second step is empiric, as knowledge about the photon dose response curve (for LEM) or the lethality of iDSB and cDSB (for GLOBLE) is needed as reference. Hence both models can be categorized as *semiempiric*.
- LEM and GLOBLE make both use of the conjecture that one class of critical targets of DNA damage are *chromatin loop domains*. This is a distinct feature not used in other modeling approaches and an interpretation of damage complexity.
- Both approaches can express cell survival based on the DSB induction. Hence two different endpoints are linked, one referring to *initial damage* and the other at more distant consequences after all repair processes have ended. In contrast, most other modeling work focuses at remaining damage after repair processes only.
- The models are capable to describe both spatial and temporal aspects of DSB induction and repair. They exploit assumptions on the *spatial scales* of radiation damage (DNA size and chromatin loop size, nm and μm scale) and *temporal scales* (two components of DNA repair with repair times of about 15 minutes and 2 hours), and comparison to experimental results supports the assumption of the existence of these scales.
- Both models can be regarded as a synthesis of concepts which have already found application in other modeling approaches: Similar as in microdosimetry, *interaction sites* are considered in which lesion accumulation leads to more complex damage [283, 284]. In LEM the exploitation of *amorphous track structure* and using the photon dose response as a *reference radiation* is similar to the concept of the Katz model [151]. The explicit modeling of DSB distributions is comparable to the output of Monte Carlo transport codes or in combination with a DNA model on top [179, 285]

Inspired by these similarities between LEM and GLOBLE, a unification of both approaches should be feasible by using the GLOBLE dose response instead of the LQ model as input for LEM.

This has not yet been accomplished, and the reason are differences in the photon dose response curves of the GLOBLE and the LQ models at higher doses. As pointed out in section 3.3, the shape of dose response curves at high doses is still under debate. Further work is needed to verify or falsify current approaches and might help to unify the concepts of LEM and GLOBLE.

One of the most remarkable insights one can gain from the modeling concepts of LEM and GLOBLE is that space and time to certain extent act in a similar way regarding radiation damage: Radiation effects are the higher, the more condensed radiation is delivered in both space and time. Inhomogeneous, acute irradiation is thus more effective than homogeneous, protracted irradiation of same dose. Hence a spatiotemporal symmetry becomes evident. On the level of radiation effects, RBE parameterizes the degree of ionization inhomogeneity in space, while the dose and dose rate effectiveness factor (DDREF) is a related quantity (mostly used in quantifying carcinogenic potential of radiation) parameterizing the effect modification for deviations from instantaneous irradiation delivery [286–288]. Furthermore, the enhanced effect of ion radiation results from different contributions, corresponding to the underlying spatial scales of radiation damage.

Current research exploiting microbeam irradiation of cells with a specified number of ions focuses at a generalization of the RBE interpretation in terms of the underlying spatial scales and the characterization of the underlying ionization patterns [234]. At the time when this thesis was completed, experimental results are in full agreement with the proposed coexistence of μm and nm scales, and a corresponding publication is in preparation. These findings are complementary to the study of ultrasoft X-rays (c.f. article [A3]), where primarily the nm scale is of relevance and strongly underpin the list of necessary ingredients of RBE models as proposed in section 3.1.

At the level of model application it is very convincing that with a fixed set of model parameters shared by LEM and GLOBLE different endpoints and phenomena in radiobiology can be modeled within one consistent picture. Figure 5.1 visualizes the various applications of the models. The broad utilization of the LEM / GLOBLE formalism is an important support for the underlying model ingredients and is hardly accomplished by any other competing modeling approach. The simultaneous applicability to a wide range of phenomena is a strong support of the consistency of the model concepts and the underlying assumptions.

5.2 Uncertainty considerations: Articles A4-A6

The emergence of uncertainty in radiobiologic data partially goes back to the probabilistic nature of interaction of radiation with matter. Inter-individual differences in the radiation response contribute additionally to the overall uncertainty, as outlined in article [A6]. In a physical perspective this means that the biologic targets of radiation exposure are not fully identical. Moreover, derived experimental quantities might suffer from bias errors which further enhance the uncertainty, c.f. article [A5].

On the theoretic side, any model that is simple and only uses a few parameters has limits of validity. To test a model, it should be challenged, and only as long no disagreement with data can be found, it can be taken as valid. Disagreement will reveal model limits. However, in the last step the uncertainty of the experimental data used for benchmarking needs to be taken into account as well. Radiobiologic models might use experimental data as input parameters and thus will transport the associated uncertainties to their predictions, as discussed in

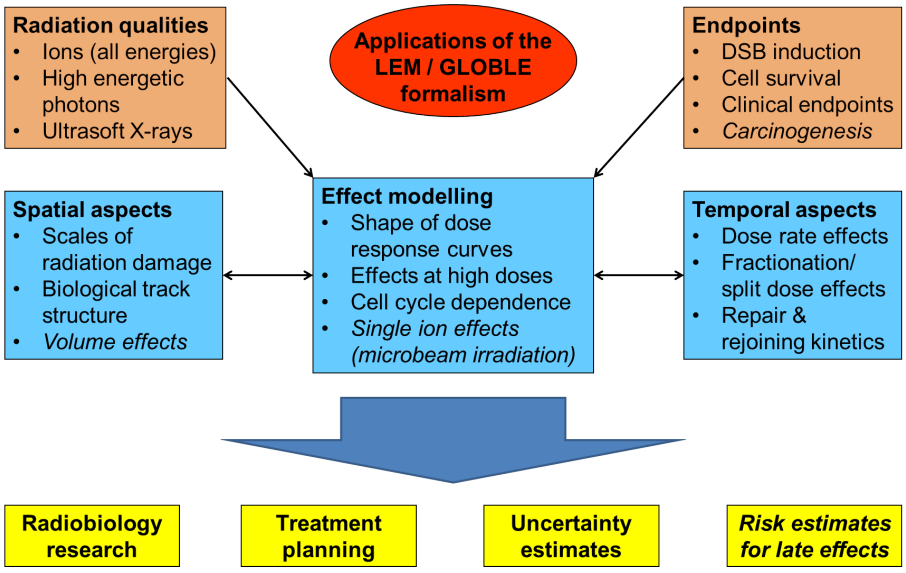

Figure 5.1: Overview of possible applications of the LEM and GLOBLE models for various scenarios, endpoints and phenomena. The top line boxes specify the various radiation qualities and biologic endpoints for which model calculations can be performed. The center line refers to the effect calculations which might consider specific aspects of dose response, involving spatial and / or temporal aspects of damage induction and processing. The calculations are aiming at the topics presented in the bottom line, summarizing the main fields of model application.

article [A4]. Further systematic deviations between model predictions and data then arise from insufficiencies in the models.

Having these different sources of uncertainties in mind, a number of lessons can be learned for testing radiobiological models:

- To reveal the model limits and uncertainties induced by the model, the fluctuation properties of experimental data used within the model and for comparison of model predictions need to be known.
- The accuracy a model is aiming at is limited by the accuracy of the experimental data used for model benchmarking.
- In the clinical context, radiobiological models are used in a framework of specified procedures with impact to radiation delivery to the patient. Uncertainty might either arise from treatment planning which accounts for this framework, or the underlying biological models. Hence model tests are frequently performed on the basis of in-vitro assays which are much less demanding in its interpretation.
- Model parameters used as constant numbers might actually turn out to be representative values of distributions. A sensitivity analysis as presented in article [A4] gives insight in the key parameters which induce most uncertainty by using average values. For LEM it turns out that in particular photon dose response parameters are the largest source of uncertainty, while uncertainties of the internal model parameters have less impact on the predictions.

LEM and GLOBLE are designed based on various concepts, abstractions and assumptions. Both models have been applied to situations, where comparison to experimental data was considered in order to perform model tests. It thereby was confirmed that the GLOBLE model reliably predicts the shape of dose response curves and that LEM gives accurate predictions for RBE values for all therapy relevant ions and energies. The only detected exception of this statement is the entrance channel for very high energetic ions, in particular for protons, where RBE values are slightly underestimated of the order of 10 %. The reasons for this are presumably that in the physical beam model of extended peaks target fragmentation is not yet taken into account. Furthermore, it is not clear if for high energetic ions, where the production cross sections of secondary electrons is low, the application of amorphous track structure is fully justified. Research towards these questions is on the way.

Besides of these considerations one has to keep in mind that LEM and GLOBLE usually work with average values. For instance, if a population of cells consists of several subpopulations, deviations between the predicted and experimentally determined effectiveness might be expected [289]. This issue could be overcome by a component-wise application of the model. In this perspective the GLOBLE model has been used successfully for the description of the cell cycle dependence of radiation effects. A similar issue might arise due to a broad distribution of cell nuclear sizes [290], where also a multiple simulation for different size categories would allow for a better theoretic assessment.

Summarizing, in the current field of applications there are only minor systematic deviations between the presented model work and experimental observations. The techniques presented in this thesis show how point predictions of radiation effects and associated uncertainties can be derived. In most parts of the parameter space the LEM and the GLOBLE model result in predictions with are correct within the accuracy of data used for benchmarking. This has important implications for therapy, where the uncertainty of patient treatment plans might be assessed, but also for novel applications such as biodosimetry, where measured radiation effects may be used to reconstruct the absorbed dose by backward application of effect models.

To further highlight the predictive power of the presented model work, model benchmarking is a continuous process which will also be followed in future research. The combination of large data collection as presented in article [A6] with uncertainty analysis tools as outlined in articles [A4] and [A5] and discussed above is promising to gain further insight in the conceptual limits of LEM. At the end, hypothesis testing of model predictions would make up a statistically sound procedure to further verify or falsify the model capabilities of LEM and GLOBLE and with that the underlying concepts.

6 Perspectives

Although there is a vivid history in radiobiology modeling the current expansion of particle therapy triggers further developments and requires for progress in this field. Also other reasons like intended space travels to Mars or the Fukushima accident gave rise to more dedicated research in modeling radiation effects. This outlook section lists a number of topics where more research seems reasonable with respect to the formulation and benefit of radiobiological models. Notably, some of these go back to very basic questions in radiobiology, where still after decades final answers are lacking, while others resulted in emerging fields of research, mostly facilitated by means of recent clinical or experimental technological developments.

Open questions in radiobiology

- **What does track structure at extremely high and low energies look like?** The radial $1/r^2$ decay of ion track structure is well established by measurements in gaseous media for a wide range of ions and energies. However, systematic measurements in denser biologic material were just gained recently by means of biodosimetry [230,291]. However, the track structure extension is less known for very small (< 1 MeV/u) or very large energies (>1 GeV/u). Here further track structure investigations will be needed and parameterizations have to be established.

- **What is the biological effect of ion radiation at extremely high energies?** While at moderate and therapy relevant energies the radiation action of ion radiation is fairly well investigated, there is little knowledge about extremely large energy. Those energies will be available at the FAIR facility in some years from now [292]. By nuclear fragmentation processes, low energetic secondary ions are expected to give rise to a high LET component of the radiation field, thus enhancing the RBE. As possible fields of applications, usage of those beams has been proposed for *theranostics*, i.e. therapy and radiography at the same time [5, 293].

- **What are the geometric sizes and size distributions of the relevant targets for damage induction?** Considering the combination of elementary lesions to more complex lesions has turned out to be crucial to propagate the induced lesion pattern to a biological outcome. While the μm and nm scales seem relevant, the coexistence of further relevant target sizes cannot be excluded [36, 41]. A better knowledge of the relevant target sizes, the associated size distribution and biological interpretation would be desirable. Lesion statistics on the relevant targets could then help to understand radiation damage on a more mechanistic basis.

- **What is the relevant complex damage and what is the microscopic composition of lethal lesions?** Although it becomes more and more clear that the notion of complex damage as neighbored lesions combined of more basic lesions is of relevance on both the μm and nm scale, the exact nature and formation of those processes remain under discussion. At the moment it is not clear what lesions ultimately determine cell lethality.

Establishing a more detailed correlation of observed chromosome aberrations or remaining damage at late times with cell survival [188, 294] could help to better point out which lesions actually commit lethality.

- **What are preconditions for the amorphous track structure concept?** Reflecting the spatial distribution of ionization events by the ionization density or local dose in biophysical models requires a locally homogeneous distribution of these events. Hence the level of detail that has to be included in track structure needs to be considered case by case. For instance, while for ion irradiation the amorphous track structure around the primary particle's (the ion's) trajectory is evaluated, for ultrasoft X-rays it is more suggestive to consider amorphous track structure around the photoelectron, because the ultrasoft X-ray photon does not transfer its energy gradually to the surrounding medium [99].

- **To what extent can biologic soft matter replace physical detectors and vice versa?** While physical dose measurements aiming at microdosimetric quantities are usually carried out in gas filled detectors in order to obtain a good experimental resolution, biodosimetry might be an alternative way for radiation effect detection in more dense media directly instead of employing density scaling approaches [230]. In turn, availability of physical detectors mimicking dose response of biologic matter would be desirable to obtain experimental data not subject to biology inherent uncertainties.

- **What are the physical properties of particle beams apart from carbon, and what are the associated biological benefits?** For various reasons in heavy ion therapy also other ions than carbon are discussed with respect to their therapeutic benefit. The fundamental characterization of helium and oxygen beams for instance are of great interest, in particular concerning scattering properties, projectile and target cross sections and LET distribution depending on depth, but also their biological effectiveness [121–124, 295, 296].

- **What elements of repair processes have to be considered in modeling?** DNA repair processes are rich multistep processes, which in turn could give rise to remaining lesions. To remove base damages, base excision repair is able to induce further DSB, when running into mitosis. In the same context, the meaning of stalled replication forks with respect to lethality is unclear [297, 298]. At the end, this may alter the relevant lesion yields, whose uncertainty needs to be reduced.

- **What is a convenient and unbiased method for comparing radiation effect models?** Models differ in their underlying concepts as well as in the type of input data they need. As the latter might be not available to equal precision for two model approaches to be compared, it is nontrivial at the moment to disentangle limits in predictive power induced by the model limits or the accuracy of the input data used. Even sophisticated statistical concepts like the Akaike information criterion [299] which is based on entropy measures of information content do not account for different data quality of the free model parameters.

- **What is the systematics of clinical RBE?** While the general dependence on dose and radiation quality is known to be comparable to what is known from in-vitro experiments, the connection of biologic parameters such as the α/β-ratio in the transition from the in-vitro to the clinical context remains unclear [68, 300]. Furthermore the availability of tissue reaction parameters is still scarce, or available parameters are associated with large uncertainties.

- **What is the proportion of targeted and non-targeted effects?** Since about a decade there is pronounced research on the contribution of intercellular signaling and related processes, which may lead to radiation consequences of unirradiated cells or tissues. However, at the moment there is no clear picture about the relevance and quantification of these effects with respect to targeted effects. Some first model attempts try to clarify the picture [301–303], but experimental data are subject to broad variability, making model verification very subtle.

Open questions in a clinical context

- **What determines normal tissue complications?** There is no consistent understanding of side effects in healthy tissues after radiation therapy. This is due to a number of reasons: No evident mechanistic picture exists of how radiation induced lesions impact connected tissue, possibly consisting of different subunits and comprising many different cell types. Moreover, radiation damage would have to be related to organ functionality, i.e. an observable endpoint has to be selected, which is somewhat ambiguous. Finally, typically there is no uniform radiation exposure over the normal tissue organs, so the volume effect (i.e. the influence of inhomogeneous exposures) has to be considered [304, 305], but again existing models and model parameters are applicable to limited extent only [64, 65]. Progress in this point would allow for a change of paradigm from target field to side effect optimized treatment planning [306]. This question is also of particular interest in the scope of new suggested treatment modalities involving extremely high local doses delivered with microbeams [307–312].

- **What is the risk for second cancers after radiotherapy?** Due to the lack of broad epidemiological and clinical data, there is only few information about second cancer formation for conventional radiotherapy [313, 314] and almost none for particle therapy [315]. In particular for the treatment of pediatric patients optimizing treatment planning in regard to second cancer risk would be of great importance [316]. While a number of models of cancer induction and formation exist [317, 318], their justification and their performance is unclear [287, 319]. For instance, model parameters are mostly derived from low dose epidemiology studies [320]. Hence a better understanding of processes of radiation induced carcinogenesis with photon and ion irradiation and development of associated risk models is desirable [321].

- **What is the dose response at high doses?** While for low doses the framework of the LQ model is a reasonable parameterization for dose response, at higher doses this is more and more questionable. This is of particular importance with respect to hypofractionated regimens or stereotactic body radiation therapy, where high doses are delivered within one or a few fractions. The biological mechanisms of damage at high doses, presumably targeting at tissue vascularization, and the applicability of the LQ model is still under discussion (c.f. the outline in section 3.3).

- **What is the interaction of radiation and chemotherapy?** Currently, most patients receive chemotherapeutic drugs and radiation in a combined therapy regimen. While there is some evidence for cytostatic drugs that they act additively in combination with radiation when applied to in-vitro assays [322, 323], this remains unclear when interaction between radiation and the immune system is involved in the clinical context [324]. If radiation

dose and drug concentration could be optimized within one consistent picture this would help to exploit the possible advantages of such combinations [325–330].

- **Do we need to consider a variable proton RBE?** As in proton therapy up to now RBE is assumed to be 1.1 in the entrance channel and target region, neglecting a potential impact of a variable RBE [257]. In a family of empiric effect models assuming a linear dependence of RBE on LET [258, 331] as well as with LEM [242] the impact of a variable RBE was considered and quantified. In particular at the distal end of extended Bragg peaks an enhanced effect is predicted [256]. However, the translation of such enhanced effects in clinically observable endpoints is unclear [332].
- **What is the role of stem cells in human cancers?** It has been hypothesized that for tumor control it is not necessary to inactivate any cancerous cell, but rather any radioresistant cancer stem cells which have the self-renewal ability, keep up tumor growth and promote metastasis [333]. While the definition and characterization of cancer stem cells is still matter of debate, they are smaller in number, but at the same time show a higher radioresistance as compared to non-stem cancer cells [334]. Further knowledge about cancer stem cell biology promises an enhanced understanding of TCP curves, and potentially provide mechanisms on how to inhibit further differentiation [335–338]. This opens new potential for models encouraging NTCP/TCP oriented treatment planning.
- **What is the optimal choice of safety margins surrounding the target?** Safety margins embedding the target are applied in the clinics to account for uncertainties in positioning and treatment planning as well as to include parts of the tumor with infiltrating growth which are invisible in the computer tomography images. However, due to the good tumor conformity achieved with modern techniques like Volumetric arc therapy or ion therapy, conventionally chosen large margins can be challenged. This is in particular of interest for pediatric patients, where probably smaller margins scaling with the organ size would be more appropriate and reveal less side effects [339].
- **How can one account for the personalized radiosensitivity of patients?** The strong heterogeneity in local tumor control among patient populations suggests to search for biomarkers to obtain a person specific radiosensitivity. Convenient markers would allow to design personalized tumor dosages. The correlation of such markers with the response of the tumor or normal tissue to radiation and an according implementation in radiation effect models paves the way to patient specific NTCP optimized treatment planning [340–342].

All these points have a potential impact to radiation effect modeling and therefore in applications of radiobioloy models, as e.g. therapy treatment planning. Answers to these questions could be exploited in therapy to either broaden the therapeutic window or facilitate to design more patient specific tailored treatment plans. This highlights the importance of mathematical modeling in current and future research and underlines the need to combine physical concepts with emerging biological and clinical insights. Finally, it should be noted that the list given above is not complete but rather reflects a selection of current research interests in the field. While in the present thesis mainly applications of biophysical modeling for cancer therapy are followed, further questions related to modeling open up from different perspectives, e.g. considering radiation protection on earth and for astronauts in space or radiation therapy of non-cancer diseases.

7 Reprints of selected publications

7.1 Article 1: The mathematical framework of the Local Effect Model

International Journal of Radiation Biology, January–February 2012; 88(1–2): 103–107

ISSN 0955-3002 print / ISSN 1362-3095 online
DOI: 10.3109/09553002.2011.611213

informa
healthcare

Calculation of the biological effects of ion beams based on the microscopic spatial damage distribution pattern

Thomas Friedrich, Uwe Scholz, Thilo Elsässer*, Marco Durante & Michael Scholz

GSI Helmholtzzentrum für Schwerionenforschung, Darmstadt, Germany

Abstract

Purpose: **To present details of the recent version of the 'Local Effect Model' (LEM), that has been developed and implemented in treatment planning for the ion beam therapy pilot project performed at GSI Helmholtzzentrum für Schwerionenforschung in Darmstadt, Germany.**

Materials and methods: **The new version of the model is based on a detailed consideration of the spatial distribution of the initial damages, i.e., double-strand breaks (DSB). This spatial distribution of DSB is obtained from the radial dose profile of the ion track using Monte Carlo methods. These distributions are then analyzed with regard to the proximity of DSB. This version of the model also facilitates the calculation of full dose response curves up to arbitrary high doses, thus allowing to thoroughly check the approximations previously used to estimate the quadratic term (β-term) for the linear-quadratic description of dose response curves.**

Results: **The accuracy of the model predictions is demonstrated by good agreement of the relative biological effectiveness (RBE) as a function of the linear energy transfer (LET) with experimental data obtained for V79 cells after carbon irradiation. The β-values predicted by the full simulation tend to be larger as compared to the approximation in the intermediate LET range.**

Conclusion: **The new version of the model allows a more mechanistic description of the biological effects of ion radiation. The full simulation is a prerequisite for tests of the validity of the approach at high doses, which are of particular interest for application in hypofractionation studies.**

Keywords: Biophysical model, local effect model, double-strand break (DSB) distribution

Introduction

Local Effect Model: Basics

The 'Local Effect Model' (LEM) in its earlier versions (Scholz et al. 1997, Elsässer and Scholz 2007, Elsässer et al. 2008a) aims at deriving the biological effects of ion radiation directly from the response of cells or tissues to photon radiation, thus efficiently exploiting the large data base collected with conventional radiation. The effectiveness of particles is calculated based on the microscopic local dose distribution pattern of ion traversals within the cell nucleus, assuming that equal local doses should lead to equal local effects, independent on the radiation quality. Typically, the local dose around single ion tracks is determined by an amorphous description of the radial dose distribution (Elsässer et al. 2008b). For a local dose d_{loc}, in the earlier versions of the LEM the local biological effect is derived directly from the corresponding photon dose response curve denoted as $S_\gamma(D)$, where S represents the survival at dose (D). This response curve is represented by the linear-quadratic (LQ) parameters α_γ and β_γ for the specific biological endpoint under consideration, which are known from experiments or clinical data.

Since the linear-quadratic description is only valid for low and intermediate doses (Astrahan 2008), a correction for S(D) was introduced in order to account for a transition to an almost linear shape at higher doses $D > D_t$, where D_t denotes the 'threshold' dose for the transition. In addition, the induction of DNA single-strand breaks in close vicinity (< 25 bp) can lead to additional DNA double-strand breaks, thus further enhancing the biological effects at very high local doses (> 1000 Gy) (Elsässer and Scholz 2007). In analogy to the cell survival dose response curves, similar considerations also apply to other endpoints that can be characterized by a linear-quadratic dose response such as local tumor control or normal tissue complications (Karger et al. 2006).

Local Effect Model: Generalization

A key feature of the approach described above is the direct link of the local dose deposition pattern to the photon dose response curve describing the observable endpoint under consideration. For the extension recently reported (Elsässer et al. 2010), we have introduced an intermediate step, based on the premise that the biological response of a cell to radiation is primarily linked to the *initial DNA damage distribution*

*Thilo Elsässer is now at Siemens Healthcare Sector, Erlangen.
Correspondence: Dr Michael Scholz, PhD, GSI, Biophysik, Planckstrasse 1, Darmstadt, D-64291 Germany. Tel: Th 49 6159 711340. Fax: Th 49 6159 712106. E-mail: m.scholz@gsi.de

(Received 17 December 2010; revised 21 June 2011; accepted 27 July 2011)

induced by radiation rather than the local dose distribution itself. We assume that the microscopic spatial distribution of DNA damage, namely double-strand breaks (DSB) and in particular their local density, represents the relevant measure determining the fate of a cell after radiation insult. Furthermore, in line with the general concepts of the LEM, we assume that similar DSB patterns should lead to similar effects, independent of the radiation quality leading to these patterns.

In order to assess the similarity of DSB distributions, specific measures have to be defined. In the LEM, these are related to the structure of chromatin organization in the cell nucleus. It is assumed that so called 'giant loops' of DNA (Yokota et al. 1995, Solovjeva et al. 1998), comprising about 2 Mega base pairs (Mbp) DNA length, represent the critical structure of the DNA (Johnston et al. 1998, Ostashevsky 1998). We then distinguish two types of damages, namely that either only a single DSB ('isolated DSB' [iDSB]) is induced in such a loop structure or two or more DSB ('clustered DSB' [cDSB]) are induced. It is hypothesized that cDSB lead to a significant higher probability of, e.g., cell killing as compared to iDSB, since for iDSB the DNA on both sides of the DSB is still attached to the nuclear matrix, and thus repair is expected to be facilitated in general in this case. In contrast, for cDSB one or more DNA fragments can be removed from the loop, which are not any longer attached to the nuclear matrix and thus correspondingly difficult to repair (Figure 1).

Assuming that damage induced in different DNA loops can be considered to act independently, the total number of loops with iDSB and cDSB, respectively, represents a measure of the clustering of the DSB induced by a given dose deposition, as defined by the cluster-index C:

$$C = \frac{N_{cDSB}}{N_{iDSB} + N_{cDSB}},$$

where N_{cDSB} and N_{iDSB} represent the number of loops with isolated and clustered DSB, respectively.

The calculation of the spatial DSB distribution is based on the local dose derived from the radial dose profile described above and used already for the previous versions of the LEM. Assuming a homogenous distribution of the DNA within the nucleus as a first approximation, the mean number of DSB in a given small subvolume of the nucleus can be derived from experimental photon data, which indicate that the yield of radiation-induced DSB is approximately 30 DSB/Gy/cell. Based on the local average number of DSB, spatial DSB distributions are then determined by means of Monte-Carlo techniques, i.e., actual DSB distributions are determined by considering the amorphous track structure pattern as the probability density distribution of DSB. A potential enhancement of the DSB induction resulting from a combination of SSB in close vicinity (< 25 bp) as a consequence of the extremely high local doses in the track center is also taken into account (Elsässer and Scholz 2007). Furthermore, indirect effects of radicals are taken into account by smearing out the radial dose profile according to the typical diffusion length of radicals (Elsässer and Scholz 2007).

Figure 2 schematically illustrates in a two-dimensional representation the analysis of the DSB distribution pattern

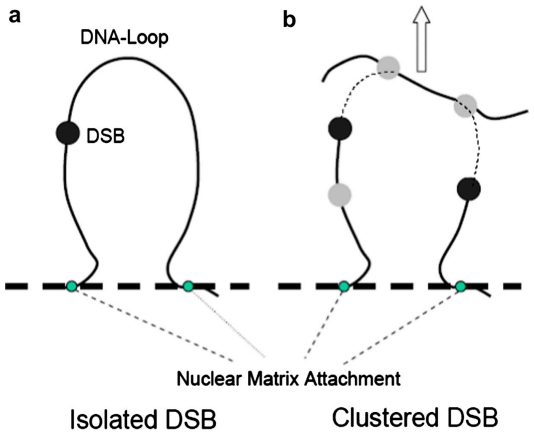

Figure 1. Illustration of the impact of isolated DSB induction (a) and clustered (b) DSB induction within a single DNA loop. In (b), the simplest case of a cDSB is indicated for the case of 2 DSB (black circles). If more than 2 DSB are induced (additional grey circles), the situation remains similar as for 2 DSB, since it is characterized by potential loss of large DNA pieces and remaining pieces attached to the nuclear matrix.

according to the method described above. The outer square represents a cell nucleus; the inner small squares represent the subvolumes covered by individual DNA loops. Assuming a homogenous distribution of DNA within the nucleus, the amount of DNA contained in a loop (approx. 2 Mbp) can be attributed to a subvolume of the nucleus, based on the knowledge of the total DNA content (approx. 6×10^9 Mbp in mammalian cells) and the typical volume of the nucleus (approx. 500 μm^3). The cell nucleus thus contains about 3000 loops of 2 Mbp size; therefore, the boxes drawn in Figure 2 are only schematic and not to scale.

In order to determine the number of isolated and clustered DSB, the cell nucleus is divided into cubic shaped subvolumes with 540 nm side length, corresponding to the volume covered by a 2 Mbp DNA content when assuming a homogenous distribution of DNA within the nucleus. The number of DSB in each subvolume is determined according to the local dose distribution within the subvolume and the subvolumes are then classified as isolated DSB or clustered DSB if exactly one DSB or two or more DSB are induced in a subvolume, respectively.

As indicated in Figure 2b, typically the overall distribution of DSB induced by a charged particle traversal largely differs from the random distribution after photon radiation (Figure 2a) because the DSB are induced essentially along the trajectory of the particle; however, the analysis of the number of iDSB and cDSB can be done exactly as for photons. The damage induced by a particle traversal can thus be interpreted as a cut-out of the distribution induced by photons at a macroscopic dose where the cluster index for photons (C_γ) is identical to the cluster index for the ion traversal (C_I); this condition $C_\gamma = C_I$ defines the 'photon equivalent dose' D_{eq}. Technically, by means of the Monte Carlo simulation average values for C_γ and C_I are obtained, from which the equivalent dose is derived. Knowing this equivalent dose, the effect of a single particle traversal can be obtained by appropriate scaling of the effect induced by photons at $D = D_{eq}$. Based on the

assumption of stochastic independence of the effects resulting from lesions induced in different loop domains, the scaling is simply based on the total number of iDSB and cDSB after photon and ion irradiation, respectively.

For the schematic representation in Figure 2a, the damage induced by the particle traversal on average would thus be 1/10 of the damage induced by photons, when averaging over a large number of individual representations. More generally, the scaling factor κ according to the condition of an equal cluster index can be determined by:

$$\kappa = \frac{\ln S_{Ion}(D_{Ion})}{\ln S_{\gamma}(D_{eq})} = \frac{\left(N_{iDSB,Ion} + N_{cDSB,Ion}\right)(D_{Ion})}{\left(N_{iDSB,\gamma} + N_{cDSB,\gamma}\right)(D_{eq})}$$

Here, D_{Ion} denotes the dose deposition by a single particle traversal, $S_{Ion}(D_{Ion})$ and $S_{\gamma}(D_{eq})$ denote the survival after ion radiation at dose D_{Ion} and photon irradiation with the photon eqivalent dose D_{eq}, respectively. N with the corresponding subscripts represents the numbers of isolated and clustered DSB after ion and photon radiation, respectively.

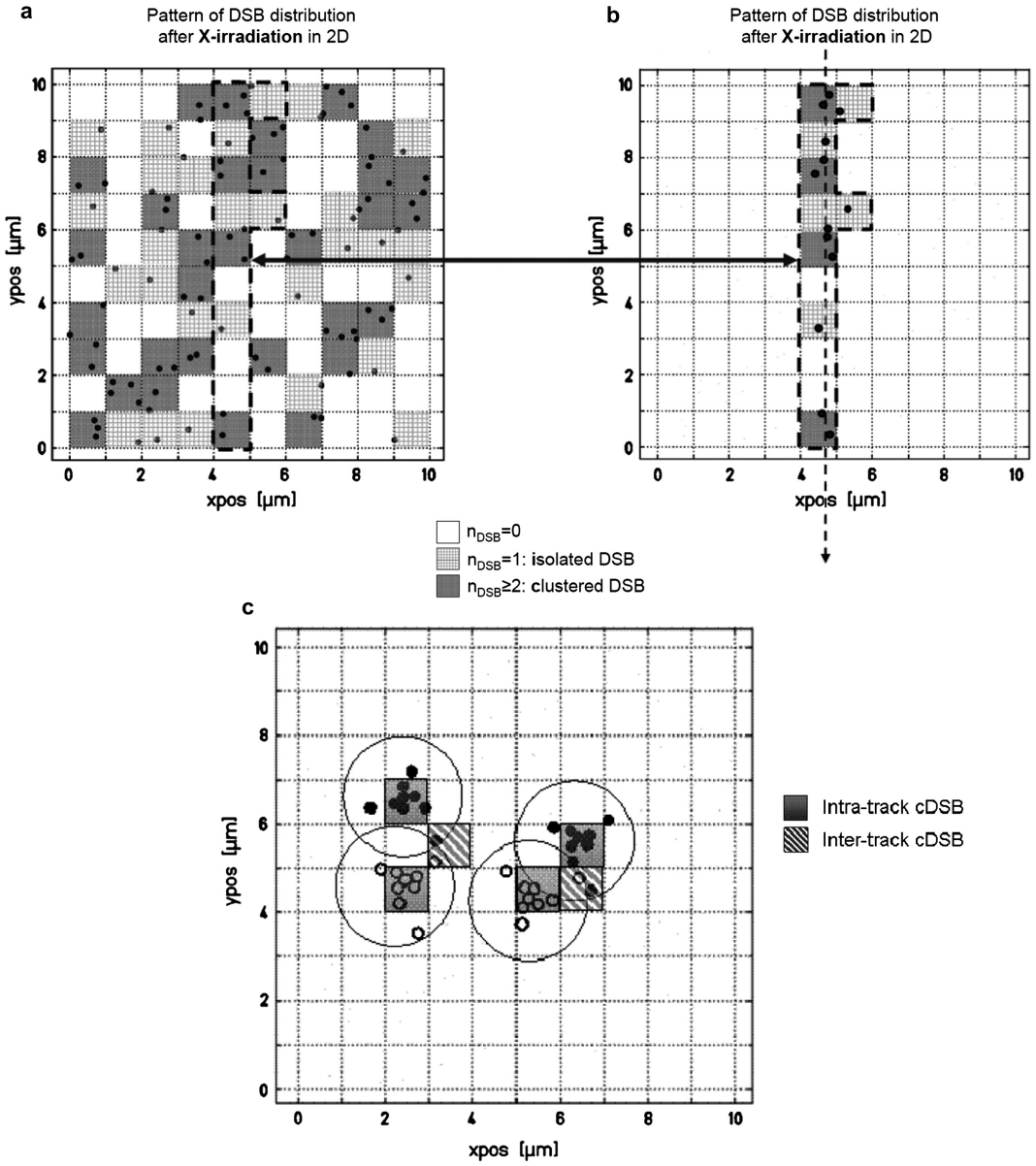

Figure 2. Schematic representation of the DSB distribution after photon radiation (a) and a single particle traversal as indicated by the arrow (b) through a cell nucleus (large square), composed of domains (small squares) representing giant DNA-loops. Different grey values represent different types of DSB. For simplicity, only 2-dimensional distributions are shown. The size of the squares representing the loop domains is not to scale. (c): Schematic illustration of the occurrence of intertrack effects by interaction of DSB from different tracks. Tracks are assumed to be perpendicular to the plane shown; circles indicate the radius of the individual tracks as defined by the maximum range of secondary electrons perpendicular to the trajectory. In order to facilitate the visualization of intertrack effects, DSB of interacting tracks are marked with different symbols.

This procedure allows calculating the effect of a single particle traversal, defining the effectiveness at low doses and thus the α_I term of the linear-quadratic representation of the dose response curve. The β_I-term can then be estimated according to the approximation described in (Krämer and Scholz 2006). This approximation has been introduced since full simulations of dose response curves would be unfeasible for applications in the framework of treatment planning; this was mainly due to the extremely time consuming calculations.

Local Effect Model: Full simulation

In extension of what has been reported by Elsässer et al. (2010), we here show for the first time that within the framework of the most recent implementation of the LEM as described above, the full simulation of dose response curves is largely simplified.

This is due to the fact that now the biological effect of interest is determined from the initial DSB distribution pattern, i.e., a discrete number of events has to be summed instead of integrating over continuous functions of local dose distribution patterns. The pattern induced by a combination of particle traversals can be deduced with good accuracy from the pattern within individual tracks, since the yield of DSB is linearly dependent on the dose up to doses of several hundred Gy, which typically occur only within a narrow region of approx. a few ten nm in the track center (Elsässer and Scholz 2007). Thus, the *induction* of DSB is not affected significantly by intertrack effects. These intertrack effects become visible only when analyzing the spatial distribution of DSB in terms of cDSB, because for cDSB distances in µm dimensions are relevant, so that even without direct overlap of the tracks interactions of the DSB induced by two tracks in µm distance might occur. Figure 2c schematically depicts this type of intertrack effect.

Results

Figure 3 shows a comparison of model predictions with experimental data for inactivation of V79 cells after carbon irradiation as published by Furusawa et al. (2000). This comparison is based on the single particle approximation as described above. The general shape of the relative biological effectiveness (RBE) as a function of linear energy transfer (LET) curve as well as the dose- and survival dependence of the RBE are reproduced reasonably well. The tendency of an underestimation in the intermediate LET range at higher doses, i.e., the RBE for 10% survival (RBE_{10}), could at least partially be due to the approximation used for the derivation of the β_I-term in the single particle approximation.

In order to further investigate the accuracy of the single particle approximation, the full simulation of dose response curves has been implemented. We first focus here on the discussion of the general differences between the single particle approximation and the full simulation based on a 'hypothetical' cell line, characterized by the linear-quadratic photon parameters α_γ and β_γ typical for in vitro cell lines. Figure 4 compares the corresponding predicted linear-quadratic parameters for ion irradiation, α_I- and β_I, for the simulation of carbon ion irradiation at different LET. The α_I-values are

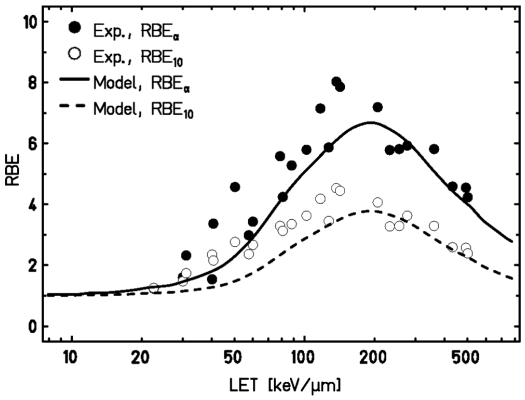

Figure 3. Comparison of model predictions with experimentally determined RBE values for cell killing obtained after carbon ion irradiation of V79 Chinese hamster cells as reported by Furusawa et al. (2000). RBE_α represents the RBE for the linear α-terms, i.e., the initial slopes of the dose response curves; RBE_{10} represents the RBE at 10% survival level. Input photon parameters for calculation: $\alpha_\gamma = 0.184\ Gy^{-1}$, $\beta_\gamma = 0.02\ Gy^{-2}$, $D_t = 17$ Gy, Radius of the cell nucleus $R_{Nucleus} = 4.7$ µm.

almost identical, which can be expected since these are fully represented by the action of individual, single particles. Systematic differences between the two approaches are observed for the β_I-term. Here, the full simulation in general predicts larger β_I-values as compared to the approximation, so that the drop of the β_I(LET)-curve is significantly shifted to higher LET values. Furthermore, there is an indication of even an increase of the β_I-term at intermediate LET values around 30 keV/µm for carbon ions. Further preliminary studies revealed that the potential enhancement of the β_I-term above the photon reference value seems to be more pronounced for lighter particles like protons.

Discussion

The generalization of the LEM based on the concept of isolated and clustered DSB in DNA giant loop domains has been shown to significantly enhance the quantitative agreement of the model predictions with experimental data (Elsässer et al. 2010). This refers in particular to the simultaneous representation of the effectiveness of light and heavier ions with the same level of accuracy. For the application to V79 cells as shown in Figure 3, a tendency of underestimation is observed in the intermediate LET range. However, this deviation seems to be specific for V79 cells and does not represent a general feature of the model, since, e.g., for other cell lines like HSG the corresponding discrepancies are much less pronounced (Elsässer et al. 2010). This could be due to the fact that at present, key parameters such as, e.g., the loop or domain size are assumed to be identical for different cell lines, but actually differences might be expected depending on the cell or tissue type.

As we have shown in this paper, the generalization of the LEM also facilitates the direct calculation of the β-term of the dose response by explicitly modeling the intertrack interaction mechanism within a full Monte Carlo simulation.

This feature is closely related to the interpretation of 'clustered damage' in terms of interaction of DSB over Mbp genomic distance or micrometer geometrical distance,

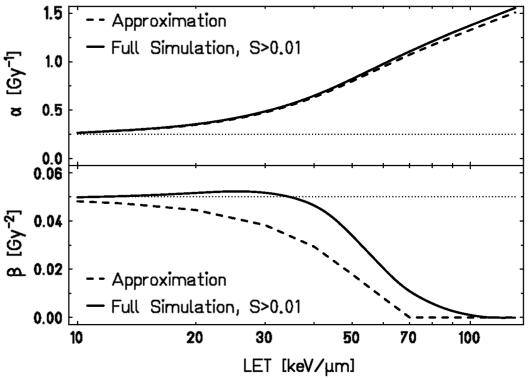

Figure 4. Comparison of α_I(LET) and β_I(LET) for the single particle approximation (dashed lines) and the full simulation (full lines) for carbon ion irradiation. Assumed linear-quadratic photon parameters: $\alpha_\gamma = 0.25$ Gy^{-1}, $\beta_\gamma = 0.05$ Gy^{-2}, $D_t = 9.5$ Gy, Radius of the cell nucleus $R_{Nucleus} = 5$ µm.

respectively. This definition of clustered damage significantly differs from that used, e.g., by Nikjoo et al. (2001) and Ottolenghi et al. (1995); they focus on 'local' cluster effects characterized by combination of damages over distances of a few basepairs only, representing what has been termed 'locally multiply damaged sites' by Ward (1994). In that respect, the most recent implementation of the LEM shares more similarities with approaches based on 'regionally multiply damaged sites' due to the consideration of interaction of DSB over significantly larger genomic distances, in line with experimental data indicating an excess of DNA fragments in the 10 kbp–1 Mbp size after ion irradiation (Radulescu et al. 2004). Our approach is also consistent with the findings by Friedland et al. (2006), who analyzed clusters on a local and regional scale and found a better correlation of regional clusters with experimental data of RBE for cell inactivation.

Underestimation of the RBE in the intermediate LET range, as visible in Figure 3, is probably due to the underestimation of the β-term in the single particle approximation, on which the predictions were based. More detailed studies of these effects are currently ongoing, based on the approach described above, which already indicated that the beta-term in the full simulation approach is systematically higher as compared to the single particle approximation.

For light particles like protons, even a simultaneous increase of α_I and β_I might occur with increasing LET, which is in contrast to conclusions that in general the β_I term tends to decrease with increasing LET. But at least for neutrons reports indicate a clear increase of the quadratic component for neutrons, $\beta_{N,}$ as compared to the corresponding component for photon radiation, β_γ (Jones 2010). The difference between the full simulation and the approximation also depends on the specific α_γ- and β_γ-values used as input for the model calculations; a detailed analysis, however, is beyond the scope of the present manuscript.

For the application of the model in treatment planning, the higher β_I-term will have significant impact mainly for higher dose levels as relevant for hypofractionation studies; we checked that at lower doses around 2–3 Gy the approximation method is sufficiently accurate.

Declaration of interest

Thilo Elsässer is now working for Siemens Healthcare Sector, Erlangen. The other authors report no conflicts of interest.

References

Astrahan M. 2008. Some implications of linear-quadratic-linear radiation dose-response with regard to hypofractionation. Medical Physics 35:4161–4172.

Elsässer T, Scholz M. 2007. Cluster effects within the Local Effect Model. Radiation Research 167:319–329.

Elsässer T, Krämer M, Scholz M. 2008a. Accuracy of the local effect model for the prediction of biologic effects of carbon ion beams in vitro and in vivo. International Journal of Radiation Oncology*Biology*Physics 71:866–872.

Elsässer T, Cunrath R, Krämer M, Scholz M. 2008b. Impact of track structure calculations on biological treatment planning in ion radiotherapy. New Journal of Physics 10:075005

Elsässer T, Weyrather WK, Friedrich T, Durante M, Iancu G, Krämer M, Kragl G, Brons S, Winter M, Weber KJ, Scholz M. 2010. Quantification of the relative biological effectiveness for ion beam radiotherapy: Direct experimental comparison of proton and carbon ion beams and a novel approach for treatment planning. International Journal of Radiation Oncology*Biology*Physics 78:1177–1183.

Friedland W, Jacob P, Paretzke HG, Ottolenghi A, Ballarini F, Liotta M. 2006. Simulation of light ion induced DNA damage patterns. Radiation Protection Dosimetry 122:116–120.

Furusawa Y, Fukutsu K, Aoki M, Itsukaichi H, Eguchi-Kasai K, Ohara H, et al. 2000. Inactivation of aerobic and hypoxic cells from three different cell lines by accelerated (3)He-, (12)C- and (20)Ne-ion beams. Radiation Research 154:485–496.

Johnston PJ, MacPhail SH, Banáth JP, Olive PL. 1998. Higher-order chromatin structure-dependent repair of DNA double-strand breaks: Factors affecting elution of DNA from nucleoids. Radiation Research 149:533–542.

Jones B. 2010. The apparent increase in the beta-parameter of the linear quadratic model with increased linear energy transfer during fast neutron irradiation. British Journal of Radiology 83:433–436.

Karger CP, Peschke P, Sanchez-Brandelik R, Scholz M, Debus J. 2006. Radiation tolerance of the rat spinal cord after 6 and 18 fractions of photons and carbon ions: Experimental results and clinical implications. International Journal of Radiation Oncology*Biology*Physics 66:1488–1497.

Krämer M, Scholz M. 2006. Rapid calculation of biological effects in ion radiotherapy. Physics in Medicine and Biology 51:1959–1970.

Nikjoo H, O'Neill P, Wilson WE, Goodhead DT. 2001. Computational approach for determining the spectrum of DNA damage induced by ionizing radiation. Radiation Research 156:577–583.

Ostashevsky J. 1998. A polymer model for the structural organization of chromatin loops and minibands in interphase chromosomes. Molecular Biology of the Cell 9:3031–3040.

Ottolenghi A, Merzagora M, Tallone L, Durante M, Paretzke HG, Wilson WE. 1995. The quality of DNA double-strand breaks: A Monte Carlo simulation of the end-structure of strand breaks produced by protons and alpha particles. Radiation Environmental Biophysics 34:239–244.

Radulescu I, Elmroth K, Stenerlöw B. 2004. Chromatin organization contributes to non-randomly distributed double-strand breaks after exposure to high-LET radiation. Radiation Research 161(1):1–8.

Scholz M, Kellerer AM, Kraft-Weyrather W, Kraft G. 1997. Computation of cell survival in heavy ion beams for therapy. The model and its approximation. Radiation and Environmental Biophysics 36:59–66.

Solovjeva L, Svetlova M, Stein G, Chagin V, Rozanov Y, Zannis-Hadjopoulos M, Price G, Tomilin N. 1998. Conformation of replicated segments of chromosome fibres in human S-phase nucleus. Chromosome Research 6:595–602.

Ward JF. 1994. The complexity of DNA damage: Relevance to biological consequences. International Journal of Radiation Biology 66: 427–432.

Yokota H, van den Engh G, Hearst JE, Sachs RK, Trask BJ. 1995. Evidence for the organization of chromatin in megabase pair-sized loops arranged along a random walk path in the human G0/G1 interphase nucleus. Journal of Cell Biology 130:1239–1249.

7.2 Article 2: The Giant Loop Binary Lesion Model

RADIATION RESEARCH **178**, 385–394 (2012)
0033-7587/12 $15.00

DOI: 10.1667/RR2964

Modeling Cell Survival after Photon Irradiation Based on Double-Strand Break Clustering in Megabase Pair Chromatin Loops

Thomas Friedrich,[a] Marco Durante[a,b] and Michael Scholz[a,1]

[a] *GSI Helmholtzzentrum für Schwerionenforschung (GSI), Department of Biophysics, Darmstadt, Germany; and* [b] *Technische Universität Darmstadt, Germany*

Friedrich, T., Durante, M. and Scholz, M. Modeling Cell Survival after Photon Irradiation Based on Double-Strand Break Clustering in Megabase Pair Chromatin Loops. *Radiat. Res*. 178, 385–394 (2012).

A new, simple mechanistic dose-response model for cell survival after photon irradiation is presented. Its ingredients are motivated by the concept of giant loops, which constitute a level of chromatin organization on a megabase pair length scale. Double-strand breaks (DSBs) that are induced within different loop domains of the DNA are assumed to be processed independently by the cell's repair mechanism. The model distinguishes between two classes of damage, characterized by either a single DSB or multiple DSBs within a single loop. Different repair fidelities are associated with these two damage classes from which lethality of damages and consequently the survival probability of cells is derived. Given the giant loop chromatin organization and the assumption of two damage classes represent the main pillars of this new approach, we propose to call it the Giant LOop Binary LEsion (GLOBLE) approach. In this paper, we discuss the motivation and the formulation of the model as well as some basic implications. First applications to experimental data obtained with 250 kV X-rays exhibit that the model is able to reveal important features of the dose-response curves describing cell survival. These comprise a linear-quadratic behavior at lower doses and a transition to a straight dose-response relationship at high doses. We establish relationships to the parameters α and β of the linear-quadratic model and discuss possible generalizations. When expressed in terms of the linear-quadratic model, we demonstrate that our new model predicts an intrinsic anticorrelation between β and α, in line with an analysis of a large set of experimental data that is based on survival curves for more than 150 cell lines.

[1]Address for correspondence: GSI Helmholtzzentrum für Schwerionenforschung, Department of Biophysics, Planckstrasse 1, D-64291 Darmstadt, Germany; e-mail: m.scholz@gsi.de.

INTRODUCTION

Precise knowledge and characterization of the dose-response curves is a prerequisite for optimal application of radiation in radiotherapy. During the past decades, the linear-quadratic model (LQ-model) has been demonstrated to be a powerful tool for the understanding and prediction of the essential biological responses that are relevant for therapy such as fractionation and dose-rate effects (*1, 2*). However, evidence has accumulated that shows that the LQ-model has certain limitations in the high-dose region. It has also been shown that the curvature of the dose-response curve is less pronounced at high doses than predicted from the shape of the dose-response curve at lower doses (*3, 4*). This is of particular clinical relevance for application of hypofractionation schemes and/or radiosurgery. Several solutions have been proposed to overcome this problem (*5–8*); however, these are more empirical approaches not aimed at a detailed consideration of the potential underlying mechanisms.

DNA double-strand breaks are considered to be the damage responsible for most end points such as chromosome aberrations and cell killing. However, due to the high number of DSBs induced by radiation at sublethal doses of only a few Gy, it is immediately obvious that a single DSB is not lethal in general, indicating that most of the induced DSBs can be rejoined or repaired correctly. It is therefore assumed that the spatial distribution of DSBs is a major factor in determining e.g. lethality (*9–13*). However, no unique strategy has emerged from these approaches allowing for the development of an improved model for the dose-response curves that would be able to overcome the drawbacks of the LQ-model mentioned above.

Fortunately, many experimental studies have been performed to better understand and characterize the factors that determine the fate of DSBs after radiation insult. The studies related to the relevance of the chromatin organization with respect to the reparability of DSBs are of particular interest for the work described below. For example, chromatin loops with a size of several megabase pairs have been identified as structural subunits that are termed ''Giant Loops'' (*14–16*). Using a different experimental technique, Johnston *et al*. (*17*) came to similar conclusions and they

identified chromatin loop structures with megabase pair size. In addition, it has now been shown that the phosphorylation of the H2AX histone in approximate 2 Mbp regions surrounding a DSB is possibly related to these giant loop structures and represents a further hint to the relevance of megabase pair chromatin structures for the response of a cell to radiation damage (*18*).

Assuming in a first approximation a homogenous distribution of DNA within the cell nucleus of 500 μm^3 volume, the amount of about 2 Mbp of DNA corresponds to an average cubical subvolume with approximately 0.5 μm side length. High-LET radiation is expected to induce multiple DSBs within such regions/subvolumes with high probability. We therefore implemented the quantification of the frequency of DSB within these subvolumes in the Local Effect Model (LEM) (*19*) and showed that it allows for the accurate prediction of the cellular response to high-LET radiation (*20, 21*).

In the present study, we investigate in more detail the implications of the chromatin loop approach for the shape of the photon dose-response curve itself. A new survival model emerges that is discussed in relationship to the conventional LQ-model and with respect to experimental photon dose-response curves. The main purpose of this investigation is to describe the principles of the model and to discuss its basic general features to allow testing of the capabilities of the model. Detailed comparison to experimental data and analysis of the corresponding model parameters will be treated elsewhere.

METHODS

The strategy for the derivation of the dose-response curve based on a mechanistic interpretation of DSB induction in megabase pair giant loops is presented below. In a first step, we restrict ourselves here to the description of *in vitro* cell survival, which does not imply that the approach is principally limited to this case. Furthermore, the stochastic nature of cell inactivation is represented by describing cell inactivation in terms of the number of the mean number of ''lethal events'' $\overline{N_{lethal}(D)}$ which are induced by irradiation with dose D. This number of lethal events is an average quantity representative for a large number of cells irradiated under the same conditions with dose D in such a way that the survival probability can be obtained by:

$$S(D) = e - \overline{N_{lethal}(D)} = e^{-\varepsilon(D)}. \quad (1)$$

where in the last step, the number of lethal events is identified with the effect ε and it is assumed that the actual number of lethal events is Poisson distributed. The basic assumption of the approach proposed here is that chromatin domains of approximately 2 Mbp size represent the key structure that determines the cellular radiation response. In agreement with the findings previously reported in refs. (*16*) and (*22*), we assume that the chromatin is organized in giant loops and are attached to the nuclear matrix at distinct points in approximately 2 Mbp distance. The response of a cell is expected to critically depend on the number of DSBs induced in each of its loop structures, as schematically illustrated in Fig. 1.

Two cases are distinguished here:

1. A single, individual DSB is induced in a loop. In this case, repair or rejoining of this loop is facilitated due to the fact that the damaged site can be accessed from both sides of the DSB for repair proteins. Furthermore, since the DNA ends are still close together, both nonhomologous end joining, as well as homologous recombination, are likely to be successful.
2. Two or more DSBs are induced in a loop. In this case, loose fragments can be produced by ''cutting out'' pieces of DNA from the loop. These fragments are no longer connected to the nuclear matrix and can easily diffuse away from its original position. Obviously, this case can be expected to represent a much more severe damage to the cell, since the DSB ends of the loop segments that remain attached to the nuclear matrix can be far apart, and the mechanism of nonhomologous end joining might fail. Two DSBs are sufficient to represent such a significant challenge to the cell, and inducing more than two DSBs does not contribute further to the complexity of the damage because only more fragments are produced.

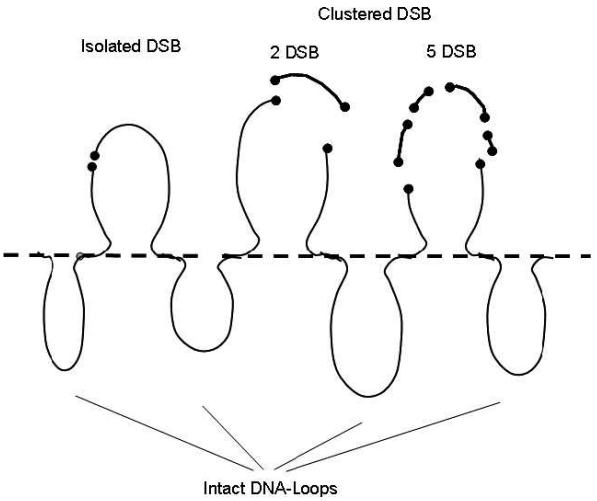

FIG. 1. Schematic representation of the chromatin giant loop structure [adapted from Yokota *et al.* (*16*)] and the consequence of isolated or clustered DSB within loops. For simplicity, only the essential topology of the chromatin loop structure is shown: the actual conformation of individual loops includes additional complicated 3-dimensional folding.

In line with the terminology introduced in refs. (*20*) and (*21*), these two cases are termed ''isolated DSB'' (iDSB) and ''clustered DSB'' (cDSB). This definition of clustered damage significantly differs from that used by Nikjoo *et al.* (*23*) and Ottolenghi *et al.* (*12*) as they focused on ''local'' cluster effects characterized by the combination of damages over distances of a few base pairs, which represents what has been termed ''locally multiply damaged sites'' by Ward (*24*). Our definition shares more similarities with approaches that are based on ''regionally multiply damaged sites'' due to the consideration of interaction of DSBs over significantly larger genomic distances, in line with experimental data indicating an excess of DNA fragments in the 10 kbp–1 Mbp size after ion irradiation (*25*).

Different effects can be attributed to the classes of iDSB and cDSB, respectively. In the first case, DSBs are likely to be repaired. The average number of lethal events of one iDSB is represented by ε_i. The average effect of one cDSB is assumed to be much more severe, represented by a number of lethal events ε_c and according to the higher severity $\varepsilon_c \gg \varepsilon_i$. Both ε_i and ε_c are smaller than 1 and can be regarded as a measure of the probability for an iDSB or a cDSB to be lethal, respectively.

The fact that ε_i and ε_c represent average quantities allows the treatment of all iDSBs and cDSBs in the same way. However, the effect of a single DSB may depend on the position in the genome where it occurs. For example, an iDSB in a single copy crucial gene might be lethal, whereas it might be well tolerated in a region of repetitive sequences. Similarly, the effect of a cDSB will depend on whether it contributes to a complex rearrangement or to a deletion. Therefore, the model can be considered as mechanistic only in the sense of the above mentioned average quantities, but not with respect to the full details of all steps involved in DNA damage processing.

If the average number of chromatin loops with isolated DSB is termed n_i and the average number of loops with complex DSB is termed n_c, the survival probability can be written as

$$S = e^{-(n_i\varepsilon_i + n_c\varepsilon_c)}. \quad (2)$$

Equation (2) represents the most general formulation of the approach and comprises the assumption that lesions in different chromatin loops are processed independently. For photon radiation, under certain simplifying assumptions, the number n_i and n_c can be easily obtained. Therefore, we assume that the yield of initial DSB is given by $\alpha_{DSB} = 30$ DSBs per Gy and per cell, independent of the cell type. This value reflects experimental data obtained for hard X rays and γ rays. In principle, the value can be easily adapted to e.g., higher values as observed for low energetic soft X rays (*26*). However, in the case of soft X rays, other factors such as significant attenuation have to be taken into account and we will analyze this in more detail separately.

Assuming a genome size S_G, this can be used to determine the number of DSBs per chromatin loop, assuming that all loops are characterized by the same size S_L. Thus, the whole genome contains $N_L = S_G/S_L$ loops, and the induction frequency of DSB is $Y_{Loop} = \alpha_{DSB}/N_L$ per Gy and per loop. From this average number, using Poisson statistics, the number of loops containing zero DSB (n_0), exactly one DSB (n_i) or two or more DSBs (n_c) can be determined as a function of the dose D from:

$$n_0 = N_L e^{-Y_{Loop}D}$$

$$n_i = N_L(Y_{Loop}D) \cdot e^{-Y_{Loop}D}$$

$$n_c = N_L - n_0 - n_i. \quad (3)$$

Inserting these values into Eq. (2) allows for the determination of the complete dose-response curve. An implicit assumption behind Eqs. (2) and (3) is that the number of lethal events as well as the number of isolated and clustered DSBs are Poisson distributed. However, for a given total number of DSBs, the corresponding possible numbers of iDSB and cDSB are not independent but are anticorrelated. Therefore, Eqs. (2) and (3) might not be strictly valid in particular at high doses. This becomes clear when the cell survival based on the assumptions of the GLOBLE is derived from a probabilistic view, where the parameters ε_i and ε_c are the probabilities for an iDSB or a cDSB to lead to cell death. Consequently, each isolated domain, e.g., does *not* lead to cell death with probability $(1 - \varepsilon_i)$, and the probability for a cell to not be killed by k_i of these is $(1 - \varepsilon_i)^{k_i}$. Hence, the survival can be calculated as

$$S = \sum_{k_i} \sum_{k_c} q(k_i, k_c)(1 - \varepsilon_i)^{k_i}(1 - \varepsilon_c)^{k_c}. \quad (4)$$

which immediately evaluates to Eq. (2) if and only if the probability function $q(k_i,k_c)$ for finding exactly k_i iDSB and k_c cDSB factorizes into two Poissonian distributions with average values n_i and n_c. This factorization is an approximation because iDSB and cDSB are not induced independently, but have a correlation by the total number of DSBs induced. We have thus performed a Monte Carlo evaluation of the survival according to Eq. (4) and compared the results of the Monte Carlo approach with the results of the analytical calculations based on Eqs. (2) and (3).

RESULTS

General Features

The general features of the model will be discussed based on the assumption of a genome size of $S_G = 6 \times 10^9$ bp and a chromatin loop size of $S_L = 2$ Mbp. The number of loops is thus $N_L = S_G/S_L = 3{,}000$ per cell. The corresponding numbers of isolated and clustered DSBs, respectively, are shown in Fig. 2 together with the resulting cell survival curve that is based on $\varepsilon_i = 0.0036$ and $\varepsilon_c = 0.18$, which represents a ratio of $R = \varepsilon_c/\varepsilon_i = 50$. As expected, the number of iDSBs rises almost linearly at lower doses. In contrast, the number of cDSBs is characterized by a highly nonlinear, initially quadratic increase with dose, which is due to the fact that simultaneous induction of at least 2 DSBs within the same loop is required to form a cDSB. This nonlinearity

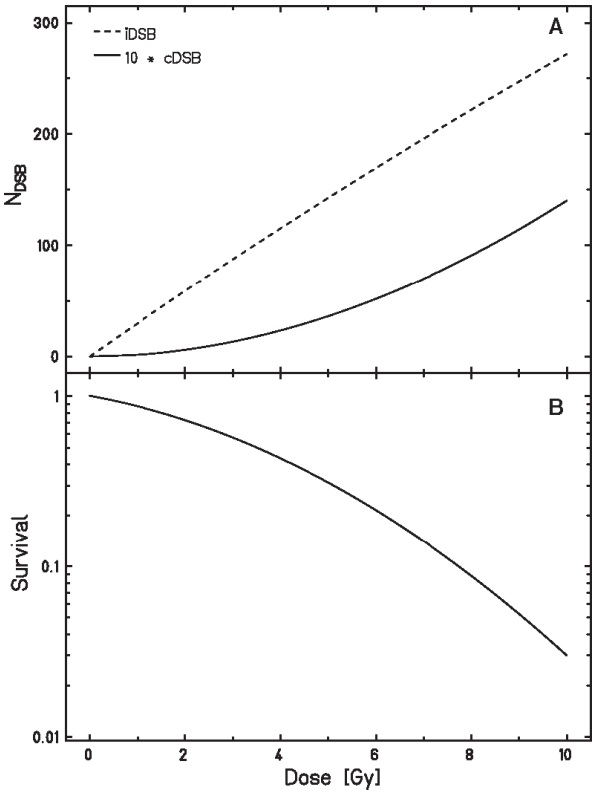

FIG. 2. Panel A: Number of isolated DSBs (iDSB) and clustered DSBs (cDSB) as a function of dose; the number of cDSB is scaled by a factor of 10 to allow a direct comparison of the dose-response curves for iDSB and cDSB. Input parameters: $S_G = 6 \times 10^9$ bp, $S_L = 2$ Mbp. Panel B: Corresponding cell survival curve based on $\varepsilon_I = 0.0036$ and $\varepsilon_c = 0.18$.

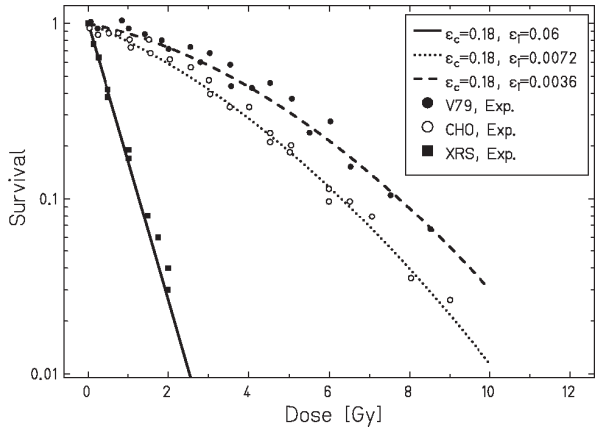

FIG. 3. Comparison of model predictions with experimental data reported by Weyrather *et al*. (*46*). Model parameters: $S_G = 6 \times 10^9$ bp, $S_L = 2$ Mbp; ε_i and ε_c as given in the legend for the different cell lines.

is also reflected in a trend toward a maximum of iDSBs at higher doses. As shown in Fig. 2B, the parameters chosen here represent a typical shape of *in vitro* cell survival curves.

When comparing different cell lines that differ mainly in their repair capacity, we assume that complex double-strand breaks (as defined in the Methods section in the sense of multiple damaged loops) are either unrepairable or misrepaired with a high probability for any cell type. This does not necessarily lead to a lethal event, as a certain level of remaining damage might be tolerable for a cell. In a first approximation, these assumptions translate into the hypothesis of a constant value for ε_c (that can be smaller than one), independent on the specific cell line. As a consequence, differences in sensitivity could then be fully attributed to the differences in the repair capability of isolated DSBs and expressed in the corresponding variation of the parameter ε_i. Figure 3 depicts survival curves based on $\varepsilon_c = 0.18$ and ε_i values of 0.06, 0.0072 and 0.0036, corresponding to ratios $R = \varepsilon_c/\varepsilon_i$ of 3, 25 and 50. The theoretical curves are compared to experimental data obtained for XRS, CHO and V79 cells, which represent cells of similar origin, but with different repair capacity; these data cover almost the full range of sensitivities found in larger sets of data for different cell lines.

The variation of R as a single variable allows for the correct reproduction of the overall difference in sensitivity as well as the transition from a significantly shouldered to an almost purely exponential survival curve. Note that the shoulder here occurs as a consequence of the enhanced lethality of cDSBs compared to iDSBs, along with the increasing abundance of cDSBs with increasing dose. The model therefore accounts for different levels of severity of DNA lesions in a very simple way.

To further investigate this impact of the R value on the shape of the dose-response curves, the corresponding slopes

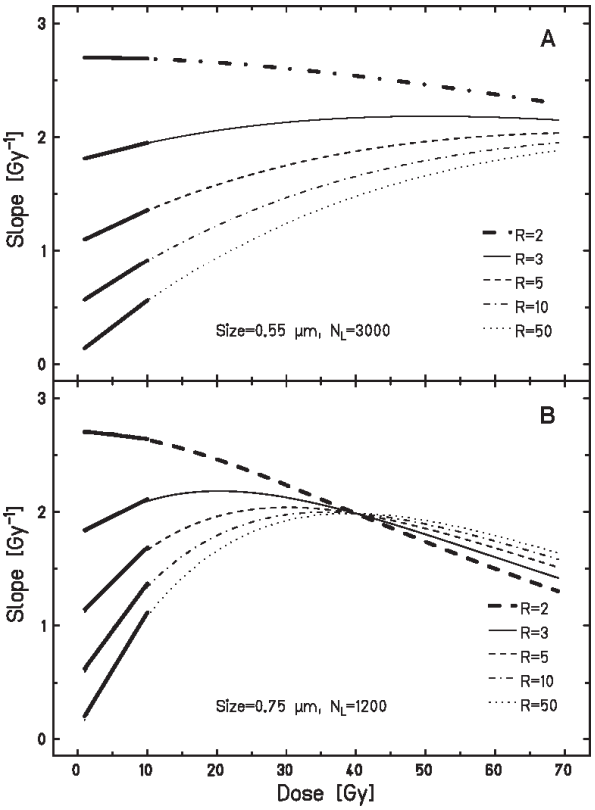

FIG. 4. Slopes of dose-response curves as a function of dose for $S_G = 6 \times 10^9$ bp, $\varepsilon_c = 0.18$, and $\varepsilon_i = \varepsilon_c/R$. Panel A: $S_L = 2$ Mbp, corresponding to $N_L = 3000$. Panel B: $S_L = 5$ Mbp, corresponding to $N_L = 1{,}200$. Straight black lines in the dose region 0–10 Gy represent linear fits to the low-dose region.

of the curves are plotted as a function of the dose over a large dose range up to 70 Gy in Fig. 4. Since the increase of this slope with the dose is a measure for the β term of the dose-response curve within the LQ model, it follows that cells characterized by a small R value are expected to show smaller β values compared to cells with higher R values. Interestingly, according to this model the slope is expected not to continuously increase, but to exhibit a maximum and a consequential decrease toward higher doses. The dose value, at which the maximum level is reached, depends on the assumption of both the R values as well as the loop size S_L and the loop DNA content, respectively. For larger loop sizes, the maximum is observed at lower doses compared to smaller loop sizes (Fig. 4B). For these loop sizes, at one specific dose at approximately 40 Gy, all curves cross and therefore become independent on ε_i. Note that the total systematics can be understood by a thorough investigation of Eq. (3).

Purely linear-quadratic behavior would correspond to straight lines, where the intersection with the y-axis and the slope correspond to the linear-quadratic parameters α and β,

TABLE 1
Ratio of the Predicted Mean Number of Lethal Events Derived from a Full Monte Carlo Simulation According to Eq. (4) Compared to the Analytical Description Based on Eqs. (2) and (3) for Different Combinations of Input Parameters ε_i and ε_c and a Constant Number of Loops $N_L = 3{,}000$

		$\overline{N_{Lethal,MC}}/\overline{N_{Lethal,analytical}}$	
ε_i	ε_c	10 Gy	50 Gy
0.05	0.2	1.005	1.030
0.05	0.1	1.003	1.014
0.05	0.5	1.019	1.177
0.01	0.2	1.003	1.031
0.10	0.2	1.008	1.040

respectively. As indicated by the fits to the dose region of up to 10 Gy, all curves shown in Fig. 4 can be approximated with sufficient accuracy by straight lines in this region. This indicates that the new approach is consistent with a linear-quadratic behavior in the low-dose region, and significant deviations are expected only in the dose region typically above 10 Gy. Therefore, the link between the new model and the LQ-approach will be analyzed in more detail in the following section.

Comparison to a Monte Carlo Based Approach

As mentioned in the Methods section, Eqs. (2) and (3) are based on the implicit assumption that n_i and n_c are Poisson distributed, which is an approximation due to the potential anticorrelation of n_i and n_c for a given number of DSBs, in particular at high doses. We therefore have compared results based on Eqs. (2) and (3) with a full Monte Carlo calculation based on Eq. (4), the results are summarized in Table 1. The deviation between the Monte Carlo calculation and the analytical description are completely negligible at 10 Gy. Additionally, at dose values of 50 Gy for four of the 5 parameter combinations, the deviations are below 5%. Only for the parameter combination using a comparably high value for ε_c, the difference is about 15% at 50 Gy. However, according to a preliminary analysis of a larger set of different survival curves, these high ε_c values are unlikely. Therefore, the analytical description using Eqs. (2) and (3) can be considered as sufficiently accurate approximation over the whole relevant dose range.

Relationship to the LQ Model

While in the widely used LQ model the effect ε is linked with dose via:

$$\varepsilon = \alpha D + \beta D^2 \tag{5}$$

in our new approach this relationship reads according to Eq. (2)

$$\varepsilon = n_i(D)\varepsilon_i + n_c(D)\varepsilon_c \tag{6}$$

where the dose dependence of n_i and n_c is nonlinear, c.f. Eq. (3).

From Eq. (5) it becomes evident that the linear and quadratic coefficients can be obtained from the limits of the first and second derivatives of the effect –lnS with respect to dose

$$\alpha = \lim_{D\to 0} \frac{d(-lnS)}{dD}; \qquad \beta = \frac{1}{2}\lim_{D\to 0} \frac{d^2(-lnS)}{dD^2}. \tag{7}$$

Applying these relationships to Eq. (6), we obtain transformation formulas between the LQ parameters and the parameter set (ε_i, ε_c) as:

$$\varepsilon_i = \frac{\alpha}{\alpha_{DSB}} \tag{8}$$

and

$$\varepsilon_c = 2\left(\frac{N_L\beta + \alpha_{DSB}\alpha}{\alpha_{DSB}^2}\right). \tag{9}$$

While the linear component α is directly linked to the lethality of iDSB, the probability for a cDSB to be lethal is given by a linear combination of both α and β.

Based on the hypothesis that the choice of a fixed, constant value of ε_c is consistent with experimental results, Eq. (9) suggests a coupling of the linear-quadratic parameters α and β:

$$\beta = \left(\frac{\varepsilon_c}{2} - \frac{\alpha}{\alpha_{DSB}}\right)\cdot\frac{\alpha_{DSB}^2}{N_L} = \frac{\varepsilon_c}{2}\frac{\alpha_{DSB}^2}{N_L} - \alpha\cdot\frac{\alpha_{DSB}}{N_L} = c_1 - c_2\alpha. \tag{10}$$

with constants c_1 and c_2.

This equation has important implications concerning the linear-quadratic parameters α and β and its correspondence to the parameters of the new model:

- When analyzing a large group of different cell lines that are characterized by different values α and β, it suggests a linear anticorrelation of β and α: i.e., the higher the α value, the lower the β value should be.
- Maximum values β_{max} should be achieved for cell lines exhibiting very small α values, and in the limit of $\alpha\to 0$ the value of β_{max} is fully characterized by the lethality of a cDSB, the overall DSB yield and the number of loops.

$$\frac{\beta_{max} = \varepsilon_c\alpha_{DSB}^2}{2N_L} \tag{11}$$

- The slope c_2 of the anticorrelation is solely dependent on the ratio of the DSB yield and the number of loops.

$$\frac{c_2 = \alpha^2 DSB}{N_L} \tag{12}$$

- A β value of zero is expected for the condition.

$$\alpha = \frac{\varepsilon_c\alpha_{DSB}}{2} \tag{13}$$

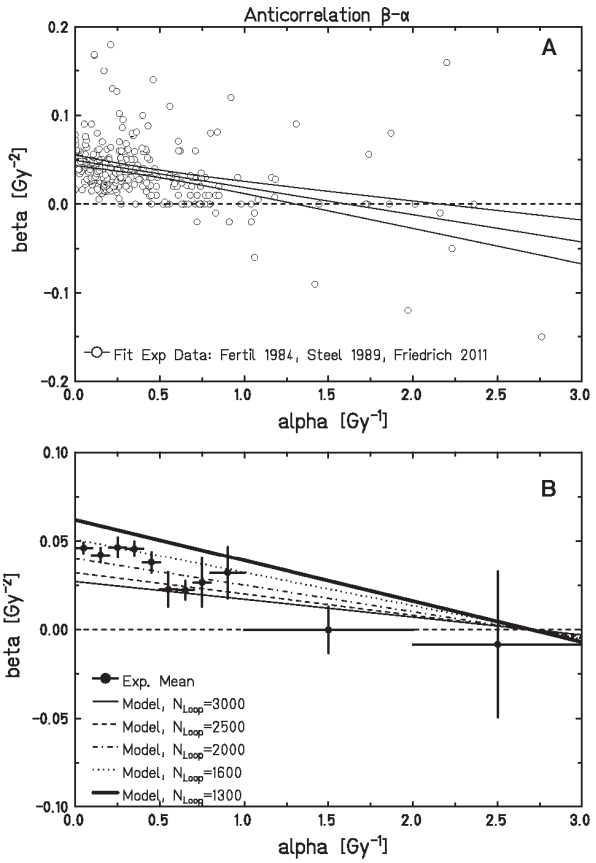

FIG. 5. Panel A: Anticorrelation of β and α as observed in experimental data reported by Fertil and Malaise (*27*), Steel *et al*. (*28*) and Friedrich *et al*. (*29*). Lines represent a linear fit with the corresponding 95% confidence intervals. Panel B: Comparison of predicted and experimentally observed anticorrelation of β and α for different values of N_L. Data points represent mean values over intervals indicated by the horizontal bars and the corresponding errors of the mean are represented by the vertical bars.

- Negative β values are predicted with the new model for high values of α. This feature will be discussed in more detail below.

The above mentioned parameters of $\varepsilon_c = 0.18$, $\alpha_{DSB} = 30$/Gy and $N_L = 3{,}000$ result in $\beta_{max} = 0.027$ Gy^{-2} and a slope c_2 of 0.01 Gy^{-1}, i.e., a β value of zero is expected for an α value of 2.7 Gy^{-1}.

To compare these model predictions to experimental data, we have compiled linear-quadratic parameters characterizing the sensitivity to high-energy photon radiation of more than 150 cell lines, as reported by Fertil and Malaise (*27*), Steel *et al*. (*28*) and Friedrich *et al*. (*29*). The experimental data are shown in Fig. 5A, together with a straight line fit and the corresponding 95% confidence intervals. Despite the large spread of the experimental data, there is a clear indication of an anticorrelation between β and α as suggested above, which is fully in line with the trend discussed by Fertil and Malaise (*27*). The corresponding fit parameters of Eq. (9) are $c_1 = 0.049 \pm 0.0029$ Gy^{-2} and $c_2 = 0.031 \pm 0.0048$ Gy^{-1}.

Figure 5B depicts the theoretically predicted anticorrelation as described above (thick line) in comparison to the mean values of β, averaged over α intervals as indicated by the horizontal bars, and the corresponding error of this mean values as indicated by the vertical bars.

The order of magnitude of the predicted values for β_{max}, as well as the slope c_2 are in reasonable agreement with the experimental data. However, with the parameters used for the comparison shown in Fig. 3, the average values for larger collections of different cell lines seem to be systematically underestimated. Based on Eq. (11), we have calculated the same anticorrelation for different loop numbers ranging from 3,000 down to 1,300; a value of about $N_L = 2{,}000$ is in the best agreement with the average values for the large data ensemble.

DISCUSSION

General Aspects

In this study, we present a simple approach to model cell survival curves after photon irradiation, which is based on the knowledge of the spatial distribution of initial DSB on the level of so called giant chromatin loops. These loops represent DNA length in the order of some Mbp and in geometrical terms regions of about 0.5 μm size. An essential feature of the model is the classification of DNA DSB in only two different classes, namely iDSB, representing loops containing exactly one DSB, or cDSB, representing loops which contain two or more DSBs. The same lethality is attributed to all cDSBs, independent of the actual total number of DSBs contained in the loop. Since the development of the new model was essentially motivated by the experimental results concerning the giant loops and only two classes of lesions are considered, we propose to call the new approach the Giant LOop Binary LEsion (GLOBLE) approach.

An important feature of the model is its compatibility with the LQ-approach in the low dose region. Here, Eqs. (8) and (9) allow for the unique translation of the linear-quadratic parameters α and β into the new parameters representing the lethality of isolated and clustered DSBs, respectively. At the same time, however, the model is able to represent the deviations from a pure LQ-behavior that is typically observed at high doses (*3, 4*). This refers to a less pronounced bending at high doses, which is in agreement with the trend predicted by the model as shown in Fig. 3. At present, this agreement has to be assessed as only qualitative. However, as the main purpose here is to describe the key features of our new approach, the full and detailed comparison to experimental

data is beyond the scope of the present paper and will be addressed in future projects.

Determination of Input Parameters

The GLOBLE approach is largely based on input parameters that can be determined experimentally. The initial yield of DSBs, α_{DSB}, has been measured for a wide variety of cell lines, and there is general agreement that this initial yield of DSB is largely independent on the specific cell line under investigation, see e.g. (*30*). The size of chromatin loops has also been determined experimentally to be in the order of 1–2 Mbp (*22*), and different cell lines are characterized by similar loop sizes in a comparably narrow range. However, it should be taken into account that using a single constant value for the loop size possibly represents an oversimplification. Therefore, analysis of the impact of an underlying loop size distribution represents an important next step for the application of the model. However, it remains open at the moment how accurately this distribution can be determined, and reasonable assumptions about the size distribution might replace the corresponding experimental information in a first step.

The link between γ-H2AX foci and chromatin loops as discussed by Rogakou *et al.* (*18*) could help to develop experimental methods for the measurement of the size distribution. If actual chromatin loops can be identified with the regions of γ-H2AX phosphorylation, measurements of foci size as reported in ref. (*31*) can give useful information about the loop size distribution.

The relevance of large scale chromatin organization for the understanding of radiation effects is also emphasized by other model approaches. Eidelman and Andreev (*32*) use subunits of 1.3–3.3 Mbp for modeling interphase chromosomes. Friedland *et al.* (*33*) assume rosette-like structures of about 0.5 Mbp size, composed of smaller loops with approximately 70 kbp each. In a more recent article, Friedland *et al.* (*34*) reported that a structure of the cell nucleus composed of approximately 6,000 subunits consisting of rosette-like structures based on multiple 100 kbp loops, corresponding to a DNA content in the order of Mbp for each subunit. A similar approach is followed by Nikjoo and Girard (*35*), subdividing chromosome domains into ''factories'' of approximately Mbp size, that also consist of rosette-like structures composed of multiple loops of approximately 100 kbp size. Ponomarev and Cucinotta (*36*) use a loop size of 120 kbp without specifically assuming higher order structures based on multiples of these loops. However, the approaches mentioned above have been mainly developed for the modeling of initial DNA damage distributions, and none of them has been applied to predict cell survival after photon radiation. According to the concept presented in this paper, correlation of DSBs on the 100 kbp scale would not be sufficient to explain the shouldered shape of the dose-response curves, and thus the results are clearly in favor of the relevance of Mbp structures.

The length scale corresponding to Mbp structures, which is in the order of micrometers, is also fully in line with the typical interaction distances discussed in the framework of chromosome aberration induction, as discussed in more detail below. Whether or not the organization of these Mbp structures as a random walk or a rosette-like structure would make a difference in respect to the model remains to be elucidated.

Anticorrelation of β and α and of Negative β Values

Mechanistically, the decrease of the curvature of the dose-response curve toward higher doses can be explained within the GLOBLE framework by the local ''effect saturation'' within individual loops. As described above, the same lethality ε_c is attributed to all types of cDSBs independent of the actual number of DSBs induced in the loop. Therefore, the highest efficiency is expected if exactly 2 DSBs are induced within a loop. If more than 2 DSBs are induced, the relative contribution to lethality per DSB is correspondingly reduced. This feature also explains the anticorrelation between β and α as shown in Fig. 5.

As mentioned above, we hypothesized that the variation of sensitivity could be mainly attributed to the variation of the lethality of iDSBs, whereas it is assumed that cDSBs should have the same lethality for all cell lines in a first approximation. The onset of saturation effects, i.e., the drop of the incremental increase of lethal events per dose increment, critically depends on the difference of lethalities between iDSBs and cDSBs. If iDSBs are much less lethal than cDSBs (i.e., $\varepsilon_i \ll \varepsilon_c$), saturation will occur only if, on average more than 2 DSBs are induced per loop. If, however, iDSBs are similarly lethal to cDSBs (i.e., $\varepsilon_i \approx \varepsilon_c$), as in the case of XRS cells, then saturation might already occur in the case of 2 DSBs, and thus the cDSB lethality per DSB is also reduced.

This effect is compatible in principle with a negative bending of the dose-response curve that corresponds to negative β values. However, this has no meaningful interpretation in the framework of the standard LQ-model. The GLOBLE approach thus represents a framework for an explanation of such an unexpected shape of dose-response curves as indicated by the negative β values in Fig. 5, and as discussed in depth by Denekamp *et al.* (*37*).

The Role of Damage Interaction

As in many other models, the curvature of the dose-response curve can be traced back in the GLOBLE approach to the accumulation and interaction of damage in the most general sense. However, no assumptions concerning a physical interaction are made here because the individual DSB of a cDSB do not necessarily have to come close together. The mere existence of 2 or more DSBs at the same time in the same loop is assumed to lead to a higher lethality due to the assumed less efficient repair of such damage.

Additionally, since interaction of DSBs over micrometer dimension is considered, the GLOBLE approach is thus consistent with experimental results that indicate the relevance of that length scale for the interpretation of chromosome aberration data (*38*). This also was the origin of the microdosimetric approach, that specifically investigates energy deposition in volumes of micrometer dimensions (*39*).

Consistent with the terminology discussed by Bedford (*38*), iDSB can be considered to be similar to the class of sublethal damage, whereas cDSB share similarity with the class of potentially lethal damage. However, in our case, both classes cannot be strictly distinguished, and are attributed only to different levels of potential lethality.

Evidence for Two Classes of Damage

An important feature of the model is that only two classes of damages are distinguished. At present, this classification is based on the hypothesis that an isolated DSB within a chromatin loop is easier to repair compared to clustered damages that consist of multiple DSBs within a loop. Based on rejoining studies, it has been proposed that the kinetics of the process can be characterized by two different time constants: a fast and a slow component. In line with the findings reported by Johnston *et al*. (*40*), it is tempting to identify the fraction of fast repairable damage with the iDSB and the fraction of slowly repairable damage with the cDSB.

One can easily estimate using Eq. (3) and the constants given above that a dose of 45 Gy [which was used for the rejoining studies reported in (*41*)] results in about 860 iDSBs and 225 cDSBs. With an average multiplicity of slightly above two at this dose, these 225 cDSBs represent a total amount of approximately 450 DSBs. If individual DSBs within a cDSB are considered to be resolvable in the assay used to measure rejoining, the iDSB thus represent a fraction of approximately 65% of the total damage induced, whereas the cDSB represent a fraction of 35% of the damage induced. The order of magnitude of these estimated fractions is in reasonable agreement with data reported by Nuñez *et al*. (*41*), indicating that for a set of 6 different cells lines, the fraction of damage attributable to the slow rejoining process is in the order of 20–30%. Similarly, Dahm-Daphi and Dikomey (*42*) found a fraction of 22 $\pm$ 5% at 60 Gy, and Stenerlöw *et al*. (*43*) report fractions of 17–45% after 100 Gy for 3 different cell lines. The value reported by Stenerlöw *et al*. (*44*), where the fraction of slow repair after 100 Gy was found to be only 7%, seems to be exceptionally low in this respect.

In contrast, when using more sensitive assays such as the γ-H2AX assay that requires doses of only a few Gy, a slow component of DSB removal is almost undetectable within experimental uncertainties (*45*). This result is in line with estimates using Eq. (3) and results in a fraction of less than 5% cDSB for doses below 5 Gy.

Kinetic Extension of the GLOBLE Approach

The possible identification of iDSB and cDSB with the fast and slow component of rejoining immediately suggests a kinetic extension of the GLOBLE approach. In principle, this can be easily implemented by using the appropriate differential equations, finally allowing the application of the approach to model e.g., dose-rate effects. First tests have already been carried out in this direction.

Potential Applications in the Framework of the Local Effect Model

The Local Effect Model (LEM) in its current implementation (*20, 21*) is based on the transfer of the known photon dose-response curve to derive the dose response to high-LET radiation. For the application of the model, the photon dose-response curve has to be known up to very high doses in the order of 100 Gy because of the extremely high local energy deposition in the center of a particle track. Since these data are not directly experimentally accessible, a simple approximation is used in the LEM, based on the assumption that the linear-quadratic shape of the dose-response curve turns into a purely linear shape at doses above a certain threshold dose D_t. This approach is in line with the independently developed approach as reported by Astrahan *et al*. (*5*) which is based on experimental findings. Since the new GLOBLE approach presented here predicts a continuous transition toward shallower slopes at high doses, it could allow a more accurate description of the dose-response curve that is based on parameters solely determined in the low-dose region according to Eqs. (8) and (9). The GLOBLE representation of the photon dose-response curve will thus be tested in the LEM framework as an alternative to the currently used linear-quadratic-linear approach.

Furthermore, the extrapolation to these extremely high doses might not be necessary since a similar approach to the one presented here could be directly used for dose deposition patterns and their corresponding spatial DSB distributions as induced by high-LET radiation. As soon as the number of iDSBs and cDSBs are known for any type of radiation quality, the same parameters ε_i and ε_c that represent the photon dose-response curve can be used to derive the corresponding survival level after light or heavier ion irradiation. This would allow for the description of the dose-response curve based solely on the knowledge of the number of iDSBs and cDSBs that are independent of the radiation quality that lead to these numbers. In mathematical terms, this corresponds to the assumption that Eq. (2) is universally valid for any radiation quality.

SUMMARY AND CONCLUSION

Starting from only a few assumptions, it was possible to set up the GLOBLE model as a new survival model that explicitly distinguishes between the effects related to

simple, isolated DSB and clustered DSB damage to the DNA, respectively. The spatial extent relevant for more severe lesions of the order of half a micrometer (corresponding to ~2 Mbp) has been identified in microdosimetry, the analysis of chromosomal aberrations and in γ-H2AX staining of DNA lesions. This scale now can be interpreted with the concept of chromatin giant loops in a biological context. Though being very simple, the GLOBLE can conveniently explain several properties of cell survival after photon irradiation, such as the systematics of survival of repair-deficient mutants and their corresponding wild-type mother cell lines, or the observed negative correlation between the linear and quadratic coefficients of the LQ model. This is promising as the latter is not an inherent feature of conventional survival models. However, in the same way we are aware that the pathways of DNA damage recognition and repair are very complex, the current implementation of the GLOBLE represents a simplification of the underlying processes. For example, we do not distinguish here between nonhomologous end-joining (NHEJ) and homologous recombination (HR), which differ in their fidelity to correctly repair DSBs. Nevertheless, there is room to extend the model in this direction by attributing different average numbers of lethal events to iDSBs processed by NHEJ and HR, respectively.

However, such extensions can only be addressed after thoroughly testing the current implementation, where the primary goal would be to check whether there is a consistent set of constants (such as the loop domain size) that allow consistent description of survival data. Another important further step will be the extension to high-LET charged particle radiation, where the abundance of cDSB is enhanced due to the extremely inhomogeneous localized dose distribution in micrometer dimensions. Finally, for applications such as radiotherapy (with photons or high-LET radiation) the GLOBLE might be of interest because it seems to overcome the shortcomings of the conventionally used LQ model at high doses.

Received: February 3, 2012; accepted: May 11, 2012; published online: September 21, 2012

REFERENCES

1. Barendsen GW. Dose fractionation, dose rate and iso-effect relationships for normal tissue responses. Int J Radiat Oncol Biol Phys 1982; 8:1981–97.
2. Dale RG. The 1989 James Kirk memorial lecture. The potential for radiobiological modelling in radiotherapy treatment design. Radiother Oncol 1990; 19:245–55.
3. Garcia LM, Wilkins DE, Raaphorst GP. Alpha/beta ratio: A dose range dependence study. Int J Radiat Oncol Biol Phys 2007; 67:587–93.
4. Skarsgard LD, Skwarchuk MW, Wouters BG, Durand RE. Substructure in the radiation survival response at low-dose in cells of human tumor cell lines. Radiat Res 1996; 146:388–98.
5. Astrahan M. Some implications of linear-quadratic-linear radiation dose-response with regard to hypofractionation. Med Phys 2008; 35:4161–72.
6. Guerrero M, Li XA. Extending the linear-quadratic model for large fraction doses pertinent to stereotactic radiotherapy. Phys Med Biol 2004; 49:4825–35.
7. Lind BK, Persson LM, Edgren MR, Hedlof I, Brahme A. Repairable-conditionally repairable damage model based on dual Poisson processes. Radiat Res 2003; 160:366–75.
8. Wang JZ, Huang Z, Lo SS, Yuh WT, Mayr NA. A generalized linear-quadratic model for radiosurgery, stereotactic body radiation therapy, and high-dose rate brachytherapy. Sci Transl Med 2010; 2:39–48.
9. Brenner DJ, Ward JF. Constraints on energy deposition and target size of multiply damaged sites associated with DNA double-strand breaks. Int J Radiat Biol 1992; 61:737–48.
10. Holley WR, Chatterjee A. Clusters of DNA induced by ionizing radiation: formation of short DNA fragments. I. Theoretical modeling. Radiat Res 1996; 145:188–99.
11. Nikjoo H, O'Neill P, Terrissol M, Goodhead DT. Quantitative modelling of DNA damage using Monte Carlo track structure method. Radiat Environ Biophys 1999; 38:31–8.
12. Ottolenghi A, Merzagora M, Tallone L, Durante M, Paretzke HG, Wilson WE. The quality of DNA double-strand breaks: a Monte Carlo simulation of the end-structure of strand breaks produced by protons and alpha particles. Radiat Environ Biophys 1995; 34:239–44.
13. Rydberg B. Clusters of DNA damage induced by ionizing radiation: formation of short DNA fragments. II. Experimental detection. Radiat Res 1996; 145:200–09.
14. Ostashevsky J. A polymer model for the structural organization of chromatin loops and minibands in interphase chromosomes. Mol Biol Cell 1998; 9:3031–40.
15. Sachs RK, van den Engh G, Trask B, Yokota H, Hearst JE. A random-walk/giant-loop model for interphase chromosomes. Proc Natl Acad Sci USA 1995; 92:2710–4.
16. Yokota H, van den Engh G, Hearst JE, Sachs RK, Trask BJ. Evidence for the organization of chromatin in megabase pair-sized loops arranged along a random walk path in the human G0/G1 interphase nucleus. J Cell Biol 1995; 130:1239–49.
17. Johnston PJ, MacPhail SH, Banath JP, Olive PL. Higher-order chromatin structure-dependent repair of DNA double-strand breaks: factors affecting elution of DNA from nucleoids. Radiat Res 1998; 149:533–42.
18. Rogakou EP, Pilch DR, Orr AH, Ivanova VS, Bonner WM. DNA double-stranded breaks induce histone H2AX phosphorylation on serine 139. J Biol Chem 1998; 273:5858–68.
19. Scholz M, Kellerer AM, Kraft-Weyrather W, Kraft G. Computation of cell survival in heavy ion beams for therapy. The model and its approximation. Radiat Environ Biophys 1997; 36:59–66.
20. Elsasser T, Weyrather WK, Friedrich T, Durante M, Iancu G, Kramer M, et al. Quantification of the relative biological effectiveness for ion beam radiotherapy: direct experimental comparison of proton and carbon ion beams and a novel approach for treatment planning. Int J Radiat Oncol Biol Phys 2010; 78:1177–83.
21. Friedrich T, Scholz U, Elsasser T, Durante M, Scholz M. Calculation of the biological effects of ion beams based on the microscopic spatial damage distribution pattern. Int J Radiat Biol 2012; 88:103–7.
22. Johnston PJ, Olive PL, Bryant PE. Higher-order chromatin structure-dependent repair of DNA double-strand breaks: modeling the elution of DNA from nucleoids. Radiat Res 1997; 148:561–7.
23. Nikjoo H, O'Neill P, Wilson WE, Goodhead DT. Computational approach for determining the spectrum of DNA damage induced by ionizing radiation. Radiat Res 2001; 156:577–83.
24. Ward JF. The complexity of DNA damage: relevance to biological consequences. Int J Radiat Biol 1994; 66:427–32.
25. Radulescu I, Elmroth K, Stenerlow B. Chromatin organization

contributes to non-randomly distributed double-strand breaks after exposure to high-LET radiation. Radiat Res 2004; 161:1–8.

26. de Lara CM, Hill MA, Jenner TJ, Papworth D, O'Neill P. Dependence of the yield of DNA double-strand breaks in Chinese hamster V79-4 cells on the photon energy of ultrasoft X rays. Radiat Res 2001; 155:440–8.

27. Fertil B, Malaise EP. Intrinsic radiosensitivity of human cell lines is correlated with radioresponsiveness of human tumors: analysis of 101 published survival curves. Int J Radiat Oncol Biol Phys 1985; 11:1699–707.

28. Steel GG, McMillan TJ, Peacock JH. The radiobiology of human cells and tissues. In vitro radiosensitivity. The picture has changed in the 1980s. Int J Radiat Biol 1989; 56:525–37.

29. Friedrich T, Scholz U, Elsässer T, Durante M, Scholz M. Systematic analysis of RBE and related quantities using a database of cell survival experiments with ion beam irradiation. J Radiat Res 2012, submitted.

30. Foray N, Priestley A, Alsbeih G, Badie C, Capulas EP, Arlett CF, et al. Hypersensitivity of ataxia telangiectasia fibroblasts to ionizing radiation is associated with a repair deficiency of DNA double-strand breaks. Int J Radiat Biol 1997; 72:271–83.

31. Ibanez IL, Bracalente C, Molinari BL, Palmieri MA, Policastro L, Kreiner AJ, et al. Induction and rejoining of DNA double strand breaks assessed by H2AX phosphorylation in melanoma cells irradiated with proton and lithium beams. Int J Radiat Oncol Biol Phys 2009; 74:1226–35.

32. Eidelman Y, Andreev SG. Biophysical study of the globular organisation of interphase chromosomes. Radiat Prot Dosim 2002; 99:217–8.

33. Friedland W, Jacob P, Bernhardt P, Paretzke HG, Dingfelder M. Simulation of DNA damage after proton irradiation. Radiat Res 2003; 159:401–10.

34. Friedland W, Dingfelder M, Kundrat P, Jacob P. Track structures, DNA targets and radiation effects in the biophysical Monte Carlo simulation code PARTRAC. Mutat Res 2011; 711:28–40.

35. Nikjoo H, Girard P. A model of the cell nucleus for DNA damage calculations. Int J Radiat Biol 2012; 88:87–97.

36. Ponomarev AL, Cucinotta FA. Chromatin loops are responsible for higher counts of small DNA fragments induced by high-LET radiation, while chromosomal domains do not affect the fragment sizes. Int J Radiat Biol 2006; 82:293–305.

37. Denekamp J, Whitmore GF, Jeggo P. Biphasic survival curves for XRS radiosensitive cells: subpopulations or transient expression of repair competence? Int J Radiat Biol 1989; 55:605–17.

38. Bedford JS. Sublethal damage, potentially lethal damage, and chromosomal aberrations in mammalian cells exposed to ionizing radiations. Int J Radiat Oncol Biol Phys 1991; 21:1457–69.

39. Rossi HH, Zaider M. Elements of microdosimetry. Med Phys 1991; 18:1085–92.

40. Johnston PJ, Bryant PE. A component of DNA double-strand break repair is dependent on the spatial orientation of the lesions within the higher-order structures of chromatin. Int J Radiat Biol 1994; 66:531–6.

41. Nunez MI, Villalobos M, Olea N, Valenzuela MT, Pedraza V, McMillan TJ, et al. Radiation-induced DNA double-strand break rejoining in human tumour cells. Br J Cancer 1995; 71:311–6.

42. Dahm-Daphi J, Dikomey E. Rejoining of DNA double-strand breaks in X-irradiated CHO cells studied by constant- and graded-field gel electrophoresis. Int J Radiat Biol 1996; 69:615–21.

43. Stenerlow B, Carlsson J, Blomquist E, Erixon K. Clonogenic cell survival and rejoining of DNA double-strand breaks: comparisons between three cell lines after photon or He ion irradiation. Int J Radiat Biol 1994; 65:631–9.

44. Stenerlow B, Hoglund E, Carlsson J, Blomquist E. Rejoining of DNA fragments produced by radiations of different linear energy transfer. Int J Radiat Biol 2000; 76:549–57.

45. Leatherbarrow EL, Harper JV, Cucinotta FA, O'Neill P. Induction and quantification of gamma-H2AX foci following low and high-LET-irradiation. Int J Radiat Biol 2006; 82:111–8.

46. Weyrather WK, Ritter S, Scholz M, Kraft G. RBE for carbon track-segment irradiation in cell lines of differing repair capacity. Int J Radiat Biol 1999; 75:1357–64.

7.3 Article 3: Modeling the radiation action of ultrasoft X-rays

RADIATION RESEARCH **181**, 485–494 (2014)
0033-7587/14 $15.00

DOI: 10.1667/RR13518.1

Modeling Cell Survival after Irradiation with Ultrasoft X Rays using the Giant Loop Binary Lesion Model

Thomas Friedrich,[a] Marco Durante[a,b] and Michael Scholz[a,1]

[a] *GSI Helmholtzzentrum für Schwerionenforschung (GSI), Department of Biophysics, Darmstadt, Germany; and* [b] *Technische Universität Darmstadt, Darmstadt, Germany*

Friedrich, T., Durante, M. and Scholz, M. Modeling Cell Survival after Irradiation with Ultrasoft X Rays using the Giant Loop Binary Lesion Model. *Radiat. Res*. 181, 485–494 (2014).

We present an application of the Giant LOop Binary LEsion (GLOBLE) model to the case of cell killing after irradiation with ultrasoft X rays. The model is based on the analysis of DSB clustering on the level of chromatin organization on a megabase pair length scale; it distinguishes between two classes of damage, characterized by either an isolated, single DSB (iDSB) or multiple, clustered DSB (cDSB) within a single giant loop. These corresponding fractions of iDSB and cDSB depend on the total number of DSB and thus on the dose as well as the yield of DSB per Gy per cell. Based on the increased yield of DSB with decreasing photon energy as reported in the literature, we demonstrate that according to the model this increased yield of DSB is sufficient to explain the increased RBE of ultrasoft X rays. Further assumptions as e.g., a higher lethality of individual DSB induced by ultrasoft X rays compared to high-energy photons, which might be a consequence of the more localized energy deposition, seem not to be a prerequisite. Since the model is also suitable to take into account local dose variations within the cell nucleus, we further analyze the impact of attenuation of low-energy photon radiation when penetrating a cell layer. We show that the inhomogenous dose distribution resulting from attenuation further increases the effectiveness and particularly affects the beta-term of the corresponding dose response curve. Finally, we compare and discuss the mechanisms of increased RBE as observed after ultrasoft X-ray irradiation with those observed after high-LET ion beam irradiation.

INTRODUCTION

Precise knowledge and characterization of the effectiveness of different radiation qualities is of utmost importance for applications in radiation protection as well as in radiation therapy. Biophysical models represent an important tool to test hypotheses about mechanisms of radiation action and are also of high practical relevance for applications e.g., in treatment planning in ion beam radiotherapy (*1, 2*).

Thorough validation of models is required for this type of application because of the precision criteria that typically have to be fulfilled in this field. Based on ideas originally implemented to model high-LET radiation in the framework of the Local Effect Model (LEM) (*3, 4*) we recently demonstrated that the general features of photon dose-response curves can be predicted by the spatial pattern of initial DSB induced by ionizing radiation (*5*). This pattern is characterized with respect to a level of chromatin organization called ''giant loops'' (*6–9*), which represent DNA segments of approximately 2 Mbp length attached to the nuclear matrix. We define two types of DSB, the first is a single, isolated DSB (iDSB) induced in the giant loop, and the second is a clustered DSB (cDSB), where two or more DSBs are induced in the giant loop. Assuming that due to their higher complexity cDSB represent a more severe damage than iDSB, we assigned different lethalities to the classes of iDSB and cDSB, respectively. We showed that essential features of photon dose-response curves e.g., the linear-quadratic behavior at low and intermediate doses as well as a transition to more straight dose-response curves at higher doses can be predicted by this classification of DSB (*5*). The application of the model, termed the ''Giant LOop Binary LEsion'' model (GLOBLE), to the case of photon radiation requires the assumption of a random distribution of DSBs within the critical target, i.e., the cell nucleus; and this condition is clearly fulfilled for high-energy photon radiation such as 250 kV X rays or ^{60}Co γ rays.

Ultrasoft X rays represent a further test case for the model, since they exhibit an increased effectiveness as compared to high-energy photons [e.g. see refs. (*10–12*)]. Potential mechanisms of this higher effectiveness might be due to the higher yield of DSB and/or to the local heterogeneity of the dose distribution because of the significant attenuation of low-energy photon radiation.

In this article we therefore analyze to what extent the GLOBLE model is consistent with the experimental results

[1] Address for correspondence: GSI Helmholtzzentrum für Schwerionenforschung, Dept. of Biophysics, Planckstrasse 1, D-64291 Darmstadt, Germany; e-mail: m.scholz@gsi.de.

obtained for cell killing after ultrasoft X-ray irradiation. Furthermore we use the model to specifically investigate the role of the target shape and geometry, which has been proposed to influence the biological effectiveness observed after ultrasoft X-ray irradiation. In addition, we discuss the potential differences between the RBE effects for ultrasoft X rays and charged particle radiation. Finally we compare the GLOBLE model with other models developed to explain the effects of ultrasoft X rays. The main purpose of this investigation is to show a proof-of-principle and to discuss the basic, general features of the model; a thorough systematic comparison to the numerous reports of experimental data and modeling approaches would be beyond the scope of this contribution.

METHODS

Basics of the GLOBLE Approach

The basic assumption of the approach which has been previously published by Friedrich *et al*. (*5*) is that chromatin loops of approximately 2 Mbp size represent the key structure determining the cellular radiation response in agreement with the findings reported by others (*6–9, 13*). In this model the response of a cell is therefore expected to critically depend on the number of DSBs induced in such a loop structure.

The average number of lethal events assigned to iDSB and cDSB is represented here by ε_i and ε_c, respectively. According to the higher severity of cDSB compared to iDSB, in general $\varepsilon_c >> \varepsilon_i$. As it turns out, both ε_i and ε_c are smaller than one and can be regarded as the probability for an iDSB or a cDSB to be lethal, respectively.

According to the definition of cDSB, dose-rate effects are expected to significantly affect the consequences of the time sequence in which DSB are induced, since repair of the first DSB might have happened before the second DSB is induced. These dose-rate effects have been neglected for the analysis shown here; however, we have demonstrated recently that GLOBLE in principle is well suited to reflect the dose-rate dependence of radiation effects (*14*).

If the average number of chromatin loops with isolated DSB is termed n_i and the average number of loops with clustered DSB is termed n_c, the survival probability can be written as:

$$S = exp^{-(n_i\varepsilon_i + n_c\varepsilon_c)} \tag{1}$$

Eq. (1) represents the general formulation of the approach and comprises the assumption of independence of the loops, i.e., the lethality of lesions in one loop is fully determined by intra-domain effects and thus by the number of initial DSBs induced within an individual loop and it does not explicitly depend on the damages induced in the neighboring domains. This does not exclude the interaction of DNA ends from different domains and thus e.g., the formation of chromosome aberrations as a consequence of misrepair or misrejoining processes. Lethal events as the result of domain interactions are comprised in the mean values ε_i and ε_c.

For photon radiation with a homogenous dose distribution, the numbers n_i and n_c can be obtained from the initial DSB yield. Therefore, we assume that for hard X rays and γ rays the yield is given by $\alpha_{DSB} = 30$ DSB per Gy and per cell, consistent with experimental data reported elsewhere (*15, 16*) and independent of the cell type.

Assuming a genome size S_G, this can be used to determine the number of DSBs per chromatin loop, assuming that all loops are characterized by the same size S_L. Then, the whole genome contains $N_L = S_G/S_L$ giant loops, and the induction frequency per loop is $Y_{Loop} = \alpha_{DSB}/N_L$ per Gy. From this average number, using the Poisson statistics the average number of loops in a cell nucleus containing zero DSB (n_0), exactly one DSB (n_i) or two or more DSB (n_c) are determined as a function of the dose from:

$$n_0 = N_L \exp^{-Y_{Loop}D}$$

$$n_i = N_L(Y_{Loop}D) \cdot \exp^{-Y_{Loop}D}$$

$$n_c = N_L - n_0 - n_i \tag{2}$$

Inserting these into Eq. (1) allows determining the complete dose response curve.

As discussed in ref. (*5*), the assumption of independent Poisson distributions for n_i an n_c leading to Eq. (1) represents an approximation, since actually, at least at very high doses, they are correlated. However, as demonstrated by a comparison with a Monte Carlo approach, the approximation underlying Eq. (1) is accurate enough for the dose range to be discussed here.

Adaptation to Ultrasoft X Rays

Essentially three aspects have to be considered for the application of the GLOBLE model to ultrasoft X rays:

- The increased yield of DSB induction
- The attenuation of X rays within the target
- The target geometry

The increased yield can be represented by the corresponding RBE value, i.e.,

$$\alpha_{DSB,UX} = RBE_{UX} \cdot \alpha_{DSB,\gamma} \tag{3}$$

where $\alpha_{DSB,US}$ and $\alpha_{DSB,\gamma}$ denote the yield of initial DSB after ultrasoft X and γ irradiation, respectively. Qualitatively, the increased yield can be explained by the pronounced clustering of ionization events as a consequence of the low energy and thus the limited range of photoelectrons emitted by ultrasoft X rays.

According to the basic assumptions of the model, the lethalities attributed to iDSB and cDSB, respectively, are hypothesized to be cell specific constants and should be independent of the radiation type.

Attenuation of ultrasoft X rays within the target at depth x is described by the attenuation length λ_{UX}:

$$D(x) = e^{-x/\lambda_{UX}} D(0) \tag{4}$$

In contrast to high-energy photon radiation, where at least for thin monolayers of cells attenuation can be neglected, in the case of ultrasoft X rays the target geometry can – depending on the attenuation length – affect the local dose distribution within the target and thus the expected effect. Therefore, the target thickness has to be specified, and in general we assume a cylindrical shape of the cell nucleus with given volume V_{Nucl}, radius R_{Cyl} and height H_{Cyl}. For comparison, we also consider a spherical shape with the same volume V_{Nucl}, but correspondingly different radius R_{Sph}. Dose values are always given as mean dose values across the thickness of the target, i.e., the cell nucleus. Additional layers of cytoplasm are not considered and taking into account that these thin layers are more or less symmetrical above and below the cell nucleus, in a first approximation the mean dose across the assumed nuclear thickness should represent the mean dose across the whole cell.

Along with the decrease of the local dose with penetration depth due to attenuation, the probability to induce iDSB or cDSB varies with depth accordingly. Therefore, the target volume is virtually divided into slices with 0.5 μm thickness, corresponding to the typical dimension of the volume covered by a giant loop. Depending on the target geometry, the number of loops contained in each slice is determined and the numbers n_i and n_c determined separately for each slice according to the local dose deposited in that slice. The total effect

TABLE 1
Characteristic Features of Different Ultrasoft X Rays with Respect to DSB Induction [taken from de Lara (*10*)] and Attenuation [taken from Nikjoo and Lindborg (*36*)]

Radiation quality	Energy (keV)	RBE_{DSB} (from de Lara *et al.*)	λ_{UX} (μm^{-1})
C-K	0.28	2.7	180
Al-K	1.49	1.9	7.9
Ti-K	4.55	1.4	1.9

is then calculated by summing up the contribution of lethal events as defined by Eq. (1) from all slices.

RESULTS

Comparison to Experimental Data

The model requires the DSB yield as input for the prediction of cell killing. de Lara *et al*. have measured DSB induction and cell killing simultaneously (*10*); this data set is thus ideally suited to test the GLOBLE model. The increased yield of DSB is implemented by assigning an RBE for DSB induction according to the data published by de Lara *et al*. and the parameters are summarized in Table 1. The RBE values for DSB induction are assumed to be valid for all cell lines. Since de Lara *et al*. performed their experiments with V79 cells, we take the corresponding values for ε_i and ε_c from our previous publication (*5*) to characterize the lethality of iDSB and cDSB, respectively, for all radiation types. The cell line specific lethalities ε_i and ε_c, are listed in Table 2, together with the values for the other cell lines as described below. Figure 1 shows the comparison of the GLOBLE prediction for high-energy photons, Ti-K soft X rays and C-K soft X rays with the experimental data. For high-energy photons and Ti-K X rays, a very good agreement is observed over the whole dose range. For C-K X rays, the model predictions are in agreement with the experimental data at least for the range from 100% to 1% survival, however at lower survival levels deviations become significant because of the saturation effects. These saturation effects are frequently reported for irradiations with extremely low-energy photons and are typically attributed to shielding effects.

Because attenuation plays a major role for very low-energy photons, the target geometry might influence the dose-response curve. Therefore, we compare curves for the standard geometry, which is a cylindrical nuclear shape to curves based on a spherical nucleus with the same nuclear volume in Fig. 1. In this case, the predicted curve is shallower for C-K X rays, whereas the curves for Ti-K X rays and high-energy photons remain unaffected. This can be attributed to the fact, that in a spherical volume the number of domains per layer in the nucleus varies with depth, whereas in a cylindrical geometry this number is constant. Consequently, in the spherical geometry in the layers close to the entrance, where the proportion of cDSB compared to iDSB is highest, the number of domains is smaller and thus the predicted effect is lower. However, calculating the mean dose in accordance with the procedure reported for the experimental data, does not consider this variation of the lateral extension of the target. Consequently, the effectiveness seems lower in the case of spherical volumes. In reality, cell nuclei have a more ellipsoidal shape and thus the corresponding prediction of the model would be between the extreme cases of cylindrical and spherical geometry.

TABLE 2
Input Parameters for the GLOBLE Model for the Different Cell Lines used for Comparison with Experimental Data

Author	Cell line	ε_i	ε_c
de Lara *et al*.	V79	0.0036	0.210
Raju *et al*.	V79	0.0048	0.163
Goodhead *et al*.	HF19	0.0315	0.150

Notes. Despite de Lara *et al*. (*10*) and Raju *et al*. (*12*) using the same cell line (V79), they report slightly different sensitivities already for high-energy photons and thus need to be characterized by correspondingly different parameters. For details see text.

Since for C-K X rays only a few data points are available in the low-dose region, which is not affected by saturation effects, we also compared the model predictions to the data reported by Raju *et al*. (*12*) (Fig. 2). Although they also used V79 cells for their studies, the dose-response curve after high-energy photon irradiation slightly differs from the one reported by de Lara *et al*. Consequently, to represent this dose-response curve correctly, the parameters ε_i and ε_c have been adapted based on the linear-quadratic parameters and the transformation formula given in Eq. (6) in the article by Friedrich *et al*. (*5*). These correspondingly adapted values for ε_i and ε_c (see Table 2) have then been used to model the dose-response curve after ultrasoft X-ray irradiation. Since DSB induction was not measured by Raju *et al*., we use the same RBE values for DSB induction as reported by de Lara *et al*. Again, a very good agreement between model predictions and experimental data is observed. In particular, the pronounced shoulder predicted by the model in the low-dose region fits to the experimental data. For higher doses, Raju *et al*. (*12*) observed a saturation as de Lara *et al*., although at a lower survival level. This was simulated in the model by introducing a constant offset for the survival level as given in the Fig. 2 legend, representing a small fraction of cells receiving no dose due to shielding by other cells.

Finally, a set of experimental data reported by Goodhead *et al*. (*17*) for irradiation of human fibroblasts has been used for comparison with the GLOBLE model. Here, the shape of the dose response after high-energy photon irradiation significantly differs from the curve observed for V79 cells. This is reflected in the difference of the parameters ε_i and ε_c as summarized in Table 2. As already discussed by Friedrich *et al*. (*5*), the higher sensitivity can be modeled

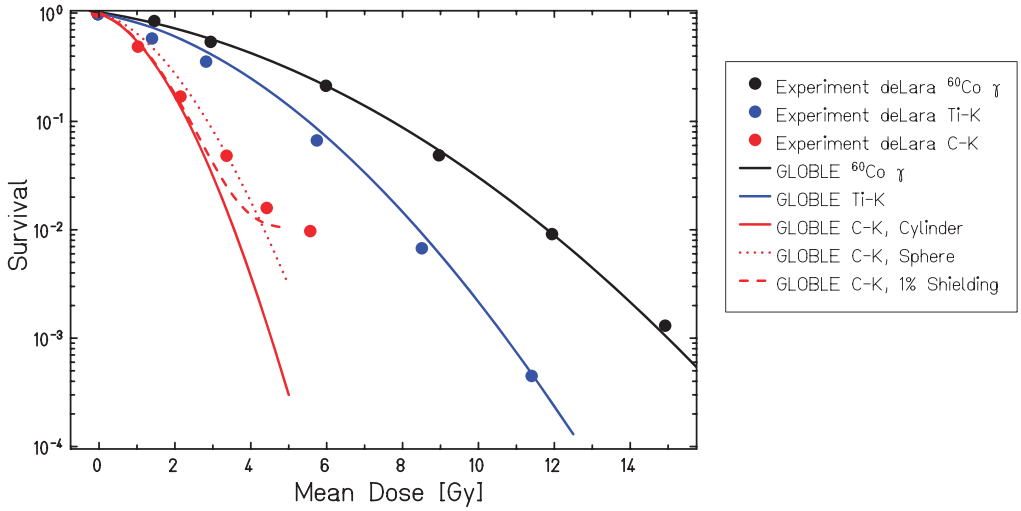

FIG. 1. Comparison of model predictions for Co-γ, Ti-K and C-K ultrasoft X rays with experimental data for V79 Chinese hamster cells reported by de Lara *et al.* (*10*). For C-K, in addition to the standard cylindrical geometry of the cell nucleus calculations are shown for a spherical shaped nucleus (dashed line). For Co-γ and Ti-K, the corresponding lines would lie exactly on top of the curves shown for the cylindrical geometry. For C-K, also the effect of shielding 1% of the cells is shown.

by a corresponding increase of ε_i with ε_c remaining in the same order of magnitude. Again, since no direct information about the RBE for DSB induction after ultrasoft X rays is available for HF19 cells, we used the same parameters as reported by de Lara *et al.* Comparison of the model predictions with the experimental data as shown in Fig. 3 shows good agreement.

The Impact of Attenuation

It has been intensively discussed whether or not the increased biological effectiveness is a consequence of the extreme attenuation of e.g., C-K X rays in combination with the nonlinearity of the dose-response curve observed for high-energy photon radiation. This could be particularly relevant for V79 cells, which are characterized by a larger

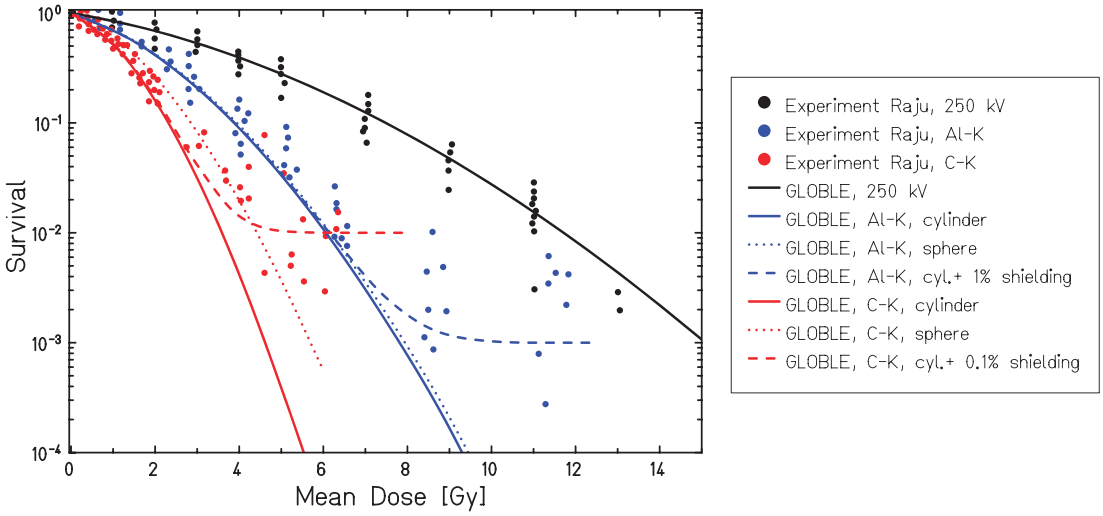

FIG. 2. Comparison of model predictions for Co-250 kV X rays, Al-K and C-K ultrasoft X rays with experimental data for V79 Chinese hamster cells reported by Raju *et al.* (*12*). Effects of shielding of the cells are illustrated for 1% shielding in the case of C-K and 0.1% shielding for Al-K.

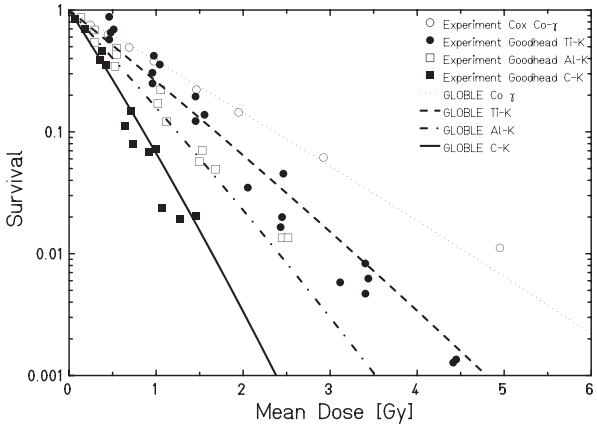

FIG. 3. Comparison of model predictions for Co-γ, Ti-K, Al-K and C-K ultrasoft X rays with experimental data for HF19 human fibroblast cells reported by Cox *et al*. (*26*) and Goodhead *et al*. (*17*).

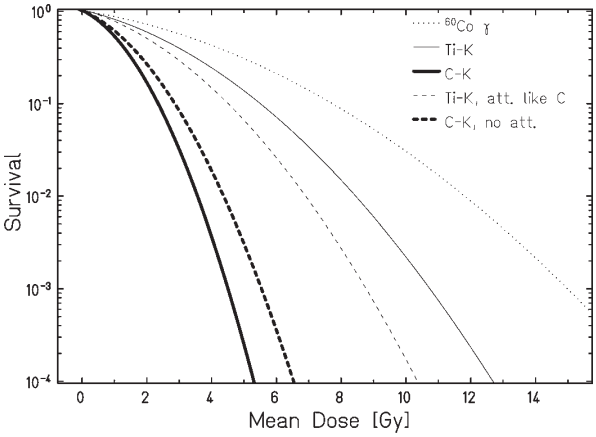

FIG. 4. Effect of attenuation on the dose-response curves for C-K and Ti-K ultrasoft X rays. The impact of attenuation is demonstrated by either artificially switching off the attenuation effect for C-K (thick dashed line) or artificially attributing a stronger attenuation as for C-K to the Ti-K X rays (thin dashed line). Simulations are performed with parameters for V79 cells; RBE_{DSB} values are kept unchanged in both cases.

cell height compared to the fibroblasts used e.g., by Cornforth *et al*.

We therefore analyzed in more detail the impact of radiation attenuation on the predicted cell survival. The GLOBLE model is ideally suited for such an analysis since cell killing is determined by summing up the number of lethal events in individual domains; inhomogeneities of the dose deposition can thus be easily taken into account.

Figure 4 illustrates the impact of attenuation by artificially switching on and off the attenuation in a cross-wise manner, i.e., for C-K X rays the attenuation was neglected, but the high RBE for DSB induction was kept. *Vice versa*, an artificially high attenuation coefficient as observed for C-K X rays has been attributed to Ti-K X rays, but again keeping the RBE for DSB inductions as reported by de Lara *et al*. for Ti ultrasoft X rays. As expected, attenuation has a significant impact if the attenuation length is in the order of micrometers, i.e., within the dimension of a typical cell nucleus, since this implies a significant dose gradient along the penetration depth of the ultrasoft X rays.

The increased effectiveness related to the strong attenuation can be explained by high local dose at the entrance side of the radiation, which increases the probability to induce cDSB in the first layer of loops. Due to the nonlinear increase of the probability of cDSB as a function of dose these high local doses lead to an over proportional increase of lethality, as reflected by the steeper slope of the corresponding survival curves.

Despite the fact that a significant impact of attenuation is predicted, it is by far not sufficient to fully explain the increased effectiveness of ultrasoft X rays.

Since the effects of attenuation will depend on the thickness of the critical target, we compared the corresponding predicted survival curves for three different heights of 2, 6 and 10 μm in Fig. 5a, where the nuclear volume has been kept constant and the cross section has been adapted accordingly. As expected, the curves get steeper with increasing thickness of the nucleus. However, this effect is only pronounced for cells showing a distinct shoulder in the case of high-energy photon irradiation, which can be traced back to a large difference in the lethality of iDSB and cDSB. If the high-energy photon dose-response curve is already almost linear – corresponding to high values of ε_i – almost no impact of attenuation is predicted even for very thick cells. This is demonstrated in Fig. 5b on the basis of the ε_i and ε_c parameters used for fibroblasts (cf. Fig. 3). A local, microscopic inhomogeneity of the dose distribution is thus expected to have impact on the dose response curve only if the corresponding high-energy photon dose-response curves are nonlinear.

Comparison of Ultrasoft X Rays and Ion Beams

In line with the experimental data the model predicts a significant bending of the dose-response curves in the region down to 10% (Fig. 2), which is a striking difference to what is typically observed after high-LET irradiation, e.g., carbon ions showing similar RBE_α. Apart from the saturation effects observed at lower survival levels, this indicates that the increased RBE of ultrasoft X rays represents a dose-modifying factor, whereas for high-LET radiation typically a drop of RBE with increasing dose is observed (*18*). Both the GLOBLE as well as the LEM are able to reproduce these features, as it is demonstrated by the comparison shown in Fig. 6. The curves for high-energy photons and C-K soft X rays are identical to the ones in Fig. 1; the curve for carbon ions is determined using the LEM, that is also based on the concept of DSB classification into

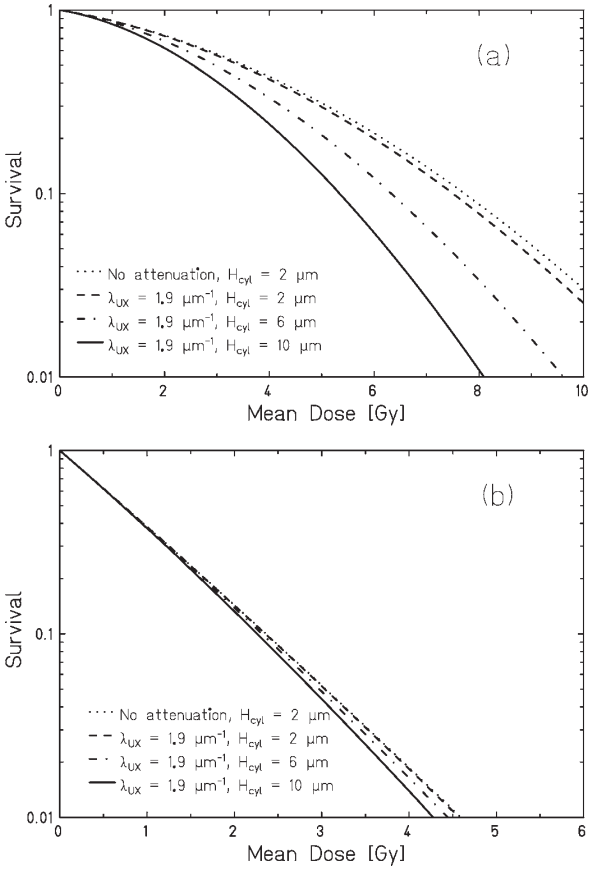

FIG. 5. Comparison of the impact of the cellular height on the predicted dose-response curves for parameters representing significantly shouldered dose-response curve after high-energy photon radiation ($\varepsilon_i = 0.0038$, $\varepsilon_c = 0.18$) (panel a) and parameters representing an almost straight-dose-response curve ($\varepsilon_i = 0.032$, $\varepsilon_c = 0.15$) (panel b). RBE_{DSB} was set to 1.0 for the calculations.

iDSB and cDSB (*3, 4*). The LET was chosen so that the RBE for the initial slope of the survival curves, RBE_α, is identical for carbon ions and C-K soft X rays. The comparison clearly demonstrates the quite different shape of the dose-response curves, despite the fact that the identical RBE_α values would indicate a similar radiation quality.

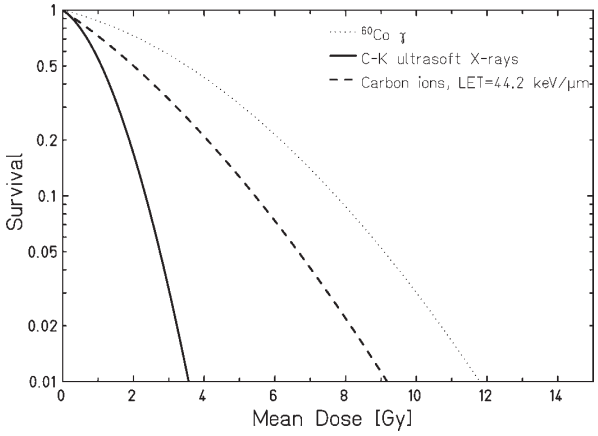

FIG. 6. Comparison of GLOBLE predictions for C-K ultrasoft X rays and LEM predictions for carbon ions at 44.2 keV/µm, characterized by the same RBE_α

DISCUSSION

Concept of Lesion Distribution Approach

Both the LEM and the GLOBLE model are based on the premise that the initial DSB distribution pattern determines the radiation response, where the pattern is characterized by the number of iDSB and cDSB induced by the radiation field. In the GLOBLE model the observable effect can be determined based on the lethalities ε_i and ε_c that are attributed to iDSB and cDSB, respectively; the lethalities are assumed to be independent of the radiation quality leading to the DSB. Based on the knowledge of the increased yield of DSB after ultrasoft X-ray irradiation and the lethalities ε_i and ε_c derived from high-energy photon radiation, the GLOBLE model can predict the cell killing effects of ultrasoft X rays with high accuracy down to survival levels of approximately 1%, that are not affected by shielding effects. This is consistent with the assumption that the quality of lesions, in particular of iDSB and cDSB, does not significantly differ between low-energy and high-energy photon radiation, and that it is mainly the different yield and thus the corresponding number of iDSB and cDSB that actually determines the effect. This conclusion concerning lesion quality is further supported by experimental results indicating that the rejoining kinetics after high-energy photon irradiation and ultrasoft X-ray irradiation is almost identical (*10*). Furthermore, a recent approach to model rejoining kinetics based on the two classes of iDSB and cDSB is consistent with these findings (*19*).

The role of the increased yield of DSB after high-LET irradiation has been discussed to be relevant for the explanation of the increased RBE in a modeling study reported by Carlson *et al*. (*20*), although that model was not able to explain the decrease of RBE typically observed for higher LET values above approximately 150 keV/µm. The authors further conclude that the *local* lesion complexity as characterized in nm-dimensions seems not to be a major factor determining radiation effectiveness, which is in agreement with the concept on which the current analysis is based.

Therefore, although lesion severity does not change with respect to individual iDSB, an increase of lesion severity on the micrometer level that is relevant for cDSB results from

the inhomogeneous dose distribution with depth in the case of C-K soft X rays. Here, the high local dose at the entrance region of the nucleus induces cDSB with a higher frequency than expected on the basis of the mean nuclear dose, because the induction of cDSB depends in a nonlinear way on the dose. Nevertheless, as demonstrated in Fig. 4, the impact of the dose attenuation on the increase in effect is comparably small, although clearly visible, compared to the impact of the higher yield of DSB.

Role of Target Geometry and Dimensions

It has been hypothesized that target geometry in combination with the strong attenuation might represent a major cause for the increased effectiveness of ultrasoft X rays (*21, 22*). In particular the experimental data reported by Cornforth *et al*., for fibroblasts that are characterized by a substantially minor thickness in contrast to other cells indicate an RBE very close to 1. Whereas this result would be in favor of the hypothesis that attenuation is responsible for the high RBE, it is at variance with the observed higher yield of DSB after ultrasoft X rays. Assuming that the increased yield of DSB is valid for fibroblasts as for V79 cells (which is in line with the general observation that the initial DSB induction does not vary significantly between cell lines), it would be difficult to understand why fibroblasts should not respond to a higher yield with a lower survival, too. However, no DSB induction were measured in the AG1522 fibroblasts after ultrasoft X ray irradiation, and thus it might be speculated that for some unknown reason the DSB induction is actually less enhanced compared to other cell lines.

In comparison to a homogeneous dose deposition to a cell nucleus, for irradiation with soft X rays with an absorption length in the order of micrometers the deposited energy is concentrated at the entrance and decreasing exponentially with increasing penetration into the nucleus. Intuitively, domains far away from the entrance are barely affected by ionization events and hence do rarely house iDSB, while domains close to the entrance are likely to show a more dense damage pattern, leading to iDSB or even cDSB more regularly. This suggests that only a reduced number of domains are accessible to the radiation, but get affected more severely in turn. Indeed a Taylor analysis for cylindrical cell nuclei irradiated with small doses of some Gy shows that absorption can be modeled by simply replacing the number of loops by a lower effective loop number, decreasing with absorption strength.

This notion of a reduced domain number with an enhanced proportion of cDSB compared to iDSB implies important consequences for the dose-response curve. While without such absorption a dose-response curve is expected to be a simple dose rescaled copy of the corresponding high-energy photon curve (i.e., it has dose modifying property), absorption will break this similarity. At the entrance where local doses are high, it becomes more likely that any two photoelectrons induce DSB into the same domain, thus giving rise to enhanced damage clustering and to a higher bending of the dose response curve at high doses. In the LQ model this results in an increased beta term.

Comparison to the Microdosimetric Approach

The experimental data obtained after ultrasoft X-ray irradiation have challenged theoretical considerations on the mechanisms of radiation action, namely the microdosimetric approach. The key argument here as raised by Goodhead (*23*) was, that the typical range of photoelectrons released by ultrasoft X rays (a few nm) is incompatible with the target dimensions of micrometer size, which is the basis of the microdosimetric approach. According to the model discussed here, these different dimensions are not in conflict.

The extreme localization of energy deposition in nm dimensions can be considered to be the cause for the increased yield of DSB, as indicated by Goodhead (*24*). The clustering of ionization events may lead to a higher probability to induce to SSB close together on opposite DNA strands, resulting in the increased yield of DSB. This increased yield is not directly modeled in the approach presented here, but information about RBE_{DSB} is taken from the experimental data and it is assumed that the spatial distribution of DSB is still random, as for higher energy photon radiation. Due to the short track length of photoelectrons, all DSB are induced independently of each other. Interaction processes get involved as soon as the doses are sufficiently high to induce a significant number of cDSB, characterized by multiple DSB within a loop. However, no physical interaction of the DSB or overlap of the dose depositions by different photoelectrons is required to lead to an interaction; instead the interaction is mediated by the target structure, because the mere simultaneous existence of two DSBs in one loop is assumed to lead to a lower survival probability compared to the product of survival probabilities for two independent iDSBs.

Thus, processes in nm as well as μm dimensions are relevant for the explanation of the increased effectiveness of ultrasoft X rays: the nm dimension is relevant for the increased induction of DSB, the micrometer dimension is relevant for the increased effectiveness of cDSB.

The Relevance of Two Damage Classes

According to the results discussed above, in the framework of the GLOBLE model the increased effectiveness of certain radiation types may result from two different processes:

1. The increased yield of DSB

2. The concentration of DSB, leading to a deviation from a random distribution

Both obviously play a role for ultrasoft X rays, although here the increased yield represents the dominant factor and the concentration of DSB seems to be a comparably minor correction leading to a further increase in the case of very low-energy photon radiation.

The discussion can be extended to the case of high-LET particle radiation, where it is much more likely that the concentration of DSB along the particle trajectories, will become dominant. This effect might be further enhanced by an increased yield of DSB, which is a consequence of the higher probability to induce SSB close together due to the high local dose within the particle track center (*25*).

Interestingly, in terms of Eq. (1) the increased effectiveness can be either attributed to a simultaneous increase of n_i and n_c or a shift in the balance between n_i and n_c for ultrasoft X rays and ions, respectively. Thus, for a given survival level, there are different potential linear combinations of ε_i and ε_c, which can be attributed to this effect.

This also explains the different shape of dose response curves for ultrasoft X rays and ion beam radiation, even if the RBE for the initial slope is identical (see. Fig. 6).

For soft X rays, the increased DSB yield seems to play the major role, and the nonrandomness of DSB distribution due to attenuation is only expected to play a role in the case of very low-energy photons with correspondingly strong attenuation. This explains why for ultrasoft X rays the increased effectiveness exhibited dose-modifying features, since as a consequence of the random distribution for a given number of DSB the same spatial patterns of microscopic DSB distributions are produced by high- and low-energy photons. The situation is entirely different for ion irradiation. Here, the nonrandom distribution of DSB is the dominant factor, caused by the track structure and the corresponding high local dose along the trajectory of the particle. As a consequence, DSBs are induced essentially along the trajectory, leading to a highly ordered distribution of DSB and resulting in a much higher probability for the induction of cDSB and thus a higher lethality. Therefore, in the case of ultrasoft X rays the increased initial slope of the dose-response curve is due to an increased number of iDSB with comparably low lethality, whereas in the case of ion irradiation the increased slope can be attributed to a comparably small number of cDSB, that however exhibit a much higher lethality compared to iDSB. In addition, according to the model assumptions, cDSB induced within individual particle tracks are not susceptible to inter-track effects, because increasing the number of DSB in a loop that already contains 2 or more DSBs does not further enhance lethality. Therefore, only iDSB induced within individual tracks can contribute to inter-track effects, and consequently the dose-response curve for ion irradiation is straighter. In contrast, since predominantly iDSB are induced by individual ultrasoft photons, all DSB can contribute to inter-track effects.

Similarly, for ultrasoft X rays a pronounced dose-rate effect would be expected similar to that of higher energy photons as described by Herr *et al*. (*14*). In contrast, since in the case of high-LET radiation cDSB are primarily formed by single ions, they are always produced simultanously and thus not susceptible to dose-rate effects.

The model prediction concerning the different shape of dose response curves after ultrasoft X-ray irradiation and high-LET irradiation is fully in line with the experimental results reported by Cox *et al*. (*26*). They compare survival curves for irradiation with Al-K X rays and 20 and 50 keV/μm He ions. Whereas both survival curves for He-ion irradiation are almost linear, the curve for Al-K X rays shows a significant bending, although the initial slope is similar to that for 20 keV/μm He-ions.

Comparison to Other Models

Several other modeling approaches have been reported in the literature for application to the case of ultrasoft X rays. Although a thorough comparison to these other approaches would be beyond the scope of this article, we will address here some conceptual aspects that might indicate directions of future work.

The experimental results obtained with ultrasoft X rays particularly challenged ideas on which the theory of dual radiation action (TDRA) (*27*) is based. The major inconsistency was related to the length scales involved; since extremely low-energy ultrasoft X rays such as C-K rays deposit their energy within nanometer ranges, this was concluded to be incompatible with the length scales relevant for the TDRA (*23*). A generalized version of the TDRA [called GTDRA (*28*)] and the appropriate accounting for the heterogeneous energy deposition caused by attenuation was then reported to be able to account for the peculiar energy deposition pattern of these low energy X rays (*29, 30*). The major impact of the attenuation has been reported to potentially lead to an increased β term, which otherwise is assumed to be constant in the TDRA and GTDRA. Interestingly, the approach shown here is consistent with the increase of beta as a consequence of the attenuation across the cell nucleus, as shown in Fig. 4. However, in general our approach predicts an increase of beta also in the case of negligible attenuation, which is even more prominent. This is a consequence of the dose modifying properties that result from the general scaling of the DSB yield by a common factor $RBE_{DSB,USX}$. If attenuation is negligible, the RBE for survival RBE_{Surv} should be constant and identical to $RBE_{DSB,UX}$ for any given survival level. With that, the linear quadratic parameter can be derived from:

$$\alpha_{Surv,UX} = \alpha_{Surv,\gamma} \cdot RBE_{DSB,UX} \quad (5)$$

$$\beta_{Surv,UX} = \beta_{Surv,\gamma} \cdot RBE^2_{DSB,UX} \quad (6)$$

Therefore, if the dose-response curves for conventional high-energy photon radiation already show a shoulder, the inter-track contribution should be particularly prominent for ultrasoft X rays, which is in line with the experimental data shown in Fig. 2.

Since the model reported by Stewart *et al*. (*31*) is able to predict the experimentally observed increase of the DSB yield with decreasing photon energy, it might be helpful in further applications of the approach presented here.

An increase of the β term with the square of the number of DSB is also predicted by the model developed for application to high-LET radiation by Carlson *et al*. (*20*). However, the model is only able to predict an increase with LET, whereas it fails to predict the decrease typically observed at LET values above approximately 150 keV/μm.

Another approach based on microdosimetric considerations has been proposed by Hawkins and adapted to the case of ultrasoft X rays [microdosimetric kinetic model (MKM) (*32, 33*)]. In this model, the increased effectiveness of low-energy photons is attributed to an increased probability to induce two potentially lethal lesions caused by one event, and the increase of β is attributed to the increased yield of potentially lethal lesions (*33*). Whereas the latter is consistent with our findings, if DSB are considered to be the potentially lethal lesions (although this is not explicitly stated so by Hawkins), the first aspect is incompatible with the approach presented here. It would require the induction of two DSB by a single-low-energy photon, and based on the average yields and the number of photons per Gy the probability of a single photon to induce one DSB is substantially smaller than 1, and therefore the simultaneous induction of two DSB thus seems to be very unlikely. However, of course this cannot be ruled out based on these simple considerations and further analysis will be required for the detailed comparison of these approaches.

Obaturov *et al*. have presented a modeling approach applicable to a wide range of radiation qualities, which resembles our approach in that it also uses a compartmentalization of the cell nucleus in about 3,000 subunits, called ''membrane attached superstructural units'' (MASSU) (*34, 35*). The model also allows for a variation of the β term, depending on the repair probability of potentially lethal damages before first postirradiation mitosis. However, the model does not allow prediction of the variation of β with radiation quality, but it rather empirically accounts for such a variation.

As discussed above, in the MKM as well as in our model the increased yield of potentially lethal damages or DSB, respectively, leads to an increased β term for ultrasoft X rays. A question we have not specifically addressed here is the mechanism leading to this increased yield. Instead, we made use of empirically determined RBE values for DSB induction as reported by de Lara *et al*. Further work thus is required to clarify in how far this increased yield of DSB can be predicted on the basis of an amorphous track structure approach as reported by Elsässer *et al*. (*25*). There, the increased yield of DSB after charged particle track traversals has been modeled by specifically considering the increased probability to induce two SSBs in close vicinity, finally leading to a DSB. Based on this concept, it might be possible to model the increased DSB yield of ultrasoft X rays based on their extremely confined energy deposition pattern.

A commonality of models based on pairwise lesion interaction, e.g., the TDRA or the MKM is the prediction of a pure linear-quadratic shape of dose-response curves. In contrast, as discussed in detail by Friedrich *et al*. (*5*), a specific prediction of the GLOBLE model resulting from the concept of DSB clustering in chromatin loops is a transition to a more straight form of the dose-response curve at high doses as well as an intrinsic anticorrelation between the LQ-parameters β and α. Experimental results are in agreement with both of these predictions and thus are further supportive of the concept on which GLOBLE is based.

SUMMARY AND CONCLUSIONS

We have compared predictions of the GLOBLE model with experimental data obtained after irradiation with ultrasoft X rays. We showed that within the framework of the GLOBLE model the increased yield of DSB is sufficient to explain the increased RBE for cell killing, assuming that the lethality of DSB is independent of radiation quality. Analyzing the impact of attenuation of ultrasoft X rays within the target, it could be demonstrated that this attenuation only plays a minor role for the increased effectiveness compared to the increased yield of DSB with decreasing photon energy. In a comparison with cell killing effects after high-LET ion-beam irradiation, we could also explain why ultrasoft X rays exhibit dose-modifying properties and nearly dose-independent RBE values, whereas for high-LET radiation a significant dose dependence is typically observed, even at the same RBE_α. Since the model predictions are fully consistent with the experimental results, we take this as further support of the general concepts on which GLOBLE is based.

Received: August 16, 2013; accepted: January 22, 2014; published online: April 22, 2014

REFERENCES

1. Inaniwa T, Furukawa T, Kase Y, Matsufuji N, Toshito T, Matsumoto Y, et al. Treatment planning for a scanned carbon beam with a modified microdosimetric kinetic model. Phys Med Biol 2010; 55:6721–37.
2. Kramer M, Scholz M. Rapid calculation of biological effects in ion radiotherapy. Phys Med Biol 2006; 51:1959–70.
3. Elsasser T, Weyrather WK, Friedrich T, Durante M, Iancu G, Kramer M, et al. Quantification of the relative biological

effectiveness for ion beam radiotherapy: direct experimental comparison of proton and carbon ion beams and a novel approach for treatment planning. Int J Radiat Oncol Biol Phys 2010; 78:1177–83.

4. Friedrich T, Scholz U, Elsasser T, Durante M, Scholz M. Calculation of the biological effects of ion beams based on the microscopic spatial damage distribution pattern. Int J Radiat Biol 2012; 88:103–7.
5. Friedrich T, Durante M, Scholz M. Modeling cell survival after photon irradiation based on double-strand break clustering in megabase pair chromatin loops. Radiat Res 2012; 178:385–94.
6. Johnston PJ, Olive PL, Bryant PE. Higher-order chromatin structure-dependent repair of DNA double-strand breaks: modeling the elution of DNA from nucleoids. Radiat Res 1997; 148:561–7.
7. Johnston PJ, MacPhail SH, Banath JP, Olive PL. Higher-order chromatin structure-dependent repair of DNA double-strand breaks: factors affecting elution of DNA from nucleoids. Radiat Res 1998; 149:533–42.
8. Ostashevsky J. A polymer model for the structural organization of chromatin loops and minibands in interphase chromosomes. Mol Biol Cell 1998; 9:3031–40.
9. Yokota H, van den Engh G, Hearst JE, Sachs RK, Trask BJ. Evidence for the organization of chromatin in megabase pair-sized loops arranged along a random walk path in the human G0/G1 interphase nucleus. J Cell Biol 1995; 130:1239–49.
10. de Lara CM, Hill MA, Jenner TJ, Papworth D, O'Neill P. Dependence of the yield of DNA double-strand breaks in Chinese hamster V79-4 cells on the photon energy of ultrasoft X rays. Radiat Res 2001; 155:440–8.
11. Goodhead DT, Thacker J. Inactivation and mutation of cultured mammalian cells by aluminium characteristic ultrasoft X-rays. I. Properties of aluminium X-rays and preliminary experiments with Chinese hamster cells. Int J Radiat Biol Relat Stud Phys Chem Med 1977; 31:541–59.
12. Raju MR, Carpenter SG, Chmielewski JJ, Schillaci ME, Wilder ME, Freyer JP, et al. Radiobiology of ultrasoft X rays. I. Cultured hamster cells (V79). Radiat Res 1987; 110:396–412.
13. Sachs RK, van den Engh G, Trask B, Yokota H, Hearst JE. A random-walk/giant-loop model for interphase chromosomes. Proc Natl Acad Sci U S A 1995; 92:2710–4.
14. Herr L, Friedrich T, Durante M, Scholz M. A Model of Photon Cell Killing Based on the Spatio-Temporal Clustering of DNA Damage in Higher Order Chromatin Structures. PLOS ONE January 2014. (DOI:10.1371/journal.pone.0083923).
15. Prise KM, Pinto M, Newman HC, Michael BD. A review of studies of ionizing radiation-induced double-strand break clustering. Radiat Res 2001; 156:572–6.
16. Stenerlow B, Karlsson KH, Cooper B, Rydberg B. Measurement of prompt DNA double-strand breaks in mammalian cells without including heat-labile sites: results for cells deficient in nonhomologous end joining. Radiat Res 2003; 159:502–10.
17. Goodhead DT, Thacker J, Cox R. Weiss Lecture. Effects of radiations of different qualities on cells: molecular mechanisms of damage and repair. Int J Radiat Biol 1993; 63:543–56.
18. Weyrather WK, Ritter S, Scholz M, Kraft G. RBE for carbon track-segment irradiation in cell lines of differing repair capacity. Int J Radiat Biol 1999; 75:1357–64.
19. Tommasino F, Friedrich T, Scholz U, Taucher-Scholz G, Durante M, Scholz M. A DNA double-strand break kinetic rejoining model based on the Local Effect Model. 2013.
20. Carlson DJ, Stewart RD, Semenenko VA, Sandison GA. Combined use of Monte Carlo DNA damage simulations and deterministic repair models to examine putative mechanisms of cell killing. Radiat Res 2008; 169:447–59.
21. Carpenter S, Cornforth MN, Harvey WF, Raju MR, Schillaci ME, Wilder ME, et al. Radiobiology of ultrasoft X rays. IV. Flat and round-shaped hamster cells (CHO-10B, HS-23). Radiat Res 1989; 119:523–33.
22. Cornforth MN, Schillaci ME, Goodhead DT, Carpenter SG, Wilder ME, Sebring RJ et al. Radiobiology of ultrasoft X rays. III. Normal human fibroblasts and the significance of terminal track structure in cell inactivation. Radiat Res 1989; 119:511–22.
23. Goodhead DT. Inactivation and mutation of cultured mammalian cells by aluminium characteristic ultrasoft X-rays. III. Implication for theory of dual radiation action. Int J Radiat Biol Relat Stud Phys Chem Med 1977; 32:43–70.
24. Goodhead DT. The initial physical damage produced by ionizing radiations. Int J Radiat Biol 1989; 56:623–34.
25. Elsasser T, Scholz M. Cluster effects within the local effect model. Radiat Res 2007; 167:319–29.
26. Cox R, Thacker J, Goodhead DT. Inactivation and mutation of cultured mammalian cells by aluminium characteristic ultrasoft X-rays. II. Dose-responses of Chinese hamster and human diploid cells to aluminium X-rays and radiations of different LET. Int J Radiat Biol Relat Stud Phys Chem Med 1977; 31:561–76.
27. Kellerer AM, Rossi HH. The theory of dual radiation action. Curr Top Radiat Res Q 1972; 8:85–158.
28. Kellerer AM, Rossi HH. A generalized formulation of dual radiation action. Radiat Res 1978; 75:471–88.
29. Brenner DJ, Zaider M. Modification of the theory of dual radiation action for attenuated fields. II. Application to the analysis of soft X-ray results. Radiat Res 1984; 99:492–501.
30. Zaider M, Brenner DJ. Modification of the theory of dual radiation action for attenuated fields. I. Basic formalism. Radiat Res 1984; 99:484–91.
31. Stewart RD, Yu VK, Georgakilas AG, Koumenis C, Park JH, Carlson DJ. Effects of radiation quality and oxygen on clustered DNA lesions and cell death. Radiat Res 2011; 176:587–602.
32. Hawkins RB. A microdosimetric-kinetic model of cell death from exposure to ionizing radiation of any LET, with experimental and clinical applications. Int J Radiat Biol 1996; 69:739–55.
33. Hawkins RB. Mammalian cell killing by ultrasoft X rays and high-energy radiation: an extension of the MK model. Radiat Res 2006; 166:431–42.
34. Obaturov GM, Filimonov AS, Moiseenko VV. Model of mammalian cell reproductive death. II. Comparison with experimental data and discussion. Radiat Environ Biophys 1993; 32:295–310.
35. Obaturov GM, Moiseenko VV, Filimonov AS. Model of mammalian cell reproductive death. I. Basic assumptions and general equations. Radiat Environ Biophys 1993; 32:285–94.
36. Nikjoo H, Lindborg L. RBE of low energy electrons and photons. Phys Med Biol 2010; 55:R65–109.

7.4 Article 4: Sensitivity analysis of high LET modelling

IOP Publishing Physics in Medicine and Biology
Phys. Med. Biol. **58** (2013) 6827–6849 doi:10.1088/0031-9155/58/19/6827

Sensitivity analysis of the relative biological effectiveness predicted by the local effect model

T Friedrich[1], R Grün[1,2,3], U Scholz[1,4], T Elsässer[1,5], M Durante[1,4] and M Scholz[1]

[1] GSI Helmholtzzentrum für Schwerionenforschung, Darmstadt, Germany
[2] Medizinische Fakultät, Philipps-Universität Marburg, Marburg, Germany
[3] Institut für Medizinische Physik und Strahlenschutz, TH Mittelhessen, Gießen, Germany
[4] Institut für Festkörperphysik, TU Darmstadt, Darmstadt, Germany

E-mail: t.friedrich@gsi.de

Received 26 April 2013, in final form 5 July 2013
Published 11 September 2013
Online at stacks.iop.org/PMB/58/6827

Abstract
The relative biological effectiveness (RBE) is a central quantity in particle radiobiology and depends on many physical and biological factors. The local effect model (LEM) allows one to predict the RBE for radiobiologic experiments and particle therapy. In this work the sensitivity of the RBE on its determining factors is elucidated based on monitoring the RBE dependence on the input parameters of the LEM. The relevance and meaning of all parameters are discussed within the formalism of the LEM. While most of the parameters are fixed by experimental constraints, one parameter, the threshold dose D_t, may remain free and is then regarded as a fit parameter to the high LET dose response curve. The influence of each parameter on the RBE is understood in terms of theoretic considerations. The sensitivity analysis has been systematically carried out for fictitious *in vitro* cell lines or tissues with $\alpha/\beta = 2$ Gy and 10 Gy, either irradiated under track segment conditions with a monoenergetic beam or within a spread out Bragg peak. For both irradiation conditions, a change of each of the parameters typically causes an approximately equal or smaller relative change of the predicted RBE values. These results may be used for the assessment of treatment plans and for general uncertainty estimations of the RBE.

(Some figures may appear in colour only in the online journal)

[5] Now working at Siemens Healthcare.

0031-9155/13/196827+23$33.00 Printed in the UK & the USA 6827

1. Introduction

The RBE is used to quantify the enhanced effect of ion beams in comparison to low LET radiation such as x-rays or gamma rays. For applications in radiobiologic research as well as in ion radiotherapy the precise characterization of RBE is of importance. Many experimental and clinical studies have been carried out to reveal the RBE under various conditions (Ando and Kase 2009, Gerweck and Kozin 1999, Friedrich *et al* 2013). However, as the RBE depends on several factors whose versatile combinations cannot be investigated solely by experiments, models for predicting the RBE have been developed. The LEM in its original version (LEM I) (Scholz *et al* 1997) and the microdosimetric kinetic model (MKM) (Hawkins 1994, 1996) are currently the only ones used for clinical treatment planning. Within the recent years, the LEM has been gradually improved (Elsässer and Scholz 2007, Elsässer *et al* 2008). The latest version LEM IV (Elsässer *et al* 2010, Friedrich *et al* 2012b) comprises a mechanistic interpretation on the level of double strand break (DSB) induction. This allowed one to significantly improve the accuracy to model the RBE for all therapy relevant ions and energies with *one unique* set of necessary parameters which have been fixed once for all model calculations. As their values, as well as other experimental parameters (e.g. those specifying the tissue considered), are associated with uncertainties the question arises how these translate into uncertainties of the predicted RBE. Hence, for applications in radiobiology and in the clinics it is of interest to quantify the consequence of a change of each input parameter for the RBE. The rates of RBE change will reflect themselves in the robustness of treatment plans for ion beam therapy.

This paper is dedicated to the sensitivity analysis of RBE, obtained by a systematic variation of parameters used within the LEM IV. The strategy is to carry out the analysis in a very systematic way, where at first all parameters are inspected and classified, then their relevance is quantitatively investigated for monoenergetic beams as well as for extended irradiated volumes[6]. This strategy finally allows one to understand the parameter sensitivity based on the physical or biological meaning of the parameter under consideration and to compare the expectations for RBE uncertainty for the different ways of beam delivery. Our approach is complementary to a recent publication (Böhlen *et al* 2012), where the authors investigated the parameter influence on RBE for extended targets and in detail discuss possible implications for ion beam therapy.

The parameters needed for calculating RBE values with LEM may be subdivided according to the model parts they are used in:

- specification of the physical aspects of track structure
- specification of the initial DNA damage distribution
- characterization of the cell and DNA conformation geometry
- characterization of the photon dose response curve.

In section 2 the basic principles of the LEM are revisited and the parameters needed for RBE calculations are introduced. The relevant parameters for LEM calculations are classified and discussed in section 3. The parameter sensitivity of the RBE values for monoenergetic beams is presented in section 4. Section 5 is dedicated to the same analysis for a clinical situation, where a SOBP is optimized in such a way that a homogenous distribution of the RBE-weighted dose covers the target volume. Finally, the results are discussed and conclusions are drawn in section 6.

[6] Throughout the paper with monoenergetic beams we understand that the samples are irradiated under track segment conditions, i.e. that energy and LET do not change along an ion track through a cell nucleus.

2. Conceptual basis of the LEM

The LEM bases on the assumptions that the nuclear DNA is the unique sensitive part of the cell to radiation, that DSB are the most relevant lesions, and that the radiation damage on a molecular level is predominantly mediated by secondary electrons and hence only depends on the local distribution of these secondaries. This includes the implicit assumption that for all radiation qualities the spectra of the slowing down secondary electrons are similar. The main idea is then to trace back the effect of ions to the effect of photons inducing locally a similar pattern of initial damage.

In a first step, ions are assumed to pass through the cell nucleus, in which the DNA is assumed to be distributed homogenously. Practically, for most applications we restrict here to one single ion passing right through the centre of the cell nucleus. This allows one to assess the effect of exactly one ion, from which the effect of a distribution of ions can be derived as outlined in (Scholz *et al* 1997). A Monte Carlo simulation of the full spatial dose distribution of a distribution of ions has also been implemented in LEM (Friedrich *et al* 2012b), but is not used for this study for the sake of computation time. We checked that this so called single particle approximation is valid up to several Gy and hence can be used for normal fractionated radiotherapy. Furthermore track segment conditions are required, i.e. the particles show no significant change of kinetic energy or LET along their way through the nucleus. According to their track structure a local dose deposition is converted into a damage pattern of DSB distributed within the nucleus. The local rate for the induction of initial DSB is proportional to the local dose in each location within the track. The proportionality factor is the DSB yield as measured in experiments with low LET radiation. In addition to these DSB, further DSB arise due to neighbouring single strand breaks (SSB) on opposite DNA strands combining to a full break of the DNA double strand (Elsässer and Scholz 2007), resulting in an overall RBE for DSB induction greater than one. In the implementation the simulation of the damage patterns is performed by means of a Monte Carlo routine simulating many cells, each being affected by one spatial DSB distribution. The procedure is stopped when the number of Monte Carlo runs is sufficient to finally determine the effect of ions within a requested accuracy.

In a second step the initial damage distribution is converted into a distribution of isolated or clustered DSBs, where the classification is defined based on the picture of a hierarchical compartmented organization of chromatin into DNA giant loops (Yokota *et al* 1995) of some Mbp size, corresponding to the micrometer length scale. The relevance of such a length scale is known since a long time in radiobiology (Neary *et al* 1959, Rossi and Zaider 1996, Goodhead 2006) and thus supportive for this conception, though its interpretation in terms of DNA conformation is under continuous debate. It is suggestive to assume that lesions can interact if they were induced in the same DNA loop, while lesions in different chromatin domains are processed independently. Consequently, the model distinguishes between domains without any DSB, with exactly one DSB (called isolated DSB), or with more than one DSB (called clustered DSB). Note that this term is not uniquely defined and used for different constellations of lesions by different authors. All definitions, however, have in common that the term means an accumulation of lesions (at least one of which is a DSB) in close neighbourhood. Indeed it is known that isolated DSB can be repaired quite efficiently by the repair mechanism of a cell, while complex damage is believed to have a higher impact on cell killing, supporting the assumption used in LEM, that the fraction of complex damage is a determining factor for the RBE.

In the third step a photon dose causing the same proportion of isolated to clustered DSBs is evaluated. The effect corresponding to that photon equivalent dose is obtained from the photon dose response curve. As for this case the local damage pattern of ion and photon irradiation

Table 1. Overview over the parameters of the LEM, classified in groups corresponding to different stages of a LEM model calculation. One can distinguish specific parameters which specify the situation to be modelled, and general parameters which have been obtained by measurements, fitted to reference data or estimated by theoretic considerations. For general parameters, the values used are given, and their origin is indicated.

Parameter class	Parameter	Type	Value	Origin
Track structure	γ	General	0.062	Measured[a]
	δ	General	1.7	Measured[a]
	r_c	General	6.5 nm	Fit + theoretic arguments[b]
	σ	General	4 nm	Theoretic arguments[a]
	E	Specific		
	LET	Specific		
Initial DNA damage	α_{DSB}	General	$30\,\mathrm{Gy}^{-1}$	Measured[a]
	α_{SSB}	General	$1250\,\mathrm{Gy}^{-1}$	Measured[a]
	h	General	25 bp	Measured[a]
	L_{Gen}	Specific		
Cell nuclear geometry	V_n	Specific		
	r_n	Specific		
	l_{DSB}	General	540 nm	Fit[b]
Photon dose response curve	α	Specific		
	β	Specific		
	D_t	Specific		

[a] See (Elsässer and Scholz 2007) and references therein.
[b] See (Elsässer *et al* 2010) and references therein.

is comparable, the effect of ions can be calculated by a proper normalization from the photon effect, and all related quantities such as the RBE are obtained easily. For a mathematical precise formulation of the LEM we refer to (Friedrich *et al* 2012b).

Note that in this general formulation up to this point no specific endpoint is considered. The LEM is appropriate for any endpoint as long as the effect is mediated primarily by the induction of DSB to DNA loops or correlating strongly with it. The difference in RBE between different endpoints originates from different associated photon dose response curves. The most prominent endpoints to which the LEM was applied up to now are cell survival for cell culture experiments and tumour control as well as normal tissue complication in carbon ion cancer therapy or *in vivo* experiments (Elsässer *et al* 2010, Scholz and Elsässer 2007, Grün *et al* 2012).

3. Parameters of the LEM

Calculating the effect of an ion impact from a photon equivalent situation requires knowledge or modelling of (i) physical properties of the ions, (ii) factors determining the DNA damage induction rates, (iii) geometric properties of the cellular nucleus and the chromatin, and (iv) the photon dose response for the endpoint under consideration. The relevant parameters are summarized in table 1 according to this classification, and their meaning will be discussed below.

Some of the parameters have been fixed once, because there is no evidence for any dependence on e.g. cell type or ion species. Their values are used for all simulations and have been either extracted from experimental results, derived by theoretic arguments, or fixed by fitting the LEM predictions to a reference set of experimentally obtained RBE data (Furusawa *et al* 2000, Suzuki *et al* 2000). They are marked with *general* in table 1 and listed along with their attributed values. All other parameters, marked as *specific* parameters, specify the experiment or clinical situation to be modelled, i.e. they characterize the cell- or tissue type

and their radiation response, define the particle species used and the energy. The distinction of general and specific input parameters of the LEM is used throughout this publication.

Note that both general and specific parameters are associated with uncertainties. For some parameters these are quite large (some ten per cents), e.g. for the radical diffusion length σ or the yield parameters α_{DSB} and α_{SSB}. However, as two general parameters, the giant loop domain size for DSB interaction l_{DSB} and the maximum inner core radius r_c, have been fixed by a fit to RBE reference data sets, the fitted parameters calibrate the model and compensate for uncertainties in the others, and therefore the uncertainties of the general parameters do not propagate to the uncertainty of the RBE. This compensation is not mathematically strict, and there might be combinations of all parameters where this procedure of calibrating the LEM model might fail, leading to systematic errors in RBEs. However, some systematic errors in the RBE predictions are only detected at low LET values, while mostly RBE predictions are reasonably correct. This strongly suggests that the model set-up and the chosen parameters are sufficiently accurate, which implies that the compensation of parameter errors works good enough to predict RBEs correctly. Moreover this is supported by the values of the two fitted parameters which are in agreement with theoretical expectations (nm range for r_c and μm range for l_{DSB}). As a consequence of the compensation of parameters, for an uncertainty analysis of RBE primarily the specific parameters characterizing an experiment or a clinical case are of relevance.

Using the set of parameters as listed in table 1 in LEM IV allows one to simulate RBE for a wide range of LET and for all therapy relevant ion species from protons to carbon in reasonable agreement with experimentally or clinically evaluated RBE values (Grün *et al* 2012). The different groups of relevant parameters needed for a LEM calculation are addressed in the following point by point.

3.1. Physical parameters of beam and track structure

The incident particle is characterized by a kinetic energy per nucleon, E, and a corresponding LET for a given particle species. Here energy and LET are determined within the cellular nucleus. The LEM assumes that the LET does not change considerably along a passage of an ion through the nucleus. If track segment conditions are violated, deviations between LEM and experimental data may occur.

Microscopically the energy is transferred from the ion to the surrounding matter in point-like ionization events. For many purposes it is sufficient to use the average dose distribution pattern around the central axis of a passing ion. This parametrization of the energy loss of particles in matter is commonly referred to as amorphous track structure (Cucinotta *et al* 1999). Note that the concept of dose used here is a local dose, being proportional to a probability density function for finding an ionization. In our implementation we follow the amorphous track structure model according to (Elsässer *et al* 2008), where the track structure consists of an inner core with a constant dose up to an energy dependent radius which is parameterized by $r_{\mathrm{min}} = \beta_{\mathrm{ion}} r_c$ with $\beta_{\mathrm{ion}} = v/c$, particle velocity v and velocity of light c. Its maximum value, $r_c = 6.5$ nm was adequately chosen in (Elsässer *et al* 2010) to fit experimental data and matches the order of magnitude expected from theoretic considerations perfectly (Mozumder 2007).

Beyond r_{min} the local dose falls off quadratically up to a maximum radius $r_{\mathrm{max}} = \gamma E^{\delta}$, where r_{max} is given in microns and E in MeV per nucleon. The parameters γ and δ have been derived by a fit to experimental data obtained in experiments using tissue equivalent proportional counters (Kiefer and Straaten 1986). In this work there is no analysis of involved uncertainties given, but it is evident that the uncertainties of γ and δ are smaller than their values, but larger than on the per cent level. Below an energy of 2 MeV u^{-1} this parametrization

does not resemble the measured doses with sufficient accuracy. Here, values different from those in table 1 are used ($\gamma = 0.124$ and $\delta = 0.7$). As the remaining range of particles of such small energy is very limited and track segment conditions might be violated, the accuracy of RBE predictions might be questionable, but for the same reason their importance within a SOBP is low.

It is known that an essential fraction of lesions is induced by an indirect effect, i.e. by free radicals which have been produced by secondary electrons. To account for this, the initial dose distribution according to the parametrization discussed previously is convoluted with a radial Gaussian of width $\sigma = 4$ nm, modelling an effective diffusion of free radicals. The value of σ was fixed in (Elsässer *et al* 2008) and is in agreement with diffusion lengths calculated by Monte Carlo codes (Nikjoo *et al* 1997, Moiseenko *et al* 2001). Here it is important to note that LEM follows an effective approach: as different radical species have different mean free path lengths, its uncertainty on the nm scale is given by the corresponding wide spread of different radical diffusion lengths.

3.2. Parameters for damage induction to the DNA

The crucial initial lesions of interest in the LEM are DSBs. Several experiments show that for photons the initial DSB yield is $\alpha_{\mathrm{DSB}} \approx 30\,\mathrm{Gy}^{-1}$ per cell for a DNA content $L_{\mathrm{Gen}} = 5.4 \times 10^9$ bp as typical for rodents (Prise *et al* 2001, Stenerlöw *et al* 2003). This DSB yield refers to the initial induction of DSB and is observed experimentally with low LET radiation. Likewise, experiments showed that the yield SSB is $\alpha_{\mathrm{SSB}} \approx 1250\,\mathrm{Gy}^{-1}$.

It is well accepted that SSB can be repaired effectively. However, for high LET radiation two SSB in close vicinity on opposite strands may combine and form an additional DSB. Hence the number of initial DSB calculated from α_{DSB} is enhanced. This amplification is explicitly modelled within the LEM. A fixed threshold of $h = 25$ bp for the maximum interaction length of SSB is used in our implementation, in agreement with experimental results using plasmids (Shao *et al* 1999), see (Elsässer and Scholz 2007) for a more detailed discussion. While it is negligible for photon irradiation, for high LET radiation qualities this effect can enhance the DSB yield up to one order of magnitude, depending on particle species, LET and genomic length (Elsässer and Scholz 2007). Concerning the uncertainties of the parameters for damage induction, in the literature typically values of 20–40 DSB and 1000–1500 SSB per cell and Gy are discussed in the literature. For the distance threshold h a huge span of 3–60 bp is reported in the literature. This motivates a reasonable fixation to 25 bp.

3.3. Parameters of the cell nucleus geometry

We assume that the DNA content of the cell is uniformly distributed in a cylindrical cell nucleus, specified by parameters for the volume of the nucleus, V_n and its radius, r_n. The impinging particles are assumed to hit the nucleus in direction of the symmetry axis of the nucleus. Note that the height of the nucleus is uniquely fixed by the two geometry parameters. Distributions of nuclear sizes are discarded up to now.

To model chromatin loop domains a three-dimensional rectangular grid is superimposed on the cell nucleus. The boxes of the grid resemble the domains in which DSBs are counted. They have equal side lengths of $l_{\mathrm{DSB}} = 540$ nm. This length was determined by a fit to survival data of Furusawa and coworkers (Furusawa *et al* 2000), and is in agreement with the typical interaction length scale derived from microdosimetric considerations (Goodhead 2006). The parameter l_{DSB} thus determines the interaction lengths of distant DSB and fixes the proportion of isolated and clustered DSB for a given dose and radiation quality.

3.4. Photon dose response parameters

Within the LEM usually the linear-quadratic (LQ) model is used, in which the effect is given by $\alpha D + \beta D^2$ with photon dose D and linear and quadratic coefficient parameters α and β. The choice of the LQ model is somewhat arbitrary but convenient, as for almost all *in vitro* and *in vivo* data as well as for most clinical reports on radiation effects are characterized in terms of this model (Friedrich *et al* 2013, Ando and Kase 2009, Steel and Peacock 1989, Fertil and Malaise 1985).

At high doses, however, it becomes more and more evident that the LQ model loses validity, as the dose response tends towards a pure linear component. This is suggested by theoretic considerations of the repair dynamics of the cell (Curtis 1986, Tobias 1985) as well as by experimental findings from both *in vitro* (Astrahan 2008, Garcia *et al* 2007, Fertil *et al* 1994) and *in vivo* experiments (Guerrero and Li 2004, Carlone *et al* 2005). In the LEM we model the different properties of the dose response curves at low and high doses by a instantaneous transition from an LQ to a linear dose response at the transition dose D_t. Then the main principle of the LEM is the mapping of the damage pattern caused by ions to a damage pattern as induced by photons. For regions of high local doses, photon irradiation will induce comparable damage patterns at doses above D_t, and hence D_t is an important parameter for RBE calculations. There are three distinct ways of asserting a numerical value to it: One can extract it from measurements, if the photon dose response curve is available to sufficient high doses. Alternatively an empirical linear relationship between D_t and α/β exists, which can serve to estimate D_t (Friedrich *et al* 2013). If one proceeds (and only if) along these ways, the LEM is free of any specific fit parameters. However, if both of these procedures are not applicable or affected with unacceptable accuracy (e.g. when the photon dose response parameters are only known within a limited low dose range), the parameter must be fitted individually to experimental high LET data from the cells or tissues under investigation.

4. Sensitivity analysis for irradiation with monoenergetic ion beams under track segment conditions

In this section the change of RBE-LET relationships for cells or tissues irradiated with a monoenergetic ion beam due to parameter variation is investigated. The results can be used to estimate the influence of parameter uncertainties on the RBE for radiobiological experiments mimicking aspects of carbon radiotherapy in the different situations with monoenergetic beams in track segment conditions. They might also be useful to understand differences in RBE values if calculated for or measured with different cell lines under comparable conditions.

Both the RBE at full survival (RBE_α) and at 10% survival level (RBE_{10}) are considered as a function of the LET. The simulations have been performed for carbon ions and two hypothetic cell- or tissue types, characterized by $\alpha/\beta = 2\,\mathrm{Gy}$ and $\alpha/\beta = 10\,\mathrm{Gy}$. The general strategy of the sensitivity analysis is to calculate for each parameter listed in table 1 (except energy and LET) three RBE-LET relationships, one for a designed value of that parameter and the other two obtained by increasing or decreasing this parameter by 25% of its initial value[7].

In particular we chose $\alpha = 0.1\,\mathrm{Gy}^{-1}$, $\beta = 0.05\,\mathrm{Gy}^{-2}$ and $D_t = 8\,\mathrm{Gy}$ as design parameters for $\alpha/\beta = 2\,\mathrm{Gy}$ and $\alpha = 0.5\,\mathrm{Gy}^{-1}$, $\beta = 0.05\,\mathrm{Gy}^{-2}$ and $D_t = 14\,\mathrm{Gy}$ for $\alpha/\beta = 10\,\mathrm{Gy}$.

[7] We chose here the reference change of 25% for all parameters to allow for an inter-comparison of the sensitivity on the RBE determining parameters. Moreover, 25% resemble the order of magnitude of the uncertainties of the input parameters, as none of the parameters is known to per cent accuracy, but also the uncertainties typically do not exceed some ten per cents. A mathematical, more rigorous treatment would require one to consider the differential expressions $\mathrm{dRBE}/\mathrm{d}x$ for any parameter x.

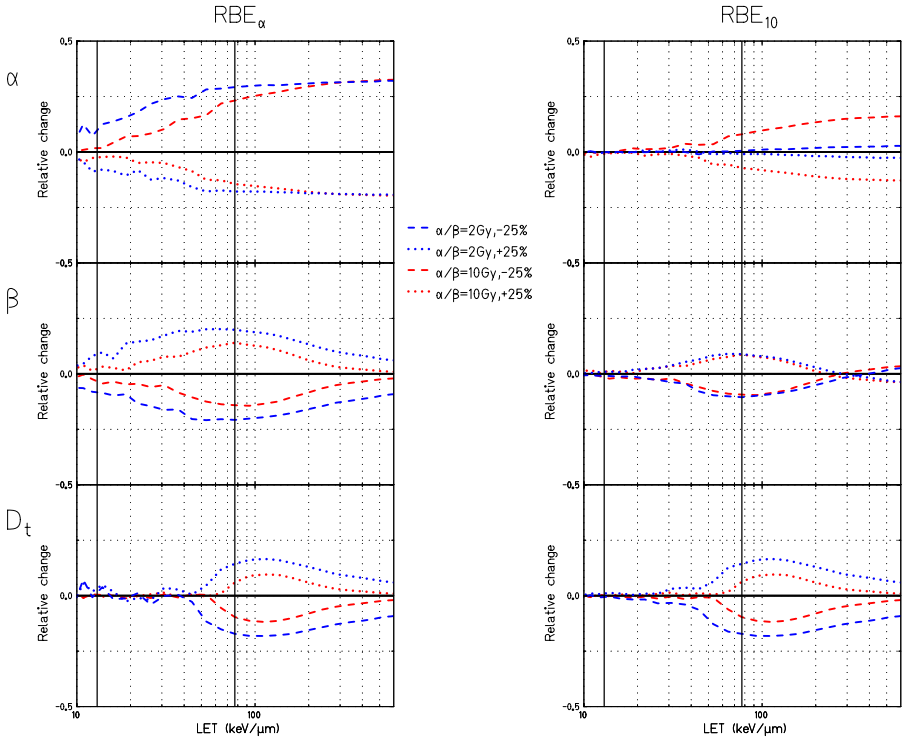

Figure 1. Relative change of RBE_α (left) and RBE_{10} (right) over LET for carbon ions and cells or tissues on the photon parameters for $\alpha/\beta = 2$ Gy (blue) and $\alpha/\beta = 10$ Gy (red). The horizontal axis corresponds to the RBE at the design parameters (see text), and the dashed and dotted curve emerge by decreasing or increasing the specific parameter about 25%, respectively. The vertical lines indicate the LET values of 13 and 77 keV μm^{-1} used in table 2.

These parameter settings are typical for *in vitro* cell survival assays (Friedrich *et al* 2013). The parameter D_t was adapted according to an empirical relation between α/β and D_t. This linear relation was found when using the LEM over a huge set of experimental cell survival data (Friedrich *et al* 2013), and is in agreement with experimental findings (Astrahan 2008). The geometric specific parameters for both cases were chosen $V_n = 500\,\mu m^3$ and $r_n = 5\,\mu m$. Again, these parameters approach typical values for mammalian cell lines.

For all combinations of effect levels for which the RBE is evaluated (RBE_α or RBE_{10}) and for both α/β ratios (2 Gy or 10 Gy), we obtained for each parameter a band in the RBE-LET characteristics which describes the variability of RBE under variation of $\pm 25\,\%$ of this parameter[8]. In all cases but one, sensitivity was investigated by varying one single parameter. As an exception, for a change of the parameter V_n we also changed l_{DSB} as a second parameter in order to keep the number of chromatin loops within the cell nuclei constant. Figure 1 shows the dependence of the RBE variation on the photon LQ parameters α, β and D_t. In figure 2 the influence of the nuclear volume V_n, nuclear radius r_n, the DNA loop domain size l_{DSB} and the DSB yield α_{DSB} on RBE is presented.

[8] Note that a change of one of the LQ parameters α or β immediately implies a modification of their ratio α/β. Here the assumed α/β ratios of 2 and 10 Gy refer to the designed (unchanged) parameter values.

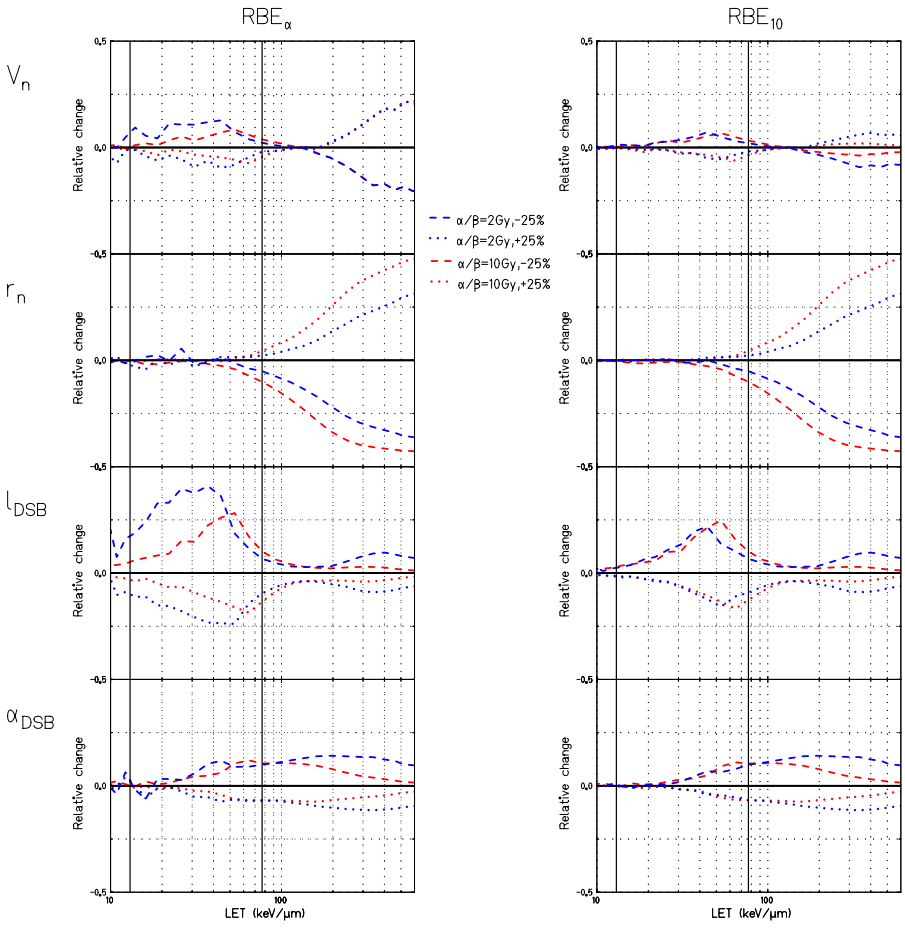

Figure 2. Relative change of RBE as presented in figure 1 for the nuclear volume, the nuclear radius, the DNA loop domain size and the DSB yield.

Generally from the figures it can be seen that in most cases there is less or at most equal sensitivity on parameter variations for $\alpha/\beta = 10$ Gy compared to $\alpha/\beta = 2$ Gy. Similarly, the RBE at 10% survival is typically less sensitive to parameter variations compared to RBE$_\alpha$. Moreover it becomes evident that the increase of some parameters leads to either a decrease or an increase of RBE. Based on some simple mechanistic interpretations within the framework of the LEM the different sensitivity patterns can be interpreted, as shall be demonstrated at some examples in the following.

To β, D_t, and α_{DSB} the RBE is primarily sensitive for intermediate LET values. These parameters show a bulb-like pattern in the plots. For very low LET they are of minor importance (as all parameters), as the nature of the radiation field converges to that of photons, and hence RBE will get close to one. At high LET the overkill effect will take place, i.e. in the limit of high LET a cell will only survive if it is not hit, and will be inactivated as consequence of any hit. Due to this simplistic picture these biologic parameters lack of importance in the high LET regime.

The parameters α and r_n in contrast show pronounced importance for high LET, which can be explained by the same argument: The probability for a cell to be hit and with that the effect increases with the nuclear radius and thus with the geometrical cross section r_n. The photon parameter α has, in contrast to β and D_t, for high LET almost no influence on the ion dose response curve within LEM. Nevertheless there is a prominent dependence of RBE on α because it directly affects the dose at which the reference effect level is reached on the photon dose response curve.

The parameter l_{DSB} shows two pronounced sensitivity regions, while there is almost no sensitivity between 100 and 200 keV $\mu\mathrm{m}^{-1}$. The reason is an interference of the length scales involved: Generally an increase of l_{DSB} allows for more DSB clustering within the photon radiation field, while this effect is not so prominent for ions, which results in a decrease of RBE. But in the intermediate LET regime the track diameter is of the order of the loop domain size. In this case an increase of the domain size will lead to an effective increase of clustering almost as much as for photons, because for increased loop domains all DSB caused in the whole track structure may contribute to DSB clusters. As there is not much differential effect between photons and ions in this case, the RBE sensitivity to changes of l_{DSB} is low. For very high LET finally a further increase of l_{DSB} will not lead to more clustered lesions caused by the ion track, hence the sensitivity recovers.

In a similar way the direction of RBE change with respect to the direction of change of the input parameter can be interpreted: An increase of the photon parameter α, e.g. implies a steeper photon dose response curve and consequently a lower dose needed to reach a desired effect level. A higher α will also correlate to a steeper ion dose response curve. But as the enhanced effect of the ion dose response is primarily caused by the inhomogeneity of the local dose deposition pattern in combination with the nonlinear response to local doses, which is parameterized by β and D_t, the steepening due to an increase in α is less pronounced than for photons. As a result the RBE will decrease, if α is increased. All parameters show a unique directional RBE change except V_n for which at low LET a parameter decrease and at high LET a parameter increase leads to RBE increase.

The analysis presented here has also been performed for other particle species (protons, helium and neon). However, the results generally follow a similar systematics, and thus no detailed discussion is presented here. The most relevant difference is that as the whole RBE-LET characteristics is shifted towards higher LET for heavier ions, they provide a lower sensitivity on the parameters for low LET, while lighter particles are more sensitive there.

To project out the findings of this sensitivity analysis with monoenergetic beams for particle therapy, the most important results of the sensitivity analysis for carbon ions are summarized for therapy relevant LET values in tables 2 and 3 for $\alpha/\beta = 2$ Gy and 10 Gy, respectively. In a treatment like situation a good conformity to a tumour in the target region is desirable and the therapy benefits from the high RBE of carbon ions just before stopping as it allows one to keep the doses applied to normal tissue low. Hence in the target region typically a high average LET and a high dose are expected, leading to low survival of tumour cells, while in the entrance channel doses should remain low, and the LET of the high energetic carbon ions is small. In the tables these situations are represented by results for RBE_{10} at a high LET and for RBE_{α} at a rather small LET, respectively. But also the complementary cases occur: At the margins of the spread out Bragg peak (SOBP), depending on the field geometry and the irradiation angles, some parts of the tissues might be covered by radiation with rather high doses of rather low LET radiation or vice versa. These interfaces between peak and plateau regions are of particular interest in therapy as all tumour cells must be inactivated, while in the same way normal tissue shall be spared as much as possible. As tumour and healthy tissue

Table 2. Parameter dependence of RBE for monoenergetic carbon ions in therapy comparable situations for $\alpha/\beta = 2$ Gy. The header part of the table contains the RBE_α and RBE_{10} for LET values typically found in the entrance channel and the Bragg peak region in carbon ion therapy, respectively. Here the design parameter settings were used. Below the header part the relative changes in RBE in per cent after change of one parameter about −25% or +25% (bottom or top numbers) are given. The second column contains the correlation direction, labelled as 0, + or − if RBE does not change, goes typically up or down with increasing parameter, respectively. Note that this information is valid below the overkill regime—for high LET the correlation might change (see text).

		Entrance (13 keV μm^{-1})		Bragg peak (77 keV μm^{-1})	
		RBE_α 1.44	RBE_{10} 1.04	RBE_α 9.08	RBE_{10} 2.31
	corr.	$\frac{\Delta RBE_\alpha}{RBE_\alpha}$ (%)	$\frac{\Delta RBE_{10}}{RBE_{10}}$ (%)	$\frac{\Delta RBE_\alpha}{RBE_\alpha}$ (%)	$\frac{\Delta RBE_{10}}{RBE_{10}}$ (%)
V_n	−/+	−4.97 7.66	−0.77 1.06	−1.98 1.98	−2.16 1.73
r_n	+	+0.46 +0.64	+0.12 −0.04	+2.23 −5.44	+2.24 −5.44
l_{DSB}	−	−9.44 +19.41	−1.29 +2.76	−9.13 +7.27	−8.84 +7.27
α	−	−6.19 +10.30	+0.04 −0.05	−17.56 +29.25	−0.63 +0.55
β	+	+7.68 −7.68	+0.74 −0.83	+19.74 −20.41	+8.77 −10.15
D_t	0/+	±0	+0.48 −0.80	+14.47 −17.05	+14.47 −17.05
γ	−	−2.39 +2.92	−0.33 +0.40	−1.78 +2.42	−1.78 +2.43
δ	−	−8.79 +13.79	−1.20 +1.95	−10.42 +12.46	−9.90 +12.46
r_c	−	−0.51 +3.26	−0.07 +0.45	−4.78 +6.14	−4.77 +6.14
σ	−	+1.96 +0.46	+0.27 +0.06	−6.16 +8.39	−6.15 +8.39
α_{DSB}	−	−0.74 +1.71	−0.10 +0.23	−6.44 +10.01	−6.44 +10.01
α_{SSB}	+	+2.27 −0.77	+0.31 −0.11	+14.86 −12.62	+14.86 −11.69
h	+	+0.03 −0.22	+0.00 −0.03	+6.46 −6.85	+6.46 −6.86
L_{Gen}	−	+0.43 +1.31	+0.06 +0.18	−5.59 +8.53	−5.59 +8.53

show often different radiosensitivities, beneath dose and LET also the α/β ratio plays a role here, which reflects the complexity of RBE.

In the tables the design RBE values as well as the RBE values after parameter change are given for typical situations in the entrance channel (LET = 13 keV μm^{-1}) as well as in the SOBP (LET = 77 keV μm^{-1}). The representative values for the LETs have been adopted from (Suzuki *et al* 2000). In the tables, also the direction of change of the RBE is given: when a parameter is increased, the RBE may either typically go up as well (as marked with a '+' sign to indicate that positive correlation) or down (as marked with a '−' sign). In the case of D_t there is for small LET no dependence for RBE_α, which is labelled by '0'. Exceptions of a unique correlation occur only for the parameter V_n where the direction of RBE change gets reverted at an LET of 150 keV μm^{-1} (thus labelled with '+/−' and for very small parameter sensitivities where an increase and a decrease may hardly change RBE, while nevertheless small changes are seen in the simulations in the same direction due to fluctuations in the Monte Carlo calculation. The dependence on energy or LET is not listed in the tables, as LET is the dependent variable in the figures presented, and for a given particle species energy is uniquely defined for a given LET in the Bethe–Bloch regime.

Note that the RBE depends on each of the quantities typically less than proportional, i.e. when a parameter is changed about 25% the RBE usually changes less than 25%. Up to few

Table 3. As table 2, for $\alpha/\beta = 10$ Gy.

		Entrance (13 keV μm^{-1})		Bragg peak (77 keV μm^{-1})	
		RBE_α 1.09	RBE_{10} 1.04	RBE_α 3.27	RBE_{10} 2.44
	corr.	$\frac{\Delta RBE_\alpha}{RBE_\alpha}$ (%)	$\frac{\Delta RBE_{10}}{RBE_{10}}$ (%)	$\frac{\Delta RBE_\alpha}{RBE_\alpha}$ (%)	$\frac{\Delta RBE_{10}}{RBE_{10}}$ (%)
V_n	+/−	−0.74 1.10	−0.48 0.58	−3.06 3.36	−3.28 3.28
r_n	+	+0.42 −0.54	+0.34 −0.55	+4.58 −9.94	+4.61 −9.96
l_{DSB}	−	−2.49 +5.12	−1.39 +2.89	−13.52 +10.49	−12.71 +10.46
α	−	−1.80 +2.90	−0.42 +0.37	−14.21 +23.44	−6.96 +8.18
β	+	+2.03 −2.02	+0.73 −0.81	+13.80 −14.49	+8.55 −9.71
D_t	0/+	±0	+0.13 −0.22	+6.08 −9.50	+6.44 −9.52
γ	−	−0.96 +0.37	−0.53 +0.21	−2.12 +2.87	−2.01 +2.85
δ	−	−2.76 +3.77	−1.54 +2.12	−12.96 +14.30	−12.19 +14.28
r_c	−	−0.21 +0.77	−0.12 +0.43	−5.33 +6.73	−5.04 +6.70
σ	−	+0.27 +0.33	+0.15 +0.18	−6.66 +8.89	−6.30 +8.87
α_{DSB}	−	−0.75 +0.47	−0.42 +0.27	−7.09 +10.78	−6.70 +10.75
α_{SSB}	+	+0.74 −0.61	+0.42 −0.34	+15.60 −13.85	+15.57 −13.02
h	+	+0.38 −0.06	+0.21 −0.03	+6.92 −7.40	+6.90 −6.99
L_{Gen}	−	+0.10 +0.64	+0.06 +0.36	−6.06 +9.06	−5.73 +9.04

exceptions RBE does not change by more than 25%. From figures 1 and 2 it is evident that for a 10% survival level only the nuclear radii r_n exceed the 25% level for RBE changes. At 77 keV μm^{-1} as representative for the target region the RBE is very sensitive on the photon dose response parameters, the track structure parameter δ and the yield of SSB.

5. Sensitivity analysis for a clinical situation

The application of carbon ions for cancer treatment in the clinics requires treatment planning which accounts for the RBE in such a way, that the target volume is covered uniformly by a described RBE-weighted dose, while the doses in the normal tissues and in particular in organs at risk remain low. This strategy is followed in the particle treatment facilities in Japan (Tsujii and Kamada 2012) as well as in Europe (Combs *et al* 2010, Schulz-Ertner *et al* 2007), although their beam characteristics and the methods in accounting for RBE differ.

The RBE in a voxel based treatment plan corresponds to a mixed radiation field, because several particle species, each having an individual energy distribution, may contribute to the overall dose deposited due to fragmentation, straggling and scattering. Because of this mixing the large sensitivities detected in the last section are balanced out, and hence the irradiation of extended targets will show a damped sensitivity of RBE to its input parameters.

In this section the same sensitivity analysis is presented for SOBPs, as before for monoenergetic beams and cells or tissues under track segment conditions. Thus, each of the specific parameters of the LEM listed in table 1 was again modified by ±25% and the induced change in RBE was monitored. To facilitate the analysis a sphere as idealized target geometry with 60 mm depth extension placed in a depth of 150 mm (isocentre) was regarded[9].

[9] Note that this choice corresponds to rather large, deep seated tumours.

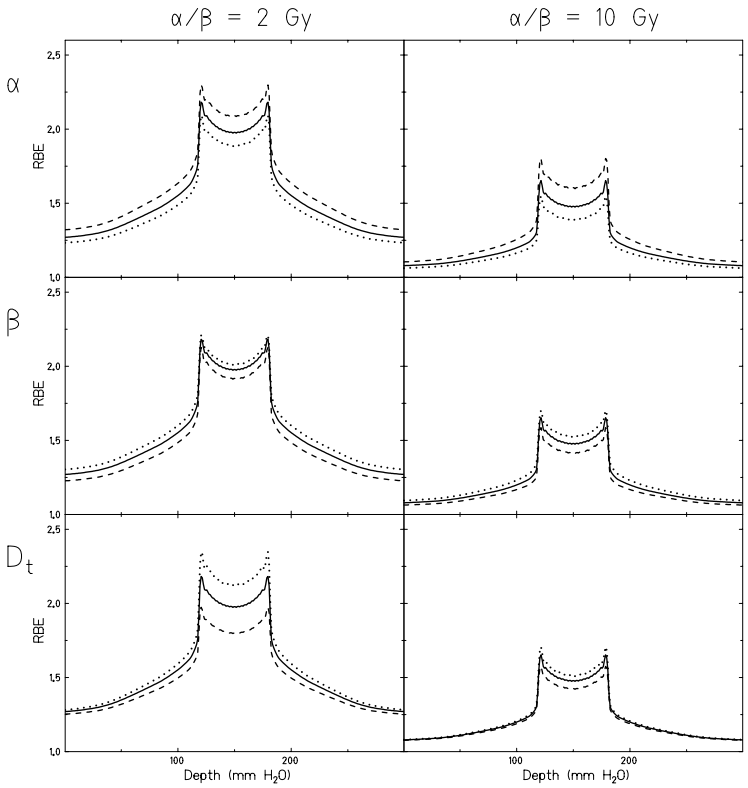

Figure 3. Dependence of RBE over water equivalent depth for carbon ions and cells or tissues with $\alpha/\beta = 2$ Gy and $\alpha/\beta = 10$ Gy on the LQ parameters. The corresponding RBE-weighted dose distributions were all optimized to 3 Gy in the target region. The solid curve corresponds to design parameters (see text), and the dashed and dotted curves emerge by decreasing or increasing the specific parameters about 25%, respectively.

The treatment planning software TRiP98 (Krämer *et al* 2000, Krämer and Scholz 2000) was used to optimize a physical dose leading to a homogeneous RBE-weighted dose throughout the SOBP. In general the RBE varies with the depth in tissue because the LET distribution changes. For this reason we here discuss depth distributions of the RBE, instead of its LET dependencies.

The strategy closest to the clinical routine is an optimization of two directly opposing fields to give a flat RBE-weighted dose of 3 Gy within the target, in line with the fraction dose used in the GSI clinical trial (Schulz-Ertner *et al* 2007). Note that for each parameter setting of the sensitivity analysis an individual optimization must be performed. As before, all calculations were performed for tissues with $\alpha/\beta = 2$ Gy and $\alpha/\beta = 10$ Gy with the same absolute values as in the previous section. The results are visualized in figures 3 and 4 where the depth distributions of the RBE values along an axis right through the isocentre (beam's eye view) are presented. We chose here to present the absolute RBEs instead of relative changes after parameter variation as in the previous figures, because for a SOBP the RBE profile is very instructive. Note that the mixed radiation field provides a variation of the average LET

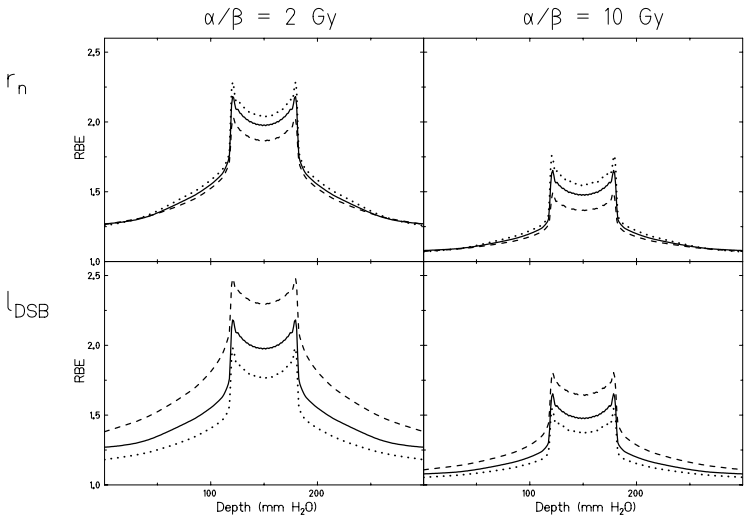

Figure 4. As figure 3, for the nuclear radius and the size of the chromatin loops.

with depth. Hence here the depth is the appropriate quantity to replace the dependence on LET, which was discussed in the last section.

At this point it is important to note that often for *in vivo* systems and clinical endpoints the LQ parameters happen to be much smaller (Brenner 1993). In order to establish comparability to the results in the previous section, here the absolute values were kept the same. However, it is known that RBE values for small and large absolute values are comparable for the same α/β ratios, with the only difference that overkill effects appear more pronounced for higher absolute values. Hence for small absolute values less sensitivity on parameters which affect overkill is expected, and we checked that conjecture at some examples (data not shown).

Generally, the curves in figures 3 and 4 show a low RBE in the entrance channels and a considerably higher RBE in the target, where particles are stopping and have a higher LET consequently. This is one of the superiorities of carbon ions compared to protons in radiotherapy. For a single field treatment plan the RBE distribution across the SOBP shows pronounced maxima towards the distal boundary of the target volume. There exclusively stopping particles (except some fragments) are present, causing a high LET, while at the proximal regions and within the SOBP broader mixtures of LETs exists. In a treatment plan consisting of two or more fields the statement holds in general, i.e. at the whole boundary of the target region. There the fraction of stopping particles is higher compared to within the target. Consequently the high LET components, causing a high RBE, are most prominent at the boundary. A relative uncertainty will therefore translate into a higher uncertainty of RBE-weighted dose at the margins of a SOBP. In contrast, in the figures the RBE distributions appear to be almost parallel for different parameter adjustments, leading to a reduced sensitivity at the margins of the target volume. This is due to the usage of two opposing fields, where at the margins high LET and comparably low LET components are mixed. Strategies for optimizing treatment plans such that the high LET components in the radiation field are more uniform distributed across the SOBP are currently discussed (Bassler *et al* 2010) and might help to diminish uncertainties of RBE (Böhlen *et al* 2012).

When varying one of the input parameters, the RBE values are shifted into the same direction as was detected in the previous section. That means that the direction of the correlation

between RBE and any specific parameter remains the same for both monoenergetic beams and SOBPs.

Regarding the quantity of the deviations a damping is observed compared to the maximum variations detected in the previous section. This is due to the mixture of LETs which is caused by the spread of pristine Bragg peaks forming the SOBP and due to fragments, which have to be taken into account properly (Lühr *et al* 2012, Gunzert-Marx *et al* 2008). The mixed radiation quality also implies a smaller overall RBE, also giving rise to smaller sensitivities. The feature of damping is of interest for the robustness of treatment plans. Furthermore, as before, the deviations typically do not exceed 25% and are therefore less than direct proportional to the change of the specific parameters.

A RBE-weighted dose of 3 Gy approximately corresponds to about 50% and 15% cell survival for the original set of specific parameters for $\alpha/\beta = 2$ Gy and 10 Gy, respectively. But in contrast to the last section, where the survival levels were fixed in advance by considering RBE_α or RBE_{10}, here the dose remains fixed at 3 Gy, when parameters are varied. Thus an optimization to 3 Gy when one of the LQ parameters is changed leads to slightly different survival levels for each parameter adjustment.

Figure 4 presents the results of the sensitivity analysis of the geometric parameters r_n and l_{DSB}. When changing the nuclear radius a variation in RBE is primarily visible in the target region and suppressed in the entrance channel. This behaviour can be again understood by looking at the case of monoenergetic ions, where there is only a marginal dependence on r_n in the low LET region. The difference in RBE after a change of the chromatin loop size l_{DSB} is, in particular for $\alpha/\beta = 2$ Gy, comparably large and in contrast to all other parameters also very prominent in the entrance channels. Again, the reason can be understood by looking at figure 2 and tables 2 and 3: while the Bragg peak typically covers LETs between 50 and 100 keV $\mu\mathrm{m}^{-1}$, in the entrance channels lower LET values occur. For RBE_α a quite high sensitivity to l_{DSB} has been found with monoenergetic beams at low LET values. Remnants of this finding cause the sensitivity in an extended treatment plan.

6. Discussion

6.1. Justification of the approach

The sensitivity analysis presented in this work is based on an approach using single parameter variations. The question arises if such a 'factorized' approach is appropriate and overall RBE changes could be calculated by a linear superposition of the RBE changes of each individual parameter. Instead, one also could expect that shifts in any two parameters act on RBE dependent on each other in a correlated way. We will argue in the following that these correlations between parameters with respect to RBE change play only a second order role.

Formally, the RBE can be regarded as a mathematical function dependent on a set of parameters $\{p_i\}$, i.e. $\mathrm{RBE} = \mathrm{RBE}(\{p_i\})$. If parameters are changed from $\{p_i\}$ to $\{p_i + \delta p_i\}$, the RBE can be expanded in a Taylor series, where the first order term contains a sum of terms $\frac{\mathrm{dRBE}}{\mathrm{d}p_i}\delta p_i$, and the second order term of type $\frac{\mathrm{d}^2\mathrm{RBE}}{\mathrm{d}p_i\mathrm{d}p_j}\delta p_i \delta p_j$. Hence the 'factorization' approach is resembled by first order terms, and correlated RBE change by second and higher order terms. So, if the values of changes are not too large, the second order contributions will be smaller than the first order contributions and thus can be neglected. For a proper uncertainty analysis this has to be fulfilled anyway: only if the uncertainties associated with the parameters are smaller than the parameter values (which is typically the case), the principles of error calculus will apply, and under this conditions the argument given is valid. We also checked that numerically for

some examples by calculating the RBE after a coexisting parameter detuning and comparing it with the RBE calculated with a linear superposition of RBE changes.

6.2. Importance of parameters for RBE uncertainty

The sensitivity analysis presented in the two previous sections reflects how RBE changes, when one of the input parameters is varied. This allows one to assess the variability of RBE based on the variability of one of the input parameters. While some of the general parameters such as δ are obtained with a quite good accuracy from experimental results, others have relatively large error bars. In this case we followed the strategy to use average values from the literature. For instance, values in the typical range between 20 and 40 DSB per Gy are reported for α_{DSB}. Recent works also indicate that the yield could be much higher, but is underestimated due to systematic experimental errors (Neumaier *et al* 2012). So, according to the state of research these parameters may be subject to change in future. However, it is important to note that the sensitivity on input parameters does not directly provide information about RBE uncertainty, as shall be explained in the following.

Despite remarkable uncertainties in the input parameters, in combination all general parameters form a consistent input parameter set, as two of them, l_{DSB} and r_c (cf table 1), were fitted once to experimental data (Furusawa *et al* 2000, Suzuki *et al* 2000) to calibrate the model. By this procedure they compensate for possible misadjustments of the measured general parameters and minimize the model inherent systematic uncertainties of RBE. Indeed, a large contribution of the general parameters to the overall uncertainty of RBE values has not been observed, which indicates that the systematic errors of the LEM are small. For *in vitro* cell survival experiments (Elsässer *et al* 2010) and clinical cases (Grün *et al* 2012) we showed in several publications that the LEM predicts RBEs with reasonable accuracy for different LET values or depths, dose levels and cell types.

The specific parameters characterize the experiment or clinical situation and have to be evaluated in order to use the LEM. Among them, the genomic length and the geometric parameters are usually known or can be obtained without too much effort. Thus the interesting consequence is that the predominant source of uncertainty of RBE, which is a quantity for *high* LET radiation is due to the uncertainty of the photon parameters α, β, and D_t, i.e. the response parameters of the *low* LET radiation. Thus in the following we focus on these parameters only.

Moreover for RBE simulations it is usually sufficient to fix the ratio α/β, because the RBE does only marginally depend on a common scaling factor of the absolute values of α and β, for small and intermediate LET. A plausible reasoning for this is, that the nonlinear dose response curve leads to a high RBE foremost by means of high local doses. A measure for the excess effect due to the nonlinearity, normalized to the linear component is just the inverse of the α/β ratio. Indeed, RBE seems to scale linearly with $(\alpha/\beta)^{-1}$ (Friedrich *et al* 2013). The α/β ratio can also be used to find an estimate for D_t by means of an empirical relationship. Another strategy could be to replace the linear quadratic linear model used within the current LEM implementation by a different photon dose response model which provides the saturation of effect increments without an explicit threshold parameter. Investigations towards this direction are on the way, and one possible option is to use the GLOBLE model (Friedrich *et al* 2012a) which fulfills these requirements.

6.3. RBE uncertainty for monoenergetic beams and SOBPs

In this section we want to make use of the presented sensitivity analysis and provide examples for an uncertainty analysis. To understand the influence of the composition of a radiation field

Table 4. Parameter dependence of RBE for monoenergetic carbon ions in therapy comparable situations at 3 Gy and for a SOBP composed of two opposing fields and optimized to 3 Gy (RBE) formed by carbon ions for $\alpha/\beta = 2$ and 10 Gy. The upper part contains the LET or dose averaged LET and the reference RBE values. In the middle section of the table the relative changes in RBE after change of one parameter about −25% or +25% (bottom or top numbers) are given in per cent. In the bottom line the overall uncertainty of the RBE value is given, provided the uncertainties of α, β and D_t are 10%, 20% and 30%, respectively.

	$\alpha/\beta = 2$ Gy		$\alpha/\beta = 10$ Gy	
	Monoenergetic	SOBP	Monoenergetic	SOBP
LET or LET_D	77 keV $\mu\mathrm{m}^{-1}$	54 keV $\mu\mathrm{m}^{-1}$	77 keV $\mu\mathrm{m}^{-1}$	52 keV $\mu\mathrm{m}^{-1}$
RBE	3.63	1.98	2.52	1.48
	$\frac{\Delta\mathrm{RBE}}{\mathrm{RBE}}$(%)	$\frac{\Delta\mathrm{RBE}}{\mathrm{RBE}}$(%)	$\frac{\Delta\mathrm{RBE}}{\mathrm{RBE}}$(%)	$\frac{\Delta\mathrm{RBE}}{\mathrm{RBE}}$(%)
α	−6.3 +7.7	−4.5 +5.7	−10.1 +32.8	−5.9 +8.5
β	+4.1 −6.4	+1.9 −3.0	+7.7 −9.3	+3.4 −4.3
D_t	+14.5 −17.1	+7.6 −9.0	+6.4 −9.5	+2.5 −3.7
Δ(%)	20.2	10.7	18.1	7.0

on the parameter sensitivity of RBE in more detail, the centre of a carbon SOBP composed from two opposing beams and representing a mixed radiation field, was compared with a monoenergetic beam of high LET, mimicking the distal end of a one-sided SOBP. While in the former case the radiation field is composed of an overlay of low and high LET components, in the latter only one high LET component is contributing. Table 4 contains the relative change of the RBE after an initial change of one of the specific parameters α, β and D_t of $\pm 25\%$ for both cases, where the restriction to the photon parameters is justified by arguments given in the last subsection. The SOBP has been chosen as in section 5 with two opposing fields optimized to a RBE-weighted dose of 3 Gy and extended to 60 mm in a depth of 150 mm in the isocentre. There, the dose averaged LET is 54 keV $\mu\mathrm{m}^{-1}$ and 52 keV $\mu\mathrm{m}^{-1}$ for $\alpha/\beta = 2$ Gy and $\alpha/\beta = 10$ Gy, respectively, where there is a small difference as the dose optimization respects the α/β ratio and hence results in different LET compositions of the fields. For the monoenergetic beam an LET of 77 keV $\mu\mathrm{m}^{-1}$ was chosen as in section 4, but to allow comparison on the same dose level the RBE was here evaluated at 3 Gy RBE-weighted dose instead of considering RBE_α or RBE_{10} as before.

For any varied parameter, the relative change of the RBE in the SOBP is damped compared to the change detected for the monoenergetic beam. The damping can still be observed for a comparison of the SOBP with a monoenergetic beam of comparable LET (about 50 keV $\mu\mathrm{m}^{-1}$, data not shown). Thus it is obviously a consequence of the broader LET distribution within a SOBP. But the damping of RBE sensitivity goes along with a smaller RBE. Hence for clinical applications a compromise between the RBE and its uncertainties has to be found. If the RBE is large, so will be its relative uncertainty, and vice versa.

When a photon dose response curve is known, often one of the parameters α and β can be determined quite well, while the other has a higher uncertainty. The most crucial part, however, is to determine an appropriate value for D_t, which is hardly accessible in experiments or clinical data. As a good estimate one can apply an empirical relationship between D_t and the α/β ratio, or determine D_t by a fit to high LET data, if available. Exemplarily we here assume that α, β and D_t are known with uncertainties of 10%, 20% and 30%, respectively, which seem to be typical estimates. We calculated the corresponding partial uncertainties of RBE by scaling the numbers given in table 4 from a 25% variation to these uncertainty levels. By calculating the propagation of the errors one can now evaluate an overall uncertainty in the following way:

bearing in mind that there is an anti-correlation between α and β induced by the common LQ fit procedures we simply added their relative errors, which is a rather pessimistic way of propagating errors, as it does not allow for mutual uncertainty compensation. From this sum and the uncertainty of D_t then a total uncertainty was calculated by means of Gaussian error propagation, allowing for such partial compensation of uncertainties. As a result, the overall relative uncertainties Δ given in the bottom line of table 4 are obtained.

These numbers are on the one hand typical and indicate the order of magnitude of uncertainty which is usually expected for RBE simulations with the LEM. They clearly demonstrate the damping of RBE uncertainties within a SOBP compared to monoenergetic irradiations. In particular the detected deviations for the irradiation within a SOBP is about 10%, which is in the order of magnitude acceptable for clinical applications. But this calculation is an example and specific for the choice of the parameters and uncertainty levels of the specific parameters as well as on the irradiation geometry. The numbers given should hence not be understood as a general uncertainty analysis. They rather indicate the order of magnitude of RBE uncertainty to be expected, while for any particular case such an analysis should be considered individually.

6.4. Sensitivity on photon and ion dose response

As RBE is a relative quantity comparing the doses needed with photons and ions for the same effect, the question arises if the RBE sensitivity on an input parameter is caused by the sensitivity of either the ion or the photon dose response curve. This was approached by monitoring the relative change of doses for ion and photon radiation at the same effect under parameter variation.

Generally, a change of α will result in larger dose changes for photons as compared to ions. Hence the RBE sensitivity on α is not due to the high LET dose response, but rather reflects the uncertainty of the photon dose response itself. In contrast, a change of β term will, for moderate effects, change the ion dose response curve more severely than the photon dose response curve. This is because the initial slope of ion survival curves strongly depends on the photon β parameter which quantifies the nonlinear dose response and hence scales the enhanced effects of high local doses as delivered to the tissues by individual charged particles along their tracks.

Thus, concerning α, there is a smaller level of uncertainty in ion therapy as compared to conventional photon therapies, while for β it is just the opposite. Hence a good fraction (cf table 4) of the overall uncertainty calculated in the last subsection, corresponding to α will also be present in a treatment with photon radiation.

6.5. Sensitivity for fixed α/β ratio

From clinical studies there are several ways of obtaining information of the photon dose response parameters. Quite often the α/β ratio can be fixed quite well (e.g. when found from fractionation studies) while the derived absolute parameter values α and β can be challenged. Hence it is also of interest to investigate the RBE dependence on photon parameter change when the α/β ratio stays fixed, i.e. when α and β are changed jointly by the same factor of 25%. This was checked, and we found for the therapeutic relevant LET range that there is almost no dependence of RBE_α on parameter change, and that there is about 10% or 5% maximum change of RBE_{10} for $\alpha/\beta = 2$ and 10 Gy, respectively. This can be interpreted by the principles of LEM: The action of individual ions is expressed by the linear coefficient α_I of ion dose response curves, which directly determines RBE_α. In LEM, it is obtained as an

extrapolation from photon effects, which are linear in both α and β. If they both are scaled by a common factor, so will α_I, and hence RBE_α remains constant. As for the quadratic component β_I nonlinear terms arise, describing the interaction of lesions from different ions, this argument does not hold and thus a sensitivity of RBE_{10} on parameter change is detected.

In clinical practice, however, as both α and β are affected by uncertainties (e.g. due to a limited patient number but also due to inter-individual differences), the α/β will also show an uncertainty. Thus always a sensitivity analysis for different α/β ratios should be carried out in prospective treatment planning.

6.6. Sensitivity on distributions of input parameters

In a population of cells the input parameters for estimating the RBE might not assume a single value but rather be subject to a distribution. For instance the geometrical cross section of cell nuclei shows a broad distribution for most cell lines. Then in a first approach the strategy is to rely on the mean of the parameter values, resulting in a RBE which approximates the mean RBE to first order. Associated uncertainties can be estimated using the sensitivity analysis presented here.

A full consideration of distribution effects would require to determine the contribution of each subpopulation of the distribution to the corresponding RBE distribution. However, for a more pragmatic handling the parameter distribution is replaced by an effective parameter, reproducing the mean RBE. For the nuclear geometrical cross sections at high LET where the RBE is sensitive on the nuclear cross section due to overkill, for a given distribution of cross sections an effective cross section of typically less than the mean (about 80%) will reproduce the mean RBE (Elsässer *et al* 2008).

Another example where uncertainties due to parameter distributions play a role is the variability in dose response within a patient population in therapy. It is common procedure to apply non-individualized regimens, where recommended doses are found by dose escalation studies over sufficient large patient numbers. The distribution of radiosensitivity parameters leads to a flattening of the dose response curve of tumour control (Dasu *et al* 2003). This phenomenon can be quite crucial and eventually has to be taken into account for analysis of clinical outcomes (Kanai *et al* 2006). However, as seen for the α term in this study the population heterogeneity has higher impact on dose response to photon than to ion radiation (Scholz *et al* 2006). A more personalized determination of input parameters, e.g. by means of biomarkers, could help to further reduce uncertainties.

6.7. Strategies for sensitivity minimization

The general goal of any kind of radiation therapy modality is to deliver dose in the target region and to avoid dose delivery as good as possible within the surrounding healthy tissue. Further constraints as sparing out organs at risk may apply. But regarding charged particle therapy recent work (Bassler *et al* 2010, Grassberger *et al* 2011) questions if a homogeneous dose distribution across the target should be the only objective in treatment planning. Additionally, LET homogeneity could be another promising objective. In addition to dose homogeneity, LET homogeneity promises to reduce RBE uncertainties. Other studies investigated practical applicability, e.g. by ramp fields (Krämer and Jäkel 2005) or by modifying the LET distribution by active scanning (Grassberger *et al* 2011) and quantified implications for the RBE uncertainty (Böhlen *et al* 2012). In a previous work (Grün *et al* 2012) we demonstrated that the delivery of dose in two opposing fields, both contributing equally to the overall dose, reduces the

uncertainties very effectively. Table 4 gives evidence for the reduced RBE uncertainty (damping), but also demonstrates the reduction of RBE going along.

Unavoidably, an uncertainty-free RBE model cannot exist, as the biological determinants of RBE, i.e. the radiosensitivity parameters, are subject to variability. Hence a reduction of RBE uncertainty as much as possible as a consequence of a more homogeneous LET distribution might be desirable, and could be realized by combining different fields irradiated in different angles in the target volume, or even inhomogeneous dose fields adding up to a homogeneous dose across the target volume. Finally, depending on particular aspects of the treatment plans, a compromise between a high RBE in the target (without caring about LET distribution) and a lower, but less uncertain RBE (applying a rather homogeneous LET distribution) has to be found.

6.8. Relation to other RBE models and to experimental RBE data

Throughout this paper, many aspects of RBE uncertainty have been discussed at hand of the LEM. But most of the implications of this study are also revealed by other high LET models. In the MKM, which is the only model apart from LEM used in clinical practice in recent versions (Inaniwa *et al* 2010, Sato and Furusawa 2012), the prediction of the RBE is based on the dose response to photon radiation, too, and hence their uncertainties are propagated to RBE in a similar way. The model of Carabe and Jones (Carabe-Fernandez *et al* 2007, Jones *et al* 2012) is a reformulation of the LQ model and thus input data of both radiation qualities are needed for which the RBE is to be predicted. It uses only few assumptions and also demonstrates the direct dependence of RBE on photon dose response parameters.

Finally, by investigating experimental RBE data (Friedrich *et al* 2013, Paganetti *et al* 2002), a scatter of measured RBE values of *in vitro* cell survival experiments reflects the order of magnitude of RBE uncertainty corresponding to the model predictions (calculated from typical uncertainties of the photon parameters as in table 4), except for low LET where some remaining systematic deviations of LEM predictions in comparison to experimental RBE values are present. To give an order of magnitude, for monoenergetic carbon ions with an LET of 77 keV μm^{-1} at 3 Gy the typical RBE uncertainty is 20% and almost independent on the α/β ratio. As outlined before, this number will be damped within an SOBP.

This agreement between RBE uncertainties observed in experiments and the uncertainties predicted by RBE modelling is a further strong support that LEM is able to predict essential characteristics of RBE. This also implies that the results presented in this study are not model specific, but are rather general properties of RBE.

7. Conclusions

This work provides a detailed and systematic discussion of the sensitivity of RBE to its determining parameters. It demonstrates that radiobiologic models such as LEM are suitable to predict RBE along with the RBE uncertainty for applications in radiobiologic experiments and particle therapy. In particular two findings which have been presented in the previous sections are important for the discussion of simulated RBE values. First, the RBE values depend typically less than proportional on the determining parameters, with few exceptions only. Second, going over from cells or tissues irradiated with monoenergetic beams to extended volumes irradiated with a SOBP, the influence of uncertainties on RBE values are damped due to the mix of radiation qualities at each position in the SOBP. The results and methods presented may thus be helpful for optimizing the precision of RBE predictions.

Acknowledgments

This work was partly supported by Siemens Healthcare. Work is part of HGS-HIRe.

References

Ando K and Kase Y 2009 Biological characteristics of carbon-ion therapy *Int. J. Radiat. Biol.* **85** 715–28

Astrahan M 2008 Some implications of linear-quadratic-linear radiation dose-response with regard to hypofractionation *Med. Phys.* **35** 4161–72

Bassler N, Jäkel O, Søndergaard C S and Petersen J B 2010 Dose- and LET-painting with particle therapy *Acta Oncol.* **49** 1170–6

Böhlen T T *et al* 2012 Investigating the robustness of ion beam therapy treatment plans to uncertainties in biological treatment parameters *Phys. Med. Biol.* **57** 7983–8004

Brenner D J 1993 Dose, volume, and tumor-control predictions in radiotherapy *Int. J. Radiat. Oncol. Biol. Phys.* **26** 171–9

Carabe-Fernandez A, Dale R G and Jones B 2007 The incorporation of the concept of minimum RBE (RBEmin) into the linear-quadratic model and the potential for improved radiobiological analysis of high-LET treatments *Int. J. Radiat. Biol.* **83** 27–39

Carlone M, Wilkins D and Raaphorst P 2005 The modified linear-quadratic model of Guerrero and Li can be derived from a mechanistic basis and exhibits linear-quadratic-linear behaviour *Phys. Med. Biol.* **50** L9–15

Combs S E *et al* 2010 Heidelberg ion therapy center (HIT): initial clinical experience in the first 80 patients *Acta Oncol.* **49** 1132–40

Cucinotta F A, Nikjoo H and Goodhead D T 1999 Applications of amorphous track models in radiation biology *Radiat. Environ. Biophys.* **38** 81–92

Curtis S B 1986 Lethal and potentially lethal lesions induced by radiation—a unified repair model *Radiat. Res.* **106** 252–70

Dasu A, Toma-Dasu I and Fowler J F 2003 Should single or distributed parameters be used to explain the steepness of tumour control probability curves? *Phys. Med. Biol.* **48** 387–97

Elsässer T, Cunrath R, Krämer M and Scholz M 2008 Impact of track structure calculations on biological treatment planning in ion radiotherapy *New J. Phys.* **10** 075005

Elsässer T, Krämer M and Scholz M 2008 Accuracy of the local effect model for the prediction of biologic effects of carbon ion beams *in vitro* and *in vivo* *Int. J. Radiat. Oncol. Biol. Phys.* **71** 866–72

Elsässer T and Scholz M 2007 Cluster effects within the local effect model *Radiat. Res.* **167** 319–29

Elsässer T *et al* 2010 Quantification of the relative biological effectiveness for ion beam radiotherapy: direct experimental comparison of proton and carbon ion beams and a novel approach for treatment planning *Int. J. Radiat. Oncol. Biol. Phys.* **78** 1177–83

Fertil B and Malaise E P 1985 Intrinsic radiosensitivity of human cell lines is correlated with radioresponsiveness of human tumors: analysis of 101 published survival curves *Int. J. Radiat. Oncol. Biol. Phys.* **11** 1699–707

Fertil B, Reydellet I and Deschavanne P J 1994 A benchmark of cell survival models using survival curves for human cells after completion of repair of potentially lethal damage *Radiat. Res.* **138** 61–9

Friedrich T, Durante M and Scholz M 2012a Modeling cell survival after photon irradiation based on double-strand break clustering in megabase pair chromatin loops *Radiat. Res.* **178** 385–94

Friedrich T, Scholz U, Elsässer T, Durante M and Scholz M 2013 Systematic analysis of RBE and related quantities using a database of cell survival experiments with ion beam irradiation *J. Radiat. Res.* **54** 494–514

Friedrich T, Scholz U, Elsässer T, Durante M and Scholz M 2012b Calculation of the biological effects of ion beams based on the microscopic spatial damage distribution pattern *Int. J. Radiat. Biol.* **88** 103–7

Furusawa Y *et al* 2000 Inactivation of aerobic and hypoxic cells from three different cell lines by accelerated 3He-, 12C- and 20Ne-Ion beams *Radiat. Res.* **154** 485–96

Garcia L M, Wilkins D E and Raaphorst G P 2007 Alpha/beta ratio: a dose range dependence study *Int. J. Radiat. Oncol. Biol. Phys.* **67** 587–93

Gerweck L E and Kozin S V 1999 Relative biological effectiveness of proton beams in clinical therapy *Radiother. Oncol.* **50** 135–42

Goodhead D T 2006 Energy deposition stochastics and track structure: what about the target? *Radiat. Prot. Dosim.* **122** 3–15

Grassberger C, Trofimov A, Lomax A and Paganetti H 2011 Variations in linear energy transfer within clinical proton therapy fields and the potential for biological treatment planning *Int. J. Radiat. Oncol. Biol. Phys.* **80** 1559–66

Grün R *et al* 2012 Impact of enhancements in the local effect model (LEM) on the predicted RBE-weighted target dose distribution in carbon ion therapy *Phys. Med. Biol.* **57** 7261–74
Guerrero M and Li A X 2004 Extending the linear-quadratic model for large fraction doses pertinent to stereotactic radiotherapy *Phys. Med. Biol.* **49** 4825–35
Gunzert-Marx K, Iwase H, Schardt D and Simon R S 2008 Secondary beam fragments produced by 200 MeVu^{-1}^{12}C ions in water and their dose contributions in carbon ion radiotherapy *New J. Phys.* **10** 075003
Hawkins R B 1994 A statistical theory of cell killing by radiation of varying linear energy transfer *Radiat. Res.* **140** 366–74
Hawkins R B 1996 A microdosimetric-kinetic model of cell death from exposure to ionizing radiation of any LET, with experimental and clinical applications *Int. J. Radiat. Biol.* **69** 739–55
Inaniwa T *et al* 2010 Treatment planning for a scanned carbon beam with a modified microdosimetric kinetic model *Phys. Med. Biol.* **55** 6721–37
Jones B, Wilson P, Nagano A, Fenwick J and McKenna G 2012 Dilemmas concerning dose distribution and the influence of relative biological effect in proton beam therapy of medulloblastoma *Br. J. Radiol.* **85** e912–8
Kanai T *et al* 2006 Examination of GyE system for HIMAC carbon therapy *Int. J. Radiat. Oncol. Biol. Phys.* **64** 650–6
Kiefer J and Straaten H 1986 A model of ion track structure based on classical collision dynamics *Phys. Med. Biol.* **31** 1201–9
Krämer M and Jäkel O 2005 Biological dose optimization using ramp-like dose gradients in ion irradiation fields *Phys. Medica* **21** 107–11
Krämer M, Jäkel O, Haberer H, Kraft G, Schardt D and Weber U 2000 Treatment planning for heavy-ion radiotherapy: physical beam model and dose optimization *Phys. Med. Biol.* **45** 3299–317
Krämer M and Scholz M 2000 Treatment planning for heavy-ion radiotherapy: calculation and optimization of biologically effective dose *Phys. Med. Biol.* **45** 3319–30
Lühr A, Hansen D C, Teiwes R, Sobolevsky N, Jäkel O and Bassler N 2012 The impact of modeling nuclear fragmentation on delivered dose and radiobiology in ion therapy *Phys. Med. Biol.* **57** 5169–85
Moiseenko V V, Hamm R N, Waker A J and Prestwich W V 2001 Calculation of radiation-induced DNA damage from photons and tritium beta-particles: part II. Tritium RBE and damage complexity *Radiat. Environ. Biophys.* **40** 23–31
Mozumder A 2007 Track-core radius of charged particles at relativistic speed in condensed media *J. Chem. Phys.* **60** 1145–48
Neary G J, Evans H J, Tonkinson S M and Williamson F S 1959 The relative biological efficiency of single doses of fast neutrons and gamma-rays on Vicia faba roots and the effect of oxygen: part III. Mitotic delay *Int. J. Radiat. Biol.* **1** 230–40
Neumaier T *et al* 2012 Evidence for formation of DNA repair centers and dose-response nonlinearity in human cells *Proc. Natl Acad. Sci. USA* **109** 443–8
Nikjoo H, O'Neill P, Goodhead D T and Terrissol M 1997 Computational modelling of low-energy electron-induced DNA damage by early physical and chemical events *Int. J. Radiat. Biol.* **71** 467–83
Paganetti H, Niemierko A, Ancukiewicz M, Gerweck L E, Goitein M, Loeffler J S and Suit H D 2002 Relative biological effectiveness (RBE) values for proton beam therapy *Int. J. Radiat. Oncol. Biol. Phys.* **53** 407–21
Prise K M, Pinto M, Newman H C and Michael B D 2001 A review of studies of ionizing radiation-induced double-strand break clustering *Radiat. Res.* **156** 572–76
Rossi H H and Zaider M 1996 *Microdosimetry and its Application* (Berlin: Springer)
Sato T and Furusawa Y 2012 Cell survival fraction estimation based on the probability densities of domain and cell nucleus specific energies using improved microdosimetric kinetic models *Radiat. Res.* **178** 341–56
Scholz M and Elsässer T 2007 Biophysical models in ion beam radiotherapy *Adv. Space Res.* **40** 1381–91
Scholz M, Kellerer A M, Kraft-Weyrather W and Kraft G 1997 Computation of cell survival in heavy ion beams for therapy: the model and its approximation *Radiat. Environ. Biophys.* **36** 59–66
Scholz M, Matsufuji N and Kanai T 2006 Test of the local effect model using clinical data: tumour control probability for lung tumours after treatment with carbon ion beams *Radiat. Prot. Dosim.* **122** 478–9
Schulz-Ertner D *et al* 2007 Effectiveness of carbon ion radiotherapy in the treatment of skull-base chordoma *Int. J. Radiat. Oncol. Biol. Phys.* **68** 449–57
Shao C, Saito M and Yu Z 1999 Formation of single- and double-strand breaks of pBR322 plasmid irradiated in the presence of scavengers *Radiat. Environ. Biophys.* **38** 105–9
Steel G G and Peacock J H 1989 Why are some human tumours more radiosensitive than others? *Radiother. Oncol.* **15** 63–72
Stenerlöw B, Karlsson K H, Cooper B and Rydberg B 2003 Measurement of prompt DNA double-strand breaks in mammalian cells without including heat-labile sites: results for cells deficient in nonhomologous end joining *Radiat. Res.* **159** 502–10

Suzuki M, Kase Y, Yamaguchi H, Kanai T and Ando K 2000 Relative biological effectiveness for cell-killing effect on various human cell lines irradiated with heavy-ion medical accelerator in Chiba (HIMAC) carbon-ion beams *Int. J. Radiat. Oncol. Biol. Phys.* **48** 241–50

Tobias CA 1985 The repair–misrepair model in radiobiology: comparison to other models *Radiat. Res. Suppl.* **8** S77–95

Tsujii H and Kamada T 2012 A review of update clinical results of carbon ion radiotherapy *Japan J. Clin. Oncol.* **42** 670–85

Yokota H *et al* 1995 Evidence for the organization of chromatin in megabase pair-sized loops arranged along a random walk path in the human G0/G1 interphase nucleus *J. Cell. Biol.* **130** 1239–49

7.5 Article 5: Mathematical aspects of RBE uncertainties

Radiat Environ Biophys (2010) 49:345–349
DOI 10.1007/s00411-010-0298-9

ORIGINAL PAPER

Accuracy of RBE: experimental and theoretical considerations

T. Friedrich · W. Weyrather · T. Elsässer · M. Durante · M. Scholz

Received: 15 October 2009 / Accepted: 21 May 2010 / Published online: 17 June 2010

Abstract The concept of the relative biological effectiveness (RBE) is essential for treatment planning in carbon ion therapy and for understanding the biological effects of high-LET radiation. As this quantity depends on many factors, both its experimental determination and the assessment of its uncertainty are not trivial. For the limiting case of zero dose, where the RBE takes its maximum value RBE_α, we present in this article a simple empirical-based approach to estimate its uncertainty. A Gaussian error calculus is applied to equally take into account both uncertainties from experiments with high- and low-LET radiation. From a theoretical point of view, we then infer, using a simple Monte Carlo model, the distribution of RBE_α values. This illustrates why the conventional error propagation approach is inappropriate in some cases. In these cases, likewise also the error estimates have to be obtained with a more sophisticated approach. Uncertainties of RBE, visualized by error bars, are of importance for treatment planning and also for setting up a precision goal for predicting biophysical models such as the local effect model.

This manuscript is based on a contribution given at the "Heavy Ions in Therapy and Space Symposium 2009", July 6–10, 2009, Cologne, Germany.

T. Friedrich (✉) · W. Weyrather · T. Elsässer · M. Durante · M. Scholz
GSI Helmholtzzentrum für Schwerionenforschung,
Planckstraße 1, 64291 Darmstadt, Germany
e-mail: t.friedrich@gsi.de
URL: http://www.gsi.de/forschung/bio/

M. Durante
Institut für Festkörperphysik, Technische Universität Darmstadt,
Hochschulstraße 6, 64289 Darmstadt, Germany

Introduction

Cancer therapy with carbon ions benefits, apart from an inverted depth-dose profile, from an enhanced RBE compared to conventional photon radiation (Hall and Giaccia 2006). Thus, knowing the RBE is essential for successful treatment planning (Kraft 1999). An analysis of its uncertainties is hence relevant for establishing precision goals for predictive models such as the local effect model, LEM (Scholz et al. 1997; Elsässer et al. 2008a, b) or the microdosimetric kinetic model (Hawkins 1994; Hawkins 2003).

The RBE is defined as the ratio of a photon dose D_γ and a corresponding ion dose D_I yielding the same effect:

$$\mathrm{RBE} = \left.\frac{D_\gamma}{D_I}\right|_{\mathrm{Iso-effect}} \tag{1}$$

Henceforth, the experimental determination of RBE involves both experiments with photon and ion radiation. The RBE for a particular experimental or therapeutic set-up depends on many parameters, such as tissue- or cell-type, the LET spectrum of the radiation, on dose and several more. It usually decreases with increasing dose and thus reaches its maximum for the zero-dose limit,

$$\mathrm{RBE}_\alpha = \frac{\alpha_I}{\alpha_\gamma} \tag{2}$$

where the α parameters are the linear coefficients of the linear quadratic (LQ) model (Douglas and Fowler 1976), which establishes a relationship between dose and effect level.

The biological reason for an enhanced effectiveness are high local doses restricted to small parts of the cell nuclei as deposited by ions, compared to rather moderate doses as deposited by photons over the whole cell nucleus (Kraft

1999). Due to the emergence of more complex lesions, the former case turns out to be more effective, therefore exhibiting RBE values larger than one.

As measurements of RBE are always associated with an uncertainty, RBEs are likewise affected with variability. However, a prerequisite for the prediction and the effect of different radiation qualities is the knowledge of their RBEs. To assess them, also the associated variances (usually visualized as error bars) are needed. The determination of the latter is the subject of the presented work.

The emergence of the variability in RBE is caused mainly by two distinguishable reasons. One is a composition of several stochastic processes as, e.g., those involved in preparing cell culture assays, in cell counting and in cell killing by radiation for the case of cell survival experiments. The other reason is the variable radiosensitivity of the cells that depends on many environmental conditions such as nutrient supply, growth density or the stresses experienced within culture preparation (which itself depends on several factors and may vary between different laboratories), as well as the individual cell type–specific sensitivity (Hall and Giaccia 2006; Kraft 1999). Note that the latter is not fixed but may change with time, as the properties of a cell line may change gradually. As these aspects are extremely complex, it is hardly feasible to monitor or to model them from first principles. Starting from either a huge set of experimental data or from reasonable assumptions based on experience, we approach this goal in this paper from two perspectives: In the next section, we focus on the problem from an empirical point of view. Experimental experience from ion and photon experiments allows to roughly estimate the uncertainty of the α parameters of survival curves. By means of Gaussian error calculus, those can be converted into errors of the RBE. Application to a real data set shows that the errors are a bit overestimated using this method, but the error bars are still in the expected range of magnitude. A more thorough look on the properties of RBE can be gained by looking not only at its variability, but on its whole distribution. This is carried out in the section about theoretical considerations, where the propagation of errors is monitored, starting from a hypothetical set of generated α parameters that follow Gaussian distributions. As will turn out, for a correct inference of the RBE, a bias correction has to be taken into account. Finally, we comment in the discussion section on the implications of these findings for models predicting the RBE.

Empirical approach

On a purely empirical level, we evaluated the fluctuations of α parameters for survival experiments. For the case of low-LET irradiation (X-rays), we investigated survival data of CHO cells, which have been taken over several years. We found that the α values of all survival curves were distributed with a peaked distribution with $\alpha = (0.162 \pm 0.083)\ \mathrm{Gy}^{-1}$. The observed variability is larger than that for a single set of experiments performed at one time (Kraft 1999), where several of the systematic errors listed previously do not enter in detected deviations. For the case of high-LET irradiation, we investigated the data sets provided in Furusawa et al. (2000). This work reports the dependence of α on linear energy transfer (LET) for different cell lines and ion species. An appropriate model function (Takatsuji et al. 1999) allows to successfully fit the RBE-LET dependence up to high LETs, where the overkill effect becomes dominant. We then could extract the remaining fluctuations of RBE values around the fit line. We found that the absolute fluctuation widths are almost independent from the cell–ion combination. Similarly, there seems to be no dependence on LET within the therapeutic relevant range up to about 100 keV/µm. In this range, we found for a variety of cell–ion combination as presented by Furusawa and co-workers (Furusawa et al. 2000) a standard deviation $\Delta\alpha_I = 0.140\ \mathrm{Gy}^{-1}$, which differs from the uncertainty detected in our analysis of photon experiments, but is still in the same order of magnitude. We propose thus

$$\Delta\alpha \approx \Delta\alpha_\gamma \approx \Delta\alpha_I \tag{3}$$

and assert a value of $\Delta\alpha = 0.1\ \mathrm{Gy}^{-1}$ as a rough estimate for the uncertainty in the α parameter both for high- and low-LET radiation.

To transfer these uncertainties in an uncertainty of the RBE_α, we use the conventional Gaussian error propagation on the definition of RBE_α as given in Eq. (2), resulting in

$$\frac{\Delta\mathrm{RBE}_\alpha}{\mathrm{RBE}_\alpha} = \sqrt{\left(\frac{\Delta\alpha_\gamma}{\alpha_\gamma}\right)^2 + \left(\frac{\Delta\alpha_I}{\alpha_I}\right)^2}. \tag{4}$$

Note that this equation assumes independent Gaussian distributed uncertainties of both the ion and photon parameters. While we checked the former assumption for the experimental data used in this paper with statistical tests, the latter one is not strictly true. The α parameters appear to be slightly positively correlated, which may lead to a further decrease in the corresponding error in RBE. The application of Eq. (4) requires the knowledge of uncertainties. To make use of the handy estimate $\Delta\alpha = 0.1\ \mathrm{Gy}^{-1}$, combining Eqs. (3) and (4) yields

$$\Delta\mathrm{RBE}_\alpha = \frac{\Delta\alpha}{\alpha_\gamma}\sqrt{1 + \mathrm{RBE}_\alpha^2}. \tag{5}$$

To apply this estimate for numerical values, α_γ and RBE_α have to be inferred from the experiment, and

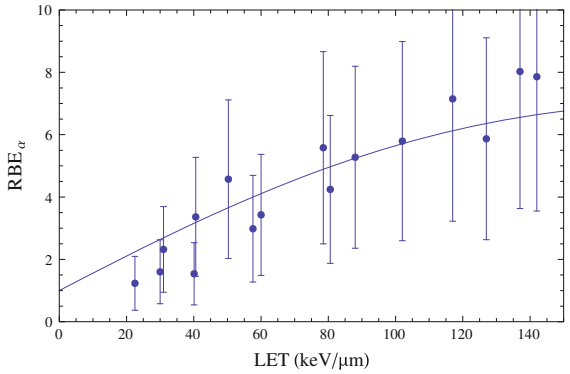

Fig. 1 RBE$_\alpha$ dependence on LET for V79 cells irradiated with carbon ions. The *solid line* shows a non-linear fit that is capable to reproduce the RBE-LET characteristics up to high LETs. The error bars were associated according to Eq. (5) and contain both contributions of uncertainties experiments with photons and ions

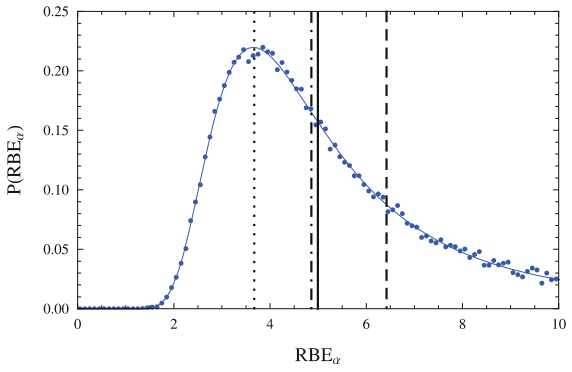

Fig. 2 Distribution of RBE$_\alpha$ values simulated by a Monte Carlo Model (points) with Gaussian distributed α parameters with $<\alpha_\gamma> = 0.2$ Gy^{-1} and $<\alpha_I> = 1$ Gy^{-1} for photon and ion experiments, respectively. A category width of 0.1 was chosen for binning. The solid curve emerges from an analytical treatment, see the "Appendix". The mean (*dashed line*) and the value where the distribution takes its maximum (*dotted line*) of the distribution deviate considerably from the design value (*thick line*). In contrast, the median value provides the best approximation (*dashed-dotted line*)

$\Delta\alpha = 0.1$ Gy^{-1} is used to estimate the uncertainty in the measurements.

In Fig. 1, we show some of the data of Furusawa et al., where experimentally obtained RBE$_\alpha$ values of V79 cells at different LETs have been associated with error bars. They were derived from deviations to a model fit (Takatsuji et al. 1999) that represents the measured data nicely as was checked by hypothesis tests. Note that the error bars appear larger in this figure than the residual deviations of the points from the fit line. This reflects the fact that a deviation in the photon parameters would result in a systematic shift of RBE$_\alpha$ of all data points in this plot. Moreover, the size of the error bars matches what is expected from experimental experience. Clearly, the uncertainties increase with rising RBE$_\alpha$, as can be seen already by the investigation of Eq. (5).

Theoretical considerations

Apart from the condition of independent Gaussian distribution, there is a further requirement for the validity of Eq. (4): The errors of $\Delta\alpha$ have to be much smaller than the α parameters. Within the range of frequently occurring values, this condition is not always fulfilled.

To investigate this situation in more detail, we performed a Monte Carlo model, in which we generated two sets of hypothetical α values. Both sets consist of independent Gaussian distributed random numbers. These sets $\{\alpha_\gamma\}$ and $\{\alpha_I\}$ mimic alpha values obtained after low- and high-LET radiation, respectively. The mean value $<\alpha_\gamma>$ obtained from the photon set is chosen smaller than $<\alpha_I>$ obtained from the ion set. By forming pairs $(\alpha_\gamma, \alpha_I)$ of elements from both sets and dividing the second by the first constituent, a set of hypothetical RBE$_\alpha$ values $\{\text{RBE}_\alpha\}$ is finally obtained whose properties can then be considered. Note that the distribution of RBE$_\alpha$ can also be elaborated analytically. The idea and the results are given in the "Appendix".

We choose $<\alpha_\gamma> = 0.2$ Gy^{-1} and $<\alpha_I> = 1$ Gy^{-1} and a universal uncertainty $\Delta\alpha = 0.1$ Gy^{-1}. Thus, RBE$_\alpha$ = $<\alpha_I>/<\alpha_\gamma> = 5$ by design. In Fig. 2, we present the distribution of 50,000 Monte Carlo simulated RBE$_\alpha$ values, together with the analytic distribution. This distribution has several interesting features: (i) it has a long tail and no symmetries (ii) its mean value overestimates the RBE$_\alpha$ (iii) the RBE$_\alpha$ at which the distribution reaches its maximum underestimates the RBE$_\alpha$ and (iv) its standard deviation diverges while the width of the prominent peak is comparable with the expected error ΔRBE$_\alpha = 2.55$ by means of Eq. (5). Moreover, the distribution has also a small negative component (not shown).

The reason for these properties can be found in the distribution of $\{\alpha_\gamma\}$, which does not vanish at values close to zero or even negative values. When the division by these numbers is carried out, the RBE$_\alpha$ is caused to diverge or to become negative. To deal with this situation, one would have to add a bias correction for the average $<$RBE$_\alpha>$ in order to approach the design value. However, this procedure is neither trivial nor illustrative.

Discussion

When comparing both approaches to obtain information about the RBE$_\alpha$ presented above, we may conclude that the empirical approach serves as a reasonable tool to estimate

the uncertainty of the RBE_α. This is confirmed by the theoretical approach, where the width of the prominent peak in the distribution of RBE_α is of comparable size as its estimated uncertainty, even though the determined mean RBE_α value is not a good predictor for the designed RBE_α. Hence, the question remains what one can do about a possibly misleading inference of the RBE_α value, which has been demonstrated by the Monte Carlo model. We suggest here two practical ways to overcome this difficulty: First, one generally should avoid to average over RBE values. A better way is to calculate averages from the linear quadratic parameters and finally compute the RBE from these averages. However, if these parameters are not at hand, the alternative approach would consist in calculating the median RBE_α. The concept of the median lacks of an easy statistical interpretation, but is by far less sensitive to extreme values. For the example presented in the last section, the median RBE_α is 4.85 and thus only deviates little from the design value, c.f. Fig. 2. The analysis presented here should be applicable for the whole spectrum of particle radiation. For light ions, also the mean value should be a good predictor, since they provide a rather small RBE and the median and mean values lie close together.

To summarize, we presented in this article an approach to understand uncertainties of the RBE. We here covered only the limiting case of RBE_α and presented practicable ways to infer its value from experimental data based on dose–effect curves (by computing arithmetic means of α_γ values) or measured RBE_α values (by computing their median). Although the RBE_α has a simple definition, a thorough development of its uncertainties is a non-trivial task (c.f. the "Appendix"). It turns out that reliable experimental data for the dose response to photon radiation imply reasonably low uncertainties in the RBE_α, as reflected yet by the empirical error model.

Generally, the dependence of RBE on the LQ parameters α and β is more complicated than in the case considered here. A rigorous error analysis for the dose-dependent RBE has to our knowledge not been developed so far. We suggest that the Monte Carlo simulations could prove as a fruitful tool to monitor error propagation in these more complicated situations, where an analytical approach is not applicable for the evaluation of realistic uncertainties. To perform tests on biophysical models such as the local effect model, predictions must be compared to experimental data. For establishing rigorous test procedures, the errors of the latter have to be known. The model is then requested to resemble the data within the experimental accuracy. Consequently, the uncertainty analysis presented in this paper will help to define precision goals for approaches to estimate RBE values for treatment planning in ion therapy.

Acknowledgments This work gained support from Siemens Healthcare.

Appendix

In order to derive the distribution of RBE_α, we set up a statistical model starting from two sets $\{\alpha_\gamma\}$ and $\{\alpha_I\}$ of artificial parameters for photon and ion irradiation, respectively. Their elements are Gaussian distributed

$$p_q(\alpha_q) = \frac{1}{\sqrt{2\pi(\Delta\alpha)^2}} \exp\left\{ -\frac{(\alpha_q - \langle\alpha_q\rangle)^2}{2(\Delta\alpha)^2} \right\} \tag{A1}$$

where the index $q = \gamma$ or $q = \mathrm{I}$ for photon or ion irradiation, respectively, and $\Delta\alpha = \Delta\alpha_\gamma = \Delta\alpha_\mathrm{I}$. Due to their statistical independence, their joint probability distribution is

$$p(\alpha_\gamma, \alpha_I) = p_\gamma(\alpha_\gamma) p_I(\alpha_I) \tag{A2}$$

The distribution of a ratio $Z = X/Y$ of two independent random variables X and Y with joint probability function $p(x, y)$ is given by

$$P(z) = \int_{-\infty}^{\infty} |y| p(zy, y) dy \tag{A3}$$

which is a result of the algebra of random variables (Springer 1979).

Combining Eqs. (A1–A3) results in the distribution of RBE_α

$$P(\mathrm{RBE}_\alpha) = \exp\left(-\frac{\langle\alpha_\gamma\rangle^2 + \langle\alpha_I\rangle^2}{2(\Delta\alpha)^2} \right) \frac{\left(1 + \sqrt{\pi y}\exp(y)\mathrm{Erf}\left(\sqrt{y}\right)\right)}{\pi\left(1 + \mathrm{RBE}_\alpha^2\right)} \tag{A4}$$

where Erf(x) is the Gaussian error function and

$$y = \frac{\left(\langle\alpha_\gamma\rangle + \langle\alpha_I\rangle \mathrm{RBE}_\alpha\right)^2}{2(\Delta\alpha)^2\left(1 + \mathrm{RBE}_\alpha^2\right)} \tag{A5}$$

The mean value of Eq. (A4) can be also calculated as

$$\begin{aligned} \langle \mathrm{RBE}_\alpha \rangle &= \int_0^\infty \mathrm{RBE}_\alpha P(\mathrm{RBE}_\alpha) \mathrm{dRBE}_\alpha \\ &= \frac{\langle\alpha_I\rangle}{\langle\alpha_\gamma\rangle} \left\{ \sqrt{\pi} c \exp\left(-c^2\right) \mathrm{Erfi}(c) \right\} \end{aligned} \tag{A6}$$

where Erfi(x) denotes the inverse error function and

$$c = \sqrt{\frac{\langle\alpha_\gamma\rangle^2}{2(\Delta\alpha)^2}} \tag{A7}$$

Note that the term in curly brackets in Eq. (A6) connects the mean of the RBE_α values with the design value and is

thus a bias correction if the mean value is used as an estimator for the RBE_{α}. The bias correction depends only on the uncertainty of photon parameters, c.f. Eq. (A7). This is plausible as they appear in the denominator of the definition of RBE_{α} as given in Eq. (2). Hence, the precise knowledge of *photon* parameters is essential for determining appropriate RBE values (ICRP 2003).

Monte Carlo calculations or the analytic treatment of ratio distributions as presented here are also applicable for other radiobiological quantities such as α/β ratios or the RBE in the zero-dose limit. However, in general, one has to take into account that the LQ parameters α/β are negatively correlated and not independent.

References

Douglas BG, Fowler JF (1976) The effect of multiple small doses of X rays on skin reactions in the mouse and a basic interpretation. Radiat Res 66:401–426

Elsässer T, Cunrath R, Krämer M, Scholz M (2008a) Impact on track structure calculations on biological treatment planning in ion radiotherapy. New J Phys 10:075005

Elsässer T, Krämer M, Scholz M (2008b) Accuracy of the local effect model for the prediction of biologic effects of carbon ion beams in vitro and in vivo. Int J Radiation Oncology Biol Phys 71:866–872

Furusawa Y, Fukutsu K, Aoki M, Itsukaichi H, Eguchi-Kasai K, Ohara H, Yatagai F, Kanai T, Ando K (2000) Inactivation of aerobic and hypoxic cells from three different cell lines by accelerated ^{3}He-, ^{12}C- and ^{20}Ne-Ion beams. Radiat Res 154:485–496

Hall EJ, Giaccia AJ (2006) Radiobiology for the radiologist. Lippincott Williams & Wilkins, Philadelphia

Hawkins RB (1994) A statistical theory of cell killing by radiation of varying linear energy transfer. Radiat Res 140:366–374

Hawkins RB (2003) A microdosimetric kinetic model for the effect of non-poisson distribution of lethal lesions on the variation of RBE with LET. Radiat Res 160:61–69

ICRP (2003) ICRP Publication 92: relative biological effectiveness (RBE), quality factor (Q) and radiation weighting factor (WR). Elsevier, Munich

Kraft G (1999) RBE and its interpretation. Strahlenther Onkol 175(Suppl II):44–47

Scholz M, Kellerer AM, Kraft-Weyrather W, Kraft G (1997) Computation of cell survival in heavy ion beams for therapy. Radiat Environ Biophys 36:59–66

Springer MD (1979) The algebra of random variables. Wiley, New York

Takatsuji T, Yoshikawa I, Sasaki M (1999) Generalized Concept of the LET-RBE Relationship of radiation-induced chromosome aberration and cell death. J Radiat Res 40:59–69

7.6 Article 6: A data base of cell survival experiments

Journal of Radiation Research, 2013, 54, 494–514
doi: 10.1093/jrr/rrs114 Advance Access Publication 23 December 2012

Systematic analysis of RBE and related quantities using a database of cell survival experiments with ion beam irradiation

Thomas FRIEDRICH[1,*], Uwe SCHOLZ[1], Thilo ELSÄSSER[1], Marco DURANTE[1,2] and Michael SCHOLZ[1]

[1]GSI Helmholtzzentrum für Schwerionenforschung, Planckstraße 1, 64291 Darmstadt, Germany
[2]Technische Universität Darmstadt, Hochschulstraße 6, 64289 Darmstadt, Germany
*Corresponding author. Tel: +49 (0)6159-71-1340; Fax: +49 (0)6159-71-2106; E-mail: t.friedrich@gsi.de

(Received 18 June 2012; revised 30 October 2012; accepted 2 November 2012)

For tumor therapy with light ions and for experimental aspects in particle radiobiology the relative biological effectiveness (RBE) is an important quantity to describe the increased effectiveness of particle radiation. By establishing and analysing a database of ion and photon cell survival data, some remarkable properties of RBE-related quantities were observed. The database consists of 855 *in vitro* cell survival experiments after ion and photon irradiation. The experiments comprise curves obtained in different labs, using different ion species, different irradiation modalities, the whole range of accessible energies and linear energy transfers (LETs) and various cell types. Each survival curve has been parameterized using the linear-quadratic (LQ) model. The photon parameters, α and β, appear to be slightly anti-correlated, which might point toward an underlying biological mechanism. The RBE values derived from the survival curves support the known dependence of RBE on LET, on particle species and dose. A positive correlation of RBE with the ratio α/β of the photon LQ parameters is found at low doses, which unexpectedly changes to a negative correlation at high doses. Furthermore, we investigated the course of the β coefficient of the LQ model with increasing LET, finding typically a slight initial increase and a final falloff to zero. The observed fluctuations in RBE values of comparable experiments resemble overall RBE uncertainties, which is of relevance for treatment planning. The database can also be used for extensive testing of RBE models. We thus compare simulations with the local effect model to achieve this goal.

Keywords: relative biological effectiveness; cell survival; ions; local effect model; linear quadratic model

INTRODUCTION

Radiation cancer therapy with carbon ions has been applied successfully in Japan and Germany and will be used in several other locations all around the world in the near future [1–6]. In earlier trials at Berkeley, other ion beams from He to Ar were used for cancer treatments. One major rationale for the application of ion beams in radiotherapy is their enhanced effectiveness compared with conventional X-rays, in particular in the target region. This has given rise to intensified research on the understanding and on the predictability of the biological effect of ions compared with respect to photons, usually parameterized by the relative biological effectiveness (RBE) [7]. The RBE is an important factor to be considered in treatment planning for ion beam therapy, since the prescribed doses have to be correspondingly reduced as compared with the doses given in conventional photon therapy [8, 9].

Generally, the RBE depends on many factors such as the linear energy transfer (LET) at a given tissue depth, the particle species, the dose and the biological endpoint. Due to these complex dependencies, full systematic characterization typically requires meta-analyses based on a combination of different studies. The primary focus of this paper is therefore to compile a large collection of experimental results and to investigate it in order to exhibit further systematic analyses of the relevant quantities. For this purpose, we established a database of cell survival experiments with both photon and ion irradiation published in the literature.

Besides these systematic analyses, such a database is also ideally suited to testing and validating biophysical models that aim to predict the biological effects of ion beams. These models are important tools, for example, in treatment planning, where they are used to estimate the RBE in situations that are not directly experimentally accessible. For example, the local effect model (LEM) has been implemented in treatment planning for a pilot project performed at Gesellschaft für Schwerionenforschung (GSI) [10, 11]; and the potential application of the microdosimetric kinetic model [12, 13] is discussed at the HIMAC/NIRS.

A prerequisite for clinical application of these models is a thorough test and validation by means of *in vitro* experimental data. Survival experiments are particularly suitable here, as they are comparably easy to perform under well-defined experimental conditions. In the design of our database we have thus put particular emphasis on its applicability for the purpose of model tests and validation.

Assessment of the accuracy of a model requires information about the uncertainty of the experimental data. Most published experiments report statistical errors, which however represent only a lower limit concerning the uncertainty of the data. Unfortunately, there is no unique established way of reporting errors in cell survival values, and indeed a full uncertainty analysis would be demanding as both stochastic and systematic errors would have to be respected. The overall uncertainty can hence be better estimated based on the combination of larger sets of experimental data, for example, from different laboratories, obtained under otherwise identical conditions. For such a dataset, a measure of uncertainty can be derived empirically from the scatter of the data, which have been obtained from comparable situations. The large database presented in this paper thus is also ideally suited to analyze fluctuations from which the overall uncertainty of RBE can be assessed directly on purely experimental grounds. In previous attempts the use of a data collection to analyze systematic variations of RBE specifically for protons has been proven to be very fruitful [14].

In this publication, we report on the set up of a database containing results of more than 800 cell survival experiments from different laboratories all over the world, using different cell types and different ions at various energies. Throughout this paper, we call this collection 'Particle Irradiation Data Ensemble,' in short, PIDE. We used the database to reveal known and new systematics of the RBE and its related quantities. We (i) evaluated statistical properties of the photon linear-quadratic (LQ) parameters and found that they are slightly anti-correlated; (ii) we investigated the evolution of the quadratic coefficient β of the LQ model with LET, which is under current discussion; and (iii) we report on a survival-dependent systematic variation of the RBE with the photon α/β ratio. Moreover we demonstrate the capability of the database for RBE model validation.

MATERIALS AND METHODS

Conception of the database

The main task in the development of the database was to combine a variety of experimental results of ion irradiation experiments with *in vitro* cell lines including the early experiments from Berkeley, the huge datasets of studies from Japan and the experiments carried out in Europe. After a thorough literature survey, we introduced some restriction for the selection of the publications that we included in the data ensemble. One of these restrictions was that we only included publications for which the LQ parameters of the response to photons as reference radiation were available or derivable. This allows the determination of the RBE values to any survival level from the LQ parameters (provided the LQ model holds, which is still under debate for high doses [15–17]). We believe that we have covered in the database a good fraction of all published survival experiments in peer-reviewed journals under these restrictions.

Currently the PIDE contains 855 measured ion cell survival curves, taken from 77 publications (see Table 1). The cell lines under investigation range from radio-resistant cells with a shoulder, to radio-sensitive cells without a visible shoulder in the photon dose–response curve. Within all experiments, 182 different photon dose–response curves were used as a reference to calculate RBE values. In the experiments about 80 different cell lines were investigated. When investigating their properties, it becomes evident that cells of the same cell line may behave differently depending on experimental factors or age of the cell line. In fact, cell lines that are equal by origin and name, but maintained for years at different institutions might not show identical responses to radiation and thus have to be better distinguished by author/institution rather than pooled in the database.

Normal cells were used for 673 curves and tumour cell lines were used for 182 curves. In some cases mutated or specially treated cells with repair deficiencies were investigated. In 52 experiments, the cells were irradiated predominantly in a specified cell cycle phase, in the other 803 experiments the cells were irradiated in an asynchronous population. In 372 experiments human cell lines were used, in 483 experiments rodent cell lines were used. Among the latter, V79 cells have been studied most often and results were reported in 29 of the 77 publications included in the PIDE. Among all the experiments, 352 were carried out with carbon ions, 186 with lighter (p-B) and 317 with heavier ions (N to U). A total of 103 experiments were carried out with a shaped beam in a spread-out Bragg peak or the entrance channel, but the majority (752 experiments) were carried out under track segment conditions with monoenergetic ion beams. Throughout the text we use the term 'monoenergetic' whenever a beam is not a shaped

beam to provide an extended peak. One should keep in mind that such a monoenergetic beam nevertheless may show an energy distribution and may be subject to fragmentation. This is in particular the case when a primary beam is decelerated by passive elements after exiting the accelerator. As can be seen from Table 1, the publications typically focus on one special aspect within all possible combinations of the factors listed above.

Technically, for each of the 855 experiments, there is one entry in the PIDE, in which the LQ parameters of the ion response curve are listed along with other information such as LQ parameters of photon response, cell type, LET, energy, etc. The entries are stored separately for each publication in two text files, one of which contains information given in the publication and the other contains information taken from related publications or quantities that have been derived (such as calculated RBE values or LET values for a given particle energy). In this way, information contained in new publications can be easily added into the PIDE. Within an entry the information is stored in variables, which are given a name and a value (such as LET and 120 keV/μm, for example). Table 2 gives an overview of all quantities required for each entry. Additional variables may be defined at any time in any entry, for example, for calculated RBE values or, for later use, oxygenation status.

The PIDE contains data obtained for a broad variety of experimental factors, both biological and physical in nature. However, the intention is not to pool all experiments. Rather the database allows one to easily extract a subset of experiments fulfilling certain requirements (such as all cells with a small α/β ratio irradiated with monoenergetic carbon ions) for which, for example, RBE dependence on further parameters (such as LET) can be investigated.

Sources of the data

Our requirements for the selection of the publications for the data ensemble were as follows. (i) We required the data included in the PIDE to be published in peer-reviewed journals or PhD theses. Both types of publications seem to be sufficiently reviewed, and in general accessible via libraries from anywhere. (ii) We only took publications into account in which data on ion radiation *and* photon radiation response were provided or where the latter were found in references or could be derived. For photon experiments generally only hard X-rays or ^{60}Co or ^{137}Cs γ-rays have been required as reference radiation. For RBE evaluations, the slightly differing effectiveness between different photon radiation qualities of these groups has been neglected. If X-rays with energies below 200 kVp were used, effectiveness could be enhanced. The corresponding publications have been indicated in Table 1. (iii) The radiation quality had to be described in the publication in sufficient detail, i.e. either LET (or track or dose-averaged LET for irradiation in a spread out Bragg peak), the specific energy on the target or the remaining range of primary particles was required to be reported in all publications included in the PIDE. The quantities not given explicitly in the publications appear in italics in Table 1. (iv) LQ parameters or related quantities (from which LQ parameters could be derived) had to be given either numerically or as figures (typically the survival curves) in the publications. If quantities other than LQ parameters or survival levels were presented in the publications, it is mentioned in Table 1. (v) Experiments with monoenergetic ions were excluded if track segment conditions were not fulfilled. (vi) Some additional information is requested. A list of all information for the required variables is given in Table 2.

Extraction of relevant parameters

Once the publications forming the basis of the PIDE were selected, the relevant information was extracted. Here the following procedures were applied:

LET and energy

If both LET and energy for a given ion species were given in a publication, both values were taken into the PIDE. If only LET or energy was given in a publication, its counterpart was determined from precalculated energy loss tables used within the treatment planning system TRiP98 [11, 99]. These encompass ions from protons to neon within the energy range of 0.1–1000 MeV/u. For ion species where no such tables are available, i.e. in particular for heavier ions that are not relevant in treatment planning, it was calculated using the computer code ATIMA developed at GSI, which performs energy loss calculations for charged particles in matter based on tabled cross sections [100]. Note that for a given energy value, slightly differing LET values may occur depending how the LET was obtained.

For irradiations in spread out bragg peak (SOBP) the dose-averaged LET was used as a representative quantity, if given in the publications. However, it should be noted that the dose-averaged LET is not always a good quantity to describe the radiation field and might be a misleading concept. This is in particular the case for SOBP with large depths and/or extensions, where the radiation field is a complex mix of LET components and hence the corresponding LET spectrum should be respected. Nevertheless, since these details cannot be represented in the database, we take (dose) average LET values as surrogates to reflect the complex radiation field.

LQ parameters of photon and ion dose–response curves

In about a third of all publications, numerical values for the LQ coefficients were presented, while in the majority the measured survival curves were shown in figures. These two cases will be discussed in more detail now. Note that in

Table 1. Content of the PIDE, sorted by publications

No.	Author/year/ ref.	No. s.c.[a]	Cell lines	Cell type[b]	Cell cycle[c]	Cell origin[d]	α/β (Gy)	Ion species	Irr. cond.[e]	LET (keV/μm)[f]	E (MeV/u)[f]	Phot.[g]	Remarks[h]
1	Chapman *et al.*, 1977 [18]	13	V79	n	s	r	2.22	^{4}He, ^{12}C, ^{20}Ne, ^{40}Ar	s	2.34–402.7	*26.1–319.0*	220	LET given
2	Chapman *et al.*, 1978 [19]	9	V79, T1	n	a, s	h, r	2.17–3.80	^{12}C	s	12.16–74.99	*26.1–319.0*	220	LET given
3	Blakely *et al.*, 1979 [20]	24	T1	n	a	r	2.13	^{12}C, ^{20}Ne, ^{40}Ar	m	11–419	*10.7–389.0*	220	
4	Raju *et al.*, 1991 [21]	5	CHO-10B, HS-23, C3H_10T1/2, V79, AG1522	n	a	r	4.33–20.0	^{4}He	m	121–136	*0.65–0.8*	Co	
5	Goodhead *et al.*, 1992 [22]	10	HeLa, HeLa S3, C3H 10 T1/2	n	a	h, r	5.39–30.0	^{1}H, ^{4}He	m	20.27–23.915	1.16–8.8	250	
6	Folkard *et al.*, 1996 [23]	10	V79	n	a	r	2.71	^{1}H, ^{2}H, ^{3}He, ^{4}He, ^{12}C, ^{16}O	m	10.1–105.8	0.465–3.66	240	
7	Eguchi-Kasai *et al.*, 1996 [24]	22	irs1, irs2, L5178Y, M10, LTA, SL3-147	n	a	r	0.06–31.1	^{4}He, ^{12}C, ^{20}Ne	m	18–327	*3.1–123.2*	200	
8	Suzuki *et al.*, 1997 [25]	7	HE20	n	s	h	0.67	^{20}Ne	m	63–335	*14.3–120.3*	Cs	
9	Bettega *et al.*, 1998 [26]	8	C3H 10T1/2	n	a	r	15.0	^{1}H, ^{2}H	m	6.65–33.2	0.72–4.89	Co	
10	Tsuboi *et al.*, 1998 [27]	20	NB1RGB, ONS-76, A-172, U251MG, TK-1	n, t	a	h	0.13–6.89	^{12}C	m	20–105	*17.4–144.0*	Cs	
11	Tsuchida *et al.*, 1998 [28]	6	A172, TK1	t	a	h	2.23–2.98	^{12}C	m	20–80	*24.1–144.0*	Cs	
12	Weyrather *et al.*, 1999 [29]	21	V79, CHO-K1, xrs5	n	a	r	3.57–∞	^{12}C	m	13.7–482.7	2.4–266.4	250	Corrected
13	Furusawa *et al.*, 2000 [30]	138	V59, HSG, T1	n	a	h, r	0.52–9.2	^{3}He, ^{12}C, ^{20}Ne	m	18.5–654	1.27–131	200	Values for α and D_{10} given; Corrected
14	Suzuki *et al.*, 2000 [31]	30	NB1RGB, HFL-III, LC-1sq, A-549, C32TG, Marcus, U-251MGKO, SK-MG-1, KNS-89, KS-1, A-172, ONS-76, KNS-60, Becker, T98G, SF126	n, t	a	h	0.59–21.3	^{12}C	m	13.3–77.1	*25.1–271.2*	200	Corrected
15	Belli *et al.*, 2000 [32]	12	HF19, M10, SCC25, SQ20B	n, t	a	h	7.65–∞	^{1}H	m	7.7–33	*0.69–5.24*	Cs + Co	

Continued

Table 1. *Continued*

No.	Author/year/ ref.	No. s.c.[a]	Cell lines	Cell type[b]	Cell cycle[c]	Cell origin[d]	α/β (Gy)	Ion species	Irr. cond.[e]	LET (keV/μm)[f]	E (MeV/u)[f]	Phot.[g]	Remarks[h]
16	Tsuruoka *et al.*, 2005 [33]	41	NB1RGB	n	a	h	17.47	^{12}C, ^{20}Ne, ^{28}Si, ^{56}Fe	m	13–400	*19.5–500*	200	Values for RBE_{10} given
17	Belli *et al.*, 2008 [34]	37	HF19, M10, SCC25, SQ20B, V79	n, t	a	h, r	4.41–∞	^{12}C	m, s	13–303	*4.5–290*	Cs + Co	$<LET_D>$ given
18	Belli *et al.*, 1998 [35]	6	V79	n	a	r	2.80	^{1}H	m	7.7–34.6	0.57–5.01		No X-ray energy given; Data in parts taken from Belli *et al.*, 1993 [36]
19	Hall *et al.*, 1977 [37]	3	V79	n	a	r	3.24	^{40}Ar	s	110.9–409.2	*48–330*	250	$<LET_D>$ given
20	Bird and Burki, 1975 [38]	6	V79	n	a	r	18.6	^{4}He, ^{7}Li, ^{11}B, ^{12}C, ^{20}Ne, ^{40}Ar	m	19.1–2000	5.09–9.93	145	Low X-ray energy; X-ray curve taken from Sinclair and Morton, 1966 [39]
21	v. Neubeck, 2009 [40]	6	RAT-1, IEC-6	n, t	a	r	6.69–15.9	^{12}C	m	13.3–163	9.9–270	250	
22	Perris *et al.*, 1986 [41]	2	V79	n	a	r	25.5	^{1}H	m	*6–12*	3–7.4	Co	
23	Bettega *et al.*, 1983 [42]	3	EUE	n	a	h	211	^{1}H	m	1.83–5.8	8–31	Co	Photon data taken from Bettega *et al.*, 1979 [43]
24	Cox *et al.*, 1977 [44]	4	V79, HF19	n	a	h, r	5.52–∞	^{4}He	m	20–68	1.9–8.8	250	
25	Wouters *et al.*, 1996 [45]	11	V79	n	a	r	2.73	^{1}H	s	2.33–6.23	*6.8–22.8*	250	$<LET_D>$ given
26	Combs *et al.*, 2009 [46]	4	U87-MG, LN229	t	a	h	4.53–6.52	^{12}C	m, s	103–170	9.8–18	250	$<LET_D>$ given

27	Kitajima *et al.*, 2010 [47]	10	SuSa, AT1OS	n	s	h	∞	^{12}C	m	24–200	*35–450*	150	Low X-ray energy; values for RBE_{α} given
28	Blomquist *et al.*, 1993 [48]	2	LS-147T, V79	n, t	a	h, r	3.65–∞	^{1}H	s	4	*11.6*	Co	$<LET_D>$ given
29	Yang *et al.*, 1985 [49]	9	C3H 10T1/2	n	a	r	0.36–13.4	^{12}C, ^{20}Ne, ^{28}Si, ^{56}Fe, ^{238}U	m	*10.5–2080*	*103–990*	225	E and LET from remaining range
30	Miller *et al.*, 1995 [50]	10	C3H 10T1/2	n	a	r	2.80	^{1}H, ^{2}H, ^{3}He, ^{4}He, ^{12}C, ^{16}O	m	3.8–418	0.275–12.9	250	
31	Czub *et al.*, 2008 [51]	4	CHO	n	a	r	8.5	^{12}C, ^{20}Ne	m	438–1245	*1.69-2.78*	Co	
32	Kamlah *et al.*, 2011 [52]	1	A594	t	a	h	11.6	^{12}C	m	168	9.9	6 MV	
33	Aoki *et al.*, 2000 [53]	6	V79	n	a	r	7.95	^{12}C	m	13–237	*6.4–283*	200	
34	Han *et al.*, 1998 [54]	6	SHE	n	a	r	13.7	^{12}C, ^{26}Si	m	13–400	*18.5–283*	250	
35	Hamada *et al.*, 2010 [55]	8	H1299	t	a	h	0.95	^{12}C, ^{20}Ne, ^{26}Si, ^{40}Ar, ^{56}Fe	m	13–200	*20–600*	200	
36	Claesson *et al.*, 2011 [56]	6	V79	n	a, s	r	4.33–∞	^{4}He	m	110	1.625	100	Low X-ray energy
37	Wedenberg *et al.*, 2010 [57]	5	T1	n	a	h	9.00	^{4}He	m	25–165	*0.46–6.8*	250	
38	Miller *et al.*, 1990 [58]	1	C3H 10T1/2	n	a	h	2.80	^{2}H	m	40	*0.55*		Photon data taken from Miller, 1995 [50]
39	Tobias *et al.*, 1980 [59]	2	V79	n	s	r	11.5–21.3	^{40}Ar	m	*370*	*55*	220	E and LET from remaining range
40	Cox and Masson, 1979 [60]	7	HF19	n	a	h	∞	^{4}He, ^{11}B, ^{14}N	m	20–470	*1.24–10.3*	250	

Continued

Table 1. *Continued*

No.	Author/year/ ref.	No. s.c.[a]	Cell lines	Cell type[b]	Cell cycle[c]	Cell origin[d]	α/β (Gy)	Ion species	Irr. cond.[e]	LET (keV/μm)[f]	E (MeV/u)[f]	Phot.[g]	Remarks[h]
41	Ito *et al.*, 2006 [61]	7	HL-60	t	a	h	4.78	^{12}C, ^{26}Si, ^{56}Fe	m	20–440	26–126	4 MV	
42	Tilly *et al.*, 1999 [62]	3	V79	n	a	r	3.73	^{4}He, ^{14}N	m	6–165	*14.4–39*	Co	
43	Thacker *et al.*, 1979 [63]	6	V79	n	a	r	3.90	^{4}He, ^{11}B, ^{14}N	m	28–470	*1.24–10.3*	Co	
44	Hirayama *et al.*, 2009 [64]	5	V79	n	a	r	3.57	^{12}C, ^{56}Fe	m	20–2106	16–416	200	
45	Hirayama *et al.*, 2005 [65]	1	CHO	n	a	r	3.23	^{12}C	m	79.6	*24*	200	
46	Curtis *et al.*, 1982 [66]	28	R-1	t	a	r	2.26	^{12}C, ^{20}Ne, ^{40}Ar	s	11–750	*19.5–428*	225	$<LET_D>$ given
47	Boehrnsen *et al.*, 2002 [67]	2	V79	n	a	r	2.50	^{12}C	m	27.5–153	10.2–92.5	6 MV	
48	Fournier *et al.*, 2001 [68]	4	AG1522B, PS1	n	a	h	13.5–25.6	^{12}C, ^{48}Ni	m	16.6–2455	9.9–195	250	
49	Wulf *et al.*, 1985 [69]	106	B14FAF28, V79	n	a	r	11.7–14.3	^{12}C, ^{16}O, ^{40}Ca, ^{40}Ar, ^{48}Ti, ^{56}Fe, ^{58}Ni, ^{84}Kr, ^{132}Xe, ^{142}Nd, ^{208}Pb, ^{238}U	m	150–15 800	0.1–400		Values for cross-sections given; photon parameters taken from Wulf, 1983 [70] and Kraft, 1987 [71]
50	Scholz, 2003 [72]	8	CHO, V79	n	a	r	3.58–11.4	^{12}C, ^{16}O, ^{20}Ne, ^{238}U	m	*13.3–16 500*	5–396		Photon parameters adapted from Weyrather *et al.*, 1999 [29]
51	Persson *et al.*, 2002 [73]	3	AA	t	a	h	0.98	^{10}B	m	40-160	6.6–36.6	Co	

52	Yang and Tobias, 1984 [74]	2	C3H 10 T1/2	n	a	r	1.07–2.07	^{56}Fe, ^{238}U	m	500–1900	300–960	225	
53	Scholz *et al.*, 1997 [10]	8	CHO	n	a	r	6.43	^{12}C, ^{16}O	m	*13.5–265*	11–395	250	
54	Prise *et al.*, 1990 [75]	4	V79	n	a	r	4.07	^{1}H, ^{4}He	m	*16.9–108*	0.76–1.9	250	
55	Terato *et al.*, 2008 [76]	4	AA8	n	a	r	30.0	^{12}C	m	13–200	*43–290*	Co	
56	Suzuki *et al.*, 1996 [77]	8	HE	n	s	h	0.66	^{12}C	m	22–230	*6.6–126*	Cs	
57	Matsumoto *et al.*, 2008 [78]	6	C32TG, Colo679, HMV-I, HMV-II, 92-1, MeWo	t	a	h	3.29–68	^{12}C	s	50	*43.4*	200	$<LET_D>$ given
58	Mehnati *et al.*, 2005 [79]	13	CHO	n	a	r	11.65	^{12}C, ^{20}Ne, ^{40}Ar, ^{56}Fe	m	20–2000	*13–144*	200	
59	Stenerloew *et al.*, 1995 [80]	10	HTh7, B16, IGR, V79, LS-174T, U-343MG, DU-145	n, t	a	h, r	0.91–∞	^{4}He, ^{14}N	s,m	40–125	*3.82–20.3*	Co	Unclear if LET or $<LET_D>$ given
60	Okayasu *et al.*, 2006 [81]	10	CHO, xrs6, xrs6-hamKu80, HFLIII, 180BR	n	a	h, r	2.70–∞	^{12}C, ^{56}Fe	m	70–200	*28.5–430*		No X-ray energy given
61	Tsuboi *et al.*, 2007 [82]	9	U87MG, TK1	n, t	a	h	2.31–6.25	^{12}C	m	20–80	*24–144*	Cs	
62	Todd, 1975 [83]	10	ChangHL, M3-1	n	a	h, r	0.64–10.42	^{7}Li, ^{11}B, ^{12}C, ^{14}N, ^{16}O, ^{20}Ne, ^{40}Ar	m	55–1940	*5.3–7*	50	Low X-ray energy
63	Hall *et al.*, 1972 [84]	1	V79	n	a	r	41.1	^{4}He	m	106	1.3	210	
64	Takahashi *et al.*, 2000 [85]	8	A172, A172neo, A172mp53, TG98G	t	a	h	0.14–0.92	^{4}He, ^{12}C	s	70–156	*0.51–28.5*	150	Low X-ray energy; $<LET_D>$ given
65	Takahashi *et al.*, 2004 [86]	12	H1299wtp53, H1299tp53, H1299tp53-null	t	a	h	0.00–2.56	^{12}C	m	30–100	*18.5–83*	200	
66	Matsuzaki *et al.*, 1998 [87]	3	OCUB-M, CRL-1500, YMB-1	t	a	h	4.45–21.3	^{12}C	s	80	*24*	200	$<LET_D>$ given; corrected

Continued

Table 1. *Continued*

No.	Author/year/ ref.	No. s.c.[a]	Cell lines	Cell type[b]	Cell cycle[c]	Cell origin[d]	α/β (Gy)	Ion species	Irr. cond.[e]	LET (keV/μm)[f]	E (MeV/u)[f]	Phot.[g]	Remarks[h]
67	Kronenberg *et al.*, 2009 [88]	1	Aprt	n	a	r	∞	^{56}Fe	m	151.4	1000	150	Values for D_0 given; low X-ray energy
68	Hamada *et al.*, 2006 [89]	6	AG01522	n	a	h	∞	^{4}He, ^{12}C, ^{20}Ne, ^{40}Ar	m	16.2–1610	*7–25.5*	Co	Values for D_0 given
69	Zhou *et al.*, 2006 [90]	1	V79	n	a	r	3.63	^{12}C	m	100	*18.5*	200	
70	Jenner *et al.*, 1993 [91]	1	V79	n	a	r	2.2	^{4}He	m	120	*0.81*	Co	
71	Furusawa *et al.*, 2002 [92]	2	V79	n	a	r	7.15–11.4	^{40}Ar, ^{58}Fe	m	86–442	*115–575*	150	Low X-ray energy
72	Takahashi *et al.*, 2001 [93]	8	SASmp53, SASneo	t	a	h	3.77–10.0	^{12}C	m	30–150	*11–83*	150	Low X-ray energy
73	Bettega *et al.*, 2005 [94]	5	AG1522	n	a	h	∞	^{26}Si, ^{48}Ti, ^{56}Fe	m	56–442	200–1000	Co	
74	Ibañez *et al.*, 2009 [95]	3	B16-F0	t	a	r	2.17	^{1}H, ^{6}Li	m	3.4–135	2.9–14.4	Cs	
75	Hellweg *et al.*, 2011 [96]	2	HEK	n	a	h	2.55	^{13}C	m	33–73	28–72	150	Low X-ray energy
76	Napolitano *et al.*, 1992 [97]	1	C3H 10T1/2	n	s	r	9.0	^{4}He	m	177	0.45	80	Low X-ray energy
77	Hill *et al.*, 2004 [98]	7	V79-4, irs1, irs2, irs3, CHO-K1, xrs5	n	a	r	3.7–∞	^{4}He	m	121	3.26	250	

Notes: For each publication, the first author, along with the year of publication, as well as the number of survival curves taken into the PIDE are given. Furthermore, summarizing properties of the used cells and radiation qualities are provided.

[a] No. s.c. = number of survival curves described in the publication.

[b] cell type: n = normal, t = tumor.

[c] cell cycle: a = asynchronous, s = synchronized in a particular phase of cell cycle.

[d] cell origin: h = human, r = rodent.

[e] irradiation conditions: m = monoenergetic, s = within a spread out Bragg peak.

[f] values given in italics if not given in the publications.

[g] X-ray energy in kVp or photon energy in MV for clinical accelerators if this unit is given, or Co = ^{60}Co and Cs = ^{137}Cs source.

[h] If linear quadratic parameters are not directly taken from figures or tables or from accessible survival values, the procedure is outlined here. Correction: shifting of one determined LQ parameters if the other is smaller than 0. Also other comments are given in this column. For spread out Bragg peaks, the quantities LET and $\langle LET_D \rangle$ refer to track and dose averaged LET values, respectively.

Table 2. Required information for each experiment in the PIDE

Quality	Content
ID	Running number labeling the publication
Paper	Short name of the publication, containing first author and year of publication
No	Running number labeling the entry within a publication
Ion	Ion species
Charge	Charge of ions
Irrmods	Irradiation modalities (monoenergetic or spread out Bragg peak)
LET	Linear energy transfer in water (in keV/μm, for irradiation in spread out Bragg peak dose mean or track averaged LET)
E	Specific energy of ions (in MeV/u, evaluated at the target)
Cell	Name of cell line
Phase	Information on cell cycle phase
Type	Tumor or normal cells
Genl	Genomic length of diploid cells (in 10^9 bp, 5.6 for rodent and 6 for human cells)
α_X	Linear coefficient of LQ model (in Gy^{-1} for response to photon reference radiation)
β_X	Quadratic coefficient of LQ model (in Gy^{-2} for response to photon reference radiation)
α_I	Linear coefficient of LQ model (in Gy^{-1} for response to ion radiation)
β_I	Quadratic coefficient of LQ model (in Gy^{-2} for response to ion radiation)

some rare cases different quantities such as RBE values or cross sections were given either numerically or in figures.

If LQ parameters were published as numbers they were simply copied into the PIDE. If other quantities were given as numbers, the corresponding LQ parameters were calculated. In some cases, one of the LQ parameters was reported or obtained with a negative value, which may occur due to either statistical fluctuations or systematic deviations from LQ behaviour. Then a purely linear or purely quadratic dose response (i.e. shifted β or α to zero) was assumed and the remaining LQ parameter was correspondingly shifted according to the formalism presented in the next section on the fit-induced anti-correlation between α and β. This formalism quantifies how a shift in one parameter approximately compensates for setting the other artificially to zero.

If no numerical values for the LQ parameters were presented but instead only the survival curves figures, the LQ parameters were derived from the graphs. For that purpose a computer program was developed and used to digitize the data points in the figures. Then the LQ parameters were been determined by fitting a second order polynomial with an ordinary χ^2 fit to the effect, i.e. the negative logarithm of the survival. We are aware that there are more sophisticated methods to derive LQ parameters from a measured survival curve, which take into account the correlation of the fit parameters by means of their covariance. However, as these methods are rarely used and the resulting fit parameters do not differ too much, we applied the conventional fit procedure, in line with most of the publications that provide numerical values for LQ parameters. If by visual inspection the quadratic coefficient β could not be reliably determined by curve fitting (e.g. when there were only a few data points and the errors of the fit parameters were large) only a straight line fit was performed and β was set to zero. Similarly, if an LQ fit yielded one negative fit parameter, a purely linear or purely quadratic fit was used, which is analogous to the shifting of parameters as described above, when numerical values are given in the publications.

Cell cycle

If no statements were made it was assumed that the cells were irradiated as an asynchronous population.

Fit induced anti-correlation of LQ parameters

In the following section the anti-correlation of LQ parameters due to the fit procedure shall be investigated. Consider an LQ dose–response curve with non-vanishing coefficients α and β. If α is set artificially to zero one can ask how β must be changed to get an appropriate quadratic fit. Likewise, if β is set artificially to zero one can ask how α must be changed to get an appropriate linear fit.

Mathematically, this question can be answered to a good approximation analytically. We assume that all dose points are continuously distributed and introduce a generalized χ^2 value on continuous functions. Let f_1 and f_2 be two functions, so the well known *sum of least squares* converts into

an integral over least squares in the continuous formulation:

$$\chi^2 = \int [f_1(x) - f_2(x)]^2 \mathrm{d}x \tag{1}$$

The integral has to be evaluated over some interval, and the χ^2 value is then a distance measure for two functions on that interval.

For approximating an LQ curve with a purely quadratic one we have to evaluate:

$$\chi^2 = \frac{1}{D_{\max}} \int_0^{D_{\max}} \left[\alpha D + \beta D^2 - \beta' D^2\right]^2 \mathrm{d}D \tag{2}$$

where β′ is the shifted β parameter used to replace the original LQ parameters α and β. In Eq. (2) $D_{\max}$ is the dose up to which the survival curve was recorded and is typically in the order of 5–10 Gy for experiments with photons and 3–7 Gy for ions.

Setting the derivative of χ^2 with respect to β' to zero and solving for β′ results in:

$$\Delta\beta = \beta' - \beta = \frac{5}{4}\frac{\alpha}{D_{\max}} \tag{3}$$

Consequently, if α <0 we may lower the β term by means of that expression to compensate for α and thus get an estimator for the best purely quadratic fit.

In the opposite case where a purely linear fit is requested the corresponding equation reads:

$$\Delta\alpha = \alpha' - \alpha = \frac{3}{4}\beta D_{\max} \tag{4}$$

Again, if β <0, which may happen 'by accident' when, for example, only a small number of dose points are available in an experiment, we may lower α by means of that expression to compensate for β and thus get an estimator for the best purely linear fit. Equations (3) and (4) were used to correct the LQ parameters in the PIDE if one of the parameters was given numerically as a negative value in the publications. The publications for which this procedure was applied were marked with 'corrected' in Table 1.

RESULTS

Photon dose response

To obtain an overview about the variety of cell lines forming the basis of the PIDE, we first looked at their photon response. Note that here with the term 'cell line', we understand not only the classification by name (such as V79) but also their sensitivity to radiation, as cell lines with the same name might show a different behaviour dependent on their history. Figure 1 shows frequency histograms of α and β among all cell lines included in the PIDE. While α shows a peak at relatively small values with a wide falloff beyond, the distribution of β is not so skewed and peaked at intermediate values. In addition the histogram of β shows a pronounced first bin, which reflects the fact that several cell lines show a purely linear response to photon radiation. Typically, α is found in the range 0.05–0.5 Gy^{-1} and β in the range 0.01–0.07 Gy^{-2}. The mean values are $<\alpha> = 0.32\ \mathrm{Gy}^{-1}$ and $<\beta> = 0.039\ \mathrm{Gy}^{-2}$, while the medians are $\alpha_m = 0.20\ \mathrm{Gy}^{-1}$ and $\beta_m = 0.033\ \mathrm{Gy}^{-2}$. Here, the brackets <.> denote averaged quantities. However, these quantities have to be taken with care, as the underlying distributions are non-symmetric and therefore the means and medians do not reflect the most likely values of the LQ parameters, i.e. the maxima of the presented histograms.

For clinical applications, often the ratio α/β of the photon LQ parameters is of interest and is used to classify the tissue type. In Fig. 2 the histogram of this quantity is shown. Clearly, the typical spectrum of α/β up to 10 Gy is covered quite uniformly in the PIDE. Values beyond occur less often. However, there are also 18 cases where β is zero and hence the α/β ratio diverges.

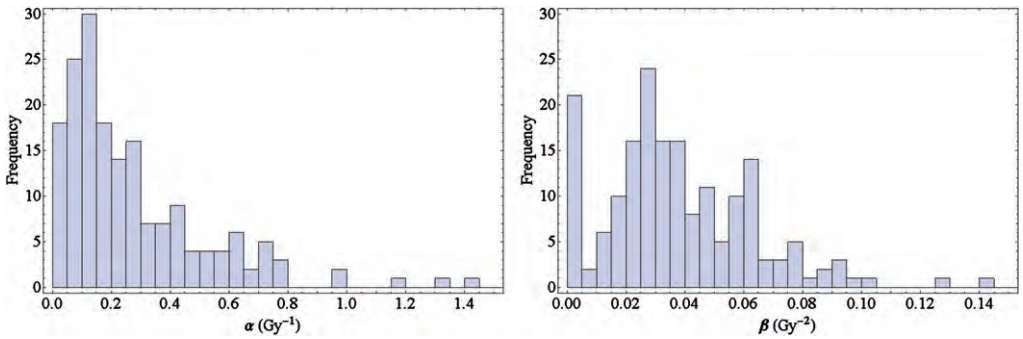

Fig. 1. Histograms of the linear-quadratic parameters α (left) and β (right) for photon dose response curves of the cell lines of the experiments included in the PIDE.

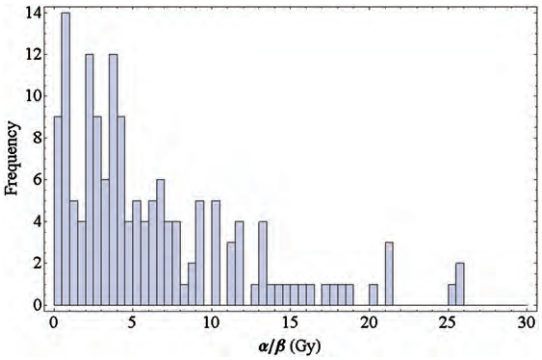

Fig. 2. Histogram of the ratio α/β for photon dose–response curves of the cell lines used in experiments included in the PIDE.

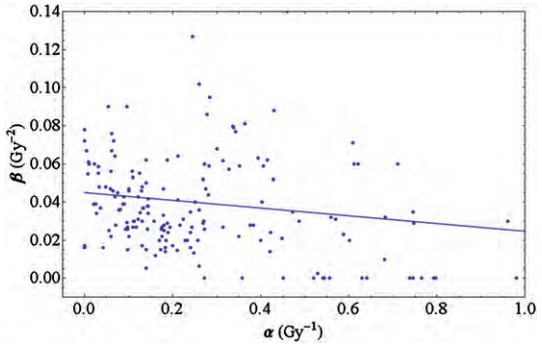

Fig. 3. Photon linear-quadratic parameters of the cell lines of the experiments included in the PIDE plotted against each other. Higher values of β occur for small values of α only. The straight line emerges from a linear fit to the data points.

In order to investigate the interdependence of the LQ parameters, Fig. 3 displays the quadratic LQ parameter β plotted against the linear parameter α. As a trend, survival curves with a very prominent β term typically are found for small α values. Likewise, very large values of α occur mostly at rather small values of β. In particular the cell lines without a β component have a steep exponential survival curve, i.e. show a large α. This trend suggests the existence of a small anti-correlation between the LQ parameters. Indeed, a linear regression reveals a negative slope of $(-0.0204 \pm 0.0056)\ \mathrm{Gy}^{-1}$, where the uncertainty is given by the standard error of the fit parameters. Figure 3 contains the corresponding linear regression line. The fit parameter errors make up a 68% confidence interval, but even the corresponding 95% confidence interval only covers negative slopes (from –0.0314 to –0.0093), thus indicating significance to that confidence level. As a further check, we performed a hypothesis test on the correlation coefficient between α and β. The coefficient is $r = -0.262$ and the P-value is $P = 0.0002$, which shows that it significantly differs from zero on a 95% confidence level.

Dose response to ion irradiation

In addition to the quantities that play a role for photon irradiation, the LET is another factor to take into account for particle irradiation. All the following analysis has been performed using information from experiments with monoenergetic beams only, to avoid peculiarities due to broad LET distributions as present in extended Bragg peaks.

Cell type specificity of RBE

For the investigation of ion dose responses in the PIDE, we calculated RBE values from the LQ parameters. Note that these may deviate from directly measured RBE values (i.e. the ratio of doses needed for a fixed effect), in particular for higher doses where it is under discussion as to whether the LQ model is valid any more [15, 16]. To investigate the impact of LET on radio-sensitivity we show the RBE plotted against LET for different particle species in Fig. 4. We restricted the analysis to the RBE_α and RBE_{10} corresponding to the initial slope (upper row) and 10% survival level (lower row), respectively. All cells were classified into two classes of low and high photon α/β ratios with values below or above 4 Gy, respectively (left and right columns, respectively). The latter distinction is somewhat arbitrary, and pooling the data in classes of intervals of α/β is a questionable procedure, as RBE generally depends on this quantity. However, as the scatter of the RBE values even for small intervals of α/β is quite large, categorizing into two classes is appropriate at least for demonstrating the dependence on α/β in a plot. Below, this dependence is investigated in more detail. For individual cell lines, systematics of this kind have been frequently evaluated [29, 30]. It was found that (i) the characteristics provide a maximum in RBE dependent on the particle species, where heavier particles have the maximum at higher LET values; (ii) that lighter particles provide higher RBEs for a fixed LET; and (iii) that the RBE decreases with increasing dose, i.e. with decreasing survival level. All findings are confirmed with the PIDE. While these trends might not be detectable due to fluctuations when only a few survival curves are considered, they are clearly observed in the present data ensemble.

LET dependence of β

There is an on-going discussion about the evolution of the β-term with increasing LET [101], debating whether β increases or decreases with rising LET. The ratio β/β_γ, where β_γ denotes the value of β for photon radiation, is an interesting quantity to look at because, at low LET where the radiation becomes photon like, this ratio converts to one. In Fig. 5 this ratio is plotted against LET for

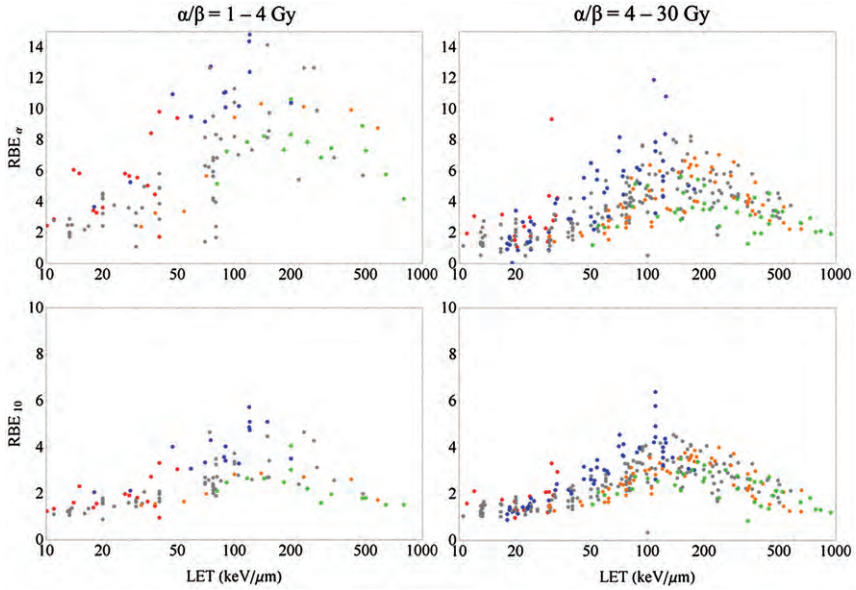

Fig. 4. RBE for monoenergetic ion beams in the limit of full survival level (upper row) and 10% survival level (lower row) vs. LET for experiments with shouldered (left column, α/β = 1–4 Gy) and less shouldered (right column, α/β = 4–30 Gy) photon dose–response curves. The colors refer to different ion species (p: red; He: blue; C: gray; Ne: orange; heavier ions than Ne: green). Note the different scales of RBE in the upper and lower row. Clearly, lighter particles show a maximum at lower LETs and have higher RBE values for a given LET.

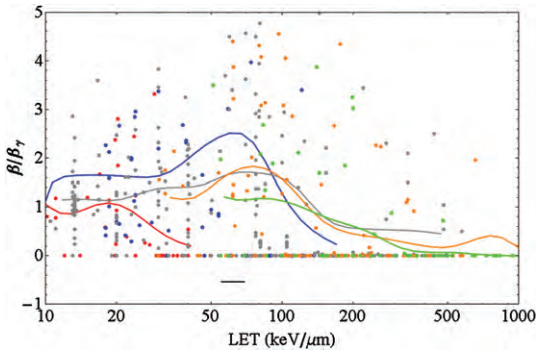

Fig. 5. Ratio of the linear-quadratic parameter β of ions to that of photons vs. LET for monoenergetic ions for different ion species with color coding as in Fig. 4. The solid lines are running averages generated by a convolution of the data points with a Gaussian function of width of 0.1 in the decadic logarithmic scale of LET values in keV/μm (i.e. a tenth of the interval between 10 and 100 keV/μm, see the black horizontal bar for an indication of that width). Lighter particles show a vanishing β at lower LET.

monoenergetic ions. The figure includes different ion species with the same colour coding as in Fig. 4.

The data shown are pooled for all photon α/β ratios, and it was checked that in contrast to the α term β depends only slightly on α/β. For intermediate and high LET values many data show a vanishing β term. For all ions a running average curve is also provided in the plot. It was calculated by summing contributions from all data points with a Gaussian weighting, i.e. for a given LET the running average is mostly determined by data points close to that LET (on the logarithmic scale), while data points further away have a smaller impact on the running average. The general trend, an increase at low LETs followed by a decrease at higher LETs, is obvious and is seen for all ion species except for protons, where the initial increase is not that obvious. Similar to the RBE maximum, the falloff for β is shifted to higher LET values for heavier ions. However, it should be noted that the fluctuations of the data points around these average curves are huge, as usually β is much harder to fix in a fit procedure than α.

Relevance of dose level and α/β ratio for RBE

In Fig. 6 we show RBE values for monoenergetic carbon ions within an LET window of 70–130 keV/μm. This range of LETs is typically found in a spread out Bragg peak, and the results may be henceforth regarded to be representative. The RBE for the initial slope (often referred to as RBE_α) and 10% survival level (RBE_{10}) are plotted vs. the inverse α/β ratio, i.e. β/α. This way of plotting [102] is motivated,

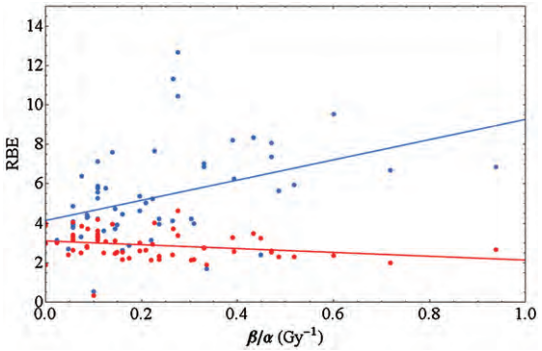

Fig. 6. RBE_{α} derived from the initial slope of survival curves (blue) and RBE_{10} for 10% survival (red) for experiments with monoenergetic carbon ions in the LET range 70–130 keV/µm vs the inverse of the photon LQ parameter ratio α/β. While for low doses the RBE increases with β/α, a decrease is observed for high doses. The data shown are restricted to α/β = 1–30 Gy. The solid lines are linear fits to the data points.

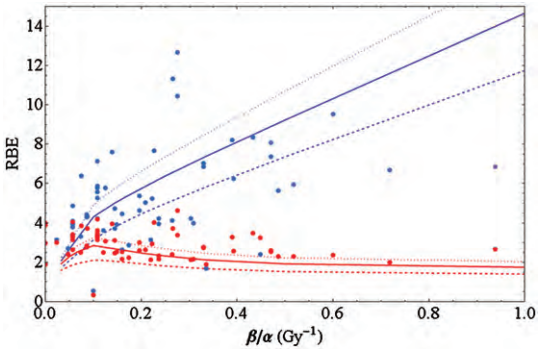

Fig. 7. Data as in Fig. 6 along with simulations of the LEM for LETs of 70, 100 and 130 keV/µm (dashed, solid and dotted lines, respectively, see text for details.

as the dependence of RBE on that quantity is consistent with a linear relationship, as can be shown by a significance analysis. Note that for large values of β/α the corresponding α/β ratio as used in Fig. 4 will be small. Again, in order to keep errors reasonably small, α/β values from 1–30 Gy have been taken into account for analysis. Data outside this interval have been excluded because the associated errors for α and/or β are enormous and the RBE values might not be sufficiently reliable. Interestingly, while for small doses the RBE increases with β/α, we find a slight decrease for doses corresponding to 10% survival. The slope for the fit to RBE_{α} is (5.1 ± 1.6) Gy and for RBE_{10} (–0.96 ± 0.52) Gy, where the errors are the standard error of the fit parameter.

Model validation

One goal of the set up of the database was to establish systematic comparisons of biophysical models for the RBE with experimental data. As a start we present here a first comparison of the RBE dependence on tissue type as seen in experiments and as predicted by the LEM. The simulations have been carried out with the most recent version of the LEM [103, 104], in which the calculation of the effect is based on the spatial distribution of double strand breaks of the DNA. All relevant parameters describing the amorphous track structure of the ions and the size of the damage sites have been chosen as in Friedrich *et al.* [104]. For all cells, an average nuclear radius of 5 µm has been assumed, which is a reasonable first order estimate. In Fig. 7 the same data points as in Fig. 6 are shown, along with LEM simulations for three different LETs where the photon parameter $\beta = 0.03\ Gy^{-2}$ has been fixed while α varies. The restriction of β is an important issue: it is artificial and, and β has been chosen as close to the median value (0.033 Gy^{-2}) of all cell lines in the PIDE. We must state here that fixing β is an approach only for revealing trends of the RBE from simulations with the LEM. A more thorough approach for the calculation of individual RBEs should take into account the LET and the photon parameters separately for each experiment, i.e. individual simulations would be performed with the specific LQ parameters α and β. Here, however, we can not expect the simulation to reflect the RBE of each individual cell line with high exactitude, but rather we have obtained an estimate for the behaviour of the ensemble of cell lines. The threshold dose D_t above which the LQ model was assumed to enter into a linear dose response [10] was chosen as $D_t = 4\ Gy + 1.1\ \alpha/\beta$. The latter relationship has been found empirically to match survival data with LEM simulations. An increase in D_t with α/β has also been suggested in a study by Astrahan [105] based on experimental motivation. The LEM clearly reveals the general systematics, i.e. the increase (decrease) of the RBE with β/α for high (low) survival levels. Moreover, for 10% survival LEM predicts a small maximum at $\beta/\alpha = 0.1\ Gy^{-1}$, which, however, is neither in contrast with nor reflected significantly by the data.

Regarding the evolution of the β term presented above, we compared the prediction of several RBE models with an individual data set, where no cell line-dependent fluctuations of β are expected. Figure 8 shows the ratio β/β_{γ} for HSG and V79 cells irradiated with carbon ions as measured by Furusawa *et al.* [30]. Again it becomes evident that for lower LET values the ratio exceeds one, while it finally decreases to zero. We indicated in the figure model predictions of the LEM, the repair–misrepair–fixation (RMF) model [106] as published recently by Frese *et al.* [107], and the microdosimetric kinetic model (MKM). Interestingly, none of the models is able to correctly reproduce the experimental findings. The LEM reveals a monotonically

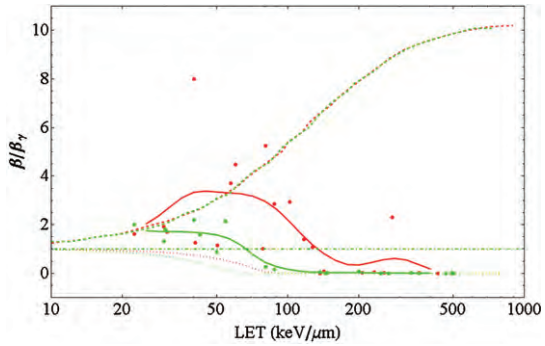

Fig. 8. Ratio of the LQ parameter β of carbon ions to that of photons vs. LET for two individual cell lines, V79 cells (red) and HSG cells (green), as measured by Furusawa *et al.* [30]. As in Fig. 5 the thick lines are obtained as a running average of the data points. The dashed, dotted and dashed–dotted lines show model predictions of the RMF (reproduced from [107] model, the LEM and the MKM, respectively. The photon parameters used for the LEM calculations are $\alpha = 0.184\ \mathrm{Gy}^{-1}$, $\beta = 0.02\ \mathrm{Gy}^{-2}$ and the threshold dose [10, 105] $D_t = 17$ Gy for V79 cells and $\alpha = 0.313\ \mathrm{Gy}^{-1}$, $\beta = 0.0615\ \mathrm{Gy}^{-2}$ and $D_t = 7.5$ Gy for HSG cells.

decreasing characteristic with increasing LET, while the RMF predicts a continuously increasing β term. The MKM predicts no changes in β/β_γ. Consequently for lower LET the LEM underestimates β, and for high LET the RMF fails to reproduce the transition to a vanishing β. The MKM suffers from both shortcomings but reveals good predictions in the intermediate LET regime. Using the PIDE model, comparisons with larger sets of data can be carried out easily and it is a useful tool to exploit the limits of RBE models.

DISCUSSION

As the PIDE comprises a large set of experiments, one may suspect that the variety of α and β values for photon dose responses is representative for all mammalian cell lines. Before discussing the properties of the particle dose–response curves, we first concentrate here on the photon properties.

Photon dose response

From Fig. 1 it is evident that both LQ parameters have a peaked distribution. However, despite the peak for very small or vanishing β, the distribution of β values is less skewed and more peaked at intermediate values, compared with the distribution of α. Consequently, the variation in the radio-sensitivity observed in cell lines is most likely due to the variability of α. Taking the average <β> as a representative quadratic parameter may be misleading, as can be seen by regarding the α/β ratio: as here β occurs in the denominator, small β values lead to large ratios as can be seen in Fig. 2. Applying <β> instead will result in artificially smaller α/β ratios, see Friedrich *et al.* [108] for details.

The large first bin of the distribution of β values is mainly reflecting the fact that many publications are concerned with repair-deficient cell lines. These cells lack the capability for repair of DNA lesions and show a linear or an almost linear dose response to low LET radiation. While this peak in the distribution seems to be non-generic because of the specific selection of cell lines, we believe the gross part of the distribution to be representative for cultured mammalian cells in general. This statement is a conjecture. However, if it holds, then the distributions shown in Fig. 1 can be used to define typical LQ parameter values for cultured cells as well as the corresponding typical intervals LQ parameters cover.

Fig. 3 suggests an anti-correlation between the LQ parameters α and β. Besides a simple expansion in powers of the dose there are several mechanistic interpretations of the LQ model in the literature [109], which give meaning to these parameters. Similarly, the LQ model emerges as a low dose approximation of many other survival models [110]. From this point of view it is interesting to note that a negative correlation observed in Fig. 3 would imply that the linear and quadratic components of the LQ model do *not* refer to totally independent processes. The anti-correlation is significant as judged by the standard error of the fit function. It is also observed in other data sets of survival curves after photon irradiation [111, 112]. The reason for this anti-correlation is still unclear. However, it can be excluded that the dependence between α and β is because of the inherent anti-correlation induced by the LQ least square fit procedure, where one parameter accounts for the other, as this only applies to multiple survival curves taken from one and the same assay. For independent survival curves no correlation is expected at all by the fit procedure. We hence believe that this observation is either because of the particular selection of cell lines studied in the literature or because there is a biological reason for the observed anti-correlation. If the latter was true the question arises as to whether this finding will influence the mechanistic interpretation of survival models. One possible explanation is a saturation of damage in organizational substructures of mega base pair size of the chromatin. We discuss the considerations about such a mechanism in a separate publication [113].

Dose response to ion irradiation

For the ion dose–response curves, the characteristics of RBE vs. LET in Fig. 4 summarizes the findings from cell survival studies during the last 50 years. Note that though fluctuations in RBE are huge, a dependence of RBE on particle species and α/β is clearly present. Having this in

mind we regard our work as an extension to the plots presented in Ando and Kase [114] where the RBE was presented as a function of LET only.

As a consequence, when modeling the RBE for therapy, its dependence on particle species and the α/β ratio has to be respected. These findings do not support the conclusions drawn in Sørensen *et al.* [115], where a collection of survival data is also considered and the authors conclude that the dependence of RBE on the particle species and the cell type is small and might be neglected for a 10% survival level. However, although a considerable scatter of the individual data points around a hypothetic 'best fit' curve is observed, the average RBE_{10} of helium ions (blue data points) turns out to exceed the one for neon ions (orange data points) for a given LET by a factor of almost two, and the maxima of RBE–LET relationships are shifted to higher LETs for heavier particles. This clearly proves that a reduction to taking the LET as the only predictor for RBE is an oversimplification of the picture. Even if one respects that the scatter of data points is large, the necessity to discriminate not only by LET but also by particle species and α/β ratios holds for therapy applications, where the RBE is desired to be known to an accuracy level of about 10% to keep the variations in tumor control reasonably low. Nevertheless the observed scatter of the data for the same particles and comparable α/β ratio corresponds to an uncertainty in RBE. This is also an important issue for the assessment of treatment plans, where the data ensemble might help to estimate the uncertainty of RBE values.

In the literature, the behavior of the LQ parameter β with varying LET is still unclear. For neutron radiation, whose radiation response is believed to be mediated by protons as secondary particles, there are indications for an increase of β with LET [116]. Other authors do not find such obvious systematics [30]. Using the data from PIDE presented in Fig. 5 an initial increase of β for low LET is suggested (except for protons), followed by a clear rapid falloff at higher LETs. Facing these partially contradictory statements one has to keep in mind that the extracted values for β are the result of a fit and therefore subject to fit errors. For instance, if a survival curve consists of a small number of dose points or an inappropriate fit interval is used, it is hardly feasible to obtain a β term with good accuracy. Currently no error analysis has been carried out with the PIDE. It is on our agenda, and maybe the question of how β varies with LET can be answered more clearly then. A clarification on this point would again be of great interest with respect to RBE models.

The trend curves in Fig. 5 show an increase in β with LET followed by a rapid falloff down to zero. These features might be understood qualitatively in a microscopic picture: The enhanced radiation response with dose is due to the track-to-track interaction ('intertrack effect') of different ions passing through a cell nucleus. This means that the β term for particle radiation emerges as a consequence of overlapping particle tracks. For high energy particles the track diameter is largest, while the local doses are rather low. When lowering the energy and thereby raising the LET, two competing processes occur: first, the inhomogeneity of the microscopic dose distribution increases, as the track radii get smaller and the energy lost by the passing particle is distributed within a smaller volume, and moreover this amount of lost energy is larger due to the increased LET. Hence the number of induced lesions within a particle track is enhanced, and thereby potentially also the rates of lesions emerging from track to track interaction are enhanced. However, on the other hand there is a second, competing process, as due to the smaller track radii the geometrical probability for tracks to overlap gets smaller. Moreover, due to the higher LET, for a given dose the overall fluence is smaller, again leading to a mitigation of overlapping of different ion tracks. For light particles and not-too-high LET the first process is more important, while for heavier particles and/or higher LETs the second one dominates the picture. Consequently, β rises first and then decreases with rising LET. At even larger LET values where one ion passing through a cell nucleus is sufficient to 'overkill' the cell, i.e. more energy than needed for cell death is deposited, there is a further argument that no β term occurs: even if tracks overlap, the consequence in terms of cell death will be just the same and no additional effect is expected, because any hit causes cell death. The same characteristics are also seen in individual cell lines, as demonstrated in Fig. 8, which is supportive of the interpretation given above.

An interesting feature in the ion dose–response curves is the increasing or decreasing course of RBE with β/α, depending on the survival level. This behavior is significant. In Fig. 6 it can be seen that for high doses (at 10% survival) where a negative slope is observed in the fit line, ion irradiation to cells with a high α/β ratio, often labeled as radio-sensitive (with respect to photon irradiation), is more effective than to cells with a small α/β ratio, which are usually labeled as radio-resistant. This is counterintuitive and we do not have an explanation for this finding yet.

For clinical applications this observation suggests two implications, provided these findings are still valid for tissues just as for cell survival assays: first, tissues with a high α/β ratio provide larger RBEs for sufficient high doses compared with tissues with smaller α/β ratios. Due to that, patients with tumors with high α/β ratios surrounded by normal tissues with smaller α/β ratios will benefit more from hypofractionated regimens than from normal fractionation schemes. This feature would constitute an additional rationale for carbon ion therapy for these tumor entities. A potential biological benefit of a small fraction number was also demonstrated with *in vivo* experiments [116]. On the other hand, if tumors with a low α/β ratio are embedded in

normal tissues with high α/β ratios, hypofractionation would be less advantageous. Second, at intermediate doses there is a survival range (~0.5–0.8) where RBE values are rather insensitive to the tissue type, i.e. to the α/β ratio. One may question the impact of these findings for biological treatment planning, but obviously in the entrance, where low doses are desired, RBE has to be taken into account as a tissue-dependent quantity.

In Fig. 7 we also present the first steps of the comparison of the experimental data in the PIDE with the LEM. Note that this comparison is carried out on a very basic level here, as the simulations have been carried out for a unique β term, while the exact properties of the individual experiments have been neglected. A 'point by point' simulation is an additional open task, where we hope to further elucidate the potential and limits of the LEM. Besides that, it is impressive to see that a less detailed simulation is capable of reproducing the increase and decrease in RBE with β/α for high and low survival levels, respectively, with reasonable accuracy. Moreover, if the peak predicted by the LEM simulations for the 10% survival level reflects reality (which cannot be assessed based on the available data), there will be a maximum RBE corresponding to $\alpha/\beta \approx 10$ Gy. Again questioning the meaning for clinical application the existence of such a peak would suggest that carbon ion therapy for tumors with that α/β ratio is particularly useful when applied as a hypofractionated regimen.

While the LEM is based on the considerations within the formalism of amorphous track structure and predicts a variation of β with LET [10], the MKM [12, 13] assumes a fixed β value for all LET. A 'saturation correction' at very high LET in the 'overkill effect' is taken into account in both models, but acts only on the α term in the MKM, leaving β constant even at high LET values. As can be seen in Fig. 8 the LEM does reveal a sudden decrease of the β term and even predicts the correct ordering, i.e. for HSG cells the falloff takes place at lower LET compared with V79 cells. While the ordering is correct, the absolute LET values for the decrease in β are not predicted correctly. Furthermore, the β term is underestimated for the lower to intermediate LET range. For obtaining the simulation results shown, we used an economic LEM algorithm, deriving the properties of the cell line after ion irradiation from the action of single hits [10]. A full Monte Carlo simulation of the damage induction processes involved in the LEM helps to partially overcome these shortcomings, allowing also a small initial increase of β/β_γ [104]. We plan to discuss this improvement in more detail in a separate publication. The RMF model (in combination with a Monte Carlo model for simulating aspects of track structure) predicts continuously increasing characteristics, which does not seem to be dependent on the cell line. In particular for the high LET regime this leads to a large overestimate of the β values. Possible reasons are discussed by the founders of the model [106]. To summarize, none of the models is able to predict the characteristics of the β term in full correspondence with the data, justifying the ongoing concentrated development in RBE models. However, in the context of the focus of this paper it becomes clear that databases generally are a powerful tool for model testing. As has been shown here the PIDE can be used conveniently to exploit the limits of RBE-predicting models. Likewise, the fluctuations in RBE observed in the database give insight into the accuracy level one can expect when applying RBE models to individual survival experiments [104].

Finally, from the discussed examples it becomes clear that the database is a powerful tool for revealing systematic properties of quantities relevant in radiobiology and therapy that may be hard to detect when reviewing a limited number of experiments only. We propose the PIDE as a standard data collection to benchmark RBE models and suggest that it is also suitable for comparing different models. From the PIDE one also can identify biological and/or physical parameters for which not so much experimental information has been available up to now and consequently further experimental work would be desirable, such as for Li, Be and B ions or for higher α/β values. We plan to share the content of the PIDE with the community and put the data on the research section (modelling group) of the website of the GSI biophysics department, where they can be downloaded after contacting the authors to obtain access. In the future we plan to maintain the PIDE continuously by inputting more data. For that reason, we invite the researchers in the field to make us aware of any suitable dataset that is missing in the PIDE.

FUNDING

This work was partially supported by Siemens Healthcare, Erlangen, Germany.

ACKNOWLEDGEMENTS

We gratefully thank G. Kraft for useful help with the literature survey. We also thank E. Scifoni for valuable remarks during manuscript preparation.

REFERENCES

1. Amaldi U, Kraft G. Radiotherapy with beams of carbon ions. *Rep Progr Phys* 2005;**68**:1861–82.
2. Kraft G. Tumor therapy with heavy charged particles. *Prog Part Nucl Phys* 2000;**45**:S473–S544.
3. Tsujii H, Kamada T, Baba M *et al*. Clinical advantages of carbon-ion radiotherapy. *New J Phys* 2008;**10**:075009.
4. Kitagawa A, Fujita T, Murumatsu M *et al*. Review on heavy ion radiotherapy facilities and related ion sources. *Rev Sci Instrum* 2010;**81**:02B909.

5. Schardt D, Elsässer T, Schulz-Ertner D. Heavy-ion tumor therapy: physical and radiobiological benefits. *Rev Mod Phys* 2010;**82**:383–425.
6. Durante M, Loeffler JS. Charged particles in radiation oncology. *Nat Rev Clin Oncol* 2010;**7**:37–43.
7. IAEA. Relative biological effectiveness in ion beam therapy. IAEA Technical Reports Series 461. 2008.
8. Emami B, Lyman J, Brown A *et al*. Tolerance of normal tissue to therapeutic irradiation. *Int J Radiat Oncol Biol Phys* 1991;**21**:109–22.
9. Withers HR, Taylor JMG, Maciejewski B. The hazard of accelerated tumor clonogen repopulation during radiotherapy. *Acta Oncol* 1988;**27**:131–46.
10. Scholz M, Kellerer AM, Kraft-Weyrather W *et al*. Computation of cell survival in heavy ion beams for therapy. The model and its approximation. *Radiat Environ Biophys* 1997;**36**:59–66.
11. Krämer M, Scholz M. Treatment planning for heavy-ion radiotherapy: calculation and optimization of biologically effective dose. *Phys Med Biol* 2000;**45**:3319–30.
12. Hawkins RB. A statistical theory of cell killing by radiation of varying linear energy transfer. *Radiat Res* 1994;**140**: 366–74.
13. Hawkins RB. A microdosimetric kinetic model for the effect of non-Poisson distribution of lethal lesions on the variation of RBE with LET. *Radiat Res* 2003;**160**:61–9.
14. Paganetti H, Niemierko A, Ancukiewicz M *et al*. Relative biological effectiveness (RBE) values for proton beam therapy. *Int J Radiat Biol Phys* 2002;**53**:407–21.
15. Guerrero M, Li XA. Extending the linear-quadratic model for large fraction doses pertinent to stereotactic radiotherapy. *Phys Med Biol* 2004;**49**:4825–35.
16. Kirkpatrick JP, Brenner DJ, Orton CG. The linear-quadratic model is inappropriate to model high dose per fraction effects in radiosurgery. *Med Phys* 2009;**38**:3381–4.
17. Brenner DJ. The linear-quadratic model is an appropriate methodology for determining isoeffective doses at large dose per fraction. *Semin Radiat Oncol* 2008;**18**:234–9.
18. Chapman JD, Blakely EA, Smith KC *et al*. Radiation biophysical studies with mammalian cells and a modulated carbon ion beam. *Radiat Res* 1978;**74**:101–11.
19. Chapman JD, Blakely EA, Smith KC *et al*. Radiobiological characterization of the inactivating events produced in mammalian cells by helium and heavy ions. *Int J Radiat Oncol Biol Phys* 1977;**3**:97–102.
20. Blakely EA, Tobias CA, Yang TCH *et al*. Inactivation of human kidney cells by high-energy monoenergetic heavy-ion beams. *Radiat Res* 1979;**80**:122–60.
21. Raju MR, Eisen Y, Carpenter S *et al*. Radiobiology of α particles. *Radiat Res* 1991;**128**:204–9.
22. Goodhead DT, Belli M, Mill AJ *et al*. Direct comparison between protons and alpha-particles of the same LET. I: irradiation methods and inactivation of asynchronous V79, HeLa and C3HT1/2 cells. *Int J Radiat Biol* 1992;**61**:611–24.
23. Folkard M, Prise KM, Voijnovic B *et al*. Inactivation of V79 cells by low-energy protons, deuterons and helium-3 ions. *Int J Radiat Biol* 1996;**69**:729–38.
24. Eguchi-Kasai K, Murakami M, Itsukaichi H *et al*. The role of DNA repair on cell killing by charged particles. *Adv Space Res* 1996;**18**:109–18.
25. Suzuki M, Kase Y, Kanai T *et al*. LET dependence of cell death and chromatin-break induction in normal human cells irradiated by neon-ion beams. *Int J Radiat Biol* 1997;**72**:497–503.
26. Bettega D, Calzolari P, Marchesini R *et al*. Inactivation of C3H10T1/2 cells by low energy protons and deuterons. *Int J Radiat Biol* 1998;**73**:303–9.
27. Tsuboi K, Tsuchida Y, Nose T *et al*. Cytotoxic effect of accelerated carbon beams on glioblastoma cell lines with p53 mutation: clonogenic survival and cell-cycle analysis. *Int J Radiat Biol* 1998;**74**:71–9.
28. Tsuchida Y, Tsuboi K, Ohyama H *et al*. Cell death induced by high-linear-energy transfer carbon beams in human glioblastoma cell lines. *Brain Tumor Pathol* 1998;**15**:71–6.
29. Weyrather WK, Ritter S, Scholz M *et al*. RBE for carbon track-segment irradiation in cell lines of differing repair capacity. *Int J Radiat Biol* 1999;**75**:1357–64.
30. Furusawa Y, Fukutsu K, Aoki M *et al*. Inactivation of aerobic and hypoxic cells from three different cell lines by accelerated ^{3}He-, ^{12}C- and ^{20}Ne beams. *Radiat Res* 2000;**154**:485–96.
31. Suzuki M, Kase Y, Yamaguchi H *et al*. Relative biological effectiveness for cell-killing effect on various human cell lines irradiated with heavy-ion medical accelerator in Chiba (HIMAC) carbon-ion beams. *Int J Radiat Oncol Biol Phys* 2000;**48**:241–50.
32. Belli M, Bettega D, Calzolari P *et al*. Inactivation of human normal and tumour cells irradiated with low energy protons. *Int J Radiat Biol* 2000;**76**:831–9.
33. Tsuruoka C, Suzuki M, Fujitaka K *et al*. LET and ion species dependence for cell killing in normal human skin fibroblasts. *Radiat Res* 2005;**163**:494–500.
34. Belli M, Bettega D, Calzolari P *et al*. Effectiveness of monoenergetic and spread-out Bragg peak carbon-ions for inactivation of various normal and tumour human cell lines. *J Radiat Res* 2008;**49**:597–607.
35. Belli M, Cera F, Cherubini R *et al*. RBE-LET relationships for cell inactivation and mutation induced by low energy protons in V79 cells: further results at the LNL facility. *Int J Radiat Biol* 1998;**74**:501–9.
36. Belli M, Cera F, Cherubini R *et al*. Inactivation and mutation induction in V79 cells by low energy protons: re-evaluation of the results at the LNL facility. *Int J Radiat Biol* 1993;**63**:331–7.
37. Hall EJ, Bird RP, Rossi HH *et al*. Biophysical studies with high-energy argon ions 2. Determinations of the relative biological effectiveness, the oxygen enhancement ratio, and the cell cycle response. *Radiat Res* 1977;**70**:469–79.
38. Bird RP, Burki HJ. Survival of synchronized Chinese hamster cells exposed to radiation of different linear-energy transfer. *Int J Radiat Biol* 1975;**27**:105–20.
39. Sinclair WK, Morton RA. X-ray sensitivity during the cell generation cycle of cultured Chinese hamster cells. *Radiat Res* 1966;**29**:450–74.

40. Von Neubeck C. Radiobiological experiments for carbon ion prostate cancer therapy: interplay of normal and tumor cells in co-culture and measurement of the oxygen enhancement ratio. PhD thesis, Technische Universität Darmstadt, 2009.
41. Perris A, Pialoglou P, Katsanos AA *et al*. Biological effectiveness of low energy protons. I. Survival of Chinese hamster cells. *Int J Radiat Biol* 1986;**50**:1093–101.
42. Bettega D, Tallone Lombardi L. Physical and radiobiological parameters of proton beams up to 31 MeV. *Nuovo Cim* 1983;**2D**:907–16.
43. Bettega D, Birattari C, Bombana M *et al*. Relative biological effectiveness for protons of energies up to 31MeV. *Radiat Res* 1979;**77**:85–97.
44. Cox R, Thacker J, Goodhead DT. Inactivation and mutation of cultured mammalian cells by aluminium characteristic ultrasoft X-rays. II. Dose-responses of Chinese hamster and human diploid cells to aluminium X-rays and radiations of different LET. *Int J Radiat Biol* 1977;**31**:561–76.
45. Wouters BG, Lam GKY, Oelfke U *et al*. Measurements of relative biological effectiveness of the 70 MeV proton beam at TRIUMF using Chinese hamster V79 cells and the high-precision cell sorter assay. *Radiat Res* 1996;**146**:159–70.
46. Combs SE, Bohl J, Elsässer T *et al*. Radiobiological evaluation and correlation with the local effect model (LEM) of carbon ion radiation therapy and temozolomide in glioblastoma cell lines. *Int J Radiat Biol* 2009;**85**:126–36.
47. Kitajima S, Nakamura H, Adachi M *et al*. AT cells show dissimilar hypersensitivity to heavy-ion and X-rays irradiation. *J Radiat Res* 2010;**51**:251–5.
48. Blomquist E, Russell KR, Stenerlöw B *et al*. Relative biological effectiveness of intermediate energy protons. Comparisons with ^{60}Co gamma-radiation using two cell lines. *Radiother Oncol* 1993;**28**:44–51.
49. Yang TCH, Craise LM, Mei MT *et al*. Neoplastic cell transformation by heavy charged particles. *Radiat Res* 1985;**104**: S177–S187.
50. Miller RC, Marino SA, Brenner DJ *et al*. The biological effectiveness of radon-progeny alpha particles. II. Oncogenic transformation as a function of linear energy transfer. *Radiat Res* 1995;**142**:54–60.
51. Czub J, Banaś D, Błaszczyk A *et al*. Biological effectiveness of ^{12}C and ^{20}Ne ions with very high LET. *Int J Radiat Biol* 2008;**84**:821–9.
52. Kamlah F, Hanze J, Arenz A *et al*. Comparison of the effects of carbon ion and photon irradiation on the angiogenic response in human lung adenocarcinoma cells. *Int J Radiat Oncol Biol Phys* 2011;**80**:1541–9.
53. Aoki M, Furusawa Y, Yamada T. LET dependency of heavy-ion induced apoptosis in V79 cells. *J Radiat Res* 2000;**41**:163–75.
54. Han ZB, Suzuki H, Suzuki F *et al*. Relative biological effectiveness of accelerated heavy ions for induction of morphological transformation in Syrian hamster embryo cells. *J Radiat Res* 1998;**39**:193–201.
55. Hamada N, Imaoka T, Masunaga S *et al*. Recent advances in the biology of heavy-ion cancer therapy. *J Radiat Res* 2010;**51**:365–83.
56. Claesson K, Magnander K, Kahu H *et al*. RBE of α-particles from ^{211}At for complex DNA damage and cell survival in relation to cell cycle position. *Int J Radiat Biol* 2011;**87**:72–84.
57. Wedenberg M, Lind BK, Toma-Daşu I *et al*. Analytical description of the LET dependence of cell survival using the repairable-conditionally repairable damage model. *Radiat Res* 2010;**174**:517–25.
58. Miller RC, Brenner DJ, Randers-Pehrson G *et al*. The effects of the temporal distribution of dose on oncogenic transformation by neutrons and charged particles of intermediate LET. *Radiat Res* 1990;**14**:S62–S68.
59. Tobias CA, Blakely EA, Ngo FQH *et al*. The repair-misrepair model of cell survival. In: Meyn RE, Withers HR (eds). *Radiation Biology in Cancer Research*. New York: Raven press, 1980, 195–230.
60. Cox R, Masson WK. Mutation, inactivation of cultured mammalian cells exposed to beams of accelerated heavy ions III. Human diploid fibroblasts. *Int J Radiat Biol* 1979;**36**:149–60.
61. Ito A, Nakano H, Kusano Y *et al*. Contribution of indirect action to radiation-induced mammalian cell inactivation: dependence on photon energy and heavy-ion LET. *Radiat Res* 2006;**165**:703–12.
62. Tilly N, Brahme A, Carlsson J *et al*. Comparison of cell survival models for mixed LET radiation. *Int J Radiat Biol* 1999;**75**:233–43.
63. Thacker J, Stretch A, Stephens MA. Mutation, inactivation of cultured mammalian cells exposed to beams of accelerated heavy ions II. Chinese hamster V79 cells. *Int J Biol* 1979;**36**:137–48.
64. Hirayama R, Ito A, Tomita M *et al*. Contributions of direct and indirect actions in cell killing by high-LET radiations. *Radiat Res* 2009;**171**:212–18.
65. Hirayama R, Furusawa Y, Fukawa T *et al*. Repair kinetics of DNA-DSB induced by X-rays or carbon ions under oxic and hypoxic conditions. *J Radiat Res* 2005;**46**:325–32.
66. Curtis SB, Schilling WA, Tenforde TS *et al*. Survival of oxygenated and hypoxic tumor cells in the extended-peak regions of heavy charged-particle beams. *Radiat Res* 1982;**90**:292–309.
67. Böhrnsen G, Weber KJ, Scholz M. Measurement of biological effects of high-energy carbon ions at low doses using a semi-automated cell detection system. *Int J Radiat Biol* 2002;**78**:259–66.
68. Fournier C, Scholz M, Weyrather WK *et al*. Changes of fibrosis-related parameters after high- and low-LET irradiations of fibroblasts. *Int J Radiat Biol* 2001;**77**:713–22.
69. Wulf H, Kraft-Weyrather W, Miltenburger HG *et al*. Heavy-ion effects on mammalian cells: inactivation measurements with different cell lines. *Radiat Res* 1985;**104**: S122–S134.
70. Wulf H. Der Einfluss von Schwerionenstrahlen auf das Überleben und Wachstum von Säugetierzellen in vitro. PhD thesis, Technische Hochschule Darmstadt, 1983.
71. Kraft G. Biologische Effekte schwerer Ionen In: zum Winkel K ed. *Wirkungssteigerung der Strahlentherapie maligner Tumoren*. Springer; Heidelberg, 1987.

72. Scholz M. Effects of ion radiation on cells and tissues. *Adv Polymer Science* 2003;**162**:95–155.
73. Persson LM, Edgren MR, Stenerlöw B *et al*. Relative biological effectiveness of boron ions human melanoma cells. *Int J Radiat Biol* 2002;**78**:743–8.
74. Yang TC, Tobias CA. Neoplastic cell transformation by energetic heavy ions and its modification with chemical agents. *Adv Space Res* 1984;**4**:207–18.
75. Prise KM, Folkard M, Davies S *et al*. The irradiation of V79 mammalian cells by protons with energies below 2 MeV. Part II. Measurement of oxygen enhancement ratios and DNA damage. *Int J Radiat Biol* 1990;**58**:261–77.
76. Terato H, Tanaka R, Nakaarai Y *et al*. Quantitative analysis of isolated and clustered DNA damage induced by gamma-rays, carbon ion beams, and iron ion beams. *J Radiat Res* 2008;**49**:133–46.
77. Suzuki M, Watanabe M, Kanai Y *et al*. LET dependence of cell death, mutation induction and chromatin damage in human cells irradiated with accelerated carbon ions. *Adv Space Res* 1996;**18**:127–36.
78. Matsumoto Y, Iwakawa M, Furusawa Y *et al*. Gene expression analysis in human malignant melanoma cell lines exposed to carbon beams. *Int J Radiat Biol* 2008;**84**:299–314.
79. Mehnati P, Morimoto S, Yatagai F, Exploration of *et al*. 'over kill effect' of high-LET Ar- and Fe-ions by evaluating the fraction of non-hit cell and interphase death. *J Radiat Res* 2005;**46**:343–50.
80. Stenerlöw B, Petterson OA, Essand M *et al*. Irregular variations in radiation sensitivity when the linear energy transfer is increased. *Radiother Oncol* 1995;**36**:133–42.
81. Okayasu R, Okada M, Okabe A *et al*. Repair of DNA damage induced by accelerated heavy ions in mammalian cells proficient and deficient in the non-homologous end-joining pathway. *Radiat Res* 2006;**165**:59–67.
82. Tsuboi K, Moritake T, Tsuchida Y *et al*. Cell cycle checkpoint and apoptosis induction in glioblastoma cells and fibroblasts irradiated with carbon beam. *J Radiat Res* 2007;**48**:317–25.
83. Todd PW. Heavy-ion irradiation of human and Chinese hamster cells in vitro. *Radiat Res* 1975;**61**:288–97.
84. Hall EJ, Gross W, Dvorak RF *et al*. Survival curves and age response functions for Chinese hamster cells exposed to X-rays or high-LET alpha-particles. *Radiat Res* 1972;**52**:88–98.
85. Takahashi A, Ohnishi K, Tsuji K *et al*. WAF1 accumulation by carbon-ion beam and α-particle irradiation in human glioblastoma cultures cells. *Int J Radiat Biol* 2000;**76**:335–41.
86. Takahashi A, Matsumoto H, Yuki K *et al*. High-LET radiation enhanced apoptosis but not necrosis regardless of pp53 status. *Int J Radiat Oncol Biol Phys* 2004;**60**:591–7.
87. Matsuzaki H, Miyamoto T, Miyazawa Y *et al*. Biological effects of heavy ion beam on human breast cancers. *Breast Cancer* 1998;**5**:261–8.
88. Kronenberg A, Gauny S, Kwoh E *et al*. Comparative analysis of cell killing and autosomal mutation in mouse kidney epithelium exposed to 1 GeV/nucleon iron ions in vitro or in situ. *Radiat Res* 2009;**172**:550–7.
89. Hamada N, Funayama T, Wada S *et al*. LET-dependent survival of irradiated normal human fibroblasts and their descendants. *Radiat Res* 2006;**166**:24–30.
90. Zhou G, Wang P, Tao L *et al*. Protective effect of melatonin against low- and high-LET irradiation. *J Radiat Res* 2006;**47**:175–8.
91. Jenner TJ, deLara CM, O'Neill P *et al*. Induction and rejoining of DNA double-strand breaks in V79-4 mammalian cells following γ- and α-irradiation. *Int J Radiat Biol* 1993;**64**:265–73.
92. Furusawa Y, Aoki M, Durante M. Simultaneous exposure of mammalian cells to heavy ions and X-rays. *Adv Space Res* 2002;**30**:877–84.
93. Takahashi A, Ohnishi K, Ota I *et al*. p53–dependent thermal enhancement of cellular sensitivity in human squamous cell carcinoma in relation to LET. *Int J Radiat Biol* 2001;**77**:1043–51.
94. Bettega D, Calzolari P, Doneda L *et al*. Early and delayed reproductive death in human cells exposed to high energy iron ion beams. *Adv Space Res* 2005;**35**:280–5.
95. Ibañez IL, Bracalente C, Molinari BL *et al*. Induction and rejoining of DNA double strand breaks assessed by H2AX phosphorylation in melanoma cells irradiated with proton and lithium beams. *Int J Radiat Oncol Biol Phys* 2009;**74**:1226–35.
96. Hellweg CE, Baumstark-Khan C, Schmitz C *et al*. Carbon-ion-induced activation of the NF-κB pathway. *Radiat Res* 2011;**175**:424–31.
97. Napolitano M, Durante M, Grossi GF *et al*. Inactivation of C3H 10T1/2 cells by monoenergetic high LEt alpha-particles. *Int J Radiat Biol* 1992;**61**:813–20.
98. Hill MA, Herdman MT, Stevens DL *et al*. Relative sensitivities of repair-deficient mammalian cells for clonogenic survival after α-particle irradiation. *Radiat Res* 2004;**162**:667–76.
99. Krämer M, Jäkel O, Haberer T *et al*. Treatment planning for heavy-ion radiotherapy: physical beam model and dose optimization. *Phys Med Biol* 2000;**45**:3299–317.
100. Geissel H, Weick H, Scheidenberger C *et al*. Experimental studies of heavy-ions slowing down in matter. *Nucl Instr and Meth B* 2002;**195**:3–54.
101. Jones B. The apparent increase in the β-parameter of the linear quadratic model with increased linear energy transfer during fast neutron irradiation. *Br J Radiol* 2009;**83**:433–6.
102. Weyrather WK. Medical applications of accelerated ions. *Lect Notes Phys* 2004;**651**:469–90.
103. Elsässer T, Weyrather WK, Friedrich T *et al*. Quantification of the relative biological effectiveness for ion beam radiotherapy: direct experimental comparison of proton and carbon ion beams and a novel approach for treatment planning. *Int J Radiat Oncol Biol Phys* 2010;**78**:1177–83.
104. Friedrich T, Scholz U, Elsässer T *et al*. Calculation of the biological effects of ion beams based on the microscopic spatial damage distribution pattern. *Int J Radiat Biol* 2012;**88**:115–22.
105. Astrahan M. Some implications of linear-quadratic-linear radiation dose-response with regard to hypofractionation. *Med Phys* 2008;**35**:4161–72.
106. Carlson DJ, Stewart RD, Semenenko VA *et al*. Combined use of Monte Carlo DNA damage simulations and deterministic repair models to examine putative mechanisms of cell killing. *Radiat Res* 2008;**169**:447–59.

107. Frese MC, Yu VK, Stewart RD, Carlson DJ. A mechanism-based approach to predict the relative biological effectiveness of protons and carbon ions in radiation therapy. *Int J Radiat Oncol Biol Phys* 2012;**83**:442–50.
108. Friedrich T, Weyrather W, Elsässer T *et al*. Accuracy of RBE: experimental and theoretical considerations. *Radiat Environ Biophys* 2010;**49**:345–9.
109. Sachs RK, Hahnfeld PJ, Brenner DJ. The link between low-LET dose-response relations and the underlying kinetics of damage production/repair/misrepair. *Int J Radiat Biol* 1997;**72**:351–74.
110. Brenner DJ, Hlatky LR, Hahnfeldt PJ *et al*. The linear-quadratic model and most other common radiobiological models result in similar predictions of time-dose relationships. *Radiat Res* 1998;**150**:83–91.
111. Fertil B, Malaise EP. Intrinsic radiosensitivity of human cell lines is correlated radioresponsiveness of human tumors: analysis of 101 published survival curves. *Int J Radiat Oncol Biol Phys* 1985;**11**:1699–707.
112. Steel GG, Peacock JH. Why are some human tumours more radiosensitive than others? *Radiother Oncol* 1989;**15**:63–72.
113. Friedrich T, Durante M, Scholz M. Modelling cell survival after photon irradiation based on double strand break clustering in megabase pair chromatin loops. *Radiat Res.* 2012;**178**:385–94.
114. Ando K, Kase Y. Biological characteristics of carbon ion-therapy. *Int J Radiat Biol* 2009;**85**:715–28.
115. Sørensen BS, Overgaard J, Bassler N. In vitro RBE-LET dependence for multiple particle types. *Acta Oncol* 2011;**50**:757–62.
116. Ando K. Biological gain of carbon-ion radiotherapy for the early response of tumor growth delay and against early response of skin reaction in mice. *J Radiat Res* 2005;**46**:51–7.

Bibliography

[1] E.J. Hall and A.J. Giaccia, Radiobiology for the Radiologist (Lipponcott, Williams & Wilkins, Philadelphia, 2012).

[2] T. Alper, Cellular Radiobiology (Cambridge University Press, Cambridge, 1979).

[3] American Cancer Society, Global Cancer Facts & Figures, 3rd Edition (American Cancer Society, Atlanta, 2015).

[4] American Cancer Society, The science behind radiation therapy, available online: `http://www.cancer.org/acs/groups/cid/documents/webcontent/003019-pdf.pdf` (2015).

[5] Nuclear Physics European Collaboration Committee (NuPECC), Nuclear physics for medicine (European Science Foundation, Strasbourg, 2014).

[6] J.S. Loeffler and M. Durante, Charged particle therapy-optimization, challenges and future directions, Nat. Rev. Clin. Oncol. **10**, 411 (2013).

[7] M. Durante, Charged Particle In Oncology: From Nuclear Physics to Cancer Treatment, Science and Culture **81**, 117 (2015).

[8] G. Kraft, Tumor therapy with heavy charged particles, Prog. Part. Nucl. Phys. **45**, S473 (2000).

[9] U. Amaldi and G. Kraft, Radiotherapy with beams of carbon ions, Rep. Prog. Phys. **68**, 1861 (2005).

[10] D. Schulz-Ertner and H. Tsujii, Particle radiation therapy using proton and heavier ion beams, J. Clin. Oncol. **25**, 953 (2007).

[11] M. Jermann, Particle therapy statistics in 2013, Int. J. Part. Ther. **1**, 40 (2014).

[12] International Atomic Energy Agency (IAEA), Radiation Biology: A Handbook for Teachers and Students. IAEA Training Course Series **42** (IAEA, Vienna, 2010).

[13] D.J. Brenner and E.J. Hall, Computed Tomography - An Increasing Source of Radiation Exposure, N. Engl. J. Med. **357**, 2207 (2007).

[14] E.J. Hall and D.J. Brenner, Cancer risks from diagnostic radiology, Br. J. Radiol. **81**, 362 (2008).

[15] R. Wakeford, Radiation in the workplace - a review of studies of the risks of occupational exposure to ionising radiation, J. Radiol. Prot. **29**, A61 (2009).

[16] A. Bouville, R.E. Toohey, J.D. Boice Jr, H.L. Beck, L.T. Dauer, K.F. Eckerman, D. Hagemeyer, R.W. Leggett, M.T. Mumma, B. Napier, K.H. Pryor, M. Rosenstein, D.A. Schauer, S. Sherbini, D.O. Stram, J.L. Thompson, J.E. Till, C. Yoder and C. Zeitlin, Dose reconstruction for the million worker study: status and guidelines, Health Phys. **108**, 206 (2015).

[17] R.K. Sachs and D.J. Brenner, Solid tumor risks after high doses of ionizing radiation, Proc. Nat. Acad. Sci. **102** 1304 (2005).

[18] M. Durante, Physical basis of radiation protection in space travel, Rev. Mod. Phys. **83**, 1245 (2011).

[19] M. Durante, Space radiation protection: Destination Mars, Life Sci. Space Res. **1**, 2 (2014).

[20] D.L. Preston, Y. Shimizu, D.A. Pierce, A. Suyama and K. Mabuchi, Studies of mortality of atomic bomb survivors. Report 13: solid cancer and noncancer disease mortality: 1950-1997, Radiat. Res. **160** 381 (2003).

[21] C. Bert, R. Engenhart-Cabillic, and M. Durante, Particle therapy for noncancer diseases, Med. Phys. **39**, 1716 (2012).

[22] T. Terasawa, E.M. Balk, M. Chung, A.C. Garlitski, A.A. Alsheikh-Ali, J. Lau, and S. Ip, Systematic review: comparative effectiveness of radiofrequency catheter ablation for atrial fibrillation, Ann. Intern. Med. **151**, 191 (2009).

[23] C. Fournier, G. Kraft and A. Maier, Untersuchungen zum genetischen Risiko und der entzündungshemmenden Wirkung von Radon (GREWIS), StrahlenschutzPRAXIS **1**, 44 (2014).

[24] G.F. Whitmore, One Hundred Years of X Rays in Biological Research, Radiat. Res. **144**, 148 (1995).

[25] T. Friedrich, U. Scholz, T. Elsässer, M. Durante and M. Scholz, Calculation of the biological effects of ion beams based on the microscopic spatial damage distribution pattern, Int. J. Radiat. Biol. **88**, 103 (2012).

[26] T. Friedrich, M. Durante and M. Scholz, Modeling cell survival after photon irradiation based on double-strand break clustering in megabase pair chromatin loops, Radiat. Res. **178**, 385 (2012).

[27] T. Friedrich, M. Durante and M. Scholz, Modeling cell survival after irradiation with ultrasoft X Rays using the Giant Loop Binary Lesion Model, Radiat. Res. **181**, 485 (2014).

[28] T. Friedrich, R. Grün, U. Scholz, T. Elsässer, M. Durante and M. Scholz, Sensitivity analysis of the relative biological effectiveness predicted by the local effect model, Phys. Med. Biol. **58**, 6827 (2013).

[29] T. Friedrich, W. Weyrather, T. Elsässer, M. Durante and M. Scholz, Accuracy of RBE: experimental and theoretical considerations, Radiat. Environ. Biophys. **49**, 345 (2010).

[30] T. Friedrich, U. Scholz, T. Elsässer, M. Durante and M. Scholz, Systematic analysis of RBE and related quantities using a database of cell survival experiments with ion beam irradiation, J. Radiat. Res. **54**, 494 (2013).

[31] G.E. Adams and D.G. Jameson, Time Effects in Molecular Radiation Biology, Radiat. Environ. Biophys. **17**, 95 (1980).

[32] C.A. Tobias, E.A. Blakely, F.Q.H. Ngo and T.C.H. Yang, The Repair-Misrepair Model of Cell Survival, in: Radiation Biology in Cancer Research, ed. R.E. Meyn and H.R. Withers (Raven Press, New York, 1980).

[33] H. Nikjoo, P. O'Neill, D.T. Goodhead and M. Terissol, Computational modelling of low-energy electron-induced DNA damage by early physical and chemical events, Int. J. Radiat. Biol **71**, 467 (1997).

[34] T.R. Munro, The Relative Radiosensitivity of the Nucleus and Cytoplasm of Chinese Hamster Fibroblasts, Radiat. Res. **42**, 451 (1970).

[35] K.K. Khanna and S.P. Jackson, DNA double-strand breaks: signaling, repair and the cancer connection, Nat. Genet. **27**, 2147 (2001).

[36] A. Schipler and G. Iliakis, DNA double-strand-break complexity levels and their possible contributions to the probability for error-prone processing and repair pathway choice, Nucl. Acids Res. **41**, 7589 (2013).

[37] W.K. Sinclair and R.A. Morton, X-Ray Sensitivity during the Cell Generation Cycle of Cultured Chinese Hamster Cells, Radiat. Res. **29**, 450 (1966).

[38] D.E. Lea and D.G. Catcheside, The mechanism of the induction by radiation of chromosome aberrations in tradescantia, J. Genet. **44**, 216 (1942).

[39] G.J. Neary, Chromosome Aberrations and the Theory of RBE, Int. J. Radiat. Biol. **9**, 477 (1965).

[40] E. Bianconi, A. Piovesan, F. Facchin, A. Beraudi, R. Casadei, F. Frabetti, L. Vitale, M.C. Pelleri, S. Tassani, F. Piva, S. Perez-Amodio, P. Strippoli and S. Canaider, An estimation of the number of cells in the human body, Ann. Hum. Biol. **40**, 471 (2013).

[41] D.T. Goodhead, Energy Deposition Stochastics and Track Structure: What about the target?, Radiat. Prot. Dosim. **122**, 3 (2006).

[42] H.R. Withers, The four R's of radiotherapy, Adv. Radiat. Biol. **5**, 241 (1975).

[43] M.H. Barcellos-Hoff, C. Park and E.G. Wright. Radiation and the microenvironment tumorigenesis and therapy, Nat. Rev. Cancer **5**, 867 (2005).

[44] K.M. Prise, G. Ahnström, M. Belli, J. Carlsson, D. Frankenberg, J. Kiefer, M. Löbrich, B.D. Michael, J. Nygren, G. Simone and B. Stenerlöw, A review of dsb induction data for varying quality radiations, Int. J. Radiat. Biol **74**, 173 (1998).

[45] E.P. Rogakou, D.R. Pilch, A.H. Orr, V.S. Ivanova and W.M. Bonner, DNA double-stranded breaks induce histone H2AX phosphorylation on serine 139, J. Biol. Chem. **273**, 5858 (1998).

[46] K.M. Prise, M. Pinto, H.C. Newman and B.D. Michael, A Review of Studies of Ionizing Radiation-Induced Double-Strand Break Clustering, Radiat. Res. **156**, 572 (2001).

[47] B. Stenerlöw, K.H. Karlsson, B. Cooper and B. Rydberg, Measurement of Prompt DNA Double-Strand Breaks in Mammalian Cells without Including Heat-Labile Sites: Results for Cells Deficient in Nonhomologous End Joining, Radiat. Res. **159**, 502 (2003).

[48] K. Rothkamm and M. Löbrich, Evidence for a lack of DNA double-strand break repair in human cells exposed to very low x-ray doses, Proc. Nat. Acad. Sci. **100**, 5057 (2003).

[49] J.A. La Verne and A. Mozumder, Differential and integral W-values for ionization in gaseous water under electron and proton irradiation: consistency of inelastic collision cross sections, Radiat. Res. **131**, 1 (1992).

[50] F. Tobias, D. Löb, N. Lengert, M. Durante, B. Drossel, G. Taucher-Scholz and B. Jakob, Spatiotemporal Dynamics of Early DNA Damage Response Proteins on Complex DNA Lesions, PLoS ONE **8**, e57953 (2013).

[51] G. Iliakis, D. Blöcher, L. Metzger and G. Pantelias. Comparison of DNA double-strand break rejoining as measured by pulsed field gel electrophoresis, neutral sucrose gradient centrifugation and nonunwinding filter elution in irradiated plateau-phase CHO cells, Int. J. Radiat. Biol. **59**, 927 (1991).

[52] J.F. Fowler, Is repair of DNA strand break damage from ionizing radiation second-order rather than first-order? A simpler explanation of apparently multiexponential repair, Radiat. Res. **152**, 124 (1999).

[53] L. Herr, I. Shuryak, T. Friedrich, M. Scholz, M. Durante and D.J. Brenner, New insight into quantitative modeling of DNA double strand break rejoining, Radiat. Res. **184**, 280 (2015).

[54] J.M. Brown and L.D. Attardi, The role of apoptosis in cancer development and treatment response, Nat. Rev. Cancer **5**, 231 (2005).

[55] T.T. Puck and P.I. Marcus, Action of x-rays on mammalian cells, J. Exp. Med. **103**, 653 (1956).

[56] T.C. Stephens, J.J. Eady, J.H. Peacock and G.G. Steel, Split-dose and low dose-rate recovery in four experimental tumour systems, Int. J. Radiat. Biol. **52**, 157 (1987).

[57] R.K. Sachs, P. Hahnfeldt and D.J. Brenner, The link between low-LET dose-response relations and the underlying kinetics of damage production/repair/misrepair, Int. J. Radiat. Biol. **72**, 351 (1997).

[58] D.J. Brenner, L.R. Hlatky, P.J. Hahnfeldt, Y. Huang and R.K. Sachs, The Linear-Quadratic Model and Most Other Common Radiobiological Models Result in Similar Predictions of Time-Dose Relationships, Radiat. Res. **150**, 83 (1998).

[59] M.M. Elkind and H. Sutton, X-Ray damage and recovery in mammalian cells in culture, Nature **184**, 1293 (1959).

[60] M.M. Elkind, H. Sutton-Gilbert, W.B. Moses and C. Kamper, Sub-lethal and Lethal Radiation Damage, Nature **214**, 1088 (1967).

[61] D. Hanahan and R.A. Weinberg, The Hallmarks of Cancer, Cell **100**, 57 (2000).

[62] S. Webb and A.E. Nahum, A model for calculating tumour control probability in radiotherapy including the effects of inhomogeneous distributions of dose and clonogenic cell density, Phys. Med. Biol. **38**, 653 (1993).

[63] A.E. Nahum and B. Sanchez-Nieto, Tumor control probability modeling: basic principles and applications in treatment planning, Phys. Med. **17**, 13 (2001).

[64] C. Burman, G.J. Kutcher, B. Emami and M. Goitein, Fitting of normal tissue tolerance data to an analytic function, Int. J. Radiat. Oncol. Biol. Phys. **21**, 123 (1991).

[65] P. Källman, A. Agren and A. Brahme, Tumour and normal tissue responses to fractionated non-uniform dose delivery, Int. J. Radiat. Biol. **62**, 249 (1992).

[66] L.B. Marks, E.D. Yorke, A. Jackson, R.K. Ten Haken, L.S. Constine, A. Eisbruch, S.M. Bentzen, J. Nam and J.O. Deasy, Use of Normal Tissue Complication Probability Models in the Clinic, Int. J. Radiat. Oncol. Biol. Phys. **76**, S10 (2010).

[67] V. Moiseenko, J. Battista and J. van Dyk, Normal Tissue Complication Probabilities: Dependence on Choice of Biological Model and Dose-Volume Histogram Reduction Scheme, Int. J. Radiat. Oncol. Biol. Phys. **46**, 983 (2000).

[68] G.G. Steel, From targets to genes: a brief history of radiosensitivity, Phys. Med. Biol. **41**, 205 (1996).

[69] B. Fertil,and E.P. Malaise, Intrinsic Radiosensitivity of Human Cell Lines is Correlated with Radioresponsiveness of Human Tumors: Analysis of 101 Published Survival Curves, Int. J. Radiat. Oncol. Biol. Phys. **11** 1699 (1985).

[70] G.G. Steel, T.J. McMillan and J.H. Peacock, The picture has changed in the 1980s, Int. J. Radiat. Biol. **56**, 525 (1989).

[71] G.G. Steel and J.H. Peacock, Why are some human tumours more radiosensitive than others?, Radiother. Oncol. **15**, 63 (1989).

[72] B.G. Douglas and J.F. Fowler, The Effect of Multiple Small Doses of X Rays on Skin Reactions in the Mouse and a Basic Interpretation, Radiat. Res. **66**, 401 (1976).

[73] E.P. Malaise, B. Fertil, N. Chavaudra and M. Guichard, Distribution of radiation sensitivities for human tumor cells of specific histological types: comparison of in vitro to in vivo data, Int. J. Radiat. Oncol. Biol. Phys. **12**, 617 (1986).

[74] G. Kraft and M. Krämer, Linear energy transfer and track structure, Adv. Radiat. Biol. **17**, 1 (1993).

[75] A.M. Kellerer, Fundamentals of Microdosimetry, in: The Dosimetry of Ionizing Radiation Vol. 1, ed. K.R. Kase, B.E. Bjärngard and F.H. Attix (Academic Press, Orlando, 1985).

[76] D.T. Goodhead, Classical Approaches to Microdosimetry, with Example of Use in Radiation Protection, Medicine and Mechanistic Understanding, Radiat. Prot. Dosim. **166**, 1 (2015).

[77] J. Kiefer and H. Straaten, A model of ion track structure based on classical collision dynamics, Phys. Med. Biol. **31**, 1201 (1986).

[78] V. Michalik, Particle track structure and its correlation with radiobiological endpoint, Phys. Med. Biol. **36**, 1001 (1991).

[79] J. Kiefer, The physical basis for the biological action of heavy ions, New J. Phys. **10**, 075004 (2008).

[80] H.A. Bethe, Zur Theorie des Durchgangs schneller Korpuskularstrahlen durch Materie, Ann. Phys. **397**, 325 (1930).

[81] F. Bloch, Zur Bremsung rasch bewegter Teilchen beim Durchgang durch Materie, Ann. Phys. **408**, 285 (1933).

[82] T. Bortfeld and W. Schlegel, An analytical approximation of depth-dose distributions for therapeutic proton beams, Phys. Med. Biol. **41**, 1331 (1996).

[83] E. Rietzel, D. Schardt and T. Haberer, Range accuracy in carbon ion treatment planning based on CT-calibration with real tissue samples, Radiat. Oncol. **2**, 14 (2007).

[84] H. Geissel and C. Scheidenberger, Slowing down of relativistic heavy ions and new applications, Nucl. Instr. Meth. Phys. Res. B **136-138**, 114 (1998).

[85] C. Scheidenberger and H. Geissel, Penetration of relativistic heavy ions through matter, Nucl. Instr. Meth. Phys. Res. B **135**, 25 (1998).

[86] J. F. Ziegler, The Stopping of Energetic Light Ions in Elemental Matter, J. Appl. Phys. **85**, 1249 (1999)

[87] H. Geissel, H. Weick, C. Scheidenberger, R. Bimbot and D. Gardès, Experimental studies of heavy-ion slowing down in matter, Nucl. Instr. Meth. Phys. Res. B **195**, 3 (2002).

[88] D. Schardt and T. Elsässer, Heavy-ion tumor therapy: Physical and radiobiological benefits, Rev. Mod. Phys. **82**, 383 (2010).

[89] M. Krämer and G. Kraft, Calculations of Heavy Ion Track Structure, Radiat. Environ. Biophys. **33**, 91 (1994).

[90] M. Krämer, Calculation of heavy-ion track structure, Nucl. Instr. Meth. Phys. Res. B **105**, 14 (1995).

[91] M. Krämer and M. Durante, Ion beam transport calculations and treatment plans in particle therapy, Eur. J. Phys. D **60**, 195 (2010).

[92] C. Wälzlein, M. Krämer, E. Scifoni and M. Durante, Advancing the modeling in particle therapy: from track structure to treatment planning, Appl. Radiat. Isot. **83**, 171 (2014).

[93] A.M. Kellerer and D. Chmelevsky, Concepts of Microdosimetry. III. Mean Values of the Microdosimetric Distributions, Radiat. Environ. Biophys. **12**, 321 (1975).

[94] T. Elsässer and M. Scholz, Cluster Effects within the Local Effect Model, Radiat. Res. **167**, 319 (2007).

[95] T. Elsässer, R. Cunrath, M. Krämer and M. Scholz, Impact of track structure calculations on biological treatment planning in ion radiotherapy, New J. Phys. **10**, 075005 (2008).

[96] H. Nikjoo and L. Lindborg, RBE of low energy electrons and photons, Phys. Med. Biol. **55**, R65 (2010).

[97] D.T. Goodhead, J. Thacker and R. Cox, Is selective absorption of ultrasoft x-rays biologically important in mammalian cells?, Phys. Med. Biol. **26**, 1115 (1981).

[98] B. Winter, U. Hergenhahn, M. Faubel, O. Björneholm and I.V. Hertel, Hydrogen bonding in liquid water probed by resonant Auger-electron spectroscopy, J. Chem. Phys. **127**, 094501 (2007).

[99] T. Buch, E. Scifoni, M. Durante, M. Scholz and T. Friedrich, Modeling radiation effects of ultrasoft X-rays on the basis of amorphous track structure, manuscript in preparation (2016).

[100] D.T. Goodhead and H. Nikjoo, Track structure analysis of ultrasoft X-rays compared to high- and low-LET radiations, Int. J. Radiat. Biol. **55**, 513 (1989).

[101] H. Nikjoo and D.T. Goodhead, Track structure analysis illustrating the prominent role of low energy electrons in radiobiological effects of low-LET radiations, Phys. Med. Biol. **36**, 229 (1991).

[102] C.Z. Chen and D.E. Watt, Biophysical mechanism of radiation damage to mammalian cells by X- and γ-rays, Int. J. Radiat. Biol. **49**, 131 (1986).

[103] M. A. Hill, The Variation in Biological Effectiveness of X-Rays and Gamma Rays with Energy, Radiat. Prot. Dosim. **112**, 471 (2004).

[104] N. Hunter and C.R. Muirhead, Review of relative biological effectiveness dependence on linear energy transfer for low-LET radiations, J. Radiol. Prot. **29**, 5 (2009).

[105] M.R. Raju, S.G. Carpenter, J.J. Chmielewski, M.E. Schillaci, M.E. Wileder, J.P. Freyer, N.F. Johnson, P.L. Schor, R.J. Sebring and D.T. Goodhead, Radiobiology of ultrasoft x rays. I. Cultured hamster cells (V79), Radiat. Res. **110**, 396 (1987).

[106] M.E. Schillaci, S. Carpenter, M.R. Raju, R.J. Sebring, M.E. Wilder and D.T. Goodhead, Radiobiology of ultrasoft x rays. II. Cultured C3H mouse cells (10T1/2), Radiat. Res. **118**, 83 (1989).

[107] D.T. Goodhead and J. Thacker, Inactivation and mutation of cultured mammalian cells by aluminium characteristic ultrasoft X-rays. I. Properties of aluminium X-rays and preliminary experiments with Chinese hamster cells, Int. J. Radiat. Biol. **31**, 541 (1977).

[108] R. Cox, J. Thacker and D.T. Goodhead, Inactivation and mutation of cultured mammalian cells by aluminium characteristic ultrasoft X-rays. II. Dose-responses of Chinese hamster and human diploid cells to aluminium X-rays and radiations of different LET, Int. J. Radiat. Biol. **31**, 561 (1977).

[109] D.T. Goodhead, Inactivation and mutation of cultured mammalian cells by aluminium characteristic ultrasoft X-rays. III. Implications for theory of dual radiation action, Int. J. Radiat. Biol. **32**, 43 (1977).

[110] G. Felsenfeld and M. Groudine, Controlling the double helix, Nature **421**, 448 (2003).

[111] T. Misteli and E. Soutoglou, The emerging role of nuclear architecture in DNA repair and genome maintenance, Nat. Rev. Mol. Cell. Biol. **10**, 243 (2009).

[112] G. Kraft, Radiobiologic Effects of Very Heavy Ions: Inactivation, Induction of Chromosome Abberations and Strand Breaks, Nucl. Sci. Appl. **3**, 1 (1987).

[113] N.A.P. Franken, R. ten Cate, P.M. Krawczyk, J. Stap, J. Haveman, J. Aten and G.W. Barendsen, Comparison of RBE values of high- LET α-particles for the induction of DNA-DSBs, chromosome aberrations and cell reproductive death, Radiat. Oncol. **6**, 64 (2011).

[114] D.T. Goodhead, Mechanisms for the Biological Effectiveness of High-LET Radiations, J. Radiat. Res. **40S**, 1 (1999).

[115] IAEA, Relative Biological Effectiveness in Ion Beam Therapy, IAEA Report series 461 (IAEA, Vienna, 2008).

[116] C.X. Yu and G. Tang, Intensity-modulated arc therapy: principles, technologies and clinical implementation, Phys. Med. Biol. **56**, R31 (2011).

[117] M. Teoh, C.H. Clark, K. Wood, S. Whitaker and A. Nisbet, Volumetric modulated arc therapy: a review of current literature and clinical use in practice, Br. J. Radiol. **84**, 967 (2011).

[118] C.K. McGarry, K.T. Butterworth, C. Trainor, J.M. O'Sullivan, K.M. Prise and A.R. Hounsell, Temporal characterization and in vitro comparison of cell survival following the delivery of 3D-conformal, intensity-modulated radiation therapy (IMRT) and volumetric modulated arc therapy (VMAT), Phys. Med. Biol. **56**, 2445 (2011).

[119] R.R. Wilson, Radiological use of fast protons, Radiology **47**, 487 (1946).

[120] J.H. Lawrence, C.A. Tobias, J.L. Born, R.K. McCombs, J.E. Roberts, H. Anger, B.V. Low-Beer and C.B. Huggins, Pituitary irradiation with high-energy proton beams: a preliminary report, Cancer Res. **18** 121 (1958).

[121] R. Grün, T. Friedrich, M. Krämer, K. Zink, M. Durante, R. Engenhart-Cabillic and M. Scholz, Assessment of potential advantages of relevant ions for particle therapy: A model based study, Med. Phys. **42**, 1037 (2015).

[122] L. Burigo, I. Pshenichnov, I. Mishustin and M. Bleicher, Comparative study of dose distributions and cell survival fractions for ^{1}H, ^{4}He, ^{12}C and ^{16}O beams using Geant4 and Microdosimetric Kinetic model, Phys. Med. Biol. **60** , 3313 (2015).

[123] E. Scifoni, W. Tinganelli, W.K. Weyrather, M. Durante, A. Maier and M. Krämer, Including oxygen enhancement ratio in ion beam treatment planning: model implementation and experimental verification, Phys. Med. Biol. **58**, 3871 (2013).

[124] F. Tommasino, E. Scifoni and M. Durante, New Ions for Therapy, Int. J. Particle Ther., ahead of print (2016).

[125] H. Tsujii, T. Kamada, M. Baba, H. Tsuji, H. Kato, S. Kato, S. Yamada, S. Yasuda, T. Yanagi, H. Kato, R. Hara, N. Yamamoto and J. Mizoe, Clinical advantages of carbon-ion radiotherapy, New J. Phys. **10**, 075009 (2008).

[126] H. Tsujii and T. Kamada, A Review of Update Clinical Results of Carbon Ion Radiotherapy, Jpn. J. Clin. Oncol. **42**, 670 (2012).

[127] T. Ohno, Particle radiotherapy with carbon ion beams, EPMA J. **4**, 9 (2013).

[128] M. Uhl, M. Mattke, T. Welzel, F. Roeder, J. Oelmann, G. Habl, A. Jensen, M. Ellerbrock, O. Jäkel, T. Haberer, K. Herfarth and J. Debus, Highly Effective Treatment of Skull Base Chordoma With Carbon Ion Irradiation Using a Raster Scan Technique in 155 Patients: First Long-Term Results, Cancer **120**, 3410 (2014).

[129] M. Durante and J.S. Loeffler, Charged particles in radiation oncology, Nat. Rev. Clin. Oncol. **7**, 37 (2010).

[130] H. Suit, T. DeLaney, S. Goldberg, H. Paganetti, B. Clasie, L. Gerweck, A. Niemierko, E. Hall, J. Flanz, J. Hallman and A. Trofimov, Proton vs carbon ion beams in the definitive radiation treatment of cancer patients, Radiother. Oncol. **95** 3, (2010).

[131] E. Fokas, G. Kraft, H. An and R. Engenhart-Cabillic, Ion beam radiobiology and cancer: Time to update ourselves, Bioch. Biophys. Acta **1796**, 216 (2009).

[132] C. Bert and M. Durante, Motion in radiotherapy: particle therapy, Phys. Med. Biol. **56**, R113 (2011).

[133] D. Schardt, I. Schall, H. Geissel, H. Irnich, G. Kraft, A. Magel, M.F. Mohar, G. Münzenberg, F. Nickel, C. Scheidenberger, W. Schwab and L. Sihver, Nuclear fragmentation of high-energy heavy-ion beams in water, Adv. Space Res. **17**, 87 (1996)

[134] K. Gunzert-Marx, H. Iwase, D. Schardt and R.S. Simon, Secondary beam fragments produced by 200 MeV u^{-1} ^{12}C ions in water and their dose contributions in carbon ion radiotherapy, New J. Phys. **10**, 075003 (2008).

[135] R. Kaderka, D. Schardt, M. Durante, T. Berger, U. Ramm, J. Licher and C. La Tessa, Out-of-field dose measurements in a water phantom using different radiotherapy modalities, Phys. Med. Biol. **57**, 5059 (2012).

[136] C. La Tessa, T. Berger, R. Kaderka, D. Schardt, S. Burmeister, J. Labrenz, G. Reitz and M. Durante, Characterization of the secondary neutron field produced during treatment of an anthropomorphic phantom with x-rays, protons and carbon ions, Phys. Med. Biol. **59**, 2111 (2014).

[137] W.D. Newhauser, J.D. Fontenot, A. Mahajan, D. Kornguth, M. Stovall, Y. Zheng, P.J. Taddei, D. Mirkovic, R. Mohan, J.D. Cox and S. Woo, The risk of developing a second cancer after receiving craniospinal proton irradiation, Phys. Med. Biol. **54**, 2277 (2009).

[138] W.D. Newhauser and R. Zhang, The physics of proton therapy, Phys. Med. Biol. **60**, R155 (2015).

[139] M. Scholz, A.M. Kellerer, W. Kraft-Weyrather and G. Kraft, Computation of cell survival in heavy ion beams for therapy. The model and its approximation, Radiat. Environ. Biophys. **36**, 59 (1997).

[140] M. Krämer and M. Scholz, Treatment planning for heavy-ion radiotherapy: calculation and optimization of biologically effective dose, Phys. Med. Biol. **45**, 3319 (2000).

[141] M. Krämer and M. Scholz, Rapid calculation of biological effects in ion radiotherapy, Phys. Med. Biol. **51**, 1959 (2006).

[142] R.B. Hawkins, A Statistical Theory of Cell Killing by Radiation of Varying Linear Energy Transfer, Radiat. Res. **140**, 366 (1994).

[143] T. Kanai, M. Endo, S. Minohara, N. Miyahara, H. Koyama-Ito, H. Tomura, N. Matsufuji, Y. Futami, A. Fukumura, T. Hiraoka, Y. Furusawa, K. Ando, M. Suzuki, F. Soga and K. Kawachi, Biophysical Characteristics of HIMAC Clinical Irradiation System for Heavy-Ion Radiation Therapy, Int. J. Radiat. Oncol. Biol. Phys. **44**, 201 (1999).

[144] T. Kanai, N. Matsufuji, T. Miyamoto, J. Mizoe, T. Kamada, H. Tsuji, H. Kato, M. Baba and H. Tsujii, Examination of GyE System for HIMAC Carbon Therapy, Int. J. Radiat. Oncol. Biol. Phys. **64**, 650 (2006).

[145] T. Inaniwa, T. Furukawa, Y. Kase, N. Matsufuji, T. Toshito, Y. Matsumoto, Y. Furusawa and K. Noda, Treatment planning for a scanned carbon beam with a modified microdosimetric kinetic model, Phys. Med. Biol. **55**, 6721 (2010).

[146] T. Inaniwa, N. Kanematsu, N. Matsufuji, T. Kanai, T. Shirai, K. Noda, H. Tsuji, T. Kamada and Hirohiko Tsujii, Reformulation of a clinical-dose system for carbon-ion radiotherapy treatment planning at the National Institute of Radiological Sciences, Japan, Phys. Med. Biol. **60**, 3271 (2015).

[147] A. van der Schaaf, J.A. Langendijk, C. Fiorino and T. Rancati, Embracing Phenomenological Approaches to Normal Tissue Complication Probability Modeling: A Question of Method, Int. J. Radiat. Oncol. Biol. Phys. **91**, 468 (2015).

[148] D.E. Lea, Actions of Radiations on Living Cells (Cambridge: Cambridge University Press, 1946).

[149] M.A. Bender and P.C. Gooch, The kinetics of X-ray survival of mammalian cells in vitro, Int. J. Rad. Biol. **5**, 133 (1962).

[150] W. Sinclair, The shape of radiation survival curves of mammalian cells cultured in vitro, in: Biophysical aspects of radiation quality. IAEA, Technical report series **58** (IAEA, Vienna, 1966).

[151] J.J. Butts and R. Katz, Theory of RBE for heavy ion bombardment of dry enzymes and viruses, Radiat. Res. **30**, 855 (1967).

[152] A. Kappos and W. Pohlit, A cybernetic model for radiation reactions in living cells. I. Sparsely-ionizing radiations; stationary cells, Int. J. Radiat. Biol. **22**, 51 (1972).

[153] A.M. Kellerer and H.H. Rossi, The Theory of Dual Radiation Action, Curr. Topics Radiat. Res. Quarterly **8**, 85 (1972).

[154] K.H. Chadwick and H.P. Leenhouts, A Molecular Theory of Cell Survival, Phys. Med. Biol. **18**, 78 (1973).

[155] W. Pohlit and I.R. Heyder, The Shape of Dose-Survival Curves for Mammalian Cells and Repair of Potentially Lethal Damage Analyzed by Hypertonic Treatment, Radiat. Res. **87**, 613 (1981).

[156] D. Harder and P. Virsik-Peuckert, Kinetics of cell survival as predicted by the repair/interaction model, Br. J. Cancer **49**, 243 (1984).

[157] T. Alper, Implications of repair models for LET effects and other radiobiological phenomena, Br. J. Cancer **49**, 137 (1984).

[158] H.D. Thames, An 'incomplete-repair' model for survival after fractionated and continuous irradiations, Int. J. Radiat. Biol. **47**, 319 (1985).

[159] D.T. Goodhead, Saturable Repair Models of Radiation Action in Mammalian Cells, Radiat. Res. **104**, S58 (1985).

[160] S.B. Curtis, Lethal and Potentially Lethal Lesions Induced by Radiation - A Unified Repair Model, Radiat. Res. **106**, 252 (1986).

[161] M. Scholz and G. Kraft, A parameter-free track structure model for heavy ion action cross sections, in: Biophysical Modelling of Radiation Effects, ed. K.H. Chadwick, G. Moschini and M.N. Varma (Adam Hilger, Bristol, 1992).

[162] R. D. Stewart, Two-Lesion Kinetic Model of Double-Strand Break Rejoining and Cell Killing, Radiat. Res. **156**, 365 (2001).

[163] B.K. Lind, L.M. Persson, M.R. Edgren, I. Hedlöf and A. Brahme, Repairable-Conditionally Repairable Damage Model Based on Dual Poisson Processes, Radiat. Res. **160**, 366 (2003).

[164] M. Wedenberg, B. K. Lind, I. Toma-Daşu, H. Rehbinder and A. Brahme, Analytical Description of the LET Dependence of Cell Survival Using the Repairable-Conditionally Repairable Damage Model, Radiat. Res. **174**, 517 (2010).

[165] M. Guerrero and X.A. Li, Extending the linear-quadratic model for large fraction doses pertinent to stereotactic radiotherapy, Phys. Med. Biol. **49**, 4825 (2004).

[166] P. Kundrát, M. Lokajíček and H. Hromčíková, Probabilistic two-stage model of cell inactivation by ionizing particles, Phys. Med. Biol. **50**, 1433 (2005).

[167] J.C. Sutherland, Repair dependent radiation survival: a stochastic model with Euler gamma function solutions, Phys. Med. Biol. **51**, 4883 (2006).

[168] D.J. Carlson, R.D. Stewart, V.A. Semenenko and G.A. Sandisona, Combined Use of Monte Carlo DNA Damage Simulations and Deterministic Repair Models to Examine Putative Mechanisms of Cell Killing, Radiat. Res. **169**, 447 (2008).

[169] C. Park, L. Papiez, S. Zhang, M. Story and R.D. Timmerman, Universal Survival Curve and Single Fraction Dose: Useful Tools in Understanding Potency of Ablative Radiotherapy, Int. J. Radiat. Oncol. Biol. Phys. **70**, 847 (2008).

[170] J.Z. Wang, Z. Huang, S.S. Lo, W.T.C. Yuh and N.A. Mayr, A Generalized Linear-Quadratic Model for Radiosurgery, Stereotactic Body Radiation Therapy, and High-Dose Rate Brachytherapy, Sci. Transl. Med. **2**, 39ra48 (2010).

[171] F. Ballarini, S. Altieri, S. Bortolussi, E. Giroletti and N. Protti, A Model of Radiation-Induced Cell Killing: Insights into Mechanisms and Applications for Hadron Therapy, Radiat. Res. **180**, 307 (2013).

[172] J. Besserer and U. Schneider, Track-event theory of cell survival with second-order repair, Radiat. Environ. Biophys. **54**, 167 (2015).

[173] H.H. Rossi, Elements of Microdosimetry, Med. Phys. **18**, 1085 (1991).

[174] R.B. Hawkins, A microdosimetric-kinetic theory of the dependence of the RBE for cell death on LET, Med. Phys. **25**, 1157 (1998).

[175] V. Conte, P. Colautti, B. Grosswendt, D. Moro and L. De Nardo, Track structure of light ions: experiments and simulations, New J. Phys. **14**, 093010 (2012).

[176] B. Grosswendt, V. Conte and P. Colautti, An upgraded track structure model: experimental validation, Radiat. Prot. Dosim., **161**, 464 (2014).

[177] H. Nikjoo, S. Uehara, D. Emfietzoglou and F.A. Cucinotta, Track-structure codes in radiation research, Radiat. Meas. **41**, 1052 (2006).

[178] H. Nikjoo, S. Uehara, W.E. Wilson, M. Hoshi and D.T. Goodhead, Track structure in radiation biology: theory and applications, Int. J. Radiat. Biol. **73**, 355 (1998).

[179] W. Friedland, M. Dingfelder, P. Kundrát and P. Jacob, Track structures, DNA targets and radiation effects in the biophysical Monte Carlo simulation code PARTRAC, Mutat. Res. **711**, 28 (2011).

[180] I. Plante, A.L. Ponomarev and F.A. Cucinotta, Calculation of the energy deposition in nanovolumes by protons and HZE particles: geometric patterns of initial distributions of DNA repair foci, Phys. Med. Biol. **58**, 6393 (2013).

[181] C. Villagrasa, M. Dos Santos, D. Bianco, G. Gruel, J. F. Barquinero and I. Clairand, RBE-LET Relationship for Proton and Alpha Irradiations Studied with a Nanodosimetric Approach, Radiat. Prot. Dosim. **161**, 449 (2014).

[182] R. Katz, Track structure theory in radiobiology and in radiation detection, Nucl. Track Detect. **2**, 1 (1978).

[183] M.P.R. Waligorski, G.L. Sinclair and R. Katz, Radiosensitivity Parameters for Neoplastic Transformations in C3H10T1/2 Cells, Radiat. Res. **111**, 424 (1987).

[184] M. Scholz and G. Kraft, Track structure and the calculation of biological effects of heavy charged particles, Adv. Space Res. **18**, 5 (1996).

[185] T. Elsässer, W.K. Weyrather, T. Friedrich, M. Durante, G. Iancu, M. Krämer, G. Kragl, S. Brons, M. Winter, K.J. Weber and M. Scholz, Quantification of the Relative Biological Effectiveness for Ion Beam Therapy: Direct Experimental Comparison of Proton and Carbon Ion Beams and a Novel Approach for Treatment Planning, Int. J. Radiat. Oncol. Biol. Phys. **78**, 1177 (2010).

[186] J.F. Fowler and B.E. Stern, Dose-rate effects: some theoretical and practical considerations, Br. J. Radiol. **33**, 389 (1960).

[187] M. Wada, M. Suzuki, C. Liu, Y. Kaneko, S. Fukudai, K. Ando and N. Matsufuji, Modeling the biological response of normal human cells, including repair processes, to fractionated carbon beam irradiation, J. Radiat. Res. **54**, 798 (2013).

[188] M.N. Cornforth and J.S. Bedford, A Quantitative Comparison of Potentially Lethal Damage Repair and the Rejoining of Interphase Chromosome Breaks in Low Passage Normal Human Fibroblasts, Radiat. Res. **111**, 385 (1987).

[189] D.J. Brenner, The linear-quadratic model is an appropriate methodology for determining isoeffective doses at large doses per fraction, Semin. Radiat. Oncol. **18**, 234 (2008).

[190] L.M. Garcia, J. Leblanc, D. Wilkins and G.P. Raaphorst, Fitting the linear-quadratic model to detailed data sets for different dose ranges, Phys. Med. Biol. **51**, 2813 (2006).

[191] L.M. Garcia, D.E. Wilkins and G.P. Raaphorst, α/β Ratio: A Dose Range Dependence Study, Int. J. Radiat. Oncol. Biol. Phys. **67**, 587 (2007).

[192] M. Astrahan, Some implications of linear-quadratic-linear radiation dose-response with regard to hypofractionation, Med. Phys. **35**, 4161 (2008).

[193] C. Greco C, M.J. Zelefsky, M. Lovelock, Z. Fuks, M. Hunt, K. Rosenzweig, J. Zatcky, B. Kim and Y. Yamada, Predictors of local control after single-dose stereotactic image-guided intensity-modulated radiotherapy for extracranial metastases, Int. J. Radiat. Oncol. Biol. Phys. **79**, 1151 (2011).

[194] B. Andisheh, M. Edgren, D. Belkić, P. Mavroidis, A. Brahme and B.K. Lind, A Comparative Analysis of Radiobiological Models for Cell Surviving Fractions at High Doses, Technol. Cancer Res. Treatm. **12**, 183 (2013).

[195] T. Sheu, J. Molkentine, M.K. Transtrum, T.A. Buchholz, H.R. Withers, H.D. Thames and K.A. Mason, Use of the LQ model with large fraction sizes results in underestimation of isoeffect doses, Radiother. Oncol. **109**, 21 (2013).

[196] F.W. McKenna and S. Ahmad, Fitting techniques of cell survival curves in high-dose region for use in stereotactic body radiation therapy, Phys. Med. Biol. **54**, 1593 (2009).

[197] J.P. Kirkpatrick, D.J. Brenner and C.G. Orton, Point/Counterpoint: The linear-quadratic model is inappropriate to model high dose per fraction effects in radiosurgery, Med. Phys. **36**, 3381 (2009).

[198] I. Shuryak, D.J. Carlson, J.M. Brown and D.J. Brenner, High-dose and fractionation effects in stereotactic radiation therapy: Analysis of tumor control data from 2965 patients, Radiother. and Oncol. **115**, 327 (2015).

[199] Z. Fuks and R. Kolesnick, Engaging the vascular component of the tumor response, Cancer Cell **8**, 89 (2005).

[200] J.M. Brown, D.J. Brenner and D.J. Carlson, Dose escalation, not "new biology," can account for the efficacy of stereotactic body radiation therapy with non-small cell lung cancer, Int. J. Radiat. Oncol. Biol. Phys. **85**, 1159 (2013).

[201] S. Girdhani, R. Sachs and L. Hlatky, Biological effects of proton radiation: What we know and don't know, Radiat. Res. **179**, 257 (2013).

[202] S.H. Benedict, K.M. Yenice, D. Followill, J.M. Galvin, W. Hinson, B. Kavanagh, P. Keall, M. Lovelock, S. Meeks, L. Papiez, T. Purdie, R. Sadagopan, M.C. Schell, B. Salter, D.J. Schlesinger, A.S. Shiu, T. Solberg, D.Y. Song, V. Stieber, R. Timmerman, W.A. Tomé, D. Verellen, L. Wang and F.F. Yin, Stereotactic body radiation therapy: The report of AAPM Task Group 101, Med. Phys. **37**, 4078 (2010).

[203] J.P. Kirkpatrick, C.R. Kelsey, M. Palta, A.R. Cabrera, J.K. Salama, P. Patel, B.A. Perez, J. Lee and F.F. Yin, Stereotactic Body Radiotherapy: A Critical Review for Non-Radiation Oncologists, Cancer. **120**, 942 (2014).

[204] H. Nikjoo, P. O'Neill, W.E. Wilson and D. T. Goodhead, Computational Approach for Determining the Spectrum of DNA Damage Induced by Ionizing Radiation, Radiat. Res. **156**, 577 (2001).

[205] J.F. Ward, Biochemistry of DNA Lesions, Radiat. Res. **104**, S103 (1985).

[206] J.F. Ward, The complexity of DNA damage: relevance to biological consequences, Int. J. Radiat. Biol. **66**, 427 (1994).

[207] B. Rydberg, Clusters of DNA Damage Induced by Ionizing Radiation: Formation of Short DNA Fragments. II. Experimental Detection, Radiat. Res. **145**, 200 (1996).

[208] P.J. Johnston, S.H. MacPhail, J.P. Banáth and P.L. Olive, Higher-Order Chromatin Structure-Dependent Repair of DNA Double-Strand Breaks: Factors Affecting Elution of DNA from Nucleoids, Radiat. Res. **149**, 533 (1998).

[209] Y. Nishino, M. Eltsov, Y. Joti, K. Ito, H. Takata, Y. Takahashi, S. Hihara, A.S. Frangakis, N. Imamoto, T. Ishikawa and K. Maeshima, Human mitotic chromosomes consist predominantly of irregularly folded nucleosome fibres without a 30-nm chromatin structure, EMBO J. **31**, 1644 (2012).

[210] E. Fussner, M. Strauss, U. Djuric, R. Li, K. Ahmed, M. Hart, J. Ellis and D.P. Bazett-Jones, Open and closed domains in the mouse genome are configured as 10-nm chromatin fibres, EMBO reports **13**, 992 (2012).

[211] T. Friedrich, M. Durante and M. Scholz, Simulation of DSB Yield for High LET Radiation, Radiat. Prot. Dosim. **166**, 61 (2015).

[212] C. Hartel, A. Nikoghosyan, M. Durante, S. Sommer, E. Nasonova, C. Fournier, R. Lee, J. Debus, D. Schulz-Ertner and S. Ritter, Chromosomal aberrations in peripheral blood lymphocytes of prostate cancer patients treated with IMRT and carbon ions, Radiother. Oncol. **95**, 73 (2010).

[213] H. Yokota, G. van den Engh, J.E. Hearst, R.K. Sachs and B.J. Trask, Evidence for the Organization of Chromatin in Megabase Pair-sized Loops Arranged along a Random Walk Path in the Human G0/G1 Interphase Nucleus, J. Cell Biol. **130**, 1239 (1995).

[214] J. Ostashevsky, A Polymer Model for the Structural Organization of Chromatin Loops and Minibands in Interphase Chromosomes, Mol. Biol. Cell **9**, 3031 (1998).

[215] G. Erzgräber, M. Rosemann, K. Regel and H. Abel, DNA Structures and Radiation Injury, Adv. Space Res. **12**, 91 (1992).

[216] K. Regel, K. Günther and G. Kampf, Evidence for Existence and Compactness of DNA Superstructure Units in Mammalian Cells: a Microdosimetric Approach to Radiation-Induced DNA Release Assayed by Neutral Sucrose Gradient Sedimentation, Radiat. Environ. Biophys. **21**, 175 (1983).

[217] M. Löbrich, B. Rydberg and P.K. Cooper, Repair of x-ray-induced DNA double-strand breaks in specific Not I restriction fragments in human fibroblasts: Joining of correct and incorrect ends, Proc. Nat. Acad. Sci. **92**, 12050 (1995).

[218] E. Lieberman-Aiden, N.L. van Berkum, L. Williams, M. Imakaev, T. Ragoczy, A. Telling, I. Amit, B.R. Lajoie, P.J. Sabo, M.O. Dorschner, R. Sandstrom, B. Bernstein, M.A. Bender, M. Groudine, A. Gnirke, J. Stamatoyannopoulos, L.A. Mirny, E.S. Lander and J. Dekker, Comprehensive mapping of long range interactions reveals folding principles of the human genome, Science **326**, 289 (2009).

[219] V. Ea, M.O. Baudement, A. Lesne and T. Forné, Contribution of Topological Domains and Loop Formation to 3D Chromatin Organization, Genes **6**, 734 (2015).

[220] S.V. Costes, A. Boissière, S. Ravani, R. Romano, B. Parvin and M.H. Barcellos-Hoff, Imaging Features that Discriminate between Foci Induced by High- and Low-LET Radiation in Human Fibroblasts, Radiat. Res. **165**, 505 (2006).

[221] R.K. Sachs, G. van den Engh, B. Trask, H. Yokota and J.E. Hearst, A random-walk/giant-loop model for interphase chromosomes, Proc. Nat. Acad. Sci. **92**, 2710 (1995).

[222] J. Mateos-Langerak, M. Bohn, W. de Leeuw, O. Giromus, E.M.M. Manders, P.J. Verschure, M.H.G. Indemans, H.J. Gierman, D.W. Heermann, R. van Driel and S. Goetze, Spatially confined folding of chromatin in the interphase nucleus, Proc. Nat. Acad. Sci. **106**, 3812.

[223] A.L. Ponomarev and F.A. Cucinotta, Chromatin loops are responsible for higher counts of small DNA fragments induced by high-LET radiation, while chromosomal domains do not affect the fragment sizes, Int. J. Radiat. Biol. **82**, 293 (2006).

[224] M. Bohn and D.W. Heermann, Diffusion-Driven Looping Provides a Consistent Framework for Chromatin Organization, PLoS One **5**, e12218 (2010).

[225] P.M. Diesinger, S. Kunkel, J. Langowski and D.W. Heermann, Histone Depletion Facilitates Chromatin Loops on the Kilobasepair Scale, Biophys. J. **99**, 2995 (2010).

[226] D.A. Jackson, P. Dickinson and P.R. Cook, The size of chromatin loops in HeLa cells, EMBO J. **9**, 567 (1990).

[227] C. Münkel, R. Eils, S. Dietzel, D. Zink, C. Mehring, G. Wedemann, T. Cremer and J. Langowski, Compartmentalization of Interphase Chromosomes Observed in Simulation and Experiment, J. Mol. Biol. **285**, 1053 (1999).

[228] T. Elsässer, M. Krämer and M. Scholz, Accuracy of the Local Effect Model for the Prediction of Biologic Effects of Carbon Ion Beams in Vitro and in Vivo, Int. J. Radiat. Oncol. Biol. Phys. **71**, 866 (2008).

[229] T. Elsässer and M. Scholz, improvement of the Local Effect Model (LEM) - Implications of Clustered DNA Damage, Radiat. Prot. Dosim. **122**, 475 (2006).

[230] J. Mirsch, F. Tommasino, A. Frohns, S. Conrad, M. Durante, M. Scholz, T. Friedrich and M. Löbrich, Direct measurement of the 3-dimensional DNA lesion distribution induced by energetic charged particles in a mouse model tissue, Proc. Nat. Acad. Sci. **112**, 12396 (2015).

[231] L. Herr, T. Friedrich, M. Durante and M. Scholz, Investigation of time-dose relationships in the cellular response to ion irradiation with the Local Effect Model, manuscript in preparation.

[232] F. Tommasino, T. Friedrich, U. Scholz, G. Taucher-Scholz, M. Durante and M. Scholz, A DNA Double-Strand Break Kinetic Rejoining Model Based on the Local Effect Model, Radiat. Res. **180**, 524 (2013).

[233] F. Tommasino, T. Friedrich, U. Scholz, G. Taucher-Scholz, M. Durante and M. Scholz, Application of the Local Effect Model to Predict DNA Double-Strand Break Rejoining after Phtonon and High-LET Irradiation, Radiat. Prot. Dosim. **166**, 66 (2015).

[234] T.E. Schmid, C. Greubel, V. Hable, O. Zlobinskaya, D. Michalski, S. Girst, C. Siebenwirth, E. Schmid, M. Molls, G. Multhoff and G. Dollinger, Low LET protons focused to submicrometer shows enhanced radiobiological effectiveness, Phys. Med. Biol. **57**, 5889 (2012).

[235] M. Saager, C. Glowa, P. Peschke, S. Brons, R. Grün, M. Scholz, P.E. Huber, J. Debus and C. Karger, Split dose carbon ion irradiation of the rat spinal cord: Dependence of the relative biological effectiveness on dose and linear energy transfer, Radiother. Oncol. **117**, 358 (2015).

[236] R. Grün, T. Friedrich, T. Elsässer, M. Krämer, K. Zink, C.P. Karger, M. Durante, R. Engenhart-Cabillic and M. Scholz, Impact of enhancements in the local effect model (LEM) on the predicted RBE-weighted target dose distribution in carbon ion therapy, Phys. Med. Biol. **57** 7261 (2012).

[237] C. Gillmann, O. Jäkel, I. Schlampp and C.P. Karger, Temporal Lobe Reactions After Carbon Ion Radiation Therapy: Comparison of Relative Biological Effectivenesse Weighted Tolerance Doses Predicted by Local Effect Models I and IV, Int. J. Radiat. Oncol. Biol. Phys. **88**, 1136 (2014).

[238] O. Steinsträter, R. Grün, U. Scholz, T. Friedrich, M. Durante and M. Scholz, Mapping of RBE-Weighted Doses Between HIMAC- and LEM-Based Treatment Planning Systems for Carbon Ion Therapy, Int. J. Radiat. Oncol. Biol. Phys. **84**, 854 (2012).

[239] P. Fossati, S. Molinelli, N. Matsufuji, M. Ciocca, A. Mirandola, A. Mairani, J. Mizoe, A. Hasegawa, R. Imai, T. Kamada, R. Orecchia and Hirohiko Tsujii, Dose prescription in carbon ion radiotherapy: a planning study to compare NIRS and LEM approaches with a clinically-oriented strategy, Phys. Med. Biol. **57**, 7543 (2012).

[240] T. Friedrich, U. Scholz, M. Durante and M. Scholz, RBE of ion beams in hypofractionated radiotherapy (SBRT), Phys. Med. **30**, 588 (2014).

[241] International Commission on Radiation Units and Measurements, ICRU Report 78: Prescribing, Recording, and Reporting Proton-Beam Therapy, J. ICRU **7**, 1.

[242] R. Grün, T. Friedrich, M. Krämer, K. Zink, M. Durante, R. Engenhart-Cabillic and M. Scholz, Physical and biological factors determining the effective proton range, Med. Phys. **40**, 111716 (2013).

[243] M. Krämer, O. Jäkel, T. Haberer, G. Kraft, D. Schardt and U. Weber, Treatment planning for heavy-ion radiotherapy: physical beam model and dose optimization, Phys. Med. Biol. **45**, 3299 (2000).

[244] O. Steinsträter, U. Scholz, T. Friedrich, M. Krämer, R. Grün, M. Durante and M. Scholz, Integration of a model-independent interface for RBE predictions in a treatment planning system for active particle beam scanning, Phys. Med. Biol. **60**, 6811 (2015).

[245] J.G. Eley, T. Friedrich, K.L. Homann, R.M. Howell, M. Scholz, M. Durante and W.D. Newhauser, Comparative Risk Predictions of Second Cancers after Carbon-Ion Therapy versus Proton Therapy, manuscript submitted to Int. J. Radiat. Oncol. Biol. Phys. (2015).

[246] J. Wölfelschneider, T. Friedrich, R. Lüchtenborg, K. Zink, M. Scholz, L. Dong, M. Durante and C. Bert, Impact of fractionation and number of fields on dose homogeneity for intrafractionally moving lung tumors using scanned carbon ion treatment, Radiother. Oncol., ahead of print (2016).

[247] W.K. Weyrather, S. Ritter, M. Scholz and G. Kraft, RBE for carbon track-segment irradiation in cell lines of differing repair capacity, Int. J. Radiat. Biol **75**, 1357 (1999).

[248] F. Tommasino, T. Friedrich, B. Jakob, B. Meyer, M. Durante and M. Scholz, Induction and Processing of the Radiation-Induced Gamma-H2AX Signal and its Link to the Underlying Pattern of DSB: A Combined Experimental and Modelling Study, PLoS One **10**, e0129416 (2015).

[249] L. Herr, T. Friedrich, M. Durante and M. Scholz, A Model of Photon Cell Killing Based on the Spatio-Temporal Clustering of DNA Damage in Higher Order Chromatin Structures, PLoS One **9**, e83923 (2014).

[250] L. Herr, T. Friedrich, M. Durante and M. Scholz, Sensitivity of the Giant LOop Binary LEsion (GLOBLE) cell survival model on parameters characterising dose rate effects, Radiat. Prot. Dosim. **166**, 55 (2015).

[251] A. Hufnagl, L. Herr, T. Friedrich, M. Durante, G. Taucher-Scholz and M. Scholz, The link between cell-cycle dependent radiosensitivity and repairpathways: A model based on the local, sister-chromatid conformation dependent switch between NHEJ and HR, DNA Repair **27**, 28 (2015).

[252] E.J. Hall, R.P. Bird, H.H. Rossi, R. Coffey, J. Varga and Y.M. Lam, Biophysical Studies with High-Energy Argon Ions. 2. Determinations of the Relative Biological Effectiveness, the Oxygen Enhancement Ratio, and the Cell Cycle Response, Radiat. Res. **70**, 469 (1977).

[253] H.D. Thames, M.E. Rozell, S.L. Tucker, K.K. Ang, D.R. Fisher and E.L. Travis, Direct analysis of quantal radiation response data, Int. J. Radiat. Biol. **49**, 999 (1986).

[254] R.W. de Boer, The use of the D vs dD plot to estimate the α/β ratio from iso-effect radiation damage data, Radiother. Oncol. **11**, 361 (1988).

[255] A.M. Kellerer, Error bands for the linear-quadratic dose-effect relation, Radiat. Environ. Biophys. **42**, 77 (2003).

[256] H. Paganetti, Range uncertainties in proton therapy and the role of Monte Carlo simulations, Phys. Med. Biol. **57**, R99 (2012).

[257] H. Paganetti, Relative biological effectiveness (RBE) values for proton beam therapy. Variations as a function of biological endpoint, dose, and linear energy transfer, Phys. Med. Biol. **59** R419 (2014).

[258] A. Carabe, M. Moteabbed, N. Depauw, J. Schuemann and H. Paganetti, Range uncertainty in proton therapy due to variable biological effectiveness, Phys. Med. Biol. **57**, 1159 (2012).

[259] H. Paganetti, Relating Proton Treatments to Photon Treatments via the Relative Biological Effectiveness - Should We Revise Current Clinical Practice?, Int. J. Radiat. Oncol. Biol. Phys. **91**, 892 (2015).

[260] International Commission on Radiation Units and Measurements, ICRU Report 24: Determination of absorbed dose in a patient irradiated by beams of x- or gamma-rays in radiotherapy procedures (International Commission on Radiation Units and Measurement, Bethesda, MD, 1976).

[261] D.J. Brenner, L.R. Hlatky, P.J. Hahnfeldt, E.J. Hall and R.K. Sachs, A convenient extension of the linear-quadratic model to include redistribution and reoxygenation, Int. J. Radiat. Oncol. Biol. Phys. **32**, 379 (1995).

[262] A. Vral, H. Thierens, A. Baeyens and L. De Ridder, Chromosomal aberrations and in vitro radiosensitivity: intra-individual versus inter-individual variability, Toxic. Lett. **149**, 345 (2004).

[263] M. Scholz, N. Matsufuji and T. Kanai, Test of the local effect model using clinical data: tumour control probability for lung tumours after treatment with carbon ion beams, Radiat. Prot. Dosim. **122**, 478 (2006).

[264] T.T. Böhlen, S. Brons, M. Dosanjh, A. Ferrari, P. Fossati, T. Haberer, V. Patera and A. Mairani, Investigating the robustness of ion beam therapy treatment plans to uncertainties in biological treatment parameters, Phys. Med. Biol. **57**, 7983 (2012).

[265] M.A. Chanrion, W. Sauerwein, U. Jelen, A. Wittig, R. Engenhart-Cabillic and M. Beuve, The influence of the local effect model parameters on the prediction of the tumor control probability for prostate cancer, Phys. Med. Biol. **59**, 3019 (2014).

[266] N. Bassler, O. Jäkel, C.S. Søndergaard and J.B. Petersen, Dose- and LET-painting with particle therapy, Acta Oncol. **29**, 1170 (2010).

[267] D. Giantsoudi, C. Grassberger, D. Craft, A. Niemierko, A. Trofimov and H. Paganetti, Linear Energy Transfer-Guided Optimization in Intensity Modulated Proton Therapy: Feasibility Study and Clinical Potential, Int. J. Radiat. Oncol. Biol. Phys. **87**, 216 (2013).

[268] M. Fager, I. Toma-Dasu, M. Kirk, D. Dolney, E.S. Diffenderfer, N. Vapiwala and A. Carabe, Linear Energy Transfer Painting With Proton Therapy: A Means of Reducing Radiation Doses With Equivalent Clinical Effectiveness, Int. J. Radiat. Oncol. Biol. Phys. **91**, 1057 (2015).

[269] C.P. South, M. Partridge and P.M. Evans, A theoretical framework for prescribing radiotherapy dose distributions using patient-specific biological information, Med. Phys. **35**, 4599 (2008).

[270] F. Kamp, S. Brüningk, G. Cabal, A. Mairani, K. Parodi and J.J. Wilkens, Variance-based sensitivity analysis of biological uncertainties in carbon ion therapy, Phys. Med. **30**, 583 (2014).

[271] R. U. Haq, A. Pandey and O. Bohigas, Fluctuation Properties of Nuclear Energy Levels: Do Theory and Experiment Agree?, Phys. Rev. Lett. **48**, 1086 (1982).

[272] K. Ando and Y. Kase, Biological Characteristics of Carbon-Ion Therapy, Int. J. Radiat. Biol. **85**, 715 (2009).

[273] B. Singers-Sørensen, J. Overgaard and N. Bassler, In vitro RBE-LET dependence for multiple particle types, Acta Oncol. **50**, 757 (2011).

[274] GSI website, GSI PIDE Project: `www.gsi.de/bio-pide` (2013).

[275] M. Durante, New challenges in high-energy particle radiobiology, Br. J. Radiol. **87**, 20130626 (2014).

[276] T. Friedrich, M. Durante and M. Scholz, Particle species dependence of cell survival RBE: Evident and not negligible (Comment to: B. Singers-Sørensen et al., In vitro RBE-LET dependence for multiple particle types, Acta Oncol. **50**, 757 (2011)), Acta Oncol. **52**, 589 (2013).

[277] L. Polster, J. Schuemann, I. Rinaldi, L. Burigo, A.L. McNamara, R.D. Stewart, A. Attili, D.J. Carlson, T. Sato, J.R. Méndez, B. Faddegon, J. Perl and H. Paganetti, Extension of TOPAS for the simulation of proton radiation effects considering molecular and cellular endpoints, Phys. Med. Biol. **60**, 5053 (2015).

[278] B.L. Tracy, D.L. Stevens, D.T. Goodhead and M.A. Hill, Variation in RBE for Survival of V79-4 Cells as a Function of Alpha-Particle (Helium Ion) Energy, Radiat. Res. **184**, 33 (2015).

[279] F. Kamp, G. Cabal, A. Mairani, K. Parodi, J.J. Wilkens and D.J. Carlson, Fast Biological Modeling for Voxel-based Heavy Ion Treatment Planning Using the Mechanistic Repair-Misrepair-Fixation Model and Nuclear Fragment Spectra, Int. J. Radiat. Oncol. Biol. Phys. **93**, 557 (2015).

[280] F. Tommasino and M. Durante, Proton Radiobiology, Cancers **7**, 353 (2015).

[281] A. Mairani, G. Magro, I. Dokic, S.M. Valle, T. Tessonnier, R. Galm, M. Ciocca, K. Parodi, A. Ferrari, O. Jäkel, T. Haberer and P. Pedroni, Data-driven RBE parameterization for helium ion beams, Phys. Med. Biol. **61**, 888 (2016).

[282] B. Jones, The apparent increase in the β-parameter of the linear quadratic model with increased linear energy transfer during fast neutron irradiation, Br. J. Radiol. **83**, 433 (2010).

[283] M. Zaider and H.H. Rossi, On the Application of Microdosimetry to Radiobiology, Radiat. Res. **113**, 15 (1988).

[284] J.R.K. Savage, Insights into sites, Mutat. Res. **366**, 81 (1996).

[285] P. Pater, J. Seuntjens, I. El Naqa and M.A. Bernal, On the consistency of Monte Carlo track structure DNA damage simulations, Med. Phys. **41**, 121708 (2014).

[286] National Research Council, Health Risks from Exposure to Low Levels of Ionizing Radiation: BEIR VII (National Academy Press, Washington DC, 2006).

[287] D.J. Shah, R.K. Sachs and D.J. Wilson, Radiation-induced cancer: a modern view, Br. J. Radiol. **85**, e1166 (2012).

[288] W.U. Müller, Current Discussions of DDREF, Cataracts, Circulatory Diseases and Dose Limits, Radiat. Prot. Dosim. **164**, 34 (2015).

[289] R.B. Hawkins, Survival of a Mixture of Cells of Variable Linear-Quadratic Sensitivity to Radiation, Radiat. Res. **153**, 840 (2000).

[290] A.C. Wéra, L. Barazzuol, J.C.G. Jeynes, M.J. Merchant, M. Suzuki and K.J. Kirkby, Influence of the nucleus area distribution on the survival fraction after charged particles broad beam irradiation, Phys. Med. Biol. **59**, 4197 (2014).

[291] N.I. Nakajima, H. Brunton, R. Watanabe, A. Shrikhande, R. Hirayama, N. Matsufuji, A. Fujimori, T. Murakami, R. Okayasu, P. Jeggo and A. Shibata, Visualisation of γH2AX Foci Caused by Heavy Ion Particle Traversal; Distinction between Core Track versus Non-Track Damage, PLoS One **8**, e70107 (2013).

[292] T. Stöhlker, V. Bagnoud, K. Blaum, A. Blazevic, A. Bräuning-Demian, M. Durante, F. Herfurth, M. Lestinsky, Y. Litvinov, S. Neff, R. Pleskac, R. Schuch, S. Schippers, D. Severin, A. Tauschwitz, C. Trautmann, D. Varentsov and E. Widmann, APPA at FAIR: From fundamental to applied research, Nucl. Instr. Meth. Phys. Res. B **365**, 680 (2015).

[293] M. Durante and H. Stöcker, Relativistic protons for image-guided stereotactic radiosurgery, J. Phys. Conf. Series **373**, 012016 (2012).

[294] E. Dikomey, J. Dahm-Daphi, I. Brammer, R. Martinsen and B. Kaina, Correlation between cellular radiosensitivity and non-repaired double-strand breaks studied in nine mammalian cell lines, Int. J. Radiat. Biol. **73**, 269 (1998).

[295] D. Habermehl, K. Ilicic, S. Dehne, S. Rieken, L. Orschiedt, S. Brons, T. Haberer, K.J. Weber, J. Debus and S.E. Combs, The Relative Biological Effectiveness for Carbon and Oxygen Ion Beams Using the Raster-Scanning Technique in Hepatocellular Carcinoma Cell Lines, PLoS One **9**, e113591 (2014).

[296] W. Tinganelli, M. Durante, R. Hirayama, M .Krämer, A. Maier, W. Kraft-Weyrather, Y. Furusawa, T. Friedrich and E. Scifoni, Kill-painting of hypoxic tumours in charged particle therapy, Sci. Rep. **5** 17106 (2015).

[297] J.V. Harper, J.A. Anderson and P. O'Neill, Radiation induced DNA DSBs: Contribution from stalled replication forks?, DNA Repair **9**, 907 (2010).

[298] A.G. Georgakilas, P. O'Neill and R.D. Stewart, Induction and Repair of Clustered DNA Lesions: What Do We Know So Far?, Radiat. Res. **180**, 100 (2013).

[299] J. Kuha, AIC and BIC: Comparisons of Assumptions and Performance, Soc. Met. Res. **33**, 188 (2004).

[300] F.B. Geara, L.J. Peters, K.K. Ang, J.L. Wike and W.A. Brock, Prospective comparison of in vitro normal cell radiosensitivity and normal tissue reactions in radiotherapy patients, Int. J. Radiat. Oncol. Biol. Phys. **27**, 1173 (1993).

[301] F.A. Cucinotta and L.J. Chappell, Non-targeted effects and the dose response for heavy ion tumor induction, Mutat. Res. **687**, 49 (2010).

[302] L. Mariotti, A. Facoetti, D. Alloni, A. Bertolotti, E. Ranzaa and A. Ottolenghi, Effects of Ionizing Radiation on Cell-to-Cell Communication, Radiat. Res. **174**, 280 (2010).

[303] A.C. Heuskin, C. Michiels and S. Lucas, Toward computer simulation of high-LET in vitro survival curves, Phys. Med. Biol. **58**, 6495 (2013).

[304] B. Emami, J. Lyman, A. Brown, L. Coia, M. Goitein, J.E. Munzenrider, B. Shank, L.J. Solin and M. Wesson, Tolerance of normal tissue to therapeutic irradiation, Int. J. Radiat. Oncol. Biol. Phys. **21**, 109 (1991).

[305] S.M. Bentzen, L.S. Constine, J.O. Deasy, A. Eisbruch, A. Jackson, L.B. Marks, R.K. Ten Haken and E.D. Yorke, Quantitative Analyses of Normal Tissue Effects in the Clinic (QUANTEC): an introduction to the scientific issues, Int. J. Radiat. Oncol. Biol. Phys. **76**, S3 (2010).

[306] S.C. Brüningk, F. Kamp and J.J. Wilkens, EUD-based biological optimization for carbon ion therapy, Med. Phys. **42**, 6248 (2015).

[307] F.A. Dilmanian, Z. Zhong, T. Bacarian, H. Benveniste, P. Romanelli, R. Wang, J. Welwart, T. Yuasa, E.M. Rosen and D.J. Anschel, Interlaced x-ray microplanar beams: A radiosurgery approach with clinical potential, Proc. Nat. Acad. Sci. **103**, 9709 (2006).

[308] E. Bräuer-Krisch, R. Serduc, E.A. Siegbahn, G. Le Duc, Y. Prezado, A. Bravin, H. Blattmann and J.A. Laissue, Effects of pulsed, spatially fractionated, microscopic synchrotron X-ray beams on normal and tumoral brain tissue, Mutat. Res. **704**, 160 (2010).

[309] F.A. Dilmanian, J.G. Eley, A. Rusek and S. Krishnan, Charged Particle Therapy with Mini-Segmented Beams, Front. Oncol. **5**, 269 (2015).

[310] A.N. Fontanella, M.K. Boss, M. Hadsell, J. Zhang, T. Schroeder, K.G. Berman, M.W. Dewhirst, S. Chang and G.M. Palmer, Effects of High-Dose Microbeam Irradiation on Tumor Microvascular Function and Angiogenesis, Radiat. Res. **183**, 147 (2015).

[311] C. Fernandez-Palomo, C. Mothersill, E. Bräuer-Krisch, J. Laissue, C. Seymour and E. Schültke, γH2AX as a Marker for Dose Deposition in the Brain of Wistar Rats after Synchrotron Microbeam Radiation, PLoS One **10**, e0119924 (2015).

[312] S. Girst, C. Greubel, J. Reindl, C. Siebenwirth, O. Zlobinskaya, D.W.M. Walsh, K. Ilicic, M. Aichler, A. Walch, J.J. Wilkens, G. Multhoff, G. Dollinger and T.E. Schmid, Proton Minibeam Radiation Therapy Reduces Side Effects in an In Vivo Mouse Ear Model, Int. J. Radiat. Oncol. Biol. Phys., ahead of print (2016).

[313] I. Diallo, N. Haddy, E. Adjadj, A. Samand, E. Quiniou, J. Chavaudra, I. Alziar, N. Perret, S. Guérin, D. Lefkopoulos and F. de Vathaire, Frequency distribution of second solid cancer locations in relation to the irradiated volume among 115 patients treated for childhood cancer, Int. J. Radiat. Oncol. Biol. Phys. **74**, 876 (2009).

[314] A. Berrington de Gonzalez, E. Gilbert, R. Curtis, P. Inskip, R. Kleinerman, L. Morton, P. Rajaraman and M.P. Little, Second Solid Cancers After Radiation Therapy: A Systematic Review of the Epidemiologic Studies of the Radiation Dose-Response Relationship, Int. J. Radiat. Oncol. Biol. Phys. **86**, 224 (2013).

[315] C.S. Chung, T.I. Yock, K. Nelson, Y. Xu, N.L. Keating and N.J. Tarbell, Incidence of Second Malignancies Among Patients Treated With Proton Versus Photon Radiation, Int. J. Radiat. Oncol. Biol. Phys. **87**, 46 (2013).

[316] W.D. Newhauser and M. Durante, Assessing the risk of second malignancies after modern radiotherapy, Nat. Rev. Cancer **11**, 438 (2011).

[317] M.P. Little, W.F. Heidenreich, S.H. Moolgavkar, H. Schöllnberger and D.C. Thomas, Systems biological and mechanistic modelling of radiation-induced cancer, Radiat. Environ. Biophys. **47**, 39 (2008).

[318] P. Vineis, A. Schatzkin and J.D. Potter, Models of carcinogenesis: an overview, Carcinogenesis **31**, 1703 (2010).

[319] J. Nguyen, M. Moteabbed and H. Paganetti, Assessment of uncertainties in radiation-induced cancer risk predictions at clinically relevant doses, Med. Phys. **42**, 81 (2015).

[320] D.L. Preston, E. Ron, S. Tokuoka, S. Funamoto, N. Nishi, M. Soda, K. Mabuchi and K. Kodama, Solid Cancer Incidence in Atomic Bomb Survivors: 1958-1998, Radiat. Res. **168**, 1 (2007).

[321] V.S.K. Manem, M. Kohandel, D.C. Hodgson, M.B. Sharpe and S. Sivaloganathan, The effect of radiation quality on the risks of second malignancies, Int. J. Radiat. Biol. **91**, 209 (2015).

[322] S.E. Combs, J. Bohl, T. Elsässer, K.J. Weber, D. Schulz-Ertner, J. Debus and W.K. Weyrather, Radiobiological evaluation and correlation with the local effect model, Int. J. Radiat. Biol. **85**, 126 (2009).

[323] F. Schlaich, S. Brons, T. Haberer, J. Debus, S.E. Combs and K.J. Weber, Comparison of the effects of photon versus carbon ion irradiation when combined with chemotherapy in vitro, Radiat. Oncol. **8**,260 (2013).

[324] M. Durante, N. Reppingen and K.D. Held, Immunologically augmented cancer treatment using modern radiotherapy, Trends Mol. Med. **19**, 565 (2013).

[325] A. Kalbasi, C.H. June, N. Haas and N. Vapiwala, Radiation and immunotherapy: a synergistic combination, J. Clin. Invest. **123**, 2756 (2013).

[326] M.M. Ahmed, C. Guha, J.W. Hodgec and E. Jaffeed, Immunobiology of Radiotherapy: New Paradigms, Radiat. Res. **182**, 123 (2014).

[327] R.E. Vatner, B.T. Cooper, C. Vanpouille-Box, S. Demaria and S.C. Formenti, Combinations of immunotherapy and radiation in cancer therapy, Front. Oncol. **4**, 325 (2014).

[328] C. Tang, X. Wang, H. Soh, S. Seyedin, M.A. Cortez, S. Krishnan, E. Massarelli, D. Hong, A. Naing, A. Diab, D. Gomez, H. Ye, J. Heymach, R. Komaki, J.P. Allison, P. Sharma and J.W. Welsh, Combining Radiation and Immunotherapy: A New Systemic Therapy for Solid Tumors?, Cancer Immunol. Res. **2**, 831 (2014).

[329] M. Durante, F. Tommasino and S. Yamada, Modelling combined chemotherapy and particle therapy for locally advanced pancreatic cancer, Front. Oncol. **5**, 145 (2015).

[330] K. Soukup and X. Wang, Radiation meets immunotherapy - a perfect match in the era of combination therapy?, Int. J. Radiat. Biol. **91**, 299 (2015).

[331] A. Dasu and I. Toma-Dasu, Impact of variable RBE on proton fractionation, Med. Phys. **40**, 011705 (2013).

[332] M.F. Gensheimer, T.I. Yock, N.J. Liebsch, G.C. Sharp, H. Paganetti, N. Madan, P.E. Grant and T. Bortfeld, In vivo proton beam range verification using spine MRI changes, Int. J. Radiat. Oncol. Biol. Phys. **78**, 268 (2010).

[333] M. Baumann, M. Krause, H. Thames, K. Trotts and D. Zips, Cancer stem cells and radiotherapy, Int. J. Radiat. Biol. **85**, 391 (2009).

[334] M. Baumann, M. Krause and R. Hill, Exploring the role of cancer stem cells in radioresistance, Nat. Rev. Cancer **8**, 545 (2008).

[335] L.E. Ailles and I.L. Weissman, Cancer stem cells in solid tumors, Curr. Opin. Biotech. **18**, 460 (2007).

[336] J.E. Visvader and G.J. Lindeman, Cancer Stem Cells: Current Status and Evolving Complexities, Cell Stem Cell **10**, 717 (2012).

[337] J.A. Magee, E. Piskounova and S.J. Morrison, Cancer Stem Cells: Impact, Heterogeneity, and Uncertainty, Cancer Cell **21**, 283 (2012).

[338] A. Mansouri, M.R. Abbaszadegan and M. Gholamin, A Review on the Biology of Cancer Stem Cells, Stem Cell Disc. **4**, 83 (2014).

[339] F. Albertini F, E.B. Hug and A.J. Lomax, Is it necessary to plan with safety margins for actively scanned proton therapy?, Phys. Med. Biol. **56**, 4399 (2011).

[340] G.C. Barnett GC, C.M. West, A.M. Dunning, R.M. Elliott, C.E. Coles, P.D. Pharoah and N.G. Burnet, Normal tissue reactions to radiotherapy: towards tailoring treatment dose by genotype, Nat. Rev. Cancer **9**, 134 (2009).

[341] S.M. Bentzen, M. Parliament, J.O. Deasy, A. Dicker, W.J. Curran, J.P. Williams and B.S. Rosenstein, Biomarkers and surrogate endpoints for normal-tissue effects of radiation therapy: the importance of dose-volume effects, Int. J. Radiat. Oncol. Biol. Phys. **76**, S145 (2010).

[342] A. Yaromina, M. Krause and M. Baumann, Individualization of cancer treatment from radiotherapy perspective, Mol. Oncol. **6**, 211 (2012).

Acknowledgements

I would like to thank all persons who helped that this work has become possible and who accompanied my scientific development during the last years.

First of all I would like to express deep gratitude to my academic mentors in the field of radiation biophysics, Prof. Dr. Marco Durante and PD Dr. Michael Scholz, who greatly supported me and steadily motivated me to think about interpretation and relevance of my research results. They gave me the chance to work in a truly interdisciplinary field within the entire spectrum between basic research and applied science. On both a scientific and personal level I could not have found better mentors.

I also would like to thank Prof. Dr. Barbara Drossel who is acting as adviser for the Habilitation procedure - it is very helpful to have a reliable contact person at TUD and, besides, highly enjoyable to discuss ideas and thoughts with somebody having a great background in theoretical physics.

Of course, much of this work would not have been possible without many inspiring scientific discussions and problem solving sessions with current and former colleagues of the 'RBE modeling group'. Especially I am grateful for the support of Dr. Rebecca Grün, for sharing all goods and bads we encounter in our work, and at last for proofreading this thesis.

Likewise, I would like to thank all staff of the GSI biophysics group. I am happy to work in such a cooperative and helpful environment, where doors and minds are open. This gave me the opportunity to meet great people, learn much about biology and discuss my views on statistical aspects in radiobiology and data analysis.

I also thank all collaboration partners - numerous fascinating projects have been developed during the last years and I am very glad working with them, combining expertise from different disciplines of science.

The 'Scholars in Training' section of the Radiation Research Society gave me the opportunity to work together with many young researchers in a society committee within an international and interdisciplinary environment. I am grateful for having met all these people, sharing issues of our scientific work and career development, and I am confident to stay in good contact with those who make their way in science for many years.

At this point I do not want to forget that I was trained in another field of research. In this regard, I would like to deeply thank Prof. Dr. Dr. h.c. mult. Achim Richter, who was my former PhD supervisor, as well as Prof. Dr. Thomas Seligman as a former collaborator. They both greatly supported me in the early days of my career and sustainably influenced my way of scientific thinking.

Finally, I would like to thank my relatives, in particular my parents, but also my friends and all people I am interacting with in my non-scientific life for continuous support and for stimulating me to keep up a beneficial work-life-balance!

Erklärung zur Habilitationsschrift

Hiermit versichere ich, die vorliegende Habilitationsschrift ohne Hilfe Dritter nur mit den angegebenen Quellen und Hilfsmitteln angefertigt zu haben. Alle Stellen, die aus Quellen entnommen wurden, sind als solche kenntlich gemacht. Diese Arbeit hat in gleicher oder ähnlicher Form noch keiner Prüfungsbehörde vorgelegen.

Darmstadt, den 5. Februar 2016

(Thomas Friedrich)